Republic of Iraq

Ministry of Higher Education and Scientific Research

University of Babylon

College of Engineering

Civil Engineering Department

Structural Behavior of Spliced Hybrid Reinforced Concrete Deck Girders Under Effect of Monotonic and Cyclic Loads

A Thesis
Submitted to the College of Engineering / University of Babylon in Partial Fulfillment of the Requirements for the Degree of Doctor of Philosophy In
Engineering/ Civil Engineering/Structures

By

Mustafa Kareem Moosa Abdulhassan AL-Hassnawi

Supervised by

Prof. Dr. Ammar Yaser Ali

2023 A.D. 1444 H.D.

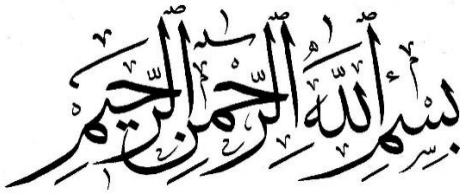

(وَيَسْأَلُونَكَ عَنِ الرُّوحِ ۖ قُلِ الرُّوحُ مِنْ أَمْرِ رَبِّي

وَمَا أُوتِيتُمْ مِنَ الْعِلْمِ إِلَّا قَلِيلًا)

﴿الاسراء ٨٥﴾

الخلاصة

الروافد الموصلة هي احد الحلول التقنية الجيدة لعمل رافدة بطول كبير بكلفة , وقت , و الات انشائية تتناسب مع المشروع المطلوب. تتلخص هذه الطريقة بعمل (صب) عدة قطع كونكريت مسبقة الصب حسب الطول المناسب و ثم توصيل و ربط التسليح و بعد ذلك صب كونكريت جديد او حقن مادة ذات ربط قوي.

في هذه الدراسة, يتم التعرف على السلوك الانشائي للروافد الموصلة ذات السقف الهجينة تحت تاثير حمل ساكن و دوري متكرر. اكمال متطلبات البحث تمت من خلال مرحلتين. الجزء الاول هو عمل تجارب مختبرية على واحد وعشرين نموذج. الروافد ذات الاسناد البسيط التي عددها اثنتاعشر نموذج تشمل دراسة المتغيرات عمق المفصل, نوع المفصل, تهجين التسليح, توصيلات اضافية , و نوع التحميل. تمتلك هذه النماذج بمقطع عرضي ذو شكل T و بأبعاد (125*200) ملم للوصلة و (100*200) ملم للشفة و بطول فضاء 1500 ملم. و تنطبق ابعاد المقطع العرضي نفسها على نماذج الاسناد المستمر لفضائين بطول 1500 ملم لكل فضاء. هذه النماذج هي تسعة نماذج فقط و تم فيها دراسة موقع المفصل, و نوع المفصل, تهجين التسليح السالب, و نوع التحميل.

تتبع السلوك الانشائي لهذه النماذج كان من خلال احمال التشقق, الحمل الاقصى, منحنيات الحمل مع الهطول, نمط الفشل و توزيع التشققات, الصلابة, المطيلية, امتصاص الطاقة, مؤشر الضرر.

بالنسبة لجميع العوارض ، تم استخدام الخرسانة فائقة الأداء (UHPC) لصب السطح والمفاصل ، حيث يتم استخدامها في سطح المقاطع مسبقة الصب للعينات ذات المفصل كامل العمق في مجموعة الاسناد البسيط وفي الوصلة كمادة مصبوبة في الموقع (CIP). بينما ، لعارضة أخرى مقسمة تستخدم لصب السطح والمفصل في نفس الوقت مثل الخرسانة CIP. أيضًا ، كذلك تم صب عوارض التحكم بنفس الوقت بالنسبة للسطح ب UHPC والخرسانة ذات القوة العادية (NSC) في الوترة (web).

نتائج الروافد البسيطة بينت ان طريقة توصيل المفصل بتخشين السطح من خلال اضهار الحصى كانت جيدة. ان وجود المفصل ادى الى نقصان بالتحمل بمقدار (4.7 – 7.7)% للمفصل ذو العمق الكامل و الجزئي تواليا. ان تهجين التسليح بنسبة 50% اضاف تحمل بنسبة 5% فوق تحمل نموذج السيطرة. مفاتيح القص اعطت مميزات جيدة لنماذج و كذلك عند اضافة وصلات اضافية حسنت التحمل ليكون بمقدار 3.6% اقل من نموذج السيطرة. عند تسليط التحميل الدوري المتكرر ضهرت نتائج قريبة لتلك النتائج في التحميل الساكن.

اما بالنسبة لنماذج الروافد المستمرة, ان وجود المفصل ادى الى نقصان التحمل بمقدار 17.2% للنموذج المفصل الوسطي و 5.7% للنموذج ذو المفصلين عند نقاط الانقلاب. ادى استبدال 50% من التسليح ب الياف الكاربون البوليمرية الى رفع قابلية التحمل لتصل الى حد قريب من نموذج السيطرة. ايضاً عند اضافة مفاتيح القص حدثت مميزات ايجابية لتلك النماذج.

عرض التشققات الناتجة من اجهادات الانحناء لم يتجاوز الحد الذي تسمح به المدونة الامريكية (ACI) خلال مرحلة الحمل الخدمي.

ان من المميزات الاصيلة لهذا البحث هو استنتاج انه عند استخدام مفصل من الخرسانة فائقة الاداء لربط عنصرين مسبقة الصب من الروافد البسيطة و تحويلها الى رافد مستمر ضهر ان التحمل قريب جداً من نموذج السيطرة و لكن بتشققات وهطول اقل.

الجزء الثاني من البحث هو نمذجة عينة لتحاكي النماذج المفحوصة عملياً من خلال طريقة العناصر المحددة و بأستخدام برنامج ال(ABAQUS) و كانت نتائج التمثيل قريبة جداً و مقبولة.

بعد نجاح تمثيل هذا النموذج تم دراسة مؤثرات اخرى على البحث لزياد الفهم و المعلومات حول السلوك الانشائي لهذه الروافد. حيث تم دراسة التحميل الدوري الانعكاسي , سمك سقف النموذج (الشفة), نسبة التسليح , طريقة معالجة سطح المفصل, طول المفصل , عدد مفاتيح القص, حالة اسناد المفصل الوسطي, مسافة تسليح القص.

Abstract

The spliced girder is one of the solutions techniques to make long-span girders with cost, time, and construction machine suitable to the project. This method concluded by casting many precast units with appropriate lengths and casting the joints with new concrete or grout.

In this study, the structural behavior of reinforced concrete (RC) hybrid spliced deck girder under Monotonic and cyclic (Repeated) load was performed. Two stages were taken to complete the study process for this research. The first part consists of the experimental work of twenty-one specimens. Simply supported girders group consist of twelve specimens with the variable of joint depth (full and partial depth), joint type (flat and key joint), hybridization of reinforcement, addition dowels, and loading type (monotonic and cyclic). Specimens of this group had T-cross section of dimensions (125x200) mm for the web and (100x200) mm for the flange and a supported length of 1500 mm. Continuous girders group consist of nine girders with variables of the location of joint (at interior support and at inflection points), type of joint (flat and key joint), hybridization of reinforcement, and loading type (monotonic and cyclic). These girders had the same T-cross section geometry with two spans of 1500 mm.

The structural behavior of girders was evaluated by tracking the cracking load, ultimate load, load-deflection response, failure mode, stiffness, ductility, energy absorption, and damage index.

For all girders, ultra high-performance concrete (UHPC) was used to cast the deck and joints, where used in deck of precast segments for full depth joint specimens in simply supported group and in joint as cast in place (CIP) concrete. While, for another spliced girder used to cast the deck and joint at same time as CIP concrete. Also, the control girders were cast monolithically with UHPC in deck and normal strength concrete (NSC) in web.

The result of tested simply supported girders showed that the UHPC joint with exposed aggregate preparation interface surface gives a good bond and some simple cracks. The presence of joint reduces the ultimate load about (5 and 8) % for full and partial-depth joints, respectively. The replacement of 50% of steel reinforcement by CFRP bar increased the ultimate load by 5% compared with the control specimen. The presence of shear key in joints provides a challenging effect of ultimate load. The addition of steel reinforcement as dowel action improved the ultimate load to reach a reduction of only 4 % compared with the control girder. In general, the girders tested with cyclic load showed closing results to the girders tested monotonically .

In continuous girders, the inclusion of joints in the girder resulted in a reduction of approximately 17 % and 6% in the ultimate load for girders with one joint at the interior support and two joints at the inflection points, respectively. However, when the steel reinforcement was replaced by 50% with CFRP bar, the load-carrying capacity was improved and was comparable to that of the control girder. Additionally, the inclusion of a shear key provided noticeable improvement in the ultimate load.

The employment of the UHPC joint to link the two segments to form a continuous girder met the peak load of the simply supported beam, but with higher cracking load and less service deflection.

The second part in this study was performed the FEM model by using ABAQUS computer program. This model was used in the numerical analysis to validate the results with the experimental results to achieve an acceptable agreement with a difference of about 2% to 3.5 % compared to experimental results in terms of the ultimate load. After the acceptance of the simulated model, A parametric study was performed to provide more understanding of the structural behavior of spliced girders, such as the reverse cyclic load, reinforcement ratio, interface type, the thickness of deck, length of the joint, number of shear keys, type of support, and the spacing of stirrups.

Appendix A

Design of Girders

Use three point loading to insure shear and moment in joint region.

- Check limitations of T-section beams

1- $b \leq \frac{l}{4} \rightarrow \frac{1500}{4} = 375\ mm\ > 200\ mm\ o.k$

2- $\frac{b-b_w}{2} \leq 8\ h_f\ \rightarrow \frac{200-125}{2} \leq 8 * 100$

37.5 < 800 O.K.

- Check for Deep Beam limitations:

*L_{span} < 4*h* ⟶ *1500 < 1200 o.k*

*Distance of (P) > 2*h* ⟶ *750 mm > 600 mm o.k*

- The beam classified as shallow beam (ACI 318-19, 2019) item (9.9.1.1)

- Check for Flexure

(Simply support)

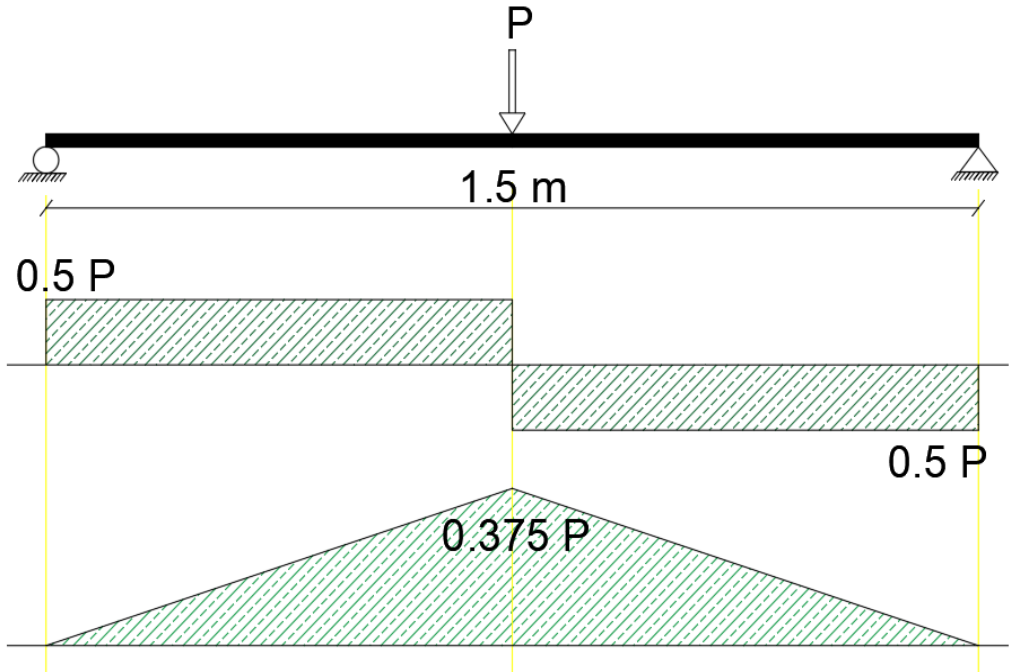

Figure A1: Load, shear & bending diagram of simply support girder.

$f_y = 585\ MPa$ ($\emptyset 10\ mm$) and f_y=317 MPa ($\emptyset 6\ mm$)

$f'_c = 145\ \ mpa$ for UHPC

$$a = \frac{A_s . f_y}{0.85\ f'_c * b_f}$$

$$a = \frac{312 * 585}{0.85 * 145 * 200} = 8\ mm < 100$$

∴ rectangular section

$$M_n = \ A_s . f_y \left(d - \frac{a}{2}\right)$$

$$\text{d} = \ 300 - 20 - 6 - 10 - 13 = 251\ \text{mm}$$

$$M_n = \ 312 * 585 \left(251 - \frac{8}{2}\right)$$

Mn= 45 kN.m

$$\text{Mn} = \frac{\text{Pn} * \text{L}}{4}$$

Pn = 120 kN

$$\rho = \frac{312}{200 * 251} = 0.006$$

$\rho_{max} = 0.05$ o.k

$\rho_{min} = 0.003$ o.k

(Continuous)

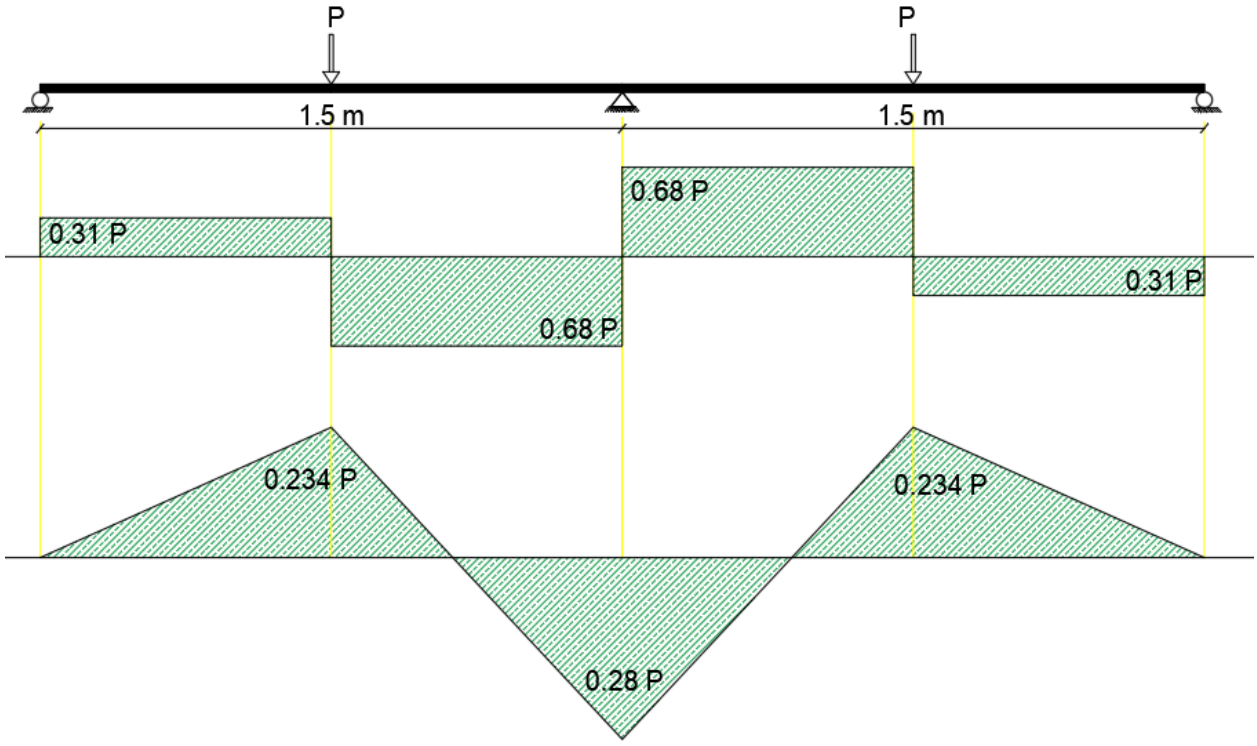

Figure A2: Load, shear & bending diagram of continuous girder.

$f_y = 317\ Mpa$ (Ø8 mm) and f_y=617 Mpa (Ø6 mm)

$f'_c = 40\ \ mpa$ for NSC

$$a = \frac{A_s . f_y}{0.85\ f'_c * b_f}$$

$$a = \frac{200.4 * 317}{0.85 * 40 * 125} = 14.94\ mm < 200$$

∴ rectangular section

$$M_n = A_s . f_y \left(d - \frac{a}{2}\right)$$

$$d = 300 - 20 - 6 - 8 = 265\ \text{mm}$$

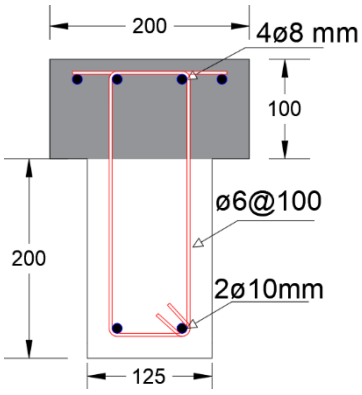

$$M_n = 200.4 * 317\left(265 - \frac{14.94}{2}\right)$$

Mn= 16.36 kN.m

$$\text{Mn} = 0.28 * \text{Pn}$$

Pn = 58.4 kN

$$\rho = \frac{200.4}{125 * 265} = 0.006$$

- Check the shear

Reinforcement of Stirrups $\emptyset$ 6@ 100 mm , $A_v = 28.3\ mm^2$

$V_s = \frac{A_v.f_y.d}{S}$, $S_{max} = \frac{d}{2} = 125\ mm$

$V_c = 0.17\sqrt{f'_c} b_w.d$

For simply support

$$V_s = \frac{2 * 28.3 * 617 * 250}{100} * 10^{-3} = 87.3\ kN$$

$$V_c = 0.17\sqrt{40} * 125 * 250 * 10^{-3} = 33.6\ kN$$

$V_n = V_c + V_s = 120.9\ kN$

$V_n = \frac{P_n}{2} \rightarrow P_n = 241.8\ kN$

For continuous support

$V_n = 1.375\ Pn \rightarrow P_n = 88\ kN$

- Check the shear-Friction

Reinforcement of Stirrups $\emptyset$ 6@ 100 mm , $A_v = 28.3\ mm^2$

$A_{vf} = 2 * 28.3 * 15 = 849\ mm^2\ total\ Area\ of\ shear\ Reinf.$

, $S_{max} = \frac{d}{2} = 125\ mm$

$V_n = \mu . A_{vf} . f_y$

$\mu = 1 \quad (coeff. of\ friction)$

$V_n = 1 * 849 * 450 * 10^{-3} = 382\ kN$

Check limitation

$0.2 * f'_c . A_c = 1125 > 382\ \ o.k$

$3.3 + 0.85 * f'_c . A_c = 1068 > 382 \quad o.k$

$11 * A_c = 2062.5 > 382 \quad o.k$

Length of splice joint

From thesis of (Al-Khazragy, 2016) used UHPC(RPC) , Ls= 30 d_b for repeated load without hook. So,

Ls with hook = 0.5 Ls of without hook bar (ACI 318-19, 2019) items [(25.3.1),(25.4.2.1),(25.4.3.1)]

Ls= 15 d_b = 15*10 =150 mm

Length of joint (L_j)= Ls + cover

Length of joint = 150 +2*20 = 190 mm

Reference

ACI 318-19, C. (2019). *Building Code Requirements for Concrete and Commentary*. 628.

Al-Khazragy, F. F. S. (2016). *Effect of Tensile Reinforcement Lap Splices on the Behavior of Reinforced Reactive Powder Concrete Beams Under Repeated Loading*. Ph.D. thesis , University of Technology.

Appendix B

Test Result and Data Sheet for Material Used in Experimental Program

B-1 Cement

Table B1:Test result for Chemical analysis of cement used in NSC and UHPC.

Compound Composition	Oxide	Test Result	Limit according to I.Q.S. 5/1984	Conformed to I.Q.S
Lime Oxide	CaO %	62.43	----------	
Silica Dioxide	SiO2 %	19.44	----------	
Alumina Oxide	Al2O3 %	4.98	----------	
Iron Oxide	Fe2O3 %	3.4	----------	
Magnesia Oxide Contino	MgO %	2.57	≤ 5%	OK
Sulfate Trioxide	SO3 %	2.41	≤2.5%ifC3A< 5% ≤2.8%ifC3A> 5%	OK
Free Lime	F.L. %	1.18		
Loss on Ignition	L.O.I. %	4.0	≤4%	OK
Insoluble Resdue	I. R. %	1.25	≤1.5 %	OK
Lime Saturation Factor	L.S.F	0.95	0.66-1.02	OK
	M.S	2.32	----------	
	M.A	1.46	----------	
	Total	99.22		

Key Compounds Percentage by Weight of Cement (Bogue's Equation)

C3S	Tricalcium Silicate	50.12
C2S	Dicalcium Silicate	21.26
C3A	Tricalcium Aluminate	9.29
C4AF	Tetra calcium Alumina ferrite	9.98

*The test was made in the Environmental Laboratory in College of Engineering in University of Babylon

Table B2:Test result of Physical properties of cement used in NSC and UHPC.

Setting Time minute	Initial	122	≥ 45	OK
	Final	240	≤ 600	OK
Fineness (Blaine), m_2/kg		314	≥ 230	OK
Compressive Strength (MPa)	7days	33.2	≥ 23	OK

*Physical tests are conducted in Construction Materials Laboratory of College of Engineering in Babylon University.

B-2 Fine Aggregate

Table B3: Classification of fine aggregate.

Size of Sieve (mm)	Passing (%)	
	Fine aggregate	Limitations for zone No2. (IQS 45/1984)
10	100	100
4.75	98.9	90-100
2.36	90.7	75-100
1.18	76.5	55-90
0.60	55.1	35-59
0.30	13.8	8-30
0.15	4.9	0-10

Table B4: Physical and chemical properties of fine aggregate.

Physical properties		
Properties	Test Results	Iraqi Specification No.45/1984
Specific Gravity	2.65	
Absorption	0.94%	
Fine Material Passing from Sieve (75 μm)	2.99%	Max ≤ 5.0%
Fineness Modulus	2.6	
Chemical Properties		
Sulfate Content	0.351%	Max ≤ 0.5%

The chemical and physical tests were conducted in the Environmental and the Constructional Materials Laboratory of College of Engineering at Babylon University, respectively.

B-3 Coarse Aggregate

Table B5: Properties of coarse aggregate.

Sieve Size (mm)	Passing %	
	Coarse Aggregate	Iraqi specifications limits (45/1984)
14	100	100
12.5	92.2	90-100
10	67.7	50-85
4.75	6.2	0-10
Chemical and defect fine materials		
Passing from Sieve (75 μm)	1.85	Max. (3%)
SO_3	0.088	Max. (0.1%)

The chemical and physical tests were carried out in the Environmental and the Constructional Materials Laboratory of College of Engineering at Babylon University, respectively.

B-4 Steel Fiber

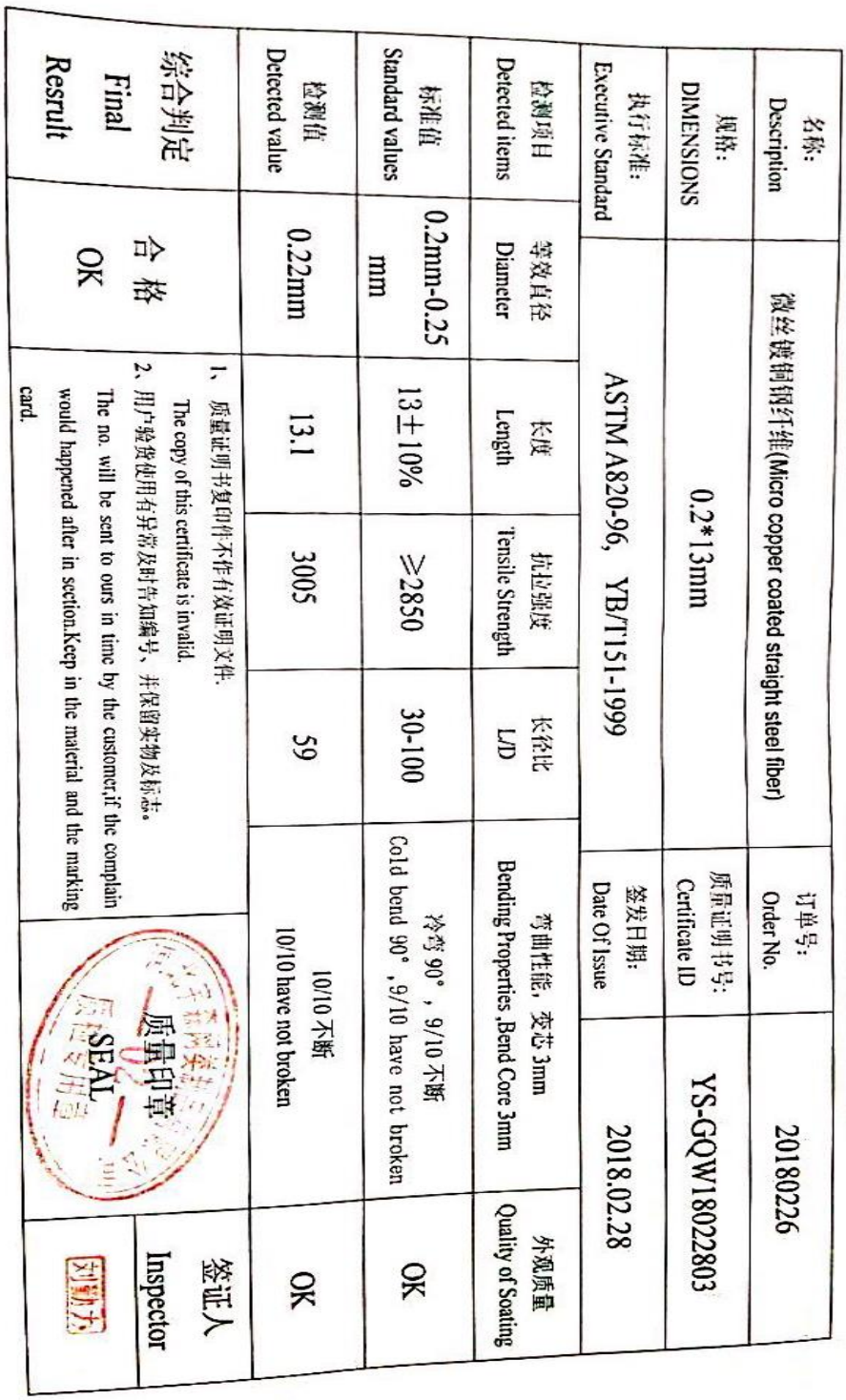

河北宇森网类制品有限公司

Hebei YuSen Metal Wire Mesh Co., Ltd.

钢纤维质量证明书

Steel fibre quality certificate

地址(ADDRESS)：河北省安平县丝网大世界开发区 Wire Mesh World Anping, Hengshui, Hebei, P. R. China

电话（TEL)： +86-318-7758858

传真（FAX)： +86-318-5288858

网址 (WEB)： www.china-steelfiber.com.cn

邮箱(EMAIL)： yusen01@metalmesh.com.cn

名称: Description	微丝镀铜钢纤维(Micro copper coated straight steel fiber)			订单号: Order No.	20180226
规格: DIMENSIONS	0.2*13mm			质保证明书号: Certificate ID	YS-GQW18022803
执行标准: Executive Standard	ASTM A820-96, YB/T151-1999			签发日期: Date Of Issue	2018.02.28
检测项目 Detected items	等效直径 Diameter	长度 Length	抗拉强度 Tensile Strength	长径比 L/D	弯曲性能，变芯 3mm Bending Properties ,Bend Core 3mm	外观质量 Quality of Soating
标准值 Standard values	0.2mm-0.25 mm	13±10%	≥2850	30-100	冷弯 90°，9/10 不断 Cold bend 90°，9/10 have not broken	OK
检测值 Detected value	0.22mm	13.1	3005	59	10/10 不断 10/10 have not broken	OK
综合判定 Final Resrult	合 格 OK	1、质量证明书复印件不作有效证明文件。 The copy of this certificate is invalid. 2、用户验货使用有异常及时告知编号，并保留实物及标志。 The no. will be sent to ours in time by the customer,if the complain would happened after in section.Keep in the material and the marking card.				签证人 Inspector 刘勤方

质量印章 SEAL

Plate B1: Data sheet of steel fiber used for UHPC mixture.

B-5 Silica Fume

BASF
We create chemistry

MasterRoc® MS 610

Densified silica fume for cast and sprayed concrete

DESCRIPTION

MasterRoc MS 610 is a high quality silica fume powder for high performance concretes. It changes the porous structure of the concrete making it denser and more resistant to any type of external influence.

FIELDS OF APPLICATION

- Wet-mix sprayed concrete applications
- Pre-cast concrete
- Cast in-situ concrete
- High strength concrete
- Underwater concrete
- Concrete with low cement content
- Annulus grouting (TBM)

FEATURES AND BENEFITS

- Wet-mix sprayed concrete applications
- Pre-cast concrete
- Cast in-situ concrete
- High strength concrete
- Underwater concrete
- Concrete with low cement content
- Annulus grouting (TBM)

PACKAGING

MasterRoc MS 610 is supplied in 20 kg plastic bags and big bags.

TECHNICAL DATA*

Form	Powder
Color	Grey
Density	0.55 - 0.7 kg/l
Chloride content	<0.1%

COMBINATION

The use of superplasticizers is recommended for any silica fume concrete. For frost resistance, an additional air-entraining agent must be added.

MIXING

MasterRoc MS 610 is added to the concrete during batching. Minimum mixing time is 90 seconds. The recommended dosage is 5 to 15% of the cement weight.

STORAGE

If stored dry and in tightly closed original bags, **MasterRoc MS 610** has a shelf life of at least 12 months.

Plate B2: Technical data sheet of silica fume used in UHPC mixture.

B-6 Super Plasticizer

MASTER® BUILDERS SOLUTIONS

MasterGlenium® 54

A high performance concrete superplasticiser based on modified polycarboxylic ether

DESCRIPTION

MasterGlenium 54 has been developed for applications primarily in precast but also readymix concrete industries where the highest durability and performance is required.

MECHANISM OF ACTION

MasterGlenium 54 is differentiated from conventional superplasticisers, such as those based on sulphonated melamine or naphthalene formaldehyde condensate as it is based on a unique carboxylic ether polymer with long lateral chains. This greatly improves cement dispersion. At the start of the mixing process the same electrostatic dispersion occurs but the presence of the lateral chains, linked to the polymer backbone, generate a steric hindrance which stabilises the cement particles capacity to separate and disperse.

This mechanism provides flowable concrete with greatly reduced water demand and enhanced early strength.

TYPICAL APPLICATIONS

The excellent dispersion properties of **MasterGlenium 54** make it the ideal admixture for precast or ready-mix where low water cement ratios are required. This property allows the production of very high early and high ultimate strength concrete with minimal voids and therefore optimum density. Due to the strength development characteristics the elimination or reduction of steam curing in precast works may be considered as an economical option.

- high workability without segregation or bleeding
- less vibration required
- can be placed and compacted in congested reinforcement
- reduced labour requirement
- improved surface finish

MasterGlenium 54 may be used in combination with **MasterMatrix** for producing Smart Dynamic Concrete (SDC). The technology produces advanced self compacting concrete, without the aid of vibration. For economic, ecological and ergonomic ready-mix / precast concrete production.

MasterGlenium 54 can be used to produce very high early strength floor screeds. For screed mix designs consult Master Builders Solutions Technical Services.

PACKAGING

MasterGlenium 54 is available in 208 litre drums and in bulk tanks upon request.

STANDARDS

ASTM C-494 Type F& G
BS EN 934-2

TYPICAL PROPERTIES*

Form	Whitish to straw coloured liquid
Relative density	1.07
pH	5-8

APPLICATION GUIDELINES

MasterGlenium 54 is a ready to use admixture that is added to the concrete at the time of batching.

The maximum effect is achieved when the **MasterGlenium 54** is added after the addition of 70% of the water. **MasterGlenium 54** must not be added to the dry materials.

Thorough mixing is essential and a minimum mixing cycle, after the addition of the **MasterGlenium 54**, of 60 seconds for forced action mixers is recommended.

Plate B3: Data sheet Super plasticizer used in UHPC and NSC mixture

MASTER® BUILDERS SOLUTIONS

MasterGlenium® 54

DOSAGE

The normal dosage for **MasterGlenium 54** is between 0.50 and 1.75 litres per 100kg of cement (cementitious material). Dosages outside this range are permissible subject to trial mixes.

COMPATIBILITY

MasterGlenium 54 is not compatible with **MasterRheobuild** superplasticizers.
MasterGlenium 54 is suitable for mixes containing all types of Portland cement and cementious materials as follows:

- microsilica
- fly ash (PFA)
- ground granulated blast furnace slag GGBS

EFFECT ON HARDENED CONCRETE

- increased early and ultimate compressive strengths
- increased flexural strength
- better resistance to carbonation
- lower permeability
- better resistance to aggressive atmospheric conditions
- reduced shrinkage and creep
- increased durability

STORAGE AND SHELF LIFE

MasterGlenium 54 should be stored above 5°C In closed containers or storage tanks to protect from evaporation and extreme temperatures.
The shelf life is 12 months when stored as above.

The occurrence of a surface layer with **MasterGlenium 54** is normal and will have no effect on the performance of the product.

HEALTH AND SAFETY

MasterGlenium 54 contains no hazardous substances requiring labelling. For further information refer to the Material Safety Data Sheet.

QUALITY AND CARE

All products originating from Master Builders Solutions Dubai, UAE facility are manufactured under a management system independently certified to conform to the requirements of the quality, environmental and occupational health & safety standards ISO 9001, ISO 14001 and ISO 45001.

* Properties listed are based on laboratory controlled tests.

® = Registered trademark of the MBCC Group in many countries.

MBS_CC-UAE/GI_54_09_07/v2/03_16

Master Builders Solutions
Construction Chemicals LLC
P.O. Box 37127, Dubai, UAE
Tel: +971 4 8090800
www.master-builders-solutions.com/en-ae

Plate B4: Continuo

B-7 Carbon Fiber Reinforced Polymer

BUILDING TRUST
CONSTRUIRE LA CONFIANCE

PRODUCT DATA SHEET
Edition 12.2018/v1
CSC Master Format™ 03 25 00
COMPOSITE REINFORCING

Sika® CarboDur® Rods

CARBON FIBER RODS FOR STRUCTURAL STRENGTHENING

Description

Sika® CarboDur® Rods are pultruded carbon fiber reinforced polymer (CFRP) rods designed for strengthening concrete, timber and masonry structures. The rods are primarily installed using the Near Surface Mounted (NSM) technique by inserting into grooves cut into the substrate and bonded with an epoxy resin. The rods can also be used for anchoring SikaWrap® fabrics for positive attachment to concrete or masonry.

Where to Use

- Negative moment reinforcing in slabs and decks.
- Anchoring of SikaWrap® fabrics.
- Strengthening of masonry walls.
- Doweling applications.
- Cathodic protection applications.

Load increases

- Increased live loads in warehouses.
- Increased loading in parking decks.
- Installation of heavy machinery.
- Vibrating structures.
- Changes of building use.

Damage to structural parts

- Aging of construction materials.
- Steel reinforcement corrosion.
- Vehicle impact.
- Fire.

Serviceability improvements

- Decrease in deformation.
- Stress reduction in steel reinforcement.
- Crack width reduction.

Change in structural system

- Removal of walls or columns.
- Removal of slab sections for openings.

Design or construction defects

- Insufficient reinforcements.
- Insufficient structural depth.

Advantages

- Very high strength.
- Lightweight.
- Non-corrosive.
- Very easy to handle.
- High modulus of elasticity.
- Can accept traffic on surface (rods are countersunk).
- High bond strength due to full encapsulation.
- Rods are not visible once installed.
- Outstanding fatigue resistance.
- Alkali resistant.

Technical Data

Packaging	Diameter:	9.52 mm (3/8 in) : 6 m (20 ft) in length
Colour	Black	
Shelf Life	Unlimited (no exposure to direct sunlight).	
Base	Carbon fiber reinforced polymer with an epoxy resin matrix.	

Plate B5: Technical data sheet of CFRP bar

Properties at 23 °C (73 °F) and 50 % R.H.

Tensile Strength	2800 MPa (4.06 x 10^5 psi)
Tensile Modulus of Elasticity	155 000 MPa (22.5 x 10^6 psi)
Strain (Elongation at Break)	1.8 %
Fiber Volumetric Content	65 %
Temperature Resistance	> 150 °C (> 300 °F)

Physical Properties

Diameter Cross	**Sectional Area**	**Tensile Strength**
6.35 mm (1/4 in)	31.67 mm^2 (0.05 sq in)	55.6 kN (12 500 lb_f)
9.52 mm (3/8 in)	71.25 mm^2 (0.11 sq in)	122.3 kN (27 500 lb_f)

Coverage

Rod (Diameter)	**Groove (Dimensions)**	**Product**	**Coverage [m (ft)/unit]**
ø = 9.52 mm (3/8 in)	16 mm x 16 mm (5/8 in x 5/8 in)	Sikadur®-32 Hi-Mod	54.1 m (177 ft)/10 L
		Sika AnchorFix®-3001	3.2 m (10 ft)/cartridge
		Sikadur®-330	20 m (65 ft)/5 kg
		Sikadur®-30	19.7 m (64 ft)/6 kg

Product properties are typically averages, obtained under laboratory conditions. Reasonable variations can be expected on-site due to local factors, including environment, preparation, application, curing and test methods.

HOW TO USE

Surface Preparation

For Near Surface Mounted Applications, cut a groove into the concrete or masonry surface using an appropriate concrete saw or diamond blade. Surface must be clean and sound. It may be dry or damp, but free of standing water and frost. Remove dust, laitance, grease, curing compounds, impregnations, waxes, foreign particles, disintegrated materials and other bond inhibiting materials from the surface. In addition, brush and clean the groove with compressed air or a vacuum prior to installation of the structural adhesive.

Preparation Work

Concrete: When using Sikadur®-30, blast clean, shotblast or use other approved mechanical means to provide an open roughened texture.

Sika® CarboDur® Rods: wipe clean with appropriate cleaner (e.g. Acetone).

Cutting the CarboDur Rods

Rods may be cut to an appropriate length with a diamond blade on a chop saw or grinder. The rods should be wrapped with duct tape in the cutting zone to minimize splintering.

Mixing

Consult Sikadur®-30, Sikadur®-330, Sikadur®-32 Hi-Mod or Sika AnchorFix®-3001 Product Data Sheet for information on epoxy resin.

Application

Near Surface Mounted Application

Grooves should be cut into the surface of the substrate to receive the Sika® CarboDur® Rods. Care must be taken not to cut through existing reinforcing steel, steel tendons, embedded ducts, or other materials within the substrate. After preparing and cleaning the surface (see above), apply the mixed Sikadur®-30, Sikadur®-32 Hi-Mod or Sika AnchorFix®-2001/3001 into the grooves approximately half-full. Sikadur®-30 and Sikadur®-330, have a paste consistency and may be use for vertical and overhead applications. Sikadur®-32 Hi-Mod has a honey-type consistency and may be used for horizontal applications. Sika AnchorFix®-2001/3001 is packaged in cartridges and can be injected directly into the grooves for horizontal, vertical, or overhead applications. Within the open time of the epoxy, depending on the temperature, press the Sika® CarboDur® Rods into the epoxy in the grooves. Apply additional epoxy over the rods to fill in the grooves. Strike the surface with a trowel to force out any air and provide a clean installation.

Limitations

Design calculations must be made and certified by an independent licensed professional engineer.

Health and Safety Information

For information and advice on the safe handling, storage and disposal of chemical products, users should refer to the most recent SAFETY DATA SHEET containing physical, ecological, toxicological and other safety-related data.

KEEP OUT OF REACH OF CHILDREN
FOR INDUSTRIAL USE ONLY

SIKA CANADA INC.

Head Office
601, avenue Delmar
Pointe-Claire, Quebec
H9R 4A9

Other locations
Toronto
Edmonton
Vancouver

1-800-933-SIKA
www.sika.ca

Certified ISO 9001 (CERT-0102780)
Certified ISO 14001 (CERT-0102791)

Plate B6: Continuo

Appendix C

The Tests of Fresh and hardened concrete

C-1 Tests of Fresh NSC

C-1-1 Slump Test

The slump test of conventional concrete was performed by (ASTM C143/C143M, 2015). The equipment for the slump test was a truncated cone and a tamping rod. The truncated cone has 30 cm in height, 20 cm in diameter at the bottom and 10 cm in diameter at the top. It is filled with concrete in three equal layers, with each layer being stroked 25 times uniformly by a steel rod and then slowly lifted. The difference in height from the average concrete level after the concrete is slumped down by its weight to the top of the mould is called the slump. Plate C-1 shows the slump values ranging from (20-100) mm, as designed.

Plate C-1: Slump test for fresh concrete.

C-2 Tests of Hardened NSC

C-2-1 Compressive strength test

For the hardened concrete, the compressive strength test was carried out according to (BS 1881: Part 116-1989) and (ASTM C39, 2016). A total of 6 cubes of (150) mm and 3 cylinder specimens, (150×300) mm, were tested using a hydraulic compression machine of 2000 kN maximum capacity. The load was applied continuously and gradually increased at a constant rate of 18 MPa per minute until failure occurred. That is available in the Structural Laboratory in the Civil Engineering Department, University of Babylon. Plate C-2 shows the compressive strength test.

The compressive strength value was evaluated from the maximum load obtained during the test divided by the cross-sectional area of the specimen (P/A).

Plate C-2:The compressive strength test for cube and cylinder.

C-2-2 Splitting tensile strength test

The splitting test was carried out according to (ASTM C496, 2011). A total number of 6 cylinders with (150×300) mm were tested. Two bearing strips of 3.0 mm thick of plywood and 300 mm in length were placed upper and lower the specimen to provide the concentrated stress and the applied uniform load on the test surface of the cylinder as shown in Plate C-3. The capacity of the testing machine 2000 kN and the load was applied continuously and without shock until the cylinder failed. The equation calculated the expression of the splitting tensile strength:

$$f_{st} = \frac{2P}{\pi LD} \qquad \text{..... (C-1)}$$

where f_{st} is splitting tensile strength in N/mm^2, P is the applied compressive load in N, D is the diameter of cylinder in mm and L is the length of cylinder in mm.

Plate C-3:The splitting tensile strength test .

C-2-3 Flexural strength test (Modulus of Rupture)

Concrete prisms of dimensions (100×100×400) mm were cast according to (ASTM C 78,2010) procedure. A total of 6 prisms were tested using a universal hydraulic machine of 2000 kN maximum capacity. The load was applied continuously and gradually increased at a constant rate until failure occurred. That was available in the Structural Laboratory in the Civil Engineering Department, University of Babylon.

Flexural strength expressed as the modulus of rupture (M.O.R) was calculated using the results obtained from a simple beam using a two-point load as shown in Plate C-4.

The Flexural strength of specimens was calculated to the nearest 0.01 MPa, using the following formula:

1- If a fracture occurs in the tension surface inside the middle one-third of the length of span, then calculate flexural strength as follows:

$$f_r = \frac{M_{max} Y_{max}}{I} = \frac{\frac{PL}{6} \cdot \frac{h}{2}}{\frac{bh^3}{12}} = \frac{PL}{bh^2} \qquad \text{..... (C-2)}$$

Where: fr is the modulus of rupture, *P* is the maximum applied in N, *l* is the length of span from center to center in mm, *h* is the average specimen depth in mm and *b* is the average specimen width in mm.

2- If fracture takes place outside the middle one-third by not more than 5% of the span length, then flexural strength is calculated as follows:

$$f_r = \frac{M_{max} Y_{max}}{I} = \frac{\frac{Pa}{2} \cdot \frac{h}{2}}{\frac{bh^3}{12}} = \frac{3Pa}{bh^2} \qquad \text{..... (C-3)}$$

Where a is the average distance measured on the tension surface of the prism between the failure crack and the nearest support.

3- If fracture takes place outside middle one-third by more than 5% of the span length, then the result is neglected.

Plate C-4:The flexural strength test (Modulus of Rupture).

C-3 Tests of Fresh UHPC

C-3-1 Flow Test

The workability of UHPC mixtures measured using the mortar flow table test according to (ASTM C1437, 2013) (ASTM C230, 2010), the flow table device and workability test is shown in Plate C-5. The procedure of the test is summarized as follows:

1) The mold is filled with concrete in 25 mm layers, each layer rodded with 20 strokes with a tamping rod uniformly over the cross-section of the mold, Plate C-5a shows the UHPC sample before the removal of the brass cone.

2) The mold is then removed from the concrete by a steady upward pull.

3) The table is then immediately dropped 25 times in 15 seconds.

4) The diameter of the spreading concrete is then measured, which is the average of four symmetrically distributed measurements read to the nearest 5 mm, as shown in Plate C-5b.

The flow table results revealed that the spreading concrete's diameter between 200 and 250 mm is adequate in providing the required flow characteristics for UHPC (ASTM C1856, 2017).

Plate C-5: Process of the flow table test.

C-4 Tests of Hardened UHPC

C-4-1 Compressive strength test of UHPC

For the hardened concrete, the compressive strength of UHPC was carried out by 6 specimens of cube 50mm in the length of the side. The result of the cube is equal to or very close to the result of the cylinder mentioned in ASTM standard (ASTM C1856 ,2017); these facts are provided by (Yuliarti, Ekkehard, and Ismail., 2015),(Graybeal and Davis, 2008),(Aziz and Ahmed, 2012).

Plate C-6:The compressive strength testof UHPC for cube and cylinder.

C-2-2 Splitting tensile strength test of UHPC

The splitting test was carried out according to (ASTM C496, 2011). A total number of 6 cylinders with (100×200) mm were tested. Two bearing strips of 3.0 mm thick of plywood and 200 mm in length were placed upper and lower the specimen to provide the concentrated stress and the applied uniform load on the test surface of the cylinder as shown in Plate C-7, The capacity of testing machine 2000 kN and the load was applied continuously and without shock until failure of the cylinder occurred. The equation calculated the expression of the splitting tensile strength:

$$f_{st} = \frac{2P}{\pi LD} \qquad \text{..... (C-3)}$$

where f_{st} is splitting tensile strength in N/mm^2, P is the applied compressive load in N, D is the diameter of cylinder in mm and L is the length of cylinder in mm.

Plate C-7:The splitting tensile strength test of UHPC.

C-2-3 Flexural strength test (Modulus of Rupture) of UHPC

Concrete prisms of dimensions (50×50×200 mm) mm were cast according to (ASTM C 78,2010) (ASTM C1609, 2012) procedure. A total of 6 prisms were tested using a universal hydraulic machine of 2000 kN maximum capacity. The load was applied continuously and gradually increased at a constant rate until failure occurred. That was available in the Structural Laboratory in the Civil Engineering Department, University of Babylon.

Flexural strength expressed as the modulus of rupture (M.O.R) was calculated using the results obtained from a simple beam using one-point load as shown in Plate C-8.

The Flexural strength of specimens was calculated to the nearest 0.01 MPa, using the following formula:

$$f_r = \frac{M_{max} Y_{max}}{I} = \frac{\frac{PL}{4}\cdot\frac{h}{2}}{\frac{bh^3}{12}} = \frac{3PL}{2bh^2} \qquad \text{.....(C-4)}$$

Where: fr is the modulus of rupture, *P* is the maximum applied in N, *l* is the length of the span from center to center in mm, *h* is the average specimen depth in mm and *b* is the average specimen width in mm.

Plate C-8:The flexural strength test (Modulus of Rupture) of UHPC.

References

ASTM C143/C143M. (2015). Standard Test Method for Slump of Hydraulic-Cement Concrete. *Astm C143*, *1*, 1–4. https://doi.org/10.1520/C0143

ASTM C1437. (2013). *C1437-13 Standard Test Method for Flow of Hydraulic Cement Mortar.pdf* (pp. 1–2).

ASTM C1609. (2012). Standard Test Method for Flexural Performance of Fiber-Reinforced Concrete. *ASTM Standard Book*, *i*(C 1609/C 1609M-05), 1–8. https://doi.org/10.1520/C1609

ASTM C1856. (2017). Standard Practice for Fabricating and Testing Specimens of Ultra-High Performance Concrete. *ASTM International*, *i*, 4. https://doi.org/10.1520/C1856

ASTM C230. (2010). Standard Specification for Flow Table for Use in Tests of Hydraulic Cement 1. *Annual Book of ASTM Standards*, 4–9. https://doi.org/10.1520/C0230

ASTM C39. (2016). Standard Test Method for Compressive Strength of Cylindrical Concrete Specimens. *American Society for Testing and Materials*, 1–7. https://doi.org/10.1520/C0039

ASTM International. (2011). Standard Test Method for Splitting Tensile Strength of Cylindrical Concrete Specimens ASTM C-496. *Astm C496/C496M*, *i*, 1–5. https://doi.org/10.1520/C0496

Aziz, O. Q., & Ahmed, G. H. (2012). Mechanical properties of Ultra High Performance Concrete (UHPC). *American Concrete Institute, ACI Special Publication*, *289 SP*, 331–346. https://doi.org/10.14359/51684273

BS 1881-116: 1983 Reprinted, incorporating Amendments No. 1 and No. 2 Testing concrete — Part 116: Method for determination of compressive strength of concrete cubes

Graybeal, B., & Davis, M. (2008). Cylinder or cube: Strength testing of 80 to 200 MPa (11.6 to 29 ksi) ultra-high-performance fiber-reinforced concrete. *ACI Materials Journal*, *105*(6), 603–609. https://doi.org/10.14359/20202

Yuliarti, K., Ekkehard, F., & Ismail., M. (2015). UHPC compressive strength test specimens: Cylinder or cube? *Procedia Engineering*, *125*, 1076 – 1080.

Appendix D

The Simulation Prosses of FEM For Abaqus Program

D-1 Modelling

The steps of modelling the specimens were illustrated in this section to understand the simulation process.

D-1-1 Materials properties and real constant

A- Modelling of elastic behavior

The elastic behavior of material represented in Abaqus by modulus of elasticity and Poisson's ratio.

A-1 Modulus of elasticity

For NSC used the Equation [$E = 4700\sqrt{\acute{f}c}$] (ACI-318, 2019)

For UHPC used the Equation [$E = 3840\sqrt{\acute{f}c}$] (Graybeal 2007)

For Steel reinforcement used [E= 200 Gpa].

A-2 Poisson's ratio

The commonly accepted value of Poisson's ratio (ν) for NSC is ranged from 0.15 to 0.25, while it is widely taken as 0.2 for analysis (Marzoq 2020).

In UHPC the Poisson's ratio ranged from 0.17 to 0.2 (Graybeal 2006), the widely use of (ν) for UHPC is 0.2 (Marzoq 2020).

For steel reinforcement (ν) taken as 0.3 (Shamass et al. 2017)

B- Modelling of Plastic behavior

ABAQUS provides three various constitutive models to analyze the concrete: the brittle cracking model, the smeared crack concrete model and the model

of concrete damaged plasticity (CDP). Each of them is proposed to supply a wide-ranging ability to model reinforced and plain concrete (besides semi-brittle materials) in several kinds of structures such as trusses, shells, beams, and solids (SIMULIA, 2014).

The CDP was adopted for this purpose. Where this model was suggested by (Lubliner et al., 1989) for monotonic loading. Concrete damaged plasticity can model all kinds of structure of plain or reinforced concrete or semi-brittle materials submitted to monotonic, dynamic or cyclic loads. In the CDP model, both compressive crushing and tensile cracking of concrete are presumed key failure mechanisms. Moreover, in this model, material degradation was considered for both compression and tension behavior.

B-1 Plasticity parameters

To model the plastic behavior of concrete in ABAQUS, the CDP utilizing several parameters as listed in Table D-1.

Table D-1: The Plastic parameters of concrete

Parameters	Standard value	Adopted value for NSC	Adopted value for UHPC
dilation angle*	15 - 56	35	40
eccentricity	0.1	0.1	0.1
fb0/fc0	1.16	1.16	1.16
Kc	0.5-1	0.667	0.667
Viscosity*	0 - 10^-20	0.00001	0.00001

*Calibrated value.

B-2 Compressive behavior

For NSC the model of (Wang and Hsu 2001) used to tracing the Stress-strain curve for compression of NSC as mentioned in chapter Four. The adopted values of compressive behavior in Abaqus as listed in Table D-2.

Table D-2: Compressive behavior of NSC

Yield Stress (MPa)	Inelastic Strain
21.22	0
24.06	0.0007
26.69	0.0008
29.12	0.0010
31.35	0.0011
33.38	0.0012
35.21	0.0013
36.84	0.0014
38.27	0.0015
39.50	0.0016
40.52	0.0017
41.35	0.0018
41.97	0.0020
42.39	0.0021
42.61	0.0022
42.63	0.0023
42.45	0.0024
42.07	0.0025
41.49	0.0026
40.71	0.0027
39.72	0.0028
38.54	0.0030
37.15	0.0031
35.56	0.0032
33.77	0.0033
31.78	0.0034

For UHPC the model of (Graybeal and Russel, 2013) used to estimate the Stress-strain curve for compression of UHPC as mentioned in chapter Four. The adopted values of compressive behavior in Abaqus were listed in Table D-3 .

Table D-3: Compressive behavior of UHPC

Yield Stress (MPa)	Inelastic strain
92.51	0.002
133.72	0.003
150.13	0.004
76.95	0.005
28.33	0.006

B-3 Tension behavior

Three ways are possible in ABAQUS for describing the curve of post cracking tension softening: crack opening (displacement), strain, and fracture energy as shown in Figure D-1.

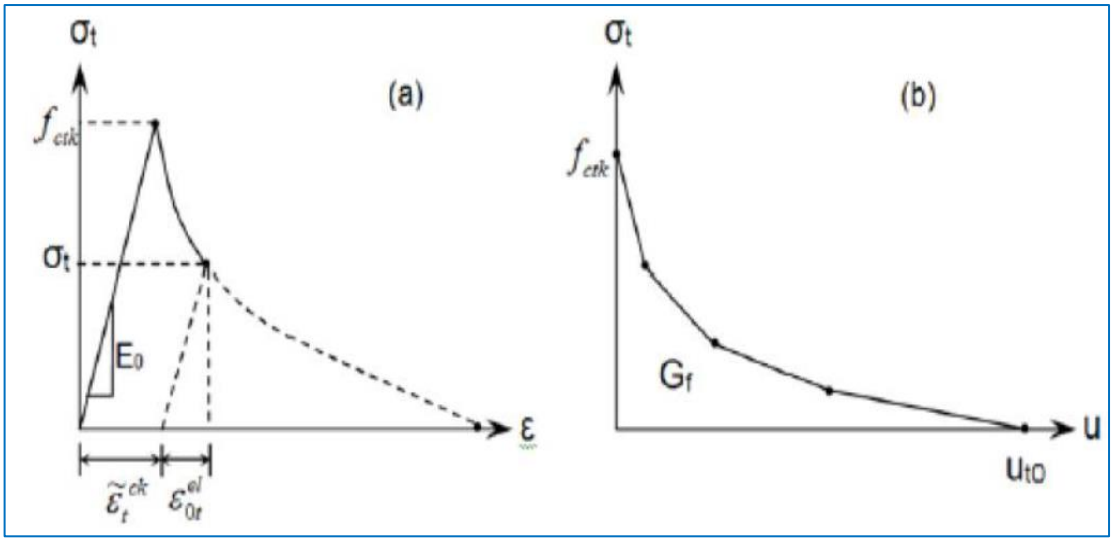

Figure D-1: Post-failure at tension: (a) Stress-strain curve, (b) Fracture curve.

In this study used the stress strain curve to represented the tensile behavior of NSC and UHPC. for NSC the tensile behavior taken as mentioned in chapter Four from the recommended formulas. Also, the UHPC as mentioned also in chapter four from the formula of (Graybeal and Russel, 2013) and adopted by (Shafieifar et al., 2017) and (Kadhim et al., 2021). ABAQUS was needed to calculate the cracking strain corresponding to tensile stress. Table D-4 and

Table D-5 show the adopted values for tension in ABAQUS for NSC and UHPC respectively.

$\epsilon_{cr} = \epsilon_t - (\frac{\sigma_t}{E_c})$..... (D-1) (Wang and Hsu, 2001)

B-4 Damage parameter

To model the initiation and propagation of a crack in the concrete, the tension damage parameter (dt) is utilized. This variable represents the damage on elastic stiffness of concrete. The tension and compression damage were determined as follow:

$d = 1 - (\frac{\sigma}{f})$..... (D-2)

Where σ is the stress of concrete at the phase of analysis where the damage parameter is to be determined and f is the yeild stress of concrete.

Table D-4: The tensile behavior of NSC

Stress	Cracking strain	Damage parameter
0	0	0
1.60	9.19E-05	0.21
1.43	0.00015	0.29
1.03	0.0004	0.49
0.98	0.00045	0.51
0.86	0.00064	0.57
0.78	0.00079	0.60
0.75	0.00094	0.63
0.73	0.00098	0.64
0.69	0.00112	0.71
0.68	0.00117	0.77

Table D-5: The tensile behavior of UHPC

Stress	Cracking strain	Damage parameter
0	0	0
6.758513	0.003357	0.59
2.027554	0.049857	0.81

B-5 Plastic properties of steel

Various stress-strain models have been utilized for steel material by various investigators, involving elastic-perfectly plastic model (Aire et al., 2005);(Hu et al., 2003);(Al-Mamory and Al-Ahmed, 2022);(Kadhim et al., 2021) and elastic-plastic model with linear hardening (Xiong and Zha, 2007) and multilinear hardening (Han et al., 2007). The Elastic-perfect plastic is utilized for modeling reinforcing steel bars materials, as can be seen in Figure D-2 and only elastic for the steel of the bearing and loading plate. The values of the stress-strain were obtained from the tensile test of steel were listed in Table D-6 to D-8.

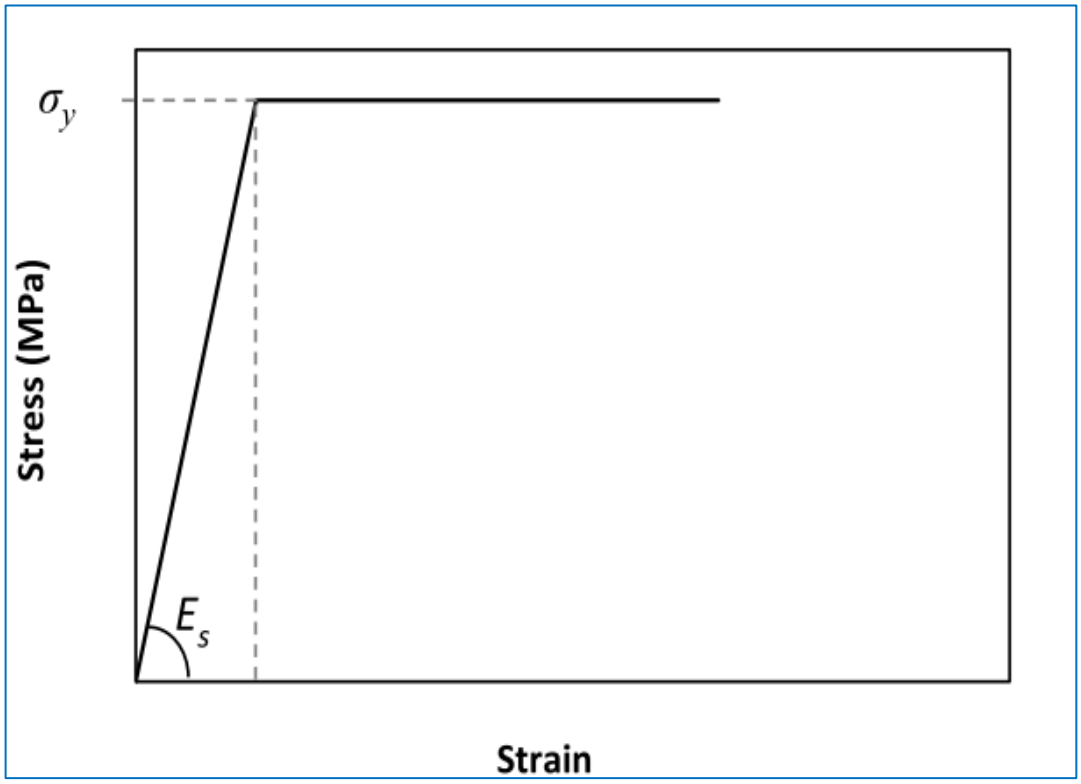

Figure D-2: Stress-strain curve of steel reinforcement (Kadhim et al., 2021).

Table D-6: Stress- Plastic strain for steel Ø10 mm

True stress	Plastic strain
585	0
668	0.050391

Table D-7: Stress- Plastic strain for steel Ø8 mm

True stress	Plastic strain
375	0
572	0.0702048

Table D-8: Stress- Plastic strain for steel Ø6 mm

True stress	Plastic strain
317	0
541	0.035277

References

ACI, 318-19. 2019. "318M-19: Building Code Requirements for Concrete and Commentary." 628.

Aire, C., R. Gettu, and J. R. Casas. 2005. "Axially Loaded Concrete-Filled Steel Tubes." *Structural Concrete and Time - Proceedings of the Fib Symposium* 2(October):777–84. doi: 10.1061/(asce)0733-9445(1998)124:10(1125).

Al-Mamory, Zainab Kareem, and Ali Hussein Ali Al-Ahmed. 2022. "Behavior of Steel Fiber Reinforced Concrete Beams with CFRP Wrapped Lap Splice Bars." *Structures* 44(June):1995–2011. doi: 10.1016/j.istruc.2022.08.096.

Graybeal, Benjamin A. 2006. "Structural Behavior of Ultra-High Performance Concrete Prestressed I-Girders." *Federal Highway Administration* (August):106.

Graybeal, Benjamin A. 2007. "Compressive Behavior of Ultra-High-Performance Fiber-Reinforced Concrete." *ACI Materials Journal* 146(104).

Graybeal, Benjamin A., and Henry G. Russel. 2013. "Ultra-High Performance Concrete: A State-of-the-Art Report for the Bridge Community. Publication N.º FHWA-HRT-13-060." (June):176.

Han, Lin Hai, Guo Huang Yao, and Zhong Tao. 2007. "Performance of Concrete-Filled Thin-Walled Steel Tubes under Pure Torsion." *Thin-Walled Structures* 45(1):24–36. doi: 10.1016/j.tws.2007.01.008.

Hu, Hsuan-Teh, Chiung-Shiann Huang, Ming-Hsien Wu, and Yih-Min Wu. 2003. "Nonlinear Analysis of Axially Loaded Concrete-Filled Tube Columns with Confinement Effect." *Journal of Structural Engineering* 129(10):1322–29. doi: 10.1061/(asce)0733-9445(2003)129:10(1322).

Kadhim, Majid M. A., Akram Jawdhari, and Abheetha Peiris. 2021. "Development of Hybrid UHPC-NC Beams: A Numerical Study." *Engineering Structures* 233(November 2020):111893. doi: 10.1016/j.engstruct.2021.111893.

Kadhim, Majid M. A., Abdul Ridah Saleh, Lee S. Cunningham, and Ali A. Semendary. 2021. "Numerical Investigation of Non-Shear-Reinforced UHPC Hybrid Flat Slabs Subject to Punching Shear." *Engineering Structures* 241(May). doi: 10.1016/j.engstruct.2021.112444.

Lubliner et .al. 1989. "A Plastic-Damage Model For Concrete." *Int.J.Solids Structures* 25(3):299–326.

Marzoq, Zahraa Hadi. 2020. "Combined Bending and Torsional Moments Effect on Hybrid Reactive Powder Concrete T-Beams." M.Sc. thesis , University of Al- Qadisiyah.

Shafieifar, Mohamadreza, Mahsa Farzad, and Atorod Azizinamini. 2017. "Experimental and Numerical Study on Mechanical Properties of Ultra High Performance Concrete (UHPC)." *Construction and Building Materials* 156:402–11. doi: 10.1016/j.conbuildmat.2017.08.170.

Shamass, Rabee, Xiangming Zhou, and Zongyi Wu. 2017. "Numerical Analysis of Shear-Off Failure of Keyed Epoxied Joints in Precast Concrete Segmental Bridges." *Journal of Bridge Engineering* 22(1):04016108. doi: 10.1061/(asce)be.1943-5592.0000971.

SIMULIA. 2014. "Abaqus Theory Manual." *Abaqus 6.13 Documentation* (Dassault Systemes Simulia Corp., Providence, RI, USA.).

Wang, Taijun, and Thomas T. C. Hsu. 2001. "Nonlinear Finite Element Analysis of Concrete Structures Using New Constitutive Models." *Computers and Structures* 79(32):2781–91.

Xiong, De Xin, and Xiao Xiong Zha. 2007. "A Numerical Investigation on the Behaviour of Concrete-Filled Steel Tubular Columns under Initial Stresses." *Journal of Constructional Steel Research* 63(5):599–611. doi: 10.1016/j.jcsr.2006.07.002.

Zhang, Qifeng, Yan Feng, Zhao Cheng, Yang Jiao, and Hang Cheng. 2022. "Large-Scale Testing and Numerical Study on an Innovative Dovetail UHPC Joint Subjected to Negative Moment Large - Scale Testing and Numerical Study on an Innovative Dovetail UHPC Joint Subjected to Negative Moment." (September). doi: 10.12989/cac.2022.30.3.175.

Chapter one

Introduction

1-1 Introduction

The splicing technique referred to connect more than one beam segment to each other by using some methods in order to made the beam to work as one unit (the same behavior of monolithic member).

The overall performance of a spliced girder is greatly governed by the performance of the cast in place (CIP) joints. The reinforced concrete (RC) spliced joints are primarily subjected to shear and bending moment. Thus, these joints should be designed to behave as structural joints in order to resist various load combinations and transfer forces between the spliced girder's components (Al-Tameemi, 2015).

The approach of constructing bridges in segments, as demonstrated in (Plate 1-1), is known as segmental construction. The segments can be created through either cast-in situ or precast methods, based on the circumstances. Segmental construction has been acknowledged as a solution to several bridge issues due to its high durability, minimal life cycle costs, and ease of quality control. It is a viable option for long spans and in regions where environmental disturbances need to be kept to a minimum. (Saibabu et al., 2013).

The splicing is not only for design of girder, whereas, it may be used for rehabilitation the damaged girder as shown in (Plate 1-2). This damaged member supported with temporary supports and makes joint has adequate splice length and CIP the joint with new concrete. Therefore, the study of splice girders must have the impact of flexure and shear simultaneously or individually. Such decks tend to suffer from issues such as corrosion, delamination, and cracking.

To extend the lifespan of bridges, it is essential to employ concrete materials with greater resistance to these conditions and superior durability (Verger-Leboeuf et al., 2017).

Plate 1-1: Splice segments of girder in a bridge(Aoun, 2018).

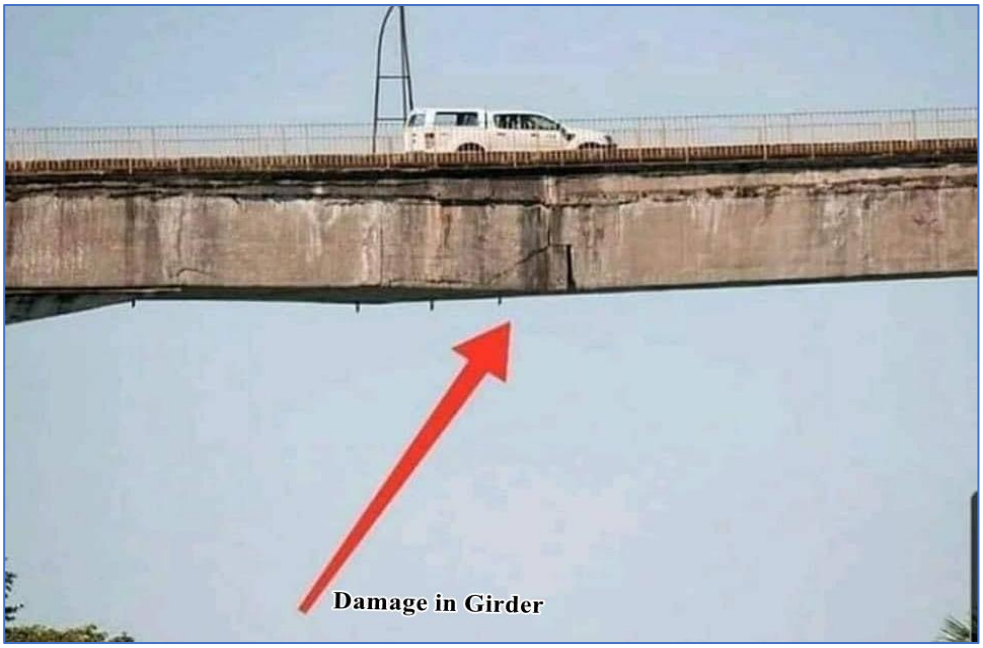

Plate 1-2: Girder damage in an old bridge .

1-2 Shear Key

Spliced girders depict regions of discontinuity through which compression and shear stresses are transferred. Joints between precast portions may have lower flexural stiffness and shear potency than adjacent solid parts. Shear keys offer superior sliding resistance and are therefore considered more effective. The keys serve three primary purposes at these joints. Firstly, they align the segments during erection. Secondly, they transfer shear forces between segments during service. Lastly, they protect the prestressing tendons from corrosion where they pass through joints, thus ensuring durability (Ahmed and Aziz, 2019). Despite the fact that the keys are more susceptible to harm during construction, the use of several keys is anticipated to guarantee more uniform distribution of stresses and offer better mechanical interlocking (Buyukozturk et al., 1991).

The majority of shear key connections are designed using standard details that are specific to a certain region. These details are of uncertain origin and do not provide information on the amount of forces that are transferred through the shear key or the capacity of a given detail to resist these loads (Russell, 2011).

The deterioration of shear key connections can be attributed to various factors, including shrinkage during grouting material curing, transfer of live load through the shear key to or from adjacent beams, thermal effects, misalignment, and deficient construction practices.(Jiqiu et al., 2018).

The shape and location of keys depends on the critical stresses that were expected in failure of specimens. The multiple shear key system gives more uniform distributed stress along the joints. Plate 1-3 shows the multiple shear keys in flange and web.

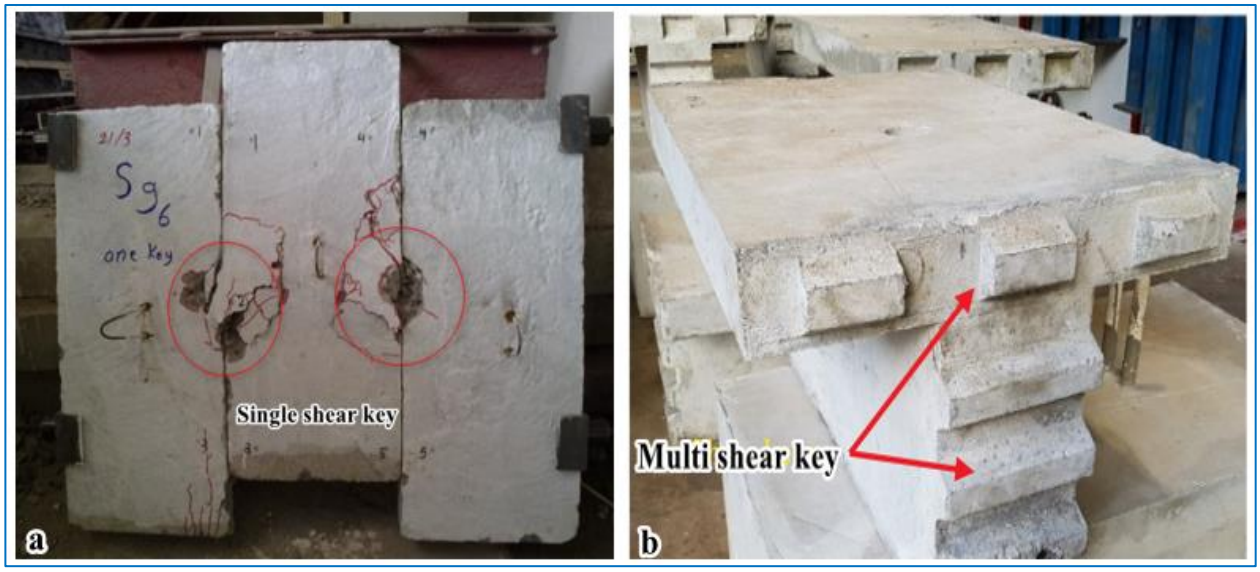

Plate 1-3 : a: Single shear key (Al-Shaarbaf and Aziz , 2012), *b: Multiple shear key in flange and web*, (Le et al., 2018).

1-3 Ultra-High-Performance Concrete (UHPC)

Ultra-high-performance concrete is a type of cementitious material that contains a high proportion of cement, along with very fine sand, micro silica fume, water, steel fiber (2- 2.5) %, and superplasticizer. UHPC has achieved to be a successful of material that capable of improving variety properties of structural members (Graybeal et al., 2020). UHPC exhibits mechanical properties that surpass those of NSC. Although there is no precise definition for UHPC in research, it is generally agreed that UHPC should possess the following characteristics: (a compressive strength greater than 120 MPa, a disconnected pore structure that significantly reduces permeability and thus enhances durability, low creep, and sufficient fiber reinforcement to allow for sustained post cracking tensile resistance more than 5 MPa (Graybeal et al., 2020);(Haber and Graybeal, 2018);(Hasgul et al., 2018);(Graybeal and Haber, 2018a);and (ASTM C1856, 2017).

By adding steel fibers to UHPC by ratio more than 0.75%in volume fraction and its homogenized microstructure, it has many demonstrated advantages such as outstanding mechanical properties, ductility, and durability((Dugat et al., 1996),(Hasgul et al., 2018),(Hung et al., 2021)**).**

The improvement in the microstructure of this special concrete, through the exact gradient of all the particles in the concrete mix, gives the maximum density. Additionally, due to this concrete high mechanical properties, the member's section size and the number of stirrups can be reduced (Zheng et al., 2018).
The structure causes premature failure for the insufficient bond resistance results. So it is very useful to accurately predict the relative slip between the rebar and concrete in the design and analysis work (Sun et al., 2016)**.**

The most blameworthy for UHPC is the high cost of production, which makes it used almost to rehabilitations, strengthening, and very special cases of members. So, many research studies provided that the bond of UHPC to other types of concrete or steel rebar is significantly stronger compared with NSC (Haber and Graybeal 2018).
This study utilized UHPC to provide high compressive strength, a good bond with reinforcement bar and old concrete (precast segments), and the presence of steel fibers to increase shear strength in the joint region.

Many applications of UHPC in structural members to achieve special requirement in view of ultimate strength, environment condition, and service requirement. UHPC has been utilized in various bridge applications as in Table 1-1 and shown in Figure 1-1 (Xue et al., 2020):

Table 1-1 : Some of applications for UHPC in bridge.

Name	Country	Year	Structure type	Application location	Achievement of using UHPC
Batu 6 Bridge	Malaysia	2016	Single span box girder bridge	Whole	To meet the international transportation requirements bridge
Shijiazhuang to Cixian Highway bridge	China	2015	Multi-span structure with three continuous box girders	Girder	To reduce the self-weight of the box girder and increase its ultimate strength.
Martinet Footbridge	Switzerland		Simply supported structure with U-shaped girder	Girder	keep crack-free condition under service stress and prevent damage from harmful fluid
Mars Hill Bridge	USA	2002	Prestressed beam bridge	I-girder	For better durability and longer service life
Sakata-Mirar Footbridge	Japan	2006	Prestressed simply supported beam bridge	Box girder	To supply guidance of the UHPC structure design in Japan
Chillon viaducts	Switzerland	2015	Twin box-girder structure	Deck slab	To improve the fatigue performance of the slabs, the stiffness of the girder and the durability of the bridge
Sherbrooke Pedestrian Bridge	Canada	1997	Space truss girder bridge	Bridge deck	To reduce the self-weight of the bridge and improve corrosion resistance
Zhaoqing Mafang Bridge	China	2011	Simply supports steel composite beam bridge	Bridge deck	The first combined application of UHPC deck with steel box girder to achieve a lighter composite girder bridge
UHPFRC Arch Bridge on the campus of Fuzhou University	China	2015	Arch bridge	Arch ring	To meet the strength requirement of the arch ring subjected to an estimated compressive strength of over 100 MPa

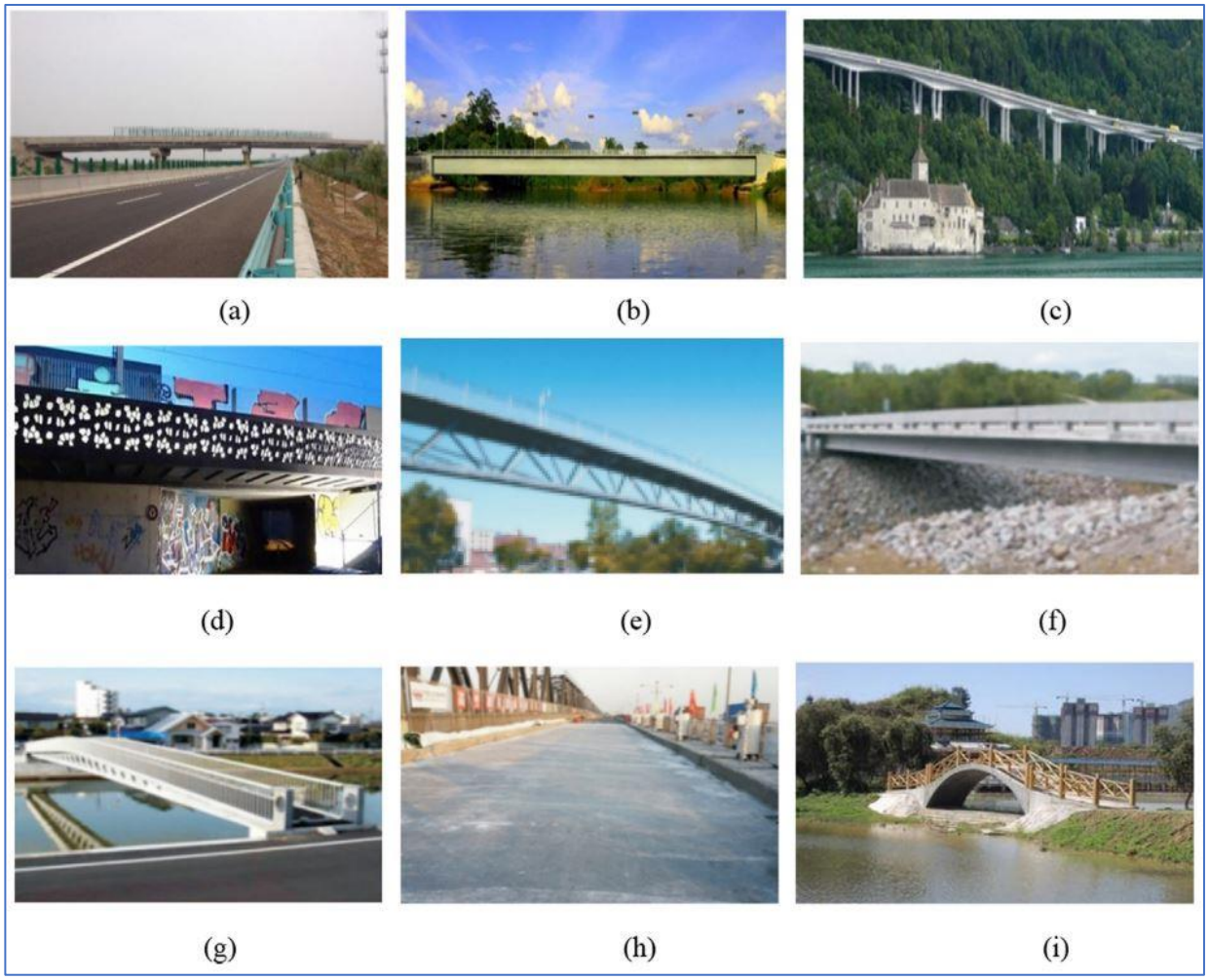

Figure 1-1: Typical applications of UHPC in bridge engineering: (a) Shijiazhuang to Cixian Highway bridge; (b) Batu 6 Bridge; (c) Chillon viaducts; (d) Martinet Footbridge; (e) Sherbrooke Pedestrian Bridge; (f) Mars Hill Bridge; (g) Sakata-Mirar Footbridge; (h) Zhaoqing Mafang Bridge; (i) UHPFRC Arch Bridge in Fuzhou University Campus.

1-4 Hybrid Reinforced Concrete

The hybrid section is an idea born to improve some of the weak properties in engineering materials. Hybrid reinforced concrete is spread extensively today (Marinela et al., 2009). The term "Hybrid reinforced concrete" is usually referred to as one of the following concepts:

1- Utilizing hybrid reinforcing bars: The first idea to improve the ductility of FRP-RC members and overcome the steel corrosion problem was to use hybrid rebars.
2- Using (FRP and steel) rebars: Another methodology was used to enhance FRP-RC members' ductility and structural performance by employing FRP and steel bars in the same section together as hybrid reinforcement.
3-Improving concrete properties: Expanding the hybrid concept to composite concrete members is made possible by advancements in concrete technology. These advancements have made it relatively simple to produce composite sections that exhibit high compressive strength, ductility, energy absorption, and tensile strength simultaneously. In this study, the second and third concepts are employed to improve the overall structural performance of the RC girder and the joint region.

1-5 Bond and Interaction Mechanism

The study focuses on two types of bonding strength: The bond strength between the steel and concrete, which is important in composite steel-concrete members, and the internal interaction between precast concrete and new concrete, which is essential to ensure that the precast and new concrete components act as a one unit.

1-5-1 Bond Mechanism of Steel bars and Concrete

Tension stresses may appear due to applied load on RC members. So, the reinforcement bars were placed to resist these stresses. A relative displacement (slip) happened between concrete and steel reinforcement due to the tensile force.

Bonding between reinforcement bar and concrete may be idealized as a shear force along the bar surface. Bonding is determined by its constituents (concrete and reinforcement) and their interaction (Wang, 2009). Figure 1-2 shows the bond mechanism of deformed steel bar and splitting force. Three primary mechanisms

determine bond behavior: chemical adhesion, mechanical interlock and friction resistance(ACI Committee 440.1R-15, 2015). The bond strength was highly dependent on the embedment length of reinforcement in concrete.

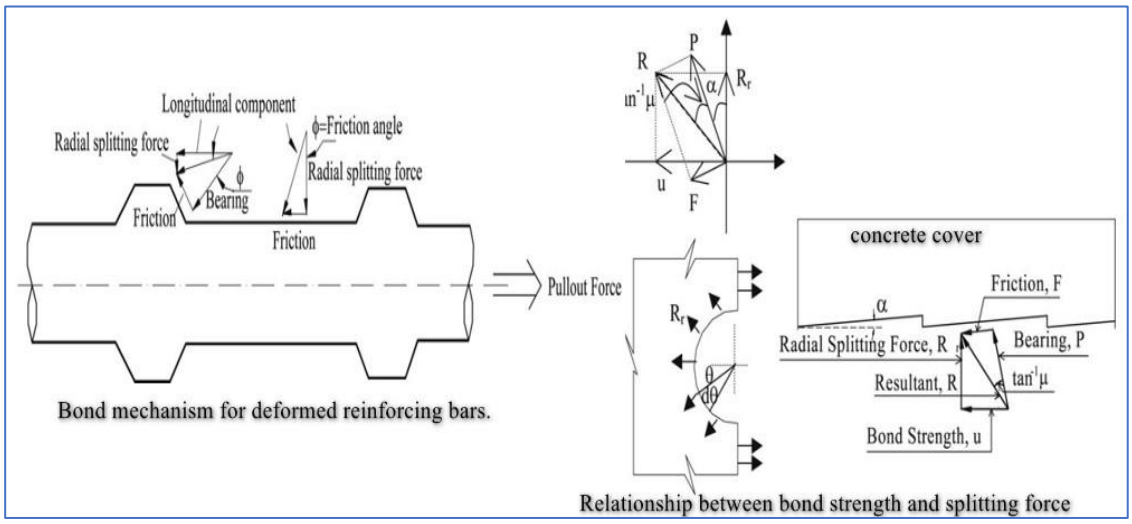

Figure 1-2: The bond of steel deformed bar and surrounding concrete (Wang 2009).

Due to the doubling of splitting pressures on the surrounding concrete, lap splices might generate a more severe mechanism of bond stress. The concrete between lapped bars is also vulnerable to significant stress concentration due to opposing signs of longitudinal bond stresses, which can cause bond degeneration and yielding at the lap splice ends. Transverse cracking at the extremities of the lap splice might exacerbate excessive local bond stress. This can grow more severe under cyclic loads due to the formation of two orthogonal fracture sets near to the bar's surface, in which concrete crumbles (Hassoon, 2021). Figure 1-3a and Figure 1-3b illustrate these mechanisms.

Generally, the length of reinforcing steel development in UHPC can be greatly decreased. The incorporation of detached the steel fiber reinforcement in UHPC enables the concrete to sustain its tensile resistance even after the cracking of the cementitious matrix. The development length of reinforcing steel bars may be

shortened as a result of this combination of matrix and fiber efficiency, which in turn provides the opportunity to redesign some structural systems. For example, this may allow for field-cast the connections between prefabricated bridge elements to be redesigned (Yuan and Graybeal, 2011),(Yuan and Graybeal, 2014), and (Haber and Graybeal 2018).

In this study, the interest was given to splice length in UHPC because the joint region would be cast with UHPC.

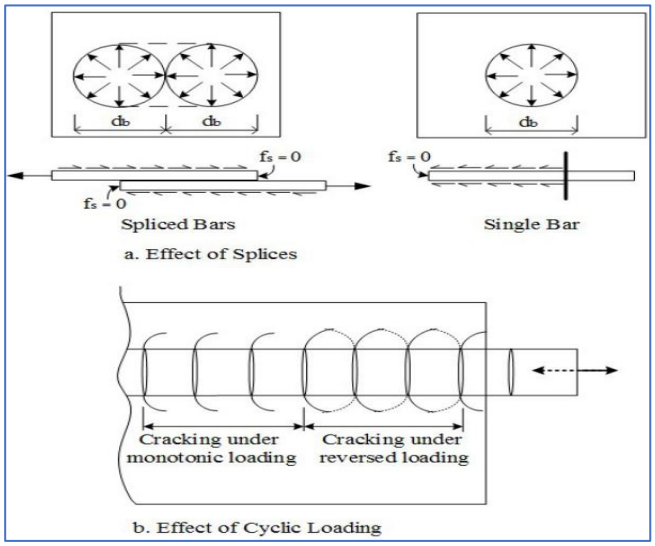

Figure 1-3: Concrete cracks around spliced reinforcing bars under cyclic and monotonic loading (Hassoon 2021)**.**

1-5-2 Interaction of precast concrete with new concrete

A poor bond between the precast and CIP concrete could result in cracks at the interface. Two critical factors that affect the bond strength at the interface area are the surface roughness and moisture present at the interface. (Graybeale et al., 2017) and (Casanova et al., 2019).

Various techniques can be used to improve the bond mechanism between precast old concrete and new cast concrete or grout. One effective approach is to increase the contact area or surface roughness, which can enhance the bond (Graybeal et

al., 2017). Different surface preparation methods can be utilized, such as wire brushing, jack hammering, pressure washing, sandblasting, or exposing the aggregate of the precast concrete. Studies have demonstrated that exposing the aggregate surface offers the most reliable method to achieve optimal bond strength. ((Graybeal and Haber, 2018b), (Tayeh et al., 2013),(Graybeal, 2014)). The exposed aggregate surface is created by applying paste-like retarders to the precast concrete formwork before casting and then washing it off after stripping. The hydration reaction of the fresh concrete contacting the retarder is delayed. This creates an open surface on the precast concrete component to which the new concrete can easily bond as shown in plate (Plate 1-4)(Graybeal, 2014)**.** (Figure 1-4) shows results from flexural beam bond-testing using different precast concrete surface preparations and different grout materials**.** This result provided the acceptance of the above recommendations.

The saturated surface dry (SSD) condition was used before placing new concrete next to the precast concrete because the bond strength was better (Casanova et al., 2019),(Graybeal et al., 2017).

Plate 1-4: Example of an exposed aggregate concrete surface(Graybeal , 2014).

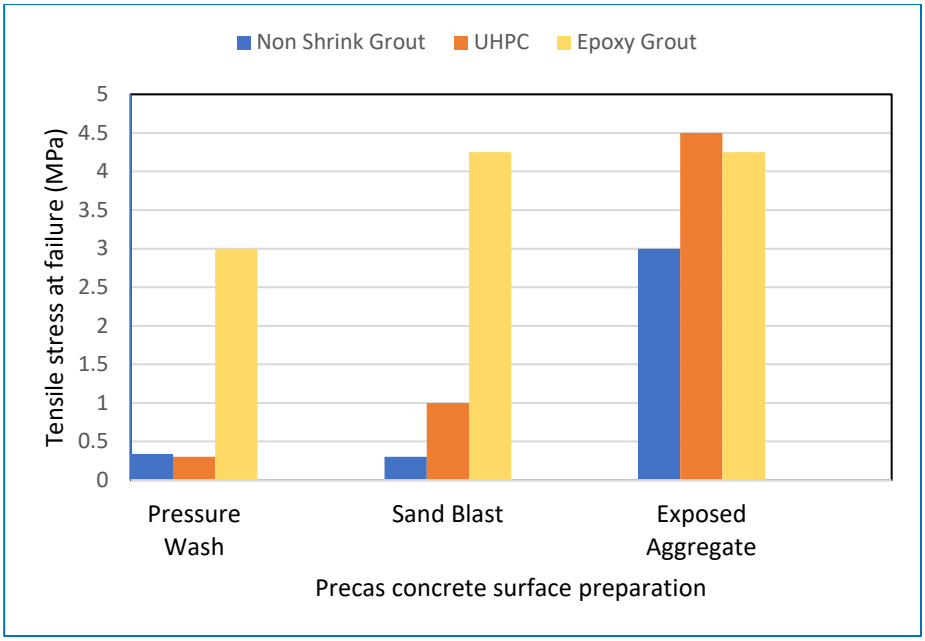

Figure 1-4: Average tensile strength from flexural beam bond tests (Graybeal et al., 2017).

1-6 Examples on Splice Girders

(Janssen and Spaans 1994) The Highland View Bridge is a 793 m long precast, the prestressed concrete bridge on U.S. 98 crossing the Gulf Intracoastal Waterway near Port Saint Joe in Gulf County, Florida (Plate 1-5).

Plate 1-5:View of Highland View Bridge(Janssen and Spaans 1994).

The total spans of the bridge are (11) spans, each one (27.1m) in length on two side with addition to three span that are located at the center have different dimensions, as shown in (Figure 1-5). The principal girder type is a continuous segmental post-tensioned precast concrete bulb-tee girder. Twenty-five precast, prestressed concrete bulb-tee girders are used in the structure.

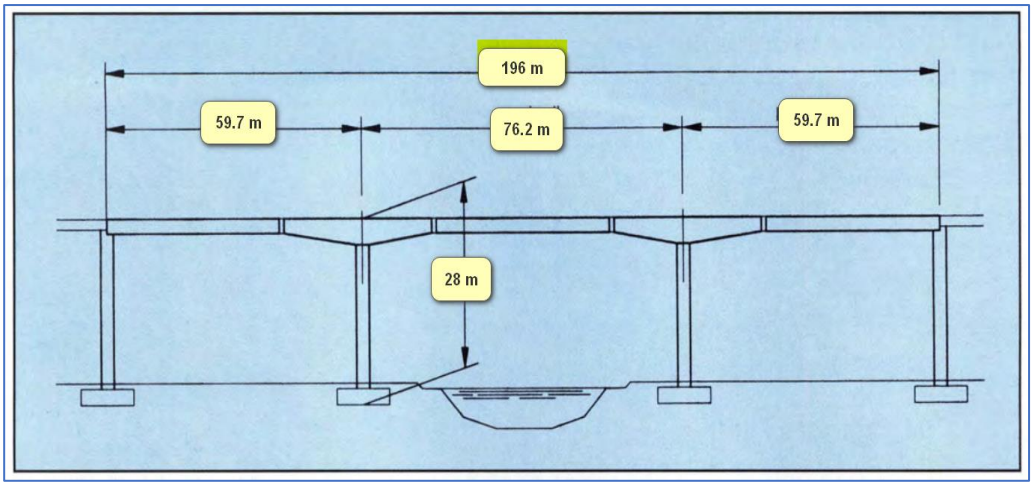

Figure 1-5: Simplified elevation of a three-span central section and the structure's total height (Janssen and Spaans 1994).

(Nicholls and Prussack 1997) The new Rock Cut Bridge (Plate 1-6) is a spliced, single-span 58.1 m precast, prestressed concrete structure. The bridge is situated in a ruggedly beautiful mountainous region just (10 km) south of the Canadian border over the Kettle River in Washington State. The problem with this bridge is that it must be having 61 m span. The key to solving the problem was to divide the "long" girder into three (19.2 m) pretension bulb-tee girder segments and transport them 240 km to a staging area near the bridge site. The segments were spliced and post-tensioned to give a total girder length of 58.1 m.

(Fowler and Stofko 2007) present some of the examples on splice girders bridge as illustrated in (Table 1-2) and shown in Figure 1-6.

Plate 1-6: View of the new Rock Cut Bridge(Nicholls and Prussack 1997).

Table 1-2: Examples of the splice girders bridge (Fowler and Stofko 2007).

Label of bridge	Details of spans	Construction way	Figure
Humber River Bridges, Toronto	3 spans - 40 m - 50 m - 40 m 2300 girders - 8/span @ 3.0 m c/c	the girders were continuously post-tensioned from abutment to abutment for structural efficiency.	1
Oldman River Bridge, Taber	5 spans - 3 main spans of 62 m and 2 end spans of 57.5 m Composite deck roadway is supported by 4 lines of 2800 NU girders spaced at 2500 mm c/c.	The center span girders were manufactured in two segments and post-tensioned together at the bridge site.	2
Perley Bridge, Hawksbury	10 Spans - total length 650 m - 8 main spans of 68.5 m, 2 end spans of 51 m Girders,	68.5 m long, consisting of a hunched segment and 3 straight segments were assembled and post-tensioned together behind one abutment. Stage post-tensioning connected the girders together before the deck was cast-in-place.	3

Label of bridge	Details of spans	Construction way	Figure
Bronte Creek Bridge, Mississauga	3 spans of 55 m/ 60 m/ 35 m 2300 girders- 7/ span @ 3.18 m c/c	The 55 and 60 m girders were assembled from 2 girder segments were stage 1 post-tensioned together behind one abutment. Continuous stage 2post-tensioning abutment/abutment was applied to each girder line.	4
Annacis Channel East Bridge, Richmond,	Total - 9 spans – 6 lanes - curved alignment 3 main spans - 60 m - 71 m - 60 m. Cantilever stub girders - 20 m long	The main span superstructure consists of two continuous spans on either side of a mid-channel simple span. Each 71.4 m continuous span is formed by erecting 10- 51.4 m girders from one pier and post-tensioning them to 10-20 m stub girders cantilevering 10 m on either side of the next pier.	5
Provencer Bridge, Winnipeg	girders ranging from 25 to 29 m for a total length of approximately 245 m.	These girders were supported on temporary supports during the construction. Drop in girders are 2250 mm deep. Girders were post-tensioned in stages as the construction progressed.	6

Figure 1-6: Pictures of different examples of splices in span girder bridges(Fowler and Stofko 2007).

1-7 Research Objectives

The main objectives of the present study are:

1. An experimental study of the overall behavior and failure modes of simply supported and continuous spliced hybrid reinforced concrete deck girders (UHPC for joint with deck and NSC for web).
2. Examining experimentally the efficiency of using UHPC concrete in joint region and flange and the effect of depth of joint, joint location, shear keys, and the internal hybridization of reinforcement for both simply supported and continuous spliced girders under static and cyclic load.
3. Carrying out a finite element model to simulate the behavior of the tested spliced girders utilizing a computer program (including the effect of interface element and bond-slip.
4. A parametric study is also carried out to explore the influence of several variables on the behavior and ultimate strength of spliced girders, such as the type of cyclic loading (reversed cyclic load), thickness of deck, type of interface, reinforcement ratio, type of support, the length of joint, spacing of stirrups, and number of the shear key.

1-8 Applications of the Study

Some of the applications of this research are:

1. Increase the efficiency of a bridge by transforming the simple span into a continuous span.
2. Reduce the cost and time of construction by assemblage more than one precast unit to make a large span of girders.
3. Repair the damaged beams or girder by removing the damaged region of concrete and replacing it with new better-reinforced concrete.
4. Replacement or strengthening of the structural members (Park et al., 2017).

1-9 Layout of Thesis

This thesis is structured as follows:

The first chapter is a simple introduction to the subject and some of the requirements and Knowlagent about shear key and UHPC. Furthermore, given a simple idea of this work's objective and originality point. **The second chapter** deals with some of the previous studies on splice girders. Some of the research and items from codes related to the present study are presented in this chapter. **The third chapter** present the laboratory and practical processes and procedures of this research and the internal material tests in it, the form and manufacture of the mold and the method and the examination device, as well as the dimensions of models and how to test the girder. **The fourth chapter** evaluate the results obtained from the tests in detail and the work of some comparisons of the results and tables that illustrate these results well. **In the fifth chapter**, a numerical analysis by finite element method of the models is carried out by a computer program **(ABAQUS)** in the **F.E.M.**, comparing results with those experimental results. Also, parametric studies are presented in this chapter.

A summary of the results and some recommendations for future research will be presented in **the sixth and final chapters**

Chapter Two

Literature Review

2-1 General Overview

This section will present a review of the previous research on spliced girders, which was considered one of the secrets of the companies implementing the bridges that were difficult to be published in scientific journals.

2-2 Bridge Constructions System

Many constructions system of bridges are illustrated in this section as follows (Tadros et al., 2003)**,**(Clark et al., 1995):

2-2-1 Full Span Segment

The precast pieces in this system span between the permanent supports (pier, abutment). This system is considered the easiest and most economical, but it is limited in shipping and handling. Four methods of creating continuity are studied to optimize this system.

2-2-1-1 Method A-Conventional Deck Reinforcement

Continuity is created by placing mild reinforcement in the deck over the piers. Consequently, method A has small negative moments and relatively high positive moments, leading to a relatively high pretension force which causes high prestress losses and bottom cracking at the piers. This method is the simplest and perhaps the least costly of existing methods.

2-2-1-2 Method B-Threaded Rod Splicing

In this method, I-girders are fabricated with 55034 MPa high strength threaded rods embedded in the top flange. The threaded rods are mechanically spliced in the field

at the diaphragms over the piers. The negative moment created by the deck slab weight, superimposed dead load and live load reduces the need for crack control bottom reinforcement over the piers. Accordingly, Method B can improve the span capacity of a given girder size by 10 to 15% over Method A.

2-2-1-3 Method C-Full Length Post-tensioning

This method is more expensive than the previous methods. It requires full-length ducts and usually necessitates widening the girder webs. It also requires end blocks to resist stress cogenerations at the anchorage zones. Continuity in this method is created through post-tensioning the full length of the bridge. This is an effective method, especially if spliced segmental I-beams are needed for spans longer than the shipping capabilities of single-piece spans. (Figure 2-1) explained the scheme of methods A, B, and C.

2-2-1-4 Method D-Stitched Splice

This type of splicing of the girder is not common. In this type of splice, the precast, pre-tensioned segments are post-tensioned across the splice, using short tendons or threaded bars. End blocks are required at the girders' spliced ends to house the post-tensioning hardware and provide the “end zone” reinforcement to resist concentrated concrete stresses due to post-tensioning forces.

Figure2-2 shows a comparison among the system capacities of methods A, B and C with a 3 m girder spacing.

2-2-2 Segmental Construction with Constant Cross Section

The post-tensioning tendon was used to splice the precast pieces of the bridge in this construction way, as shown in (Figure 2-3). Generally, for this system, the ultimate shear and the ultimate negative moment capacity are lower than the positive ultimate moment capacity and the tension service capacity, respectively.

Significant capacity in the positive region remains unused. Consequently, the system is inefficient for this reason. That is why the pier segment needs to be deepened to optimize the structure as in systems 3 or 4.

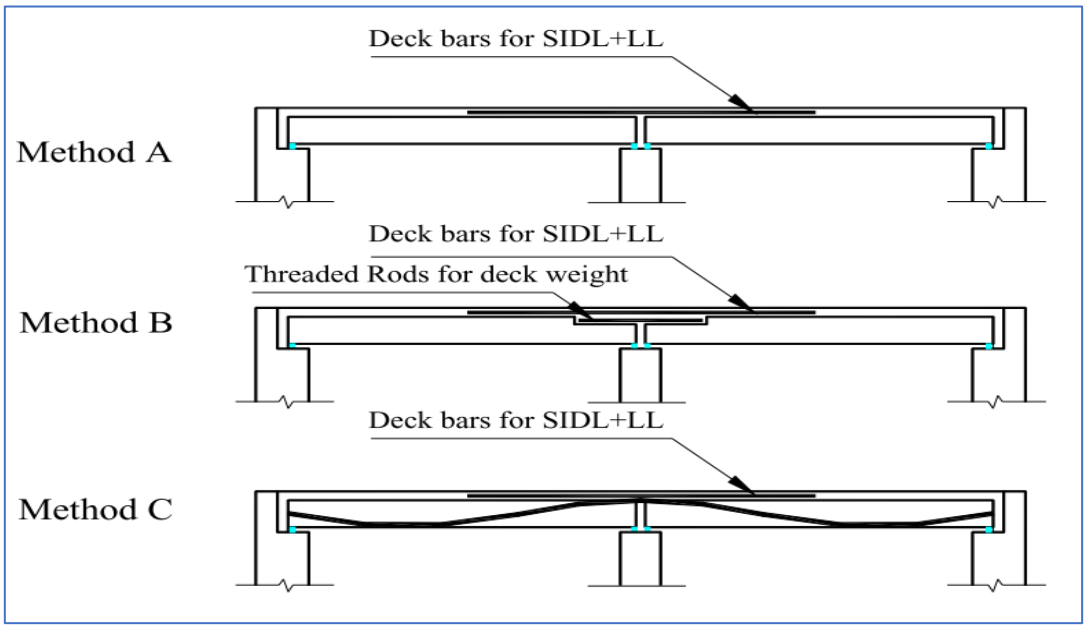

Figure 2-1: Method of full-span girders system (Tadros et al. 2003).

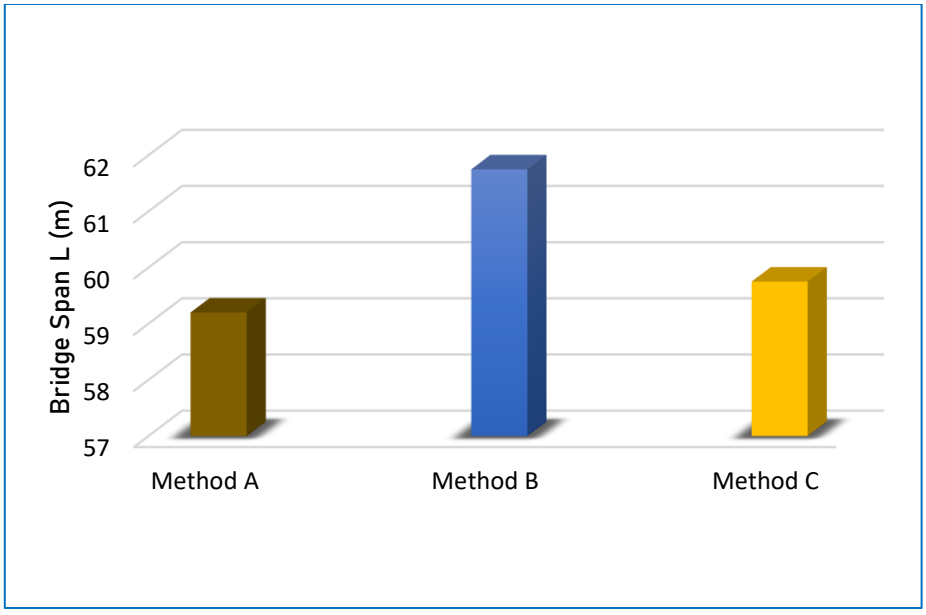

Figure2-2: Bridge span capacities of system1 methods(Tadros et al., 2003).

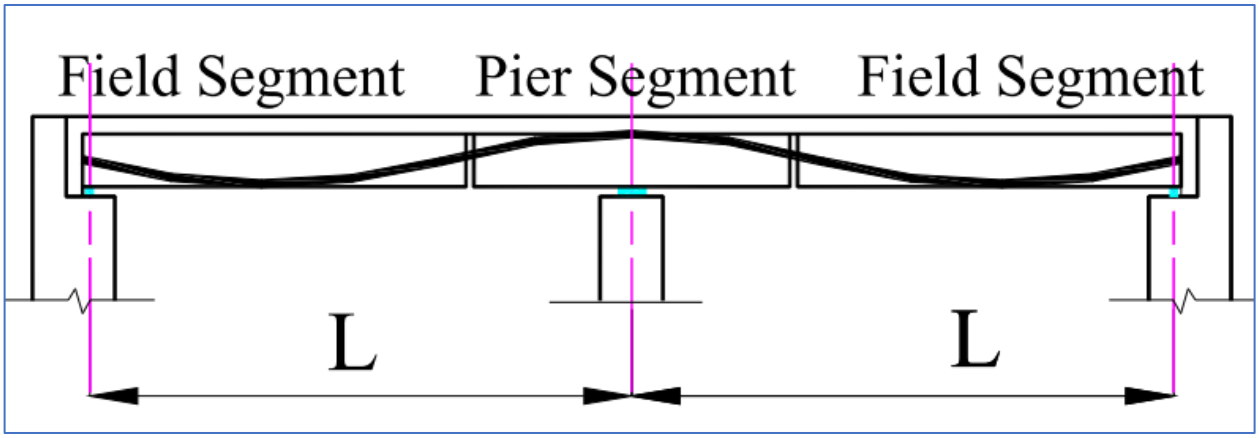

Figure 2-3: Layout of segmental construction system (Tadros et al., 2003).

2-2-3 Segmental Construction with Arched Pier Segment

This system uses three precast pieces for a two-span bridge: two field segments and a one-piece curved pier segment. This method referred to deepen the pier segment by using a curved hunched girder, as explained in (Figure 2-4). The negative moment was still controlled despite its little improvement, but the shear capacity has enhanced more. Many of the positive capacities in the field segment did not reach the design limit, thus considered redundant capacity. So, the pier segment needs to be deepened more so that all the capacities are equal.

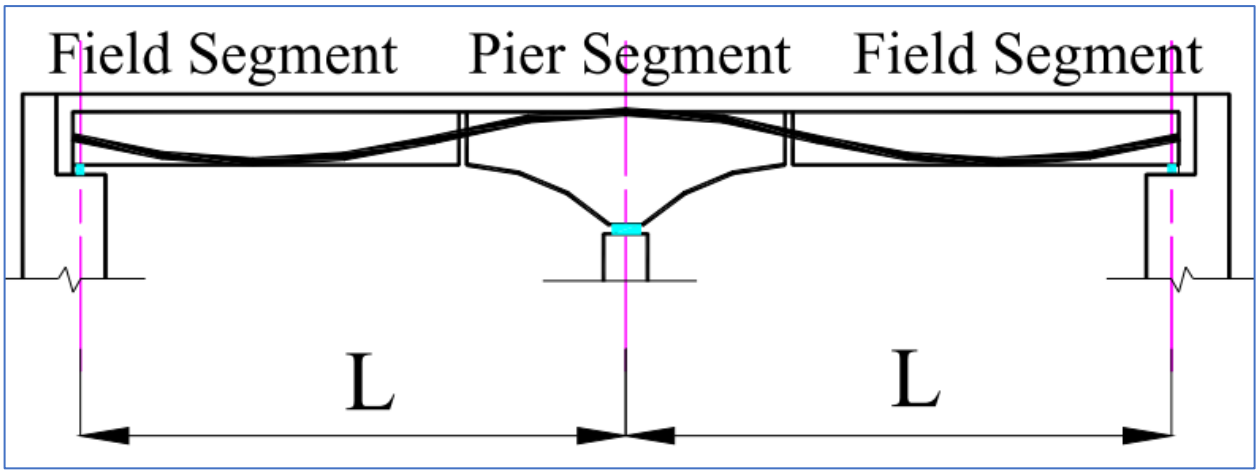

Figure 2-4: Layout of segmental construction with curved pier segment system (Tadros et al., 2003).

2-2-4 Segmental Construction with Two Pier Segment Pieces

The system utilizes a two-piece pier segment: a straight haunch block and an NU-I girder to increase the negative moment capacity as shown in (Figure 2-5). Haunch block dimensions of 0.50(L) in length and 0.9(h) deep were the most efficient haunch block size, equalizing the ultimate negative, the ultimate positive, and the shear capacities.

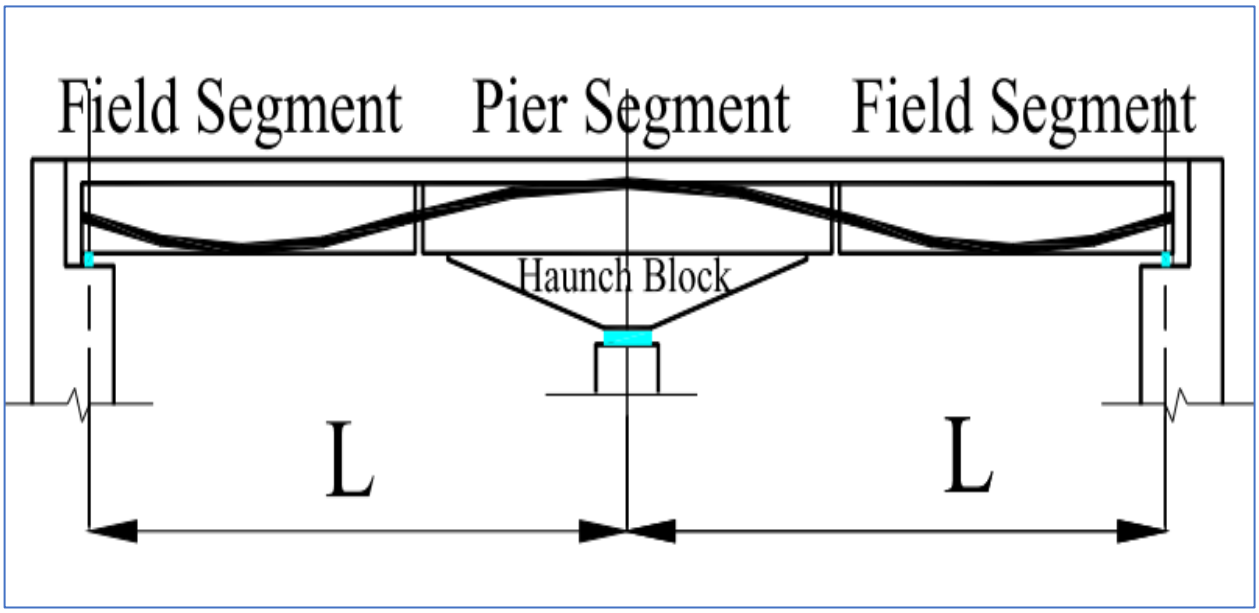

Figure 2-5: Layout of segmental construction with haunch block system (Tadros et al. 2003).

(Figure 2-6) shows a comparison between all previous systems. The span capacity of System II is about 16% less than that of the system I, because system II has a higher negative moment than the system I, which controls the design. The span capacity of system III is almost equal to that of the system I. However, in system III, the maximum transportable span is higher. System IV is superior in terms of span capacity and provides a 60% improvement in span capacity over System I.

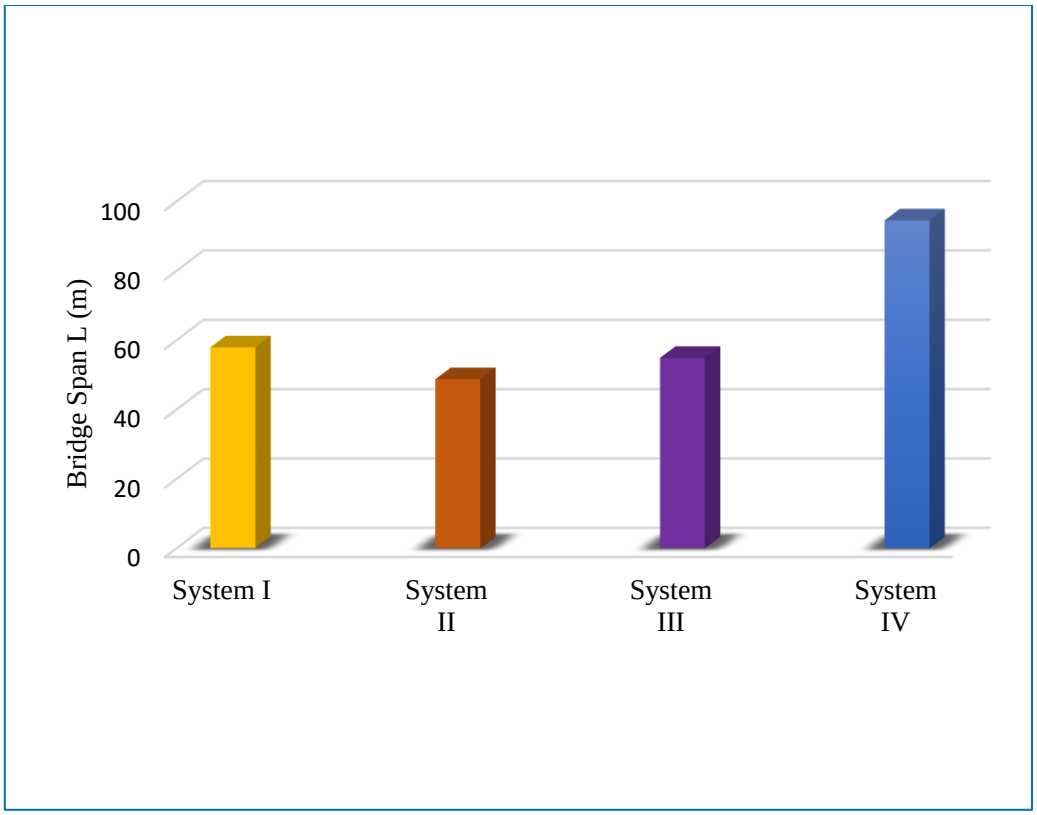

Figure 2-6: Span capacity for all systems (Tadros et al. 2003)**.**

2-3 Segmental (Splice) Girder Bridge

2-3-1 **Splicing Girder with Posttension System**

In this field, the spliced girders with post-tension were presented. The continuity of the segments is provided by prestressing force.

2-3-1-1 Cold Joint

The joint between the girder segments is connected directly and sometimes with the addition of epoxy material to increase the bond between the two pieces. The mechanical behavior of the joint was very important to specify the structural performance of the girder.

Buyukozturk et al., (1991) investigated the shear strength and deformation behavior of precast segmental bridge joints. This research studied the effect of the type of joint (flat or Keyed), the presence of epoxy in the joint or not (dry),

the thickness of the epoxy layer, and prestressing force. The results showed that epoxied joints increased the shear strength of PCSB, but it made failure sudden and brittle.

Ramos et al., (2004) It has produced an experimental study to investigates the using of carbon fiber reinforced polymer (CFRP) sheet product to strengthen the segmental dry joint bridge. This research tested two full-scale beams with a total length of 7.2 m and a box-type section. This specimen consists of seven segments with multiple shear keys in joint rejoin, as shown in (Figure 2-7). The concrete used in the beams had a normal strength grade of 40. The use of CFRPs affects the failure mode of the segmental structure, as it makes the failure due to the concentration of stresses in the joint's region and cracks between conjugated elements. The load-carrying capacity of segmental beams is increased due to strengthening by fiber reinforced polymer (FRP) product and increased stiffness of the mid-span section.

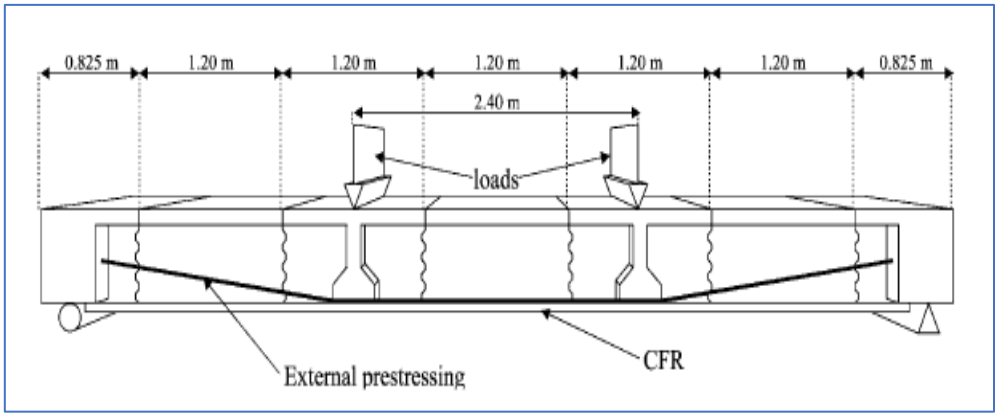

Figure 2-7: Segmental beam setup and dimensions (Ramos et al. 2004).

Huang and Liu, (2006) According to experimental research, a modified skew bending model was developed to calculate the load-carrying capacity of segmental bridges subjected to combined bending, shear, and torsion. A finite element method (FEM) was used to investigate the deflection behavior of such

a structure and to check the theoretical model. A satisfactory agreement between test and theoretical results exists. The results showed a reduction in the load-carrying capacity of the segmental bridges compared with the monolithic structures due to nonyielding the prestressing steel and opening of the joints.

Zhu et al., (2006) study the construction feasibility and structural performance of splicing techniques for concrete-filled FRP tubes. One control beam and four spliced beams were tested, three internally spliced using grouted steel or FRP bars or unbonded post-tensioning bars, and the fourth with an FRP socket commonly used in the piping industry. All specimens were tested by the two-point load method, and the max. Load, mid-span deflection, and stiffness were observed. The Posttensioned spliced beam was the optimum and easy method among this field's suggested methods.

Two full-scale prestressed concrete (PSC) box girders were fabricated and tested by (Kim et al., 2008). One of the girders was cast monolithically, and cast-in-place joints spliced the other. Both girders were simply supported over a 19.8 m span. It was demonstrated that the spliced girder provides excellent static performance that parallels the monolithic girder in the elastic range. No joint failure was observed in the spliced girder until the final load stage.

To investigate the effect of torsion on the externally prestressed segmental (EPS) bridge, as shown in (Figure 2-8). (Algorafi et al., 2010) Four series with 12 beams (with different tendon layouts and joint types) with three load cases (different load eccentricities) were tested under vertical loading. The eccentricities of load that causes the torsion significantly affect the failure load of the beam. The change in tendon layout did not affect the ultimate load with the same joint type. On the other hand, the failure load had a large change by the

joint type with the same tendon layout. Consequently, the existence of a shear key in the EPS beam increased the failure load capacities.

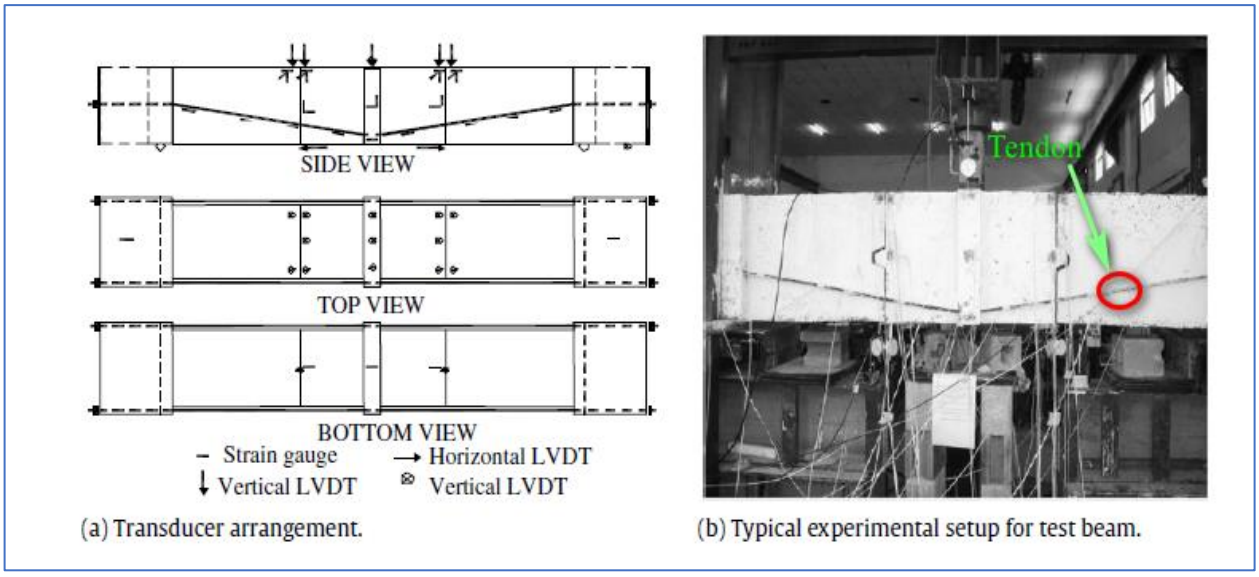

Figure 2-8: The assembling and load system of the specimen(Algorafi et al. 2010).

Al-Shaarbaf et al., (2012) were deals with experimental study of shear strength and deformation of precast segmental bridge joints. All specimens have the same cross-section and reinforcement. The dimension, strand location, load system, and shear key shape are illustrated in (Figure 2-9). These segmental specimens were made with different types of concrete, the number of shear keys, tensile stress in prestressing strands and types of joints at the interface between segments. As a conclusion, using fibers in concrete increased the ultimate load. As the number of shear keys increases, an increase in the value of the ultimate load is obtained. The deflection is reduced, and the ultimate load increases when increasing the restressing level. And it was found that the presence of epoxy increases the ultimate load by about (13.7 %).

Li et al., (2013) studied the response of key joints subjected to combined stress shear and flexure. Nine specimens of precast concrete segmental beams (PCSB) with external tendons were match cast and tested: two-thirds of them were tested under combined shear and bending; two specimens were tested under pure bending, and the remaining specimen was tested under direct shear. The type of joint (dry and epoxy), the position of joints, and the applied load were investigated as variables in this study. In conclusion, Joint position significantly affects joint resistance and the type of joint affected by the mode of failure. The tested specimens have more load capacity of dry joint than epoxied joint for the same load.

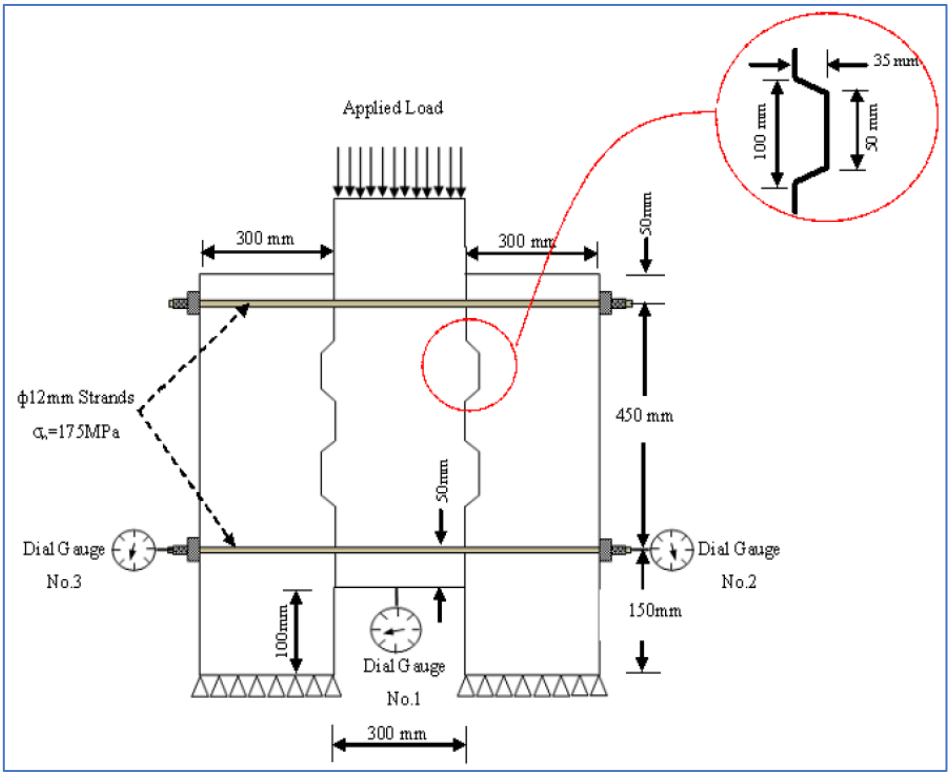

Figure 2-9: Details of Segmental Specimens (Al-Shaarbaf et al., 2012).

A small scale specimens by Saibabu et al., (2013), cast and tested as simply supported deck girders box-section. The segment construction method was used to assemble the girders with dry and epoxied joint and shear keys. Repeated

loading and unloading resulted in the opening and closing of the joints between two segments, which resulted in the loss of joint stiffness and crushing of concrete above the joint at mid-span. The phenomenon is much more severe in dry joint specimens. The results showed that the tensile strength added from using the epoxy in the joint was the reason for higher performance than a dry joint.

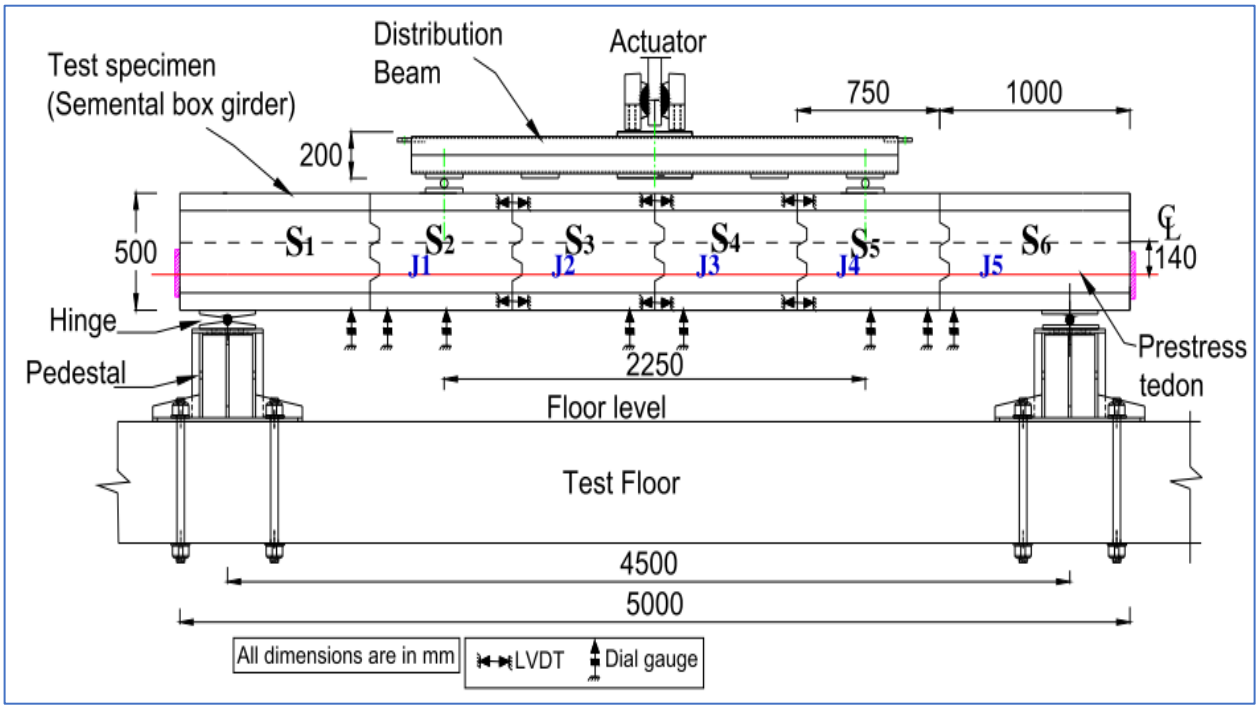

Figure 2-10:Details of the scaled model of segmental box girder (Saibabu et al. 2013).

Brenkus et al., (2016a) used five small-scale I-girders to analyze Splice's flexural static and fatigue strength behavior for prestressed precast concrete girders. In conclusion, behavior at the splice is similar to that of unbonded joints in segmental bridges.

Brenkus et al., (2016b) studied on the shear behavior of prestressed precast concrete I-girders. Four specimens were tested with three-point bending for this

evaluation. The shear and flexure capacity exceeded the strength of AASHTO-LRFD specifications. Using epoxy and an additional stirrup at the splice interface affected the cracking behavior and ultimate performance.

Jiang et al., (2016) investigated the shear behavior of different types of joint specimens with various parameter combinations, especially keyed dry joints of Steel fiber-reinforced concrete (SFRC). Using SFRC in dry joints can improve shear behavior of flat and keyed dry joint specimens in terms of effectively delaying crack initiation and enhancing the shear strength and ductility.

Jiang et al., (2018) It was found that joint location plays an important role in the shear strength of Precast concrete segmental beams (PCSBs) with dry joints when compared with monolithic specimens. The failure modes of PCSBs were independent of joint types. With a larger joint number and higher shear span-depth ratio, the shear strength of specimens with dry joints was greater than that of the corresponding monolithic specimens and segmental specimens with epoxy joints.

The shear transfer of dry joints between UHPC segments is one of the major concerns due to the discontinuity and interruption of the reinforced bars.

So, Liu et al., (2019) studied the shear strength of precast UHPC segmental bridge. A push-off test setup, as in (Plate 2-1), was adopted to investigate the shear behavior of concrete joints. Fifty-two specimens of dry concrete joints were tested, including 4 flat joints, 10 single-keyed joints, 8 three-keyed joints, and 3 large-keyed joints. The effect of different confining ratios, joint types, concrete types, and key shapes on shear strength was investigated. The increasing confined ratio and/or the number of shear keys increased the first crack load. When used fiber in concrete such as fiber reinforced concrete FRC, high strength fiber reinforced concrete HSFRC, and UHPC lead to more ductile

behavior than concrete without fibers. The large-keyed joints show a slight increase in shear capacity (9.7%) compared with the three-keyed joints.

To study the shear behavior of joints in precast box girder segmental bridges as shown in (Figure 2-11), Ahmed and Aziz, (2020) took thirteen specimens and tested them with direct shear loading. The results showed that increasing the confining pressure and/or number of shear keys can highly improve both the elastic stiffness and the plastic ductility of the segmental bridges and changes the brittle behavior of the epoxied joints to a gradual strength degradation model.

Plate 2-1: Typical experimental setup for dry joints(direct shear setup) (Liu et al., 2019).

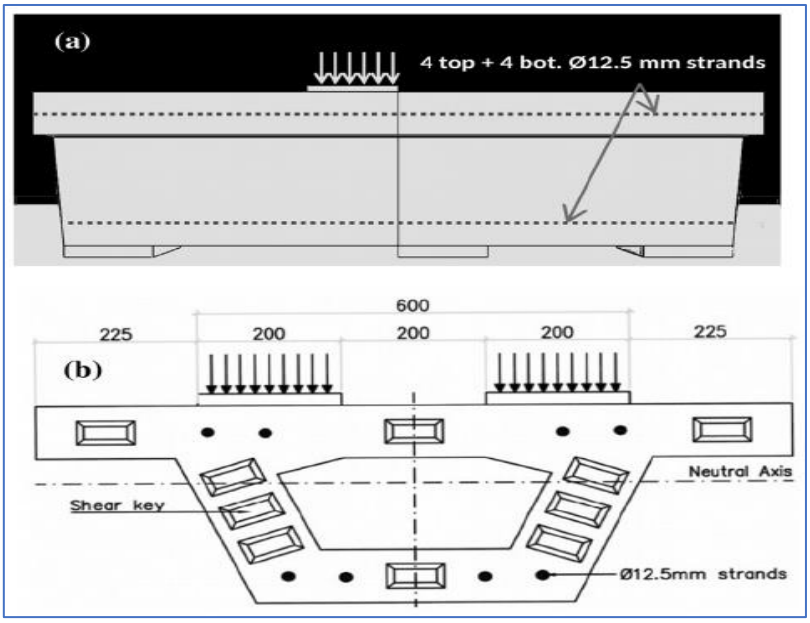

Figure 2-11: (a) Test setup in the longitudinal direction (specimen length is 2×750 mm, the width of plates is 200 mm) (b) Test setup in the transverse direction (all dimensions are in mm) (Ahmed and Aziz, 2020).

2-3-1-2 Cast in Place Joint

Brenkus, (2013) the experiment study was conducted on nine specimens to investigate the behavior of spliced girders. Three of these were cast without splices, while the other six were each composed of two precast segments linked at the spliced region, as shown in (Plate 2-2). The test program included flexural, shear and fatigue behavior. The flexural test had shown that the ultimate capacity of the spliced girder specimens exceeded the calculated capacity by 15%. Although the different test settings to study the behavior of shear in the girder specimens, there was only one of these exhibited a shear failure.

During the test, the researchers noticed that implementation of epoxy on the end of precast segments improved bending between the precast segments and concrete, which cast-in-place splice region. They also observed the importance

of adequate vibration to properly consolidate the concrete within the splice area, even using a self-consolidating mixture.

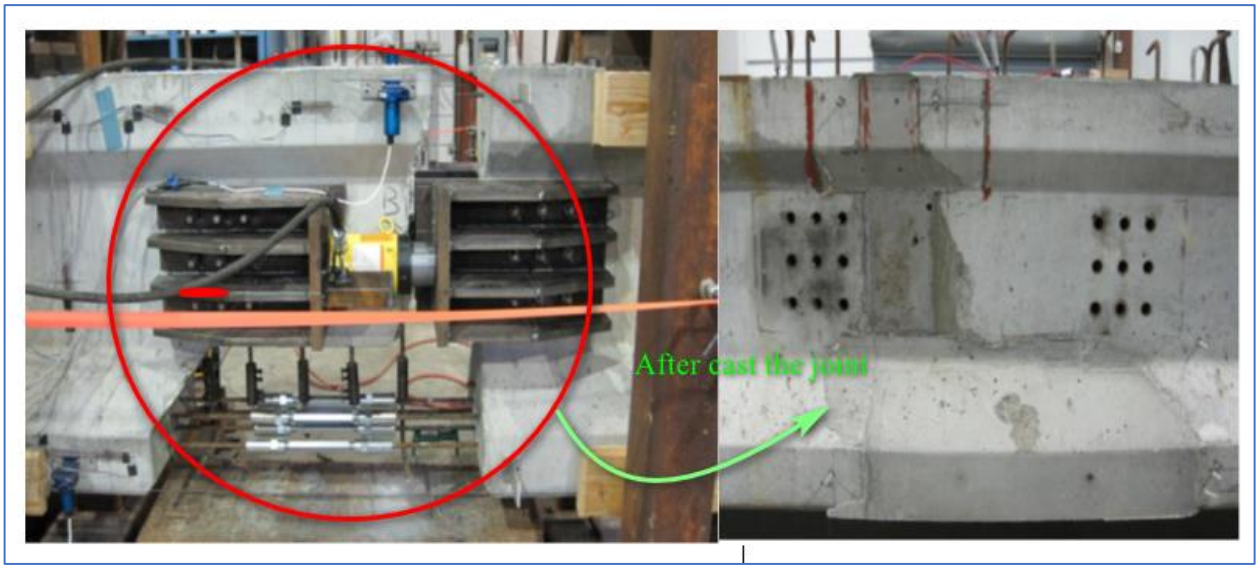

Plate 2-2: Splice the segment of girder (Brenkus, 2013).

Williams, (2015) studied the behavior of the (CIP) region of spliced I- girder bridges. The experimental program was applied to show the behavior of spliced I-girders. More specifically, the primary objective of this research was to evaluate the structural behavior of the Cast-In-Place splice region. Two large scales of simply supported concrete girders were tested, each girder consists of two precast segments joined together at a splice region, and three post-tensioning tendons were used to provide continuity along the girder length of (15.25 m). The amount of longitudinal reinforcement within the bottom flanges of the test girders was varied between the two specimens to show the effect of the bar's number on the behavior of the splice region. The girders were tested in a (8900 kN) capacity load frame until the specimen failed in shear, the load was applied in increments of (445 kN) or less. Each test girder was loaded monotonically until the specimen exhibited a shear-compression failure of the concrete web.

The results show that spliced girders failed at shear strengths exceeding calculated values. Furthermore, splice region details were recommended based on the research program results.

By Choi et al., (2015)**,** a total of nine specimens were fabricated for which prestressing has been introduced after grouting high-performance mortar (HPM), and another seven specimens for which high-strength concrete (HSC) has been placed after lap splicing. Static flexural and cyclic loading tests were conducted. The HPM series specimens performed better than the integrated specimen. The HSC series specimens showed similar static flexural behavior but lower serviceability than the integrated specimen.

Park et al., (2017) studied experimentally and analytically the deflection behavior of precast concrete beams with joints. The details of dimensions, splicing, and reinforcement are shown in (Figure 2-12). Each module was connected with a lapped splice of steel reinforcements and ultra-high-strength concrete (UHSC) with a specified concrete strength of 120 MPa. The initial deflection data from the cyclic loading test were used to review the instantaneous deflection's serviceability. As a result of explicitly including joint behavior, which is considered attached transmission length and characteristic by concrete strength, a more accurate deflection calculation is developed.

Peng and Yan, (2021) investigated the comparative study on the different type of joints in UHPC beams. Experimental tests were implemented on a complete beam and on five further specimens with vertical joint, rhombus joint, vertical joint with strips, tied rhombus joint with strips, and welded rhombus joint with strips.

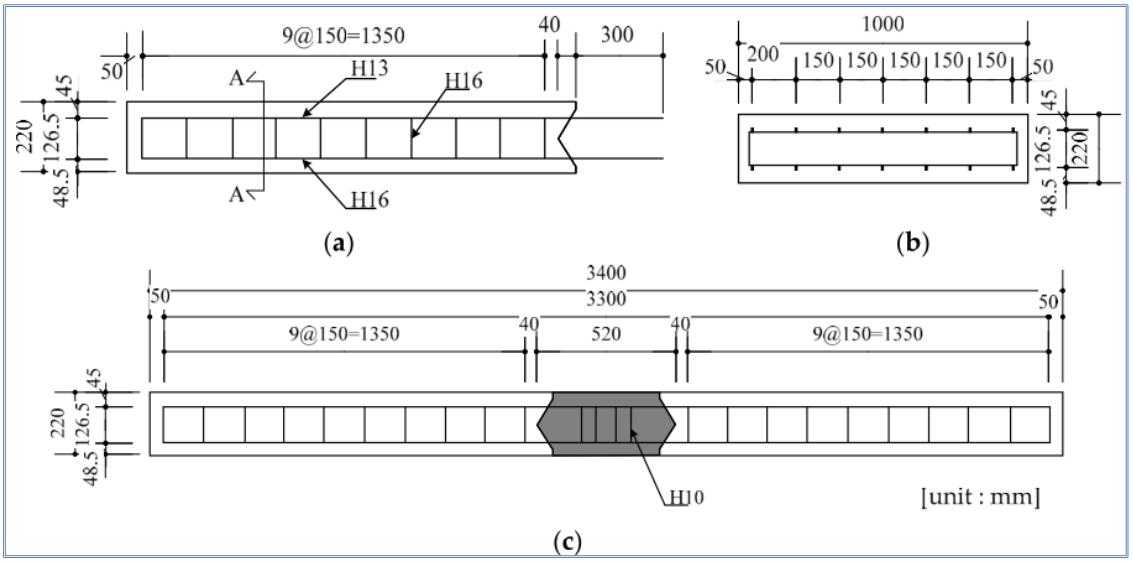

Figure 2-12: Specifications of the specimen: (a) precast module before casting ultra-high-strength concrete (UHSC); (b) cross section of A-A; (c) modular specimen after casting UHSC (Park et al., 2017).

The variables, joints' shape, and beams' dimensions are shown in (Figure 2-13). The complete beam and the main segment of the joint beam were cast with UHPC 150 premix and the same reinforcement details, then cured by steam. Joint region cast after that with same concrete and curing. All specimens were tested as simply supported conditions under a four-point bending load. From the results, the joint's presence led to significant weakness in the beam's flexure capacity. Adding strips in the top and bottom of the joint enhanced the flexure capacity, but it was causing to lose of the yield stage (sudden failure). Welded the reinforcement with top and bottom strips led to the best structural behavior of the joint beam.

2-3-2 **Splicing girder with steel lap-splice System**

This part focused on the research that depend on the steel reinforcement overlapping and CIP concrete joint to provide the continuity of the precast

segment. many parameters and results, as will show.

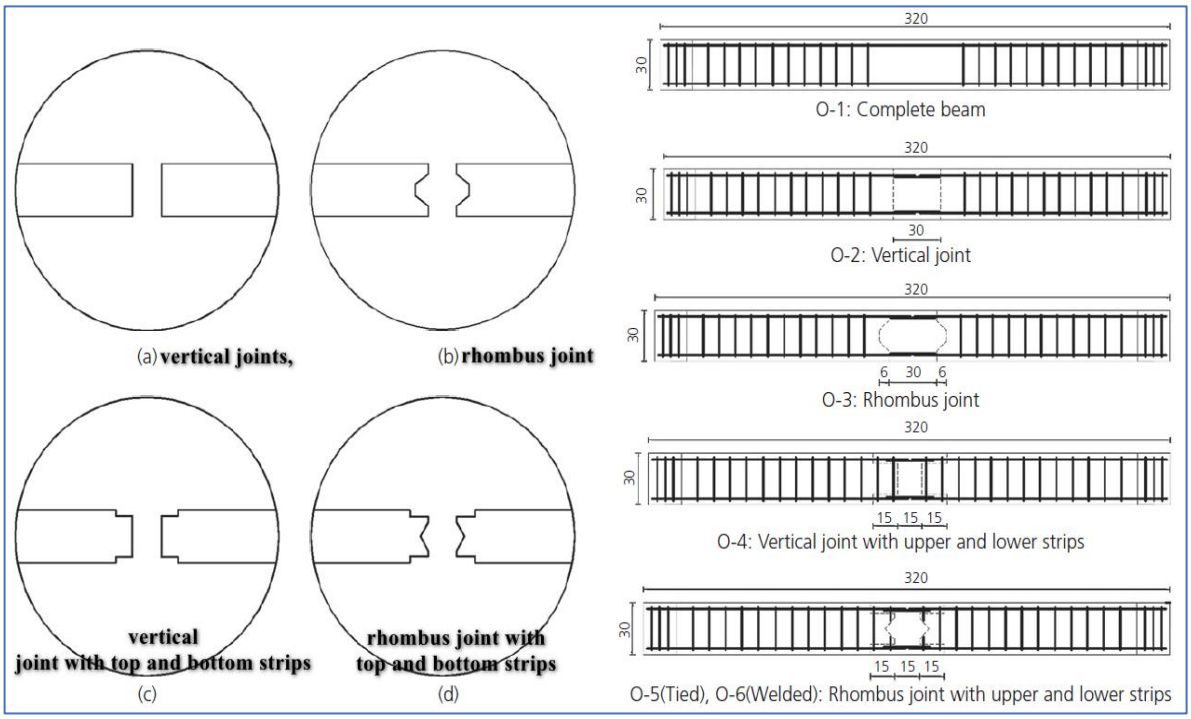

Figure 2-13: Symbols, dimensions, and type of joints of tested beams.

Al-Mamuree, (2008) studied the experimental and numerical performance of prestressed spliced and monolithic concrete beams. The experimental program consists of the cast and tested sixteen beams with simply and continuous support. The spliced girders were made with three pieces, as shown in (Figure 2-14). Tendon area, joint location, beam depth, span length, load arrangement, and segment state (pre-tensioned or not). The numerical part was adopted by using a computer program (ANSYS). From the results, the presence of joints in girders causes decreases in the failure load in the range (12- 17) %, and deflection increases by about (10-15) %. Then the ultimate load was increased by (11-16) %, and the deflection decreased in range (8-14) % when the post-tension area from 50% to 100%.

One of the drawbacks of this study is assuming perfect bond between the reinforcement and concrete and between the concrete of precast segments and cast in place concrete of the joints.

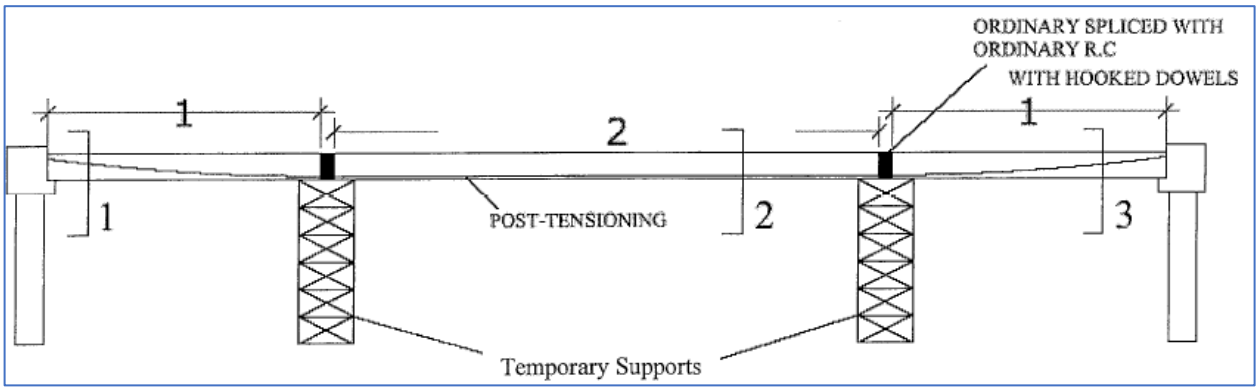

Figure 2-14: Spliced girder of three precast segments(Al-Mamuree, 2008)**.**

Al-Quraishy, (2011) investigated the behavior of precast spliced girders. Two or three segments were fabricated to achieve the required length of girders. Fifteen beams in four groups with rectangular sections were cast and tested up to failure under two points loads. The experimental variables were the supported condition, the method of strengthening (post-tensioning of all segments and steel plate with the hooked dowels in the spliced joint), number and positions of the splice joint. From the results, the number of pieces had no a large effect on the ultimate load. The use of steel plates with different thicknesses and positions had a slight enhancement in the flexural capacity of spliced beams. Post-tensioning has improved the hooked splice girder's behavior and increased the failure load. A nonlinear three-dimensional element by (ANSYS) program was used to represent all tested girders. The maximum difference between the experimental and theoretical ultimate loads for girders was in the range of (3- 11) %. In a previous study, it was assumed perfect bond between reinforcement and concrete at the splice region and the interface between new-old concrete.

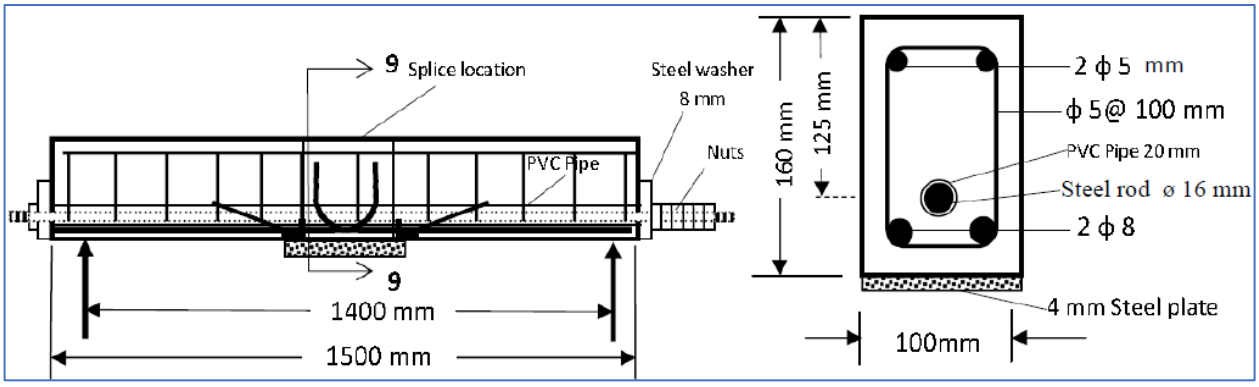

Figure 2-15:Details of the girder with post-tension and steel plate strengthening (Al-Quraishy, 2011)**.**

Al-Tameemi, (2015) studied the experimental and numerical behavior of RC spliced girders. The main objective of this research was to find an improvement in the capacity of spliced girders when using CFRP sheets to strengthen the joint region. All specimens have rectangular sections of 150 x 250 mm, and a total length of 2 m. the experimental program deals with two support conditions (simply supported and continuous support). The experimental variables were strengthening the joint region by different schemes of CFRP laminates, location and length of the joint, presence of internal stirrups at the joint region and using binder material at joint interfaces. The results showed that strengthening the simply supported spliced girders with longitudinal CFRP laminates could increase the ultimate load in a range of **(**42 to 77) %. On the other hand, the increase in ultimate load is (15 to 28) % when using transverse CFRP sheets.

It was also found that strengthening the continuous spliced girders with 45° inclined CFRP laminates led to an increase in the ultimate load in a range of (47 to 74) %. As well as strengthening the continuous spliced girder with horizontal CFRP laminates bonded at its lateral faces could increase the ultimate load by (70%). Additionally, the ultimate load of the continuous spliced girder was increased by (30%) due to the presence of the horizontal steel stirrups through the interface between the joints and the precast segments.

In the numerical part, FEM analysis by (ANSYS) was carried out to check the model's validity that simulates the structural behavior of the splice girder. Some parametric studies were investigated after the acceptance of the numerical model, such as the compressive strength of the joint concrete, the diameter of spliced hooks, the number of stirrups in the joint, and the distribution of longitudinal CFRP laminates.

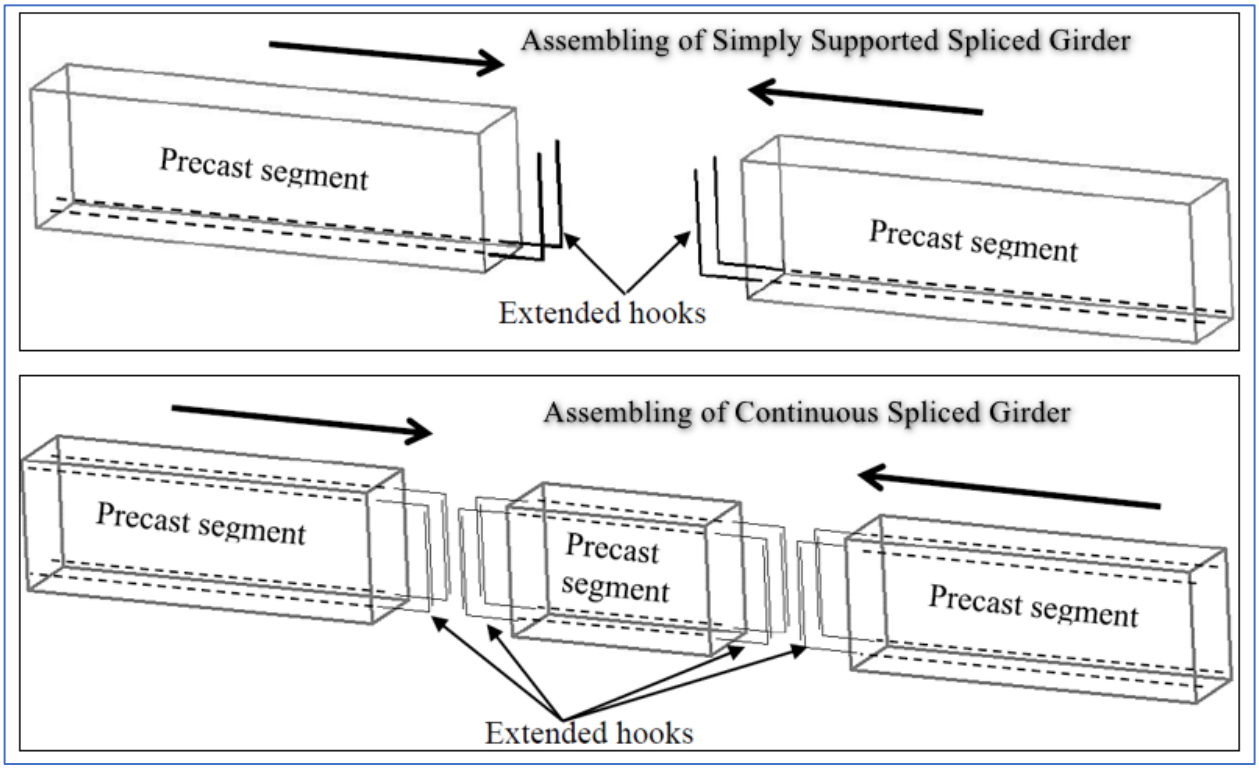

Figure 2-16:Assembling of Spliced Girders (Al-Tameemi, 2015).

Arafa et al., (2016) studied the behaviour of UHPC joints that were subjected to negative moments. The test matrix has eight panel specimens with the same dimensions illustrated in Figure 2-17. This paper deals with the reinforcement type (steel and GFRP). From the tested specimens, the presence of a joint at a negative moment led to a decreased ultimate load of steel-RC panels. In contrast, the GFRP-RC panels had no degradation effect on the ultimate load or deflection and changed the failure mode from flexure failure without joint panels for shear

in panels with UHPC joint. This change occurred due to the high tensile strength of UHPC caused an increase in flexure capacity at the maximum moment location.

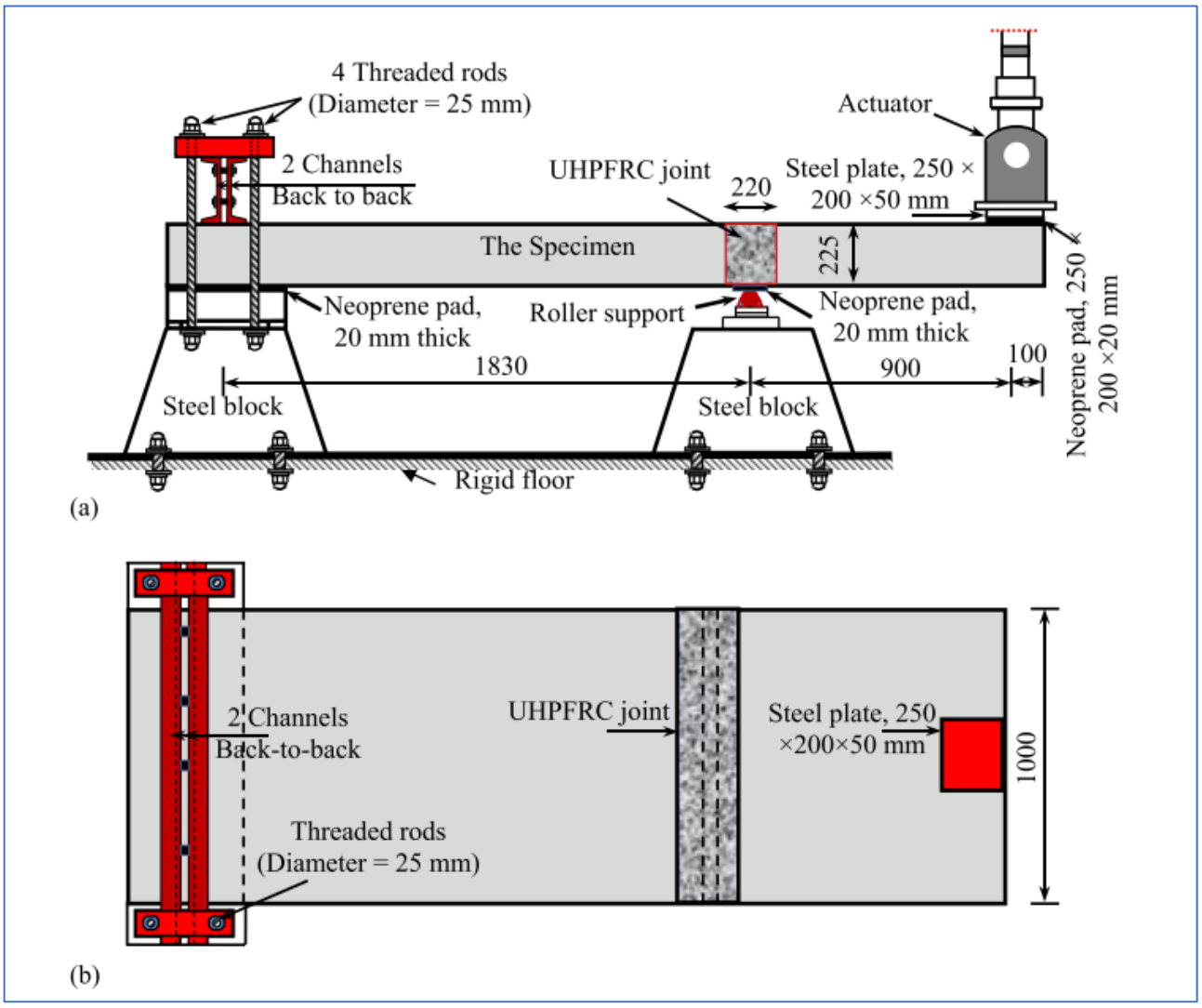

Figure 2-17:Test setup: (a) elevation; (b) plan (Arafa et al., 2016).

AL-Khafaji et al., (2018) studied the experimental behavior of rectangle spliced girder tested under two points load. The research had 8 girders with the same total length and three segments. Half of them were tested as simply supported and the others as continuous beams. The study main objective was to use the RPC in joints and change the volume of steel fiber in the mix, then explain its

structural behavior on the spliced girders. The dimensions and other details, such as joint length, location, and type of concrete in the joint region, are all shown in (Figure 2-18). The results showed that using RPC enhanced the ultimate load by (8.6-15.2) % in the case of the simply supported girder, while in the case of a continuously supported girder, the ultimate load increased by (4.7-14.7) %. The increase in steel fibers ratio leads to an improvement of the overall behavior of spliced girders, because these fibers restrict cracks and increase the stiffness and consequently reduce the deflection of the spliced girders.

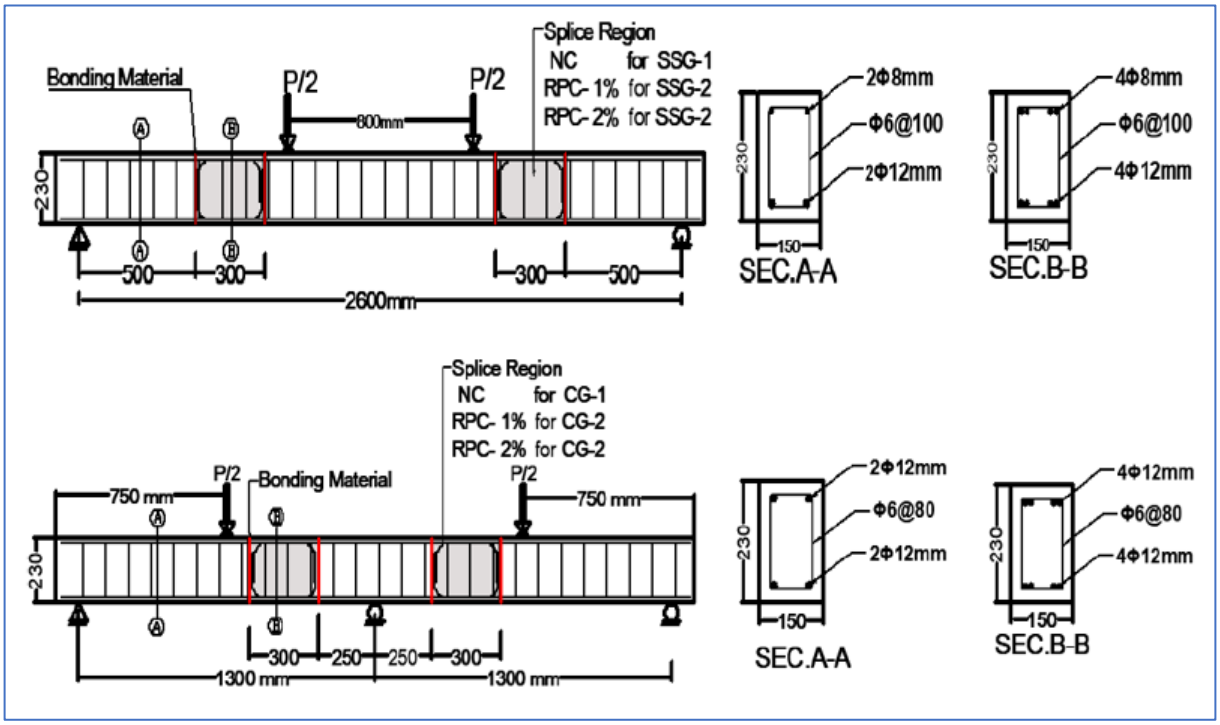

Figure 2-18: Details of the Tested Girders (AL-Khafaji et al., 2018).

In addition to the last research, Aoun, (2018) also investigate using CFRP bars to strengthen the splice region by NSM system for both simple and continuous supports. This strengthening technique improved the ultimate load by 11.25% and 3.76%, and the deflection was also increased by 15.56% and 8.7% for the simply supported and continuous girders respectively. In the same field, FEM

was adopted in this study using (ANSYS) program. The result of the numerical part had acceptance as compared with the experimental data. After that, the researcher studied some of parametric study length of splice, number of CFRP in strengthened region, and the type of FRP (glass fiber (GFRP), and basalt fiber (BFRP)) used in NSM system. The results of these parameters showed that the increased length of splice and number of CFRP bars led to an increase in the failure load by (38.63%), (18%) respectively.

Qi et al., (2020) investigated the flexural performance of the UHPC joint for connecting the precast segment. The test variables used in this research include interface preparation, joint material, lab-splice form, and prestressing level. Using the steel wire mesh to treat the interface increased the ductility by about 50% and enhanced the ultimate load by 20.1 %. These results are due to the steel fiber continuity provided by this interface treatment system. The use of prestressing tendons to increase the continuity of the precast segment increased the flexural crack capacity and the ultimate strength, while the ductility had high degradation. Also, the straight overlapping form was inadequate to transform the generated stresses.

Hassoon and Aljanabi, (2020) studied the behavior of simply supported R.C spliced girder. Seven small-scale girders with rectangular sections have been cast and tested. One of the cast one unit as a control specimen and the remaining girders were cast with spliced rejoin with different concrete types (NS and SFC). This paper found that the spliced joint is the region in which the model failure occurs, so this region must be strengthened. The method of NSM-CFRP bars was used to strengthen this region, as illustrated in (Figure 2-19). The variables in this investigation were the joint length and the type of concrete. The existence of splices and joint regions decreased the ultimate load capacity and ductility

factor of the spliced girder by 33.1% and 44.5%. The reduction in the joint length from 320 mm to 170 mm leads to a decrease in the load-carrying capacity. While the use of steel fibers and concrete increased the ultimate load capacity and ductility. When used NSM- CFRP bars to strengthening, increased the ultimate load capacity of the girder by 5.8%–83.7% but the ductility factor decreased by 2.6%–50.5%.

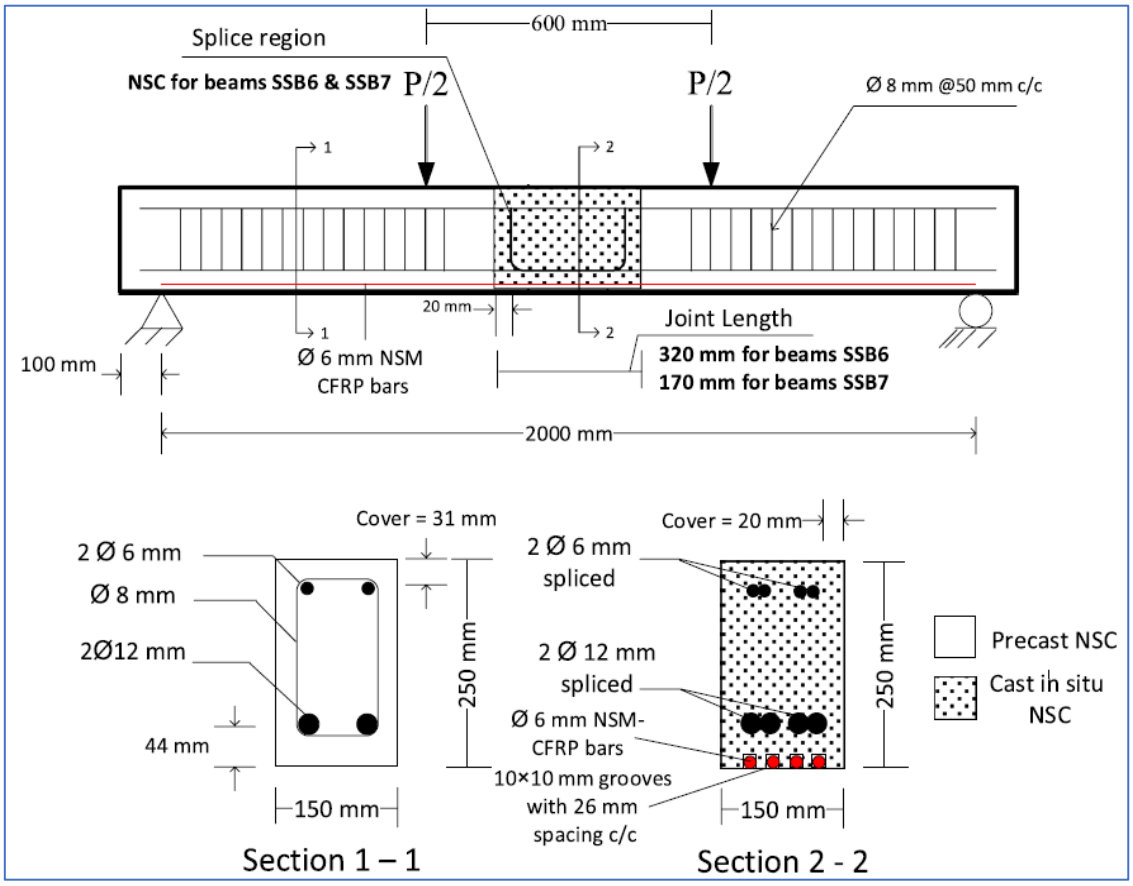

Figure 2-19: Details the spliced beams(Hassoon and Aljanabi, 2020)**.**

Aljanabi and Hassoon, (2020) investigated the behavior of two-spans continuous reinforced concrete spliced girders strengthened using steel fiber concrete of volume fraction of 1% at splice regions and side near-surface mounted carbon fiber reinforced polymer bars of 6- and 10-mm sizes. Five girders with rectangular sections were cast, connected with two joint regions, and tested a

single concentrated force at each midspan. (Figure 2-20) The girders section, the using parameters, and load setup were explained. One of the specimens is cast as a single unit (reference). The other models assemblage of three precast segments spliced together using cast-in-place concrete joints of 170 mm length located at the inflection points. The results showed that using steel fiber increases the ultimate load compared with normal concrete but does not restore the reference beam capacity. Also, it led to delayed the initial cracks and did not affect the failure mode. In the same failed, using near surface mounted CFRP bars increase the ultimate load of the spliced girders by 69.1% - 98.1%, in comparison with the non-strengthened spliced girder with lower deflection values and large first crack load.

In the same field, the researcher Hassoon, (2021) studied the effect of repeated load on the eight splice girder for both groups experimentally. The total number of cycles was 10 cycles, and each cycle was divided into two sub-cycles to ensure the same loading rate. The results have shown that the effect of repeated load seemed clear on decreased the ultimate load, ductility, energy absorption, cracking load and crack width because of the adverse effect of the loading and unloading successive load cycles. But, it had little or no effect on the failure mode.

The numerical analysis was performed using the computer program (ANSYS 16.1) to validate the adopted numerical models in predicting the overall structural response of the spliced girders. The simulated model has good approval as compared with experimental results. Thus, the other parameters were studied to give more ideas about this topic. These parameters were the effect of stirrups, the length of the splice, steel fiber ratio, the intensity of repeated load, and the effect of reversed loading. The most important in these results is that

reversed repeated loading let to decreased the failure load by (92.7) % as compared with a uni-directional repeated load.

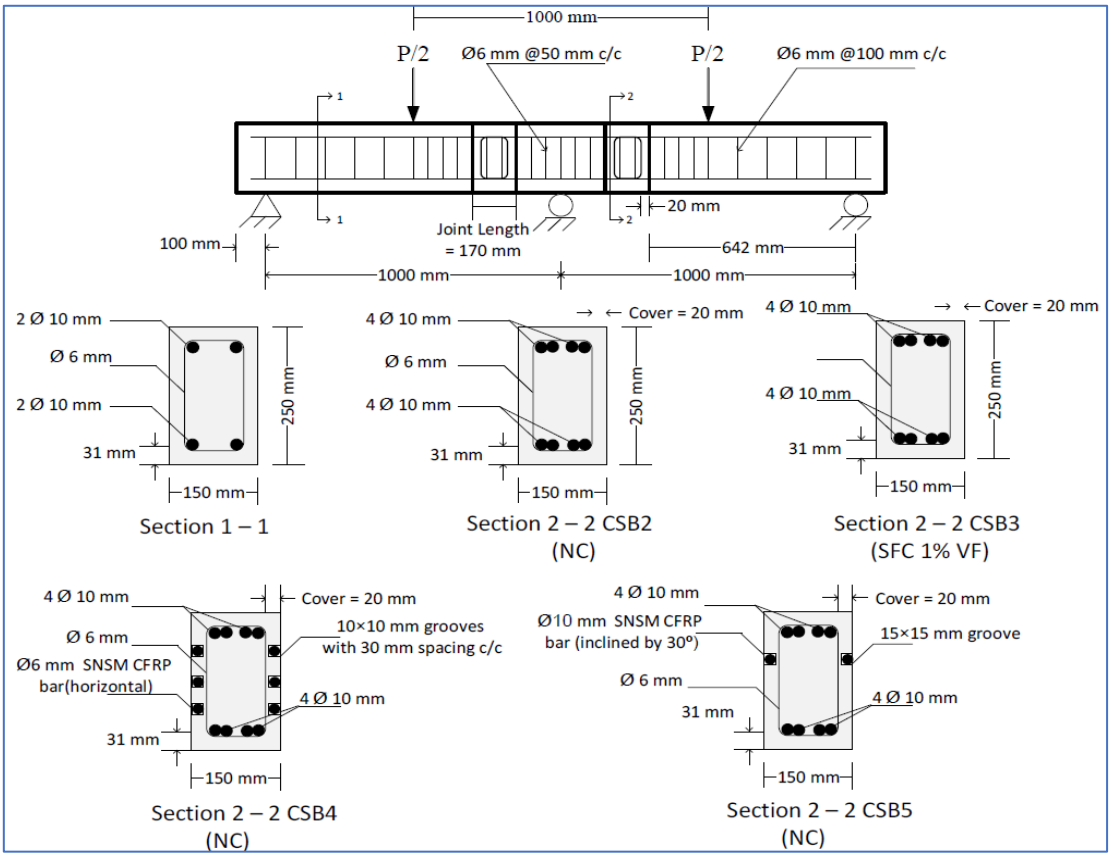

Figure 2-20: Details of the spliced girders(Aljanabi and Hassoon, 2020).

2-4 Hybrid Reinforced concrete

The hybridization utilizing to improve the performance of RC member.

Mohammed, (2013) presented an experimental and theoretical investigation of flexural behavior (strength and deformation characteristics) of hybrid rectangular beams combining conventional concrete (CC) and reactive powder concrete (RPC). Twenty-four simply supported beams with rectangular section were cast and tested to perform this study. Three of the tested beams are made with CC, five with RPC and sixteen as hybrid beams of the two concretes. RPC is used in tension in ten hybrid beams and in compression in the other six beams.

The main variables were steel fiber ratio, RPC thickness, and reinforcement ratio. From the experimental results, the reinforcement ratio has the largest effect on the increased the ultimate load and stiffness. The other parameter also increased the failure load and stiffness with less effect. Using RPC in compression is found to be more effective than using RPC in tension. After that the FEM model was simulated by using (ANSYS) program and the results given good agreement from experimental results.

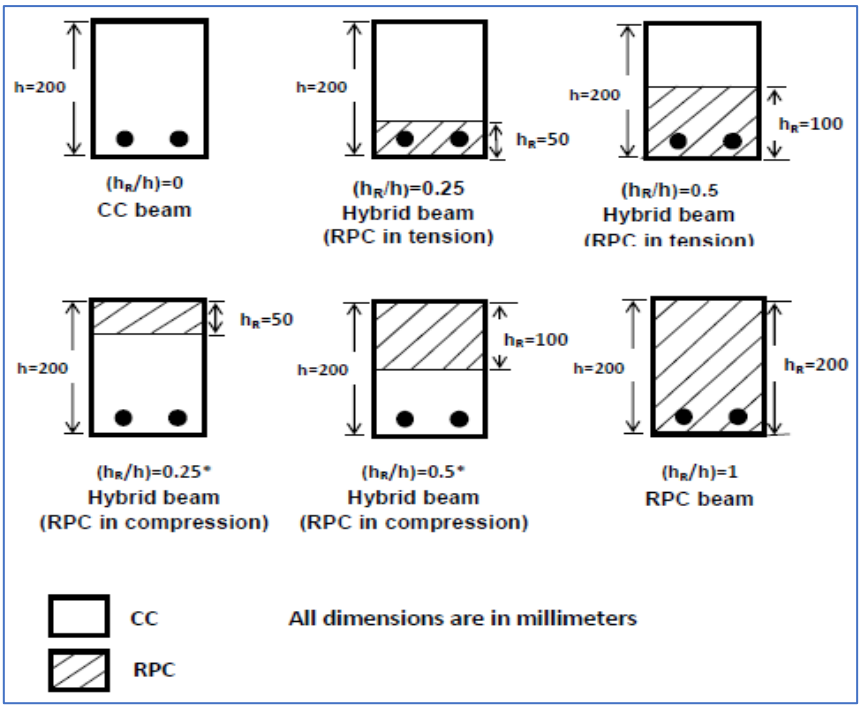

Figure 2-21: Thickness layer of RPC in the tested beams(Mohammed, 2013).

Ismael et al., (2015) introduced experimental study to investigate flexural behavior of hybrid T-section beams and study the ability of using normal strength concrete together with RPC in the same section to exploit the advantages of these two materials in optimal way. Five beam specimens were used to perform this investigation. The experimental results showed that using RPC in the web and normal strength concrete in the flange effectively enhanced performance of hybrid T-section beams when compared with normal strength

concrete T-beam, however, the increases in the first crack load, ultimate flexural load and ultimate deflection were 86.67%, 60% and 29.19% respectively, while, the increases for the case of using RPC in the flange and NSC in the web were 20%, 34.28% and 14.97 respectively when compared with NSC T-beam.

Abtan, (2016) in his research was studied the flexure behavior of hybrid reinforced concrete beams combining RPC and lightweight concrete (LWC). Twelve beams were prepared, cast, and tested as simply support to perform this study. LWC was used in bottom layer and RPC was used in top layer for all hybrid concrete beams. Increasing the thickness of RPC layer led to improve the load capacity of beams (increased load and decreased deflection). from the experimental results, the concrete with steel fiber and porecilenite had more effective than the concrete with other types of aggregate (sawdust and polystyrene).

Marzoq, (2020) studied the performance of RPC and hybrid RPC-NC under the effect of flexure only and combined flexure-torsion loading by using T-section beam as shown in (Figure 2-22). The experimental program had cast and tested 8 beams. These beams divided into two group depending on the load type. Each group had 4 specimens with different concrete section (i.e., NC only, RPC only, Hybrid section with RPC in flange and NC in web, and reversed).

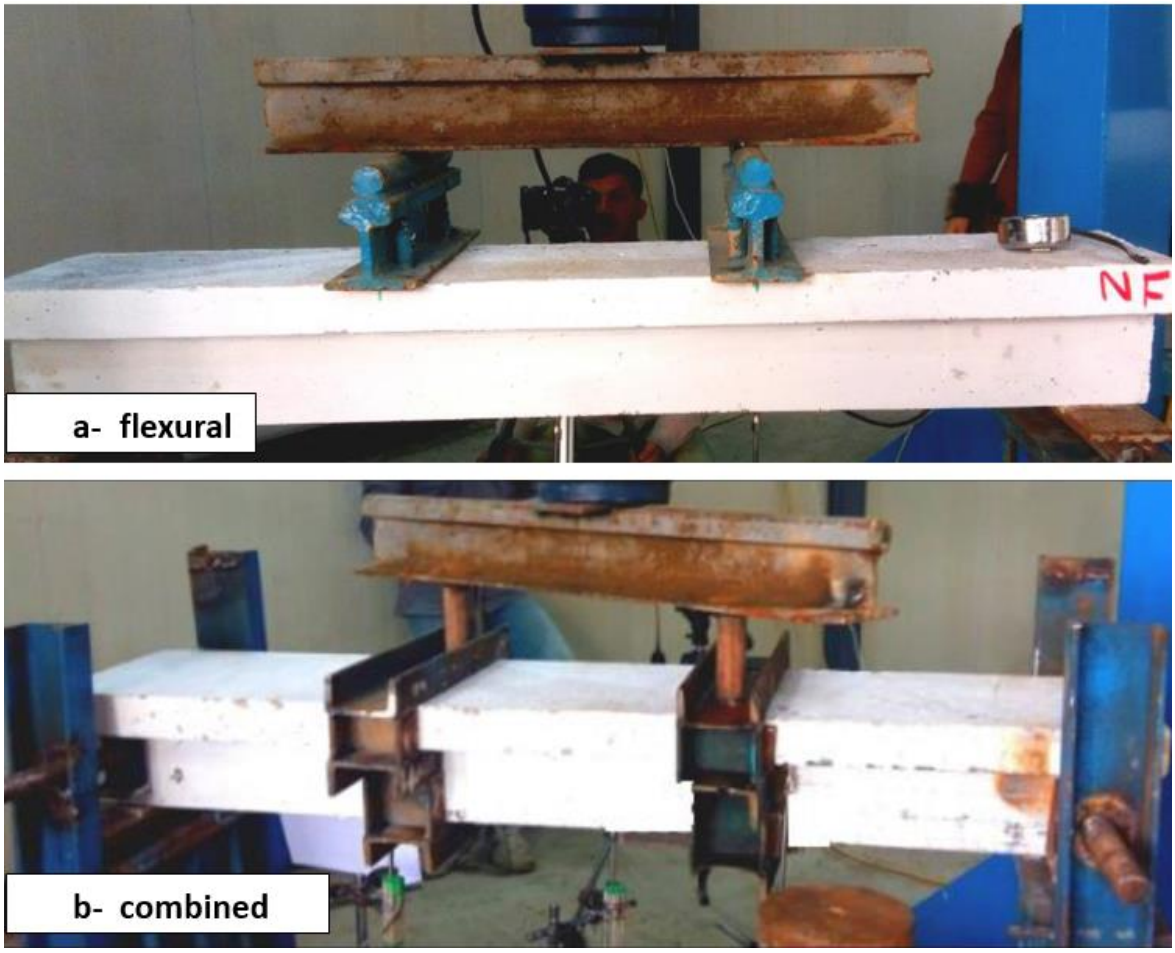

Figure 2-22: Load conditions of tested beam (Marzoq, 2020).

Results show that the flexure performance highly dependent on the type of concrete. for pure bending, the utilizing of RPC instead of NSC in the T-beams increased the first crack load, ultimate load and the maximum deflection with percentages of 100%, 40.42%, and 77.08% respectively compared with NSC T-beam. For combined load, the using of RPC instead of NSC in the T-beams increased the first crack load, the ultimate load and the maximum deflection by the percentages of 60%, 41.07%, and 70.09% respectively compared to that of NSC T-beam. Placing RPC in the web and NSC in the flange enhanced the behavior of these beams more than the other hybridization for both load conditions.

Numerical study was adopted by using FEM analysis in (ABAQUS) computer program. The simulated model has good convergence from experimental result. For thus, some of other parameters were investigated numerically.

Cao et al., (2017) five expansive concrete (EC) beams and five conventional Portland cement concrete (PC) beams were tested under flexure. Reinforcement was designed by considering different layers of CFRP as well as steel reinforcement. Cracking loads, ultimate loads, mid-span deflections, and ductility were collected and analyzed. Test results show that beams reinforced with hybrid reinforcement perform superior than those reinforced only with steel in all aspects.

Qin et al., (2017) in order to improve both its strength and flexural ductility, a hybrid reinforcement system composed of FRP and steel bars has been proposed and adopted in design the recently. main variable in this study was the hybrid reinforcement ratio between FRP and steel. Over-reinforced design for hybrid FRPRC is demonstrated to a preferable choice possessing high stiffness, high load- carrying capacity and good ductility behavior. Under-reinforced design can also be used as an economic way provided that the A_f / A_s is strictly controlled.

Al-Rousan et al., (2020) studied the enhancement the flexure capacity of RC beams by using hybrid CFRP sheet -steel reinforcement. To complete this study, 24 specimens were prepared, cast, and tested under pure bending, (Figure 2-23) shown the design of beams and test setup. The investigated parameters include the CFRP number of layers of one and two, the CFRP sheet length of (400, 500, 600, 700, 800, 900 and 1000)mm for internal reinforcement, and the CFRP sheet length of 400, 700, and 1000 mm for external strengthening. For the internal strengthening, the use of CFRP in tension region led to enhanced the load

capacity by about 52% as average for deferent length of CFRP in one layer. While the average of improvement was reached 62% for two layers of strengthening. In term of deflection, the used of CFRP sheet improved the mid span deflection with (36, 51) % for one and two layers, respectively. The beams of external strengthening have many less improvements in flexure capacity than internal strengthening.

Basim et al., (2019) this study proposed a new design to reinforce the beam-column joints with embedded CFRP rods, due to their extremely high strength and stiffness. CFRP rods are used in reinforced concrete (RC) frame and UHPC frame subjected to dynamic load. The results showed improvement in the performance of the frames reinforced with embedded CFRP in joints in terms of lateral load resistance capacity, ductility behavior, overall stiffness, and failure mechanism.

(Song et al., 2021) studied the behavior of concrete frame reinforced with CFRP-steel hybrid reinforcement under the effect of cyclic load. CFRP longitudinal reinforcements are placed in the outer layer of the section, while steel reinforcements are arranged in the inner layer. The results of the tested frame presence that the CFRP-steel hybrid reinforced concrete led to improve the overall structural performance for cyclic loading as compared with steel reinforcement only.

2-5 Lap-Splice of Reinforcement

Tighiouart et al., (1999) was the first study on the bond strength of splice FRP rebar in reinforced concrete. The parameters were studied five lap splice length with two different FRP diameter and beam cross-section. All 16 beams were having 30mm cover, 3000 mm as span and tested in third points.

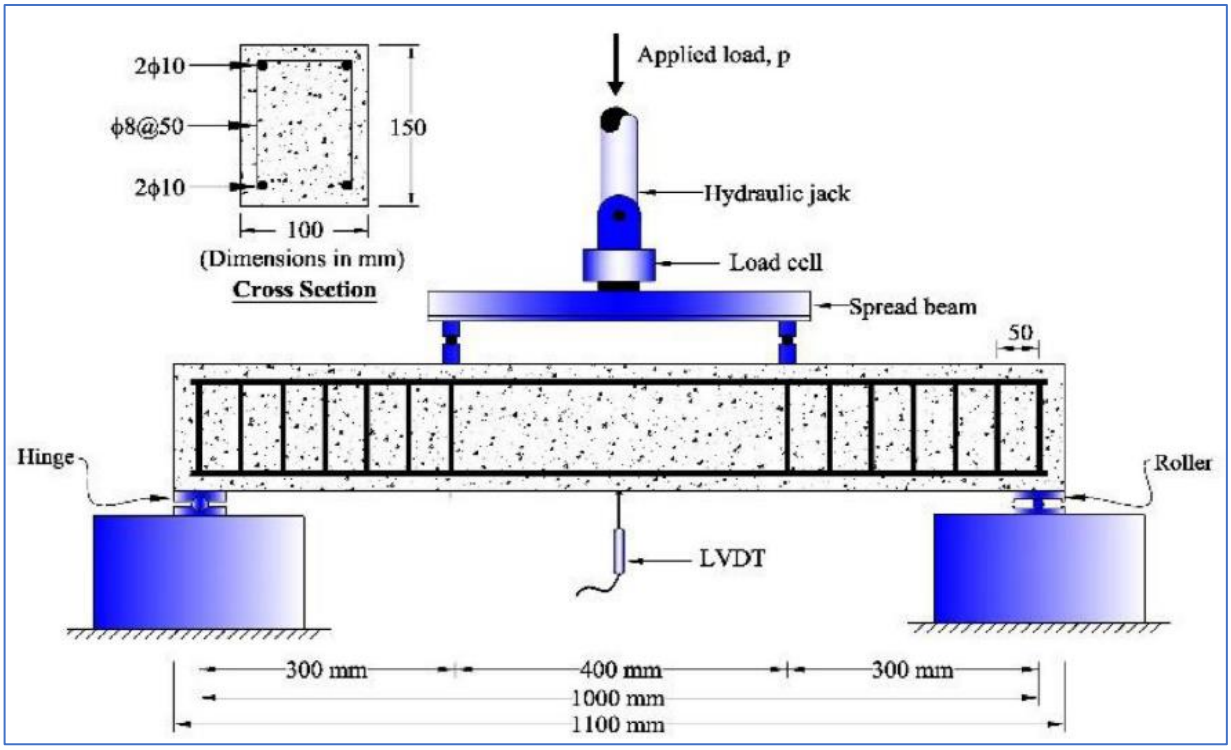

Figure 2-23: Details of dimension and loading of specimens(Al-Rousan et al., 2020).

The development length was calculated according to ACI-code. As a conclusion, when the splice length is 1.6 l_d, the bond stress permits the development of the complete glass FRP rebar tensile strength. From results, a glass FRP rebar modification factor of 1.3 should therefore be considered to be safe.

Zuo and Darwin, (2000) evaluated the effect of many parameters such as concrete strength, projection area of reinforced bar, type and ratio of coarse aggregate on the reinforcement splice strength. The total number of specimens were 64 beams that have dimensions, reinforcement, and load setup as shown in (Figure 2-24). The splice strength of bars confined by transverse reinforcement increases with an increase in relative rib area and bar diameter. The use of stronger coarse aggregate results in an increase in splice strength for bars both with and without confining reinforcement.

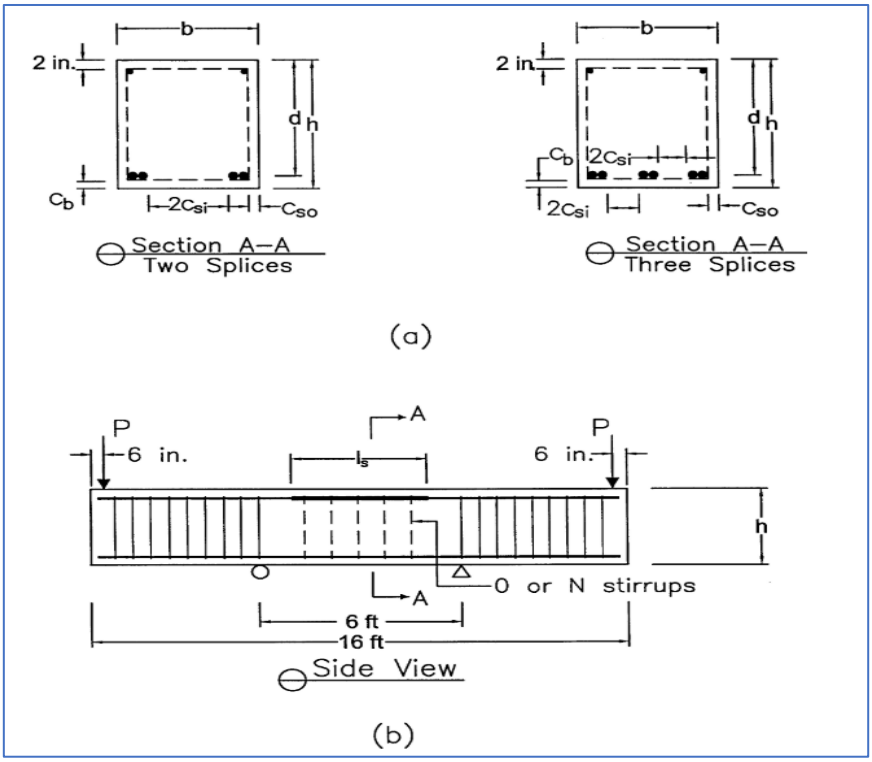

Figure 2-24: Beam splice specimens: (a) beam configuration as cast; and (b) test setup (Zuo and Darwin, 2000)**.**

Aly et al., (2006) studied the lap splice of FRP rebar under static four points loading. The effect of type of FRP, diameter, and splice length were studied. (Figure 2-25) shows the dimensions and details of 12 specimens in this research. Furthermore, an evaluation of the spliced FRP bars with (ACI 440.1R-03, CAN/CSA-S806-02, ISIS-M03-01, and CAN/ CSA-S6-00) is presented. The critical bond strength of spliced FRP bars is inversely proportional to the bar diameter and splice length.

Al-Khazragy, (2016) studied the effect of tensile lap splices on the behavior of reinforced RPC beams subjected to repeated loading. The main parameters that were studied are: repeated loading regime depending on the minimum to maximum load ratio of applied load (0%, 27% and 20), lap splice length ($20d_b$, $30d_b$ and $40d_b$), steel fiber volumetric ratio (2%, 1.75% and 1.5%), diameter of

tension spliced steel bars (12mm, 16mm and 20mm), concrete cover (30mm, 35mm and 40mm) and adding steel stirrups within the lap splice region.

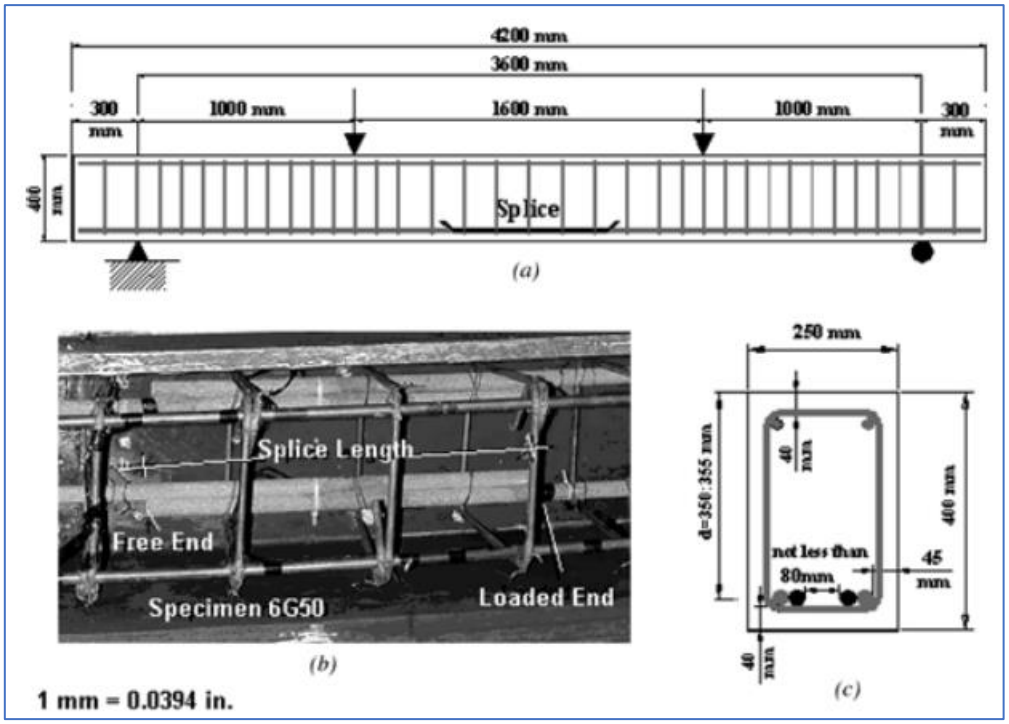

Figure 2-25: Typical cross section and details of tested beams: (a) elevation; (b) splice in beam before casting; and (c) cross section (Aly et al., 2006)**.**

All beams were simply supported and tested up to failure under the action of two-point loads. The experimental results shown that length of splice $20d_b$ was the critical value for splicing in RPC. Where this length was adequate under static load, but it is insufficient under repeated load. The splice length was improved with $30d_b$ and $40d_b$ for repeated applied load. The lap splice can be reduced with an increase in concrete cover and steel fiber ratio, also with provided stirrups at splice region. The FEM analysis was carryout to simulate model validated with experimental data. Computer program (ANSYS) used to perform the numerical part and it was obtained a good convergence from the experimental results. Thus, some of parametric study were investigated to give high understanding on the performance of lap splice in RPC.

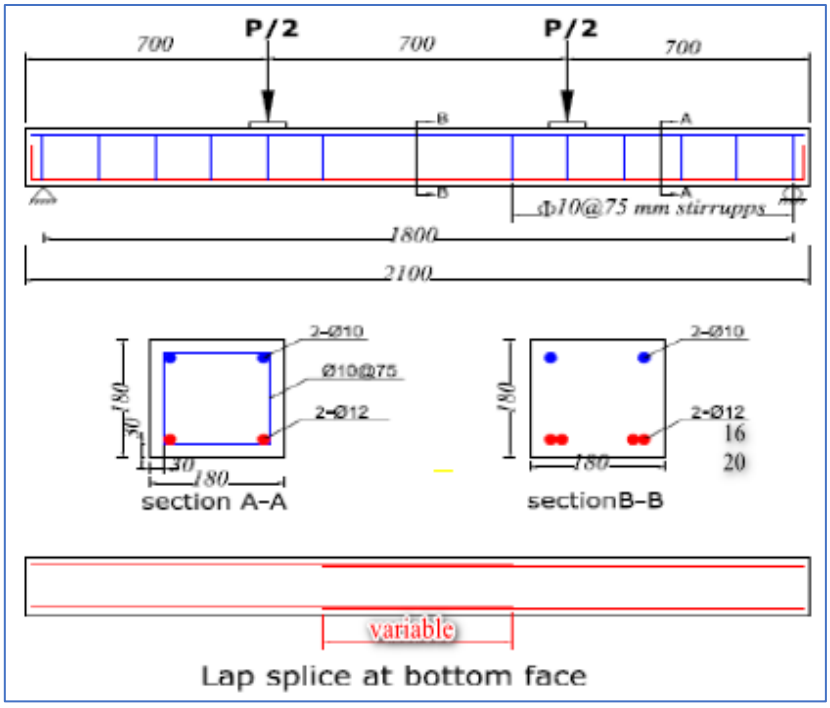

Figure 2-26: The details of beams specimens(Al-Khazragy, 2016).

Helal et al., (2016) studied the effect of posttensioned metal straps PTMS on behavior of short lap-splice RC beams. Twelve rectangular section beams were design to flexure failure, cast with two notches at mid span, and tested as simply supported. (Figure 2-27) shows the details of specimens and location of metal strap. The effect of confinement (no confinement, internal steel stirrups or external PTMS), bar diameter and concrete cover were examined. The unconfined control beams with short splices failed in a brittle manner due to splitting of the concrete cover around the splice. The use of external PTMS confinement delayed the splitting failure of the lap splices. In comparison to unconfined specimens, the PTMS confinement also enhanced the bond strength by up to 58 %.

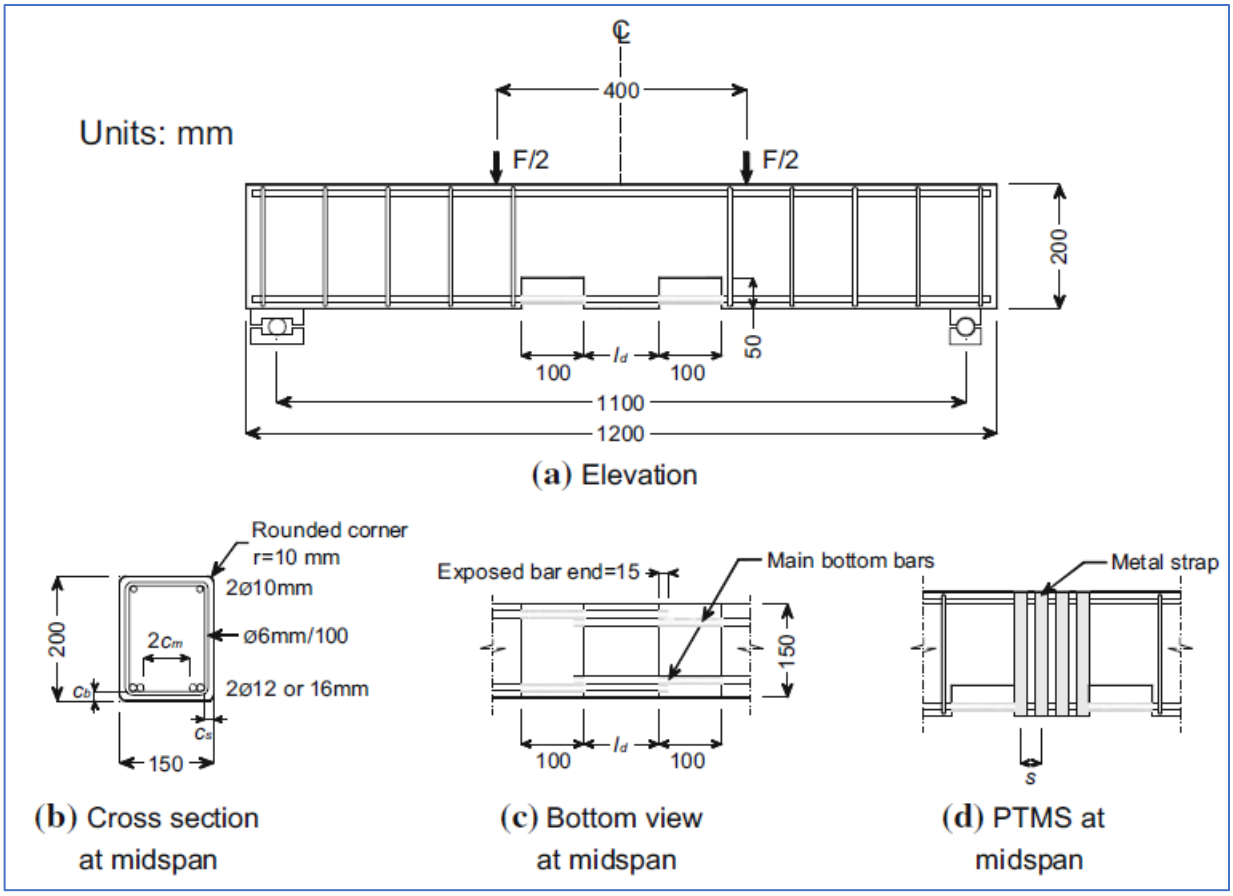

Figure 2-27: Geometry and reinforcement details of beams(Helal et al., 2016).

Tekle et al., (2017) investigated the effect of alkali activated concrete on the bond of spliced GFRP bar. For this research seven beams have dimensions (125, 180, and1600) mm as width, height, and total length, respectively. These beams were prepared, cast, and tested under flexural loading. The main investigated parameters were the splice length, compressive strength, bar diameter and stirrup confinement. The results and mode failure of all specimens show that the splitting of cover is adopted. This type of failure is caused by the radial component of the bond stress. This type of failure is referred to adequate splice length of bar and the tensile strength of concrete did not capable withstand the stress generate around GFRP. Numerical analysis by ABAQUS program was current in this study.

Dagenais and Massicotte, (2017) investigated the lab splice reinforcement in beam strengthened with UHPFRC subjected to cyclic load. Specimen reinforcement consists of two pairs of deformed bars spliced at midspan on both tension and compression faces. The strengthening technique consists of replacing normal concrete around lapped bars in the splice region by UHPFRC, which allows for keeping the original member geometry. UHPFRC with three fiber contents, 2 bar diameters, and two splice arrangements were used. The result indicates that UHPFRC with a fiber content of 2 or 3% can significantly increase the bond strength of splice bars without confinement.

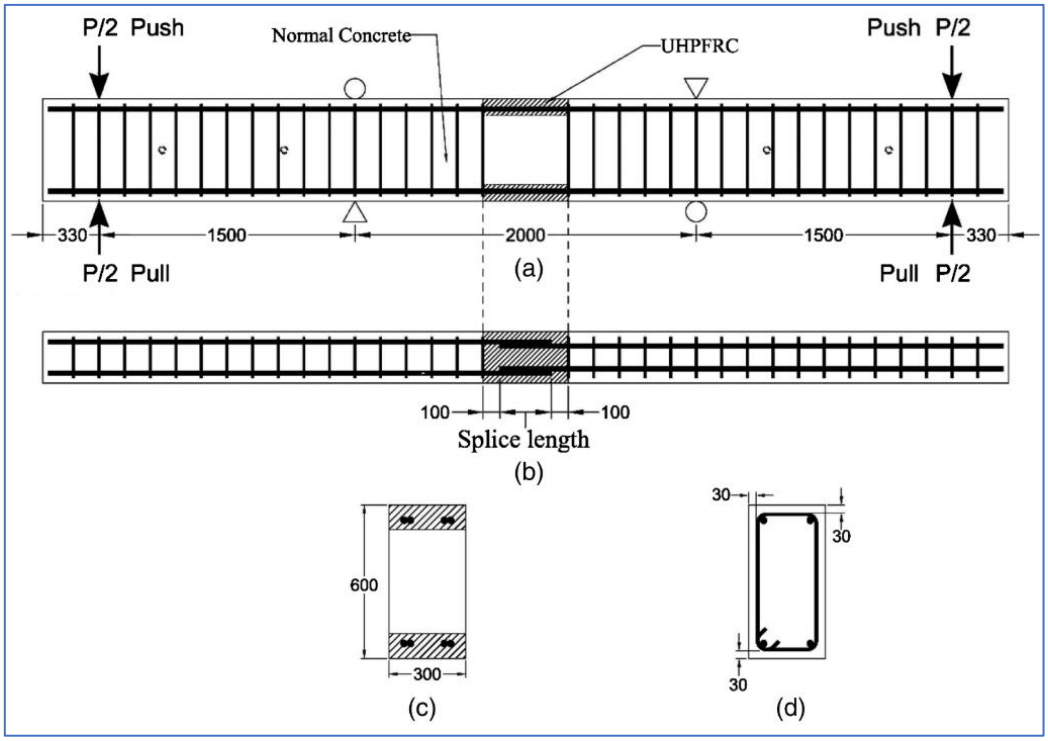

Figure 2-28: Specimen dimensions and reinforcement details: (a) side view; (b) top view; (c) cross section at midspan; (d) stirrups and cover details (Dagenais and Massicotte, 2017).

Michaud et al., (2021) aimed to estimate the development length of a commonly used sand coated GFRP standard bar size (17.2 mm) embedded in UHPC with different of used fiber and percentage. Also, this study deals with the specimens

have small clear cover in UHPC. The investigation has cast and test 28 notched beam under four point-load. The result shown that the used of steel fiber and increased its quantity led to increase the average bond strength more than PVA fiber. The percentage of steel fiber inversely proportion with embedment length.

Equation 2-1 is suggested for L_d of sand-coated GFRP bars in UHPC, based on a linear regression of the experimental results in (Figure 2-29) and take cover-to-diameter ratio of 1.0. It captures the effects of fiber type and content in the UHPC mix, indirectly, through f'$_c$. Values of L_d calculated by this equation converge to those calculated by ACI440.1R-15 and CAN/CSAS806-12 as f'c reduces towards 45–55 MPa.

$$\frac{L_d}{d_b} = \frac{1538}{\sqrt{f'_c}} - 113 \qquad \ldots\ldots\ldots\ldots\ldots\ldots\ldots\ldots \quad (2\text{-}1)$$

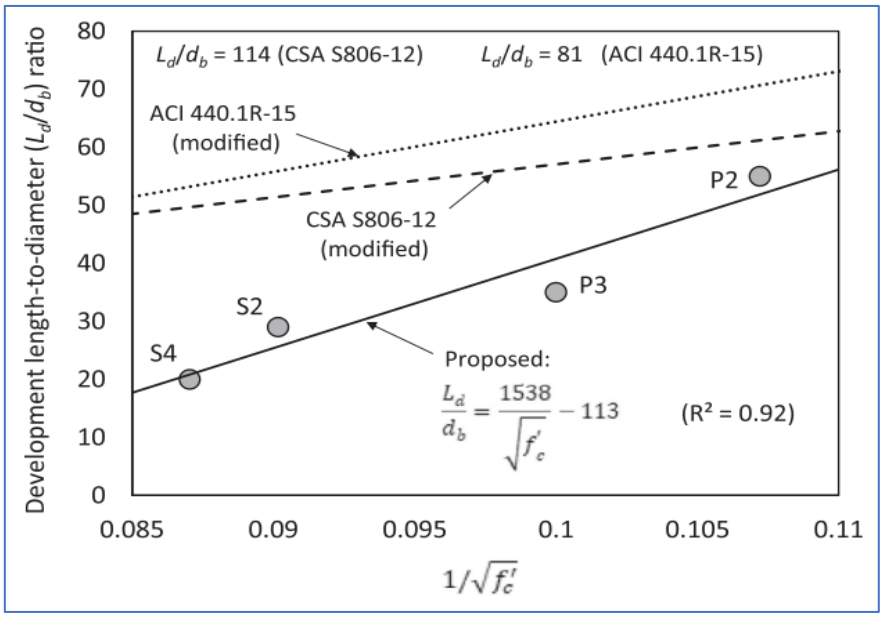

Figure 2-29:Variation of axial GFRP bar stress at failure embedment length (Michaud et al., 2021).

2-6 Summary and Concluding Remarks

From the review of the previous study on the spliced beams for many researchers, the following points can be concluded:

- The joint region is the weak point of the segmental beams due to the discontinuity of the steel reinforcement and concrete.
- The presence of epoxy in the joint region led to an increase the shear capacity for segmental girders, but it was giving a sudden failure.
- Shear keys improved the structural performance of the splice girder with a post-tension system. The provider of the shear key led to an increase in the area friction. Thus, it increased the connection and interlocking between segments.
- The segmental girders had less load capacity under combined stresses as compared with only shear or bending stress.
- Location of joint has high importance in terms of ultimate load and mode of failure due to specifying the stresses that caused the failure.
- The overall performance of spliced girders was improved when using and increasing the force of the post-tension system and the area of strands, where the ultimate load increased by 16% when increasing the tension force by 100%. This improvement increased the connection between segments and thus obstructed the failure plane.
- Utilizing the CFRP product for strengthening had the benefit of enhancing the behavior of splice girders. CFRP can be used as a sheet laminate in the joint region with a different scheme or as a bar with an NSM system. Both methods improve the ultimate load, deflection, ductility, and stiffness of splice girders.
- Utilizing the UHPC as new concrete at the joint increased the ultimate load and ductility of the splice girder, especially when the steel fiber ratio increased to 2%.

- Using a hybrid concrete section improves some of the mechanical and physical properties of the structural member.
- The presence of FRP to hybridize the reinforcement of RC members led to improve the overall structural performance.
- The length of the UHPC joint ranged from 150- 200 mm to achieve an adequate bond mechanism. For cyclic load found, the $30d_b$ for straight lap splice bar was necessary to transform the stresses safely.

From the previous literature, the use of the deck spliced girders (T cross section) with hybrid concrete were not investigated enough. Also, the depth of joint, location of joint, and reinforcement hybridization were not studied previously. At the same time, other parameters, such as the UHPC shear key, presence of dowels, and cyclic load, will be studied to increase knowledge and understand the hybrid splice girders further.

2-7 Originality of the Study

The original main points of hybrid reinforced concrete deck spliced girders of this research work are:

1. Using the UHPC in deck and joint.
2. Studying the location of joints in continuous girders.
3. Using the shear key system.
4. Hybridization of reinforcement internally.
5. Transforming the multi-simple span girders to continuous girders.

Chapter Three

Experimental Work

3-1 Introduction

The main goal of this study was to investigate the structural behavior of reinforced hybrid concrete spliced deck girders under the effect of monotonic and repeated load. This part referred to the details of experimental program deals with the description of specimens, material properties, preparation, cast, curing, and test of specimens. The design of specimen and length of joint explained in (Appendix A). In addition to definitions for the main variables and the symbols of girders with some of schemes to illustrate the groups of girders. Figure 3-1 presents a summary of the experimental program. The experimental program was performed at the Structural Laboratory of Civil Engineering Department in the University of Babylon.

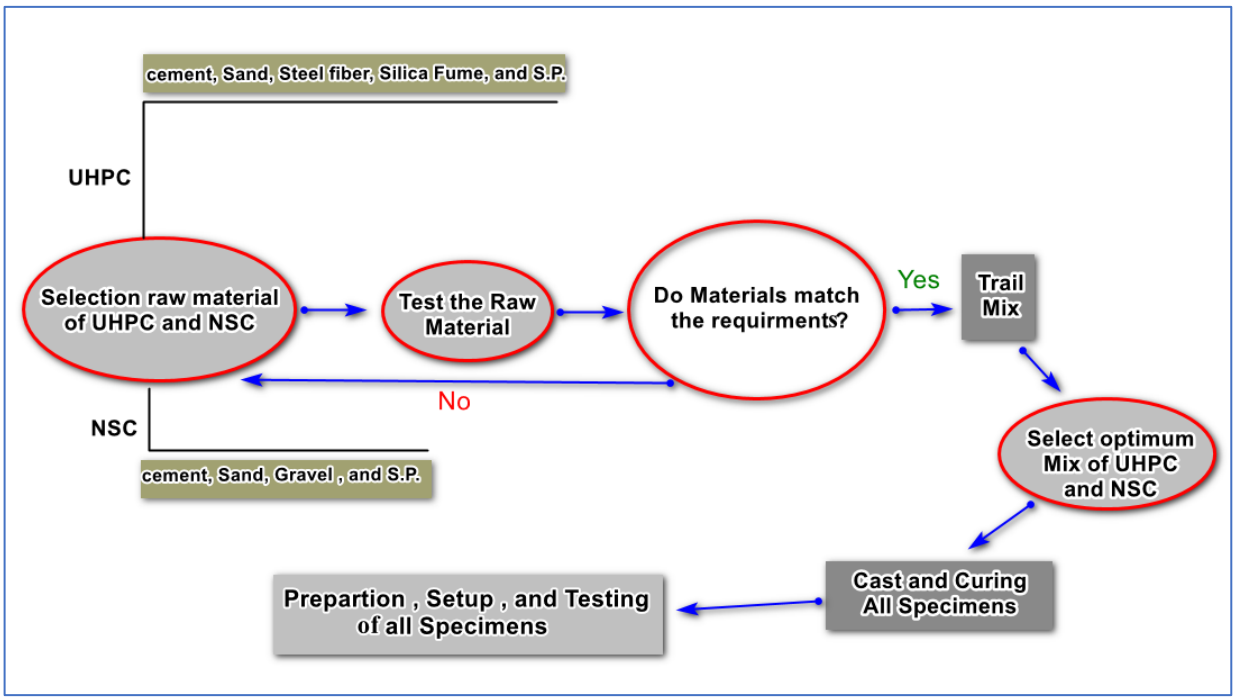

Figure 3-1: Summary of experimental program.

3-2 Description of Specimens

Twenty-one models of T-cross section girders used to perform this work. The experimental program has two main groups with respect to support condition simply supported and continuous girders. For all specimens, the web cast by NSC except the joint region and the deck cast with UHPC, and joint region also cast with UHPC have 2% steel fiber ratio to reduce shrinkage and obtained good mechanical properties of concrete (Eren and Marar, 2010).Many variables that studied in this research such as depth of joint, Hybridization of reinforcement, location of joint, and shear key. The name of symbol specimens is as shown in Figure 3-2. The variable, symbols, and all details are explained in Table 3-1 and Table 3-2.

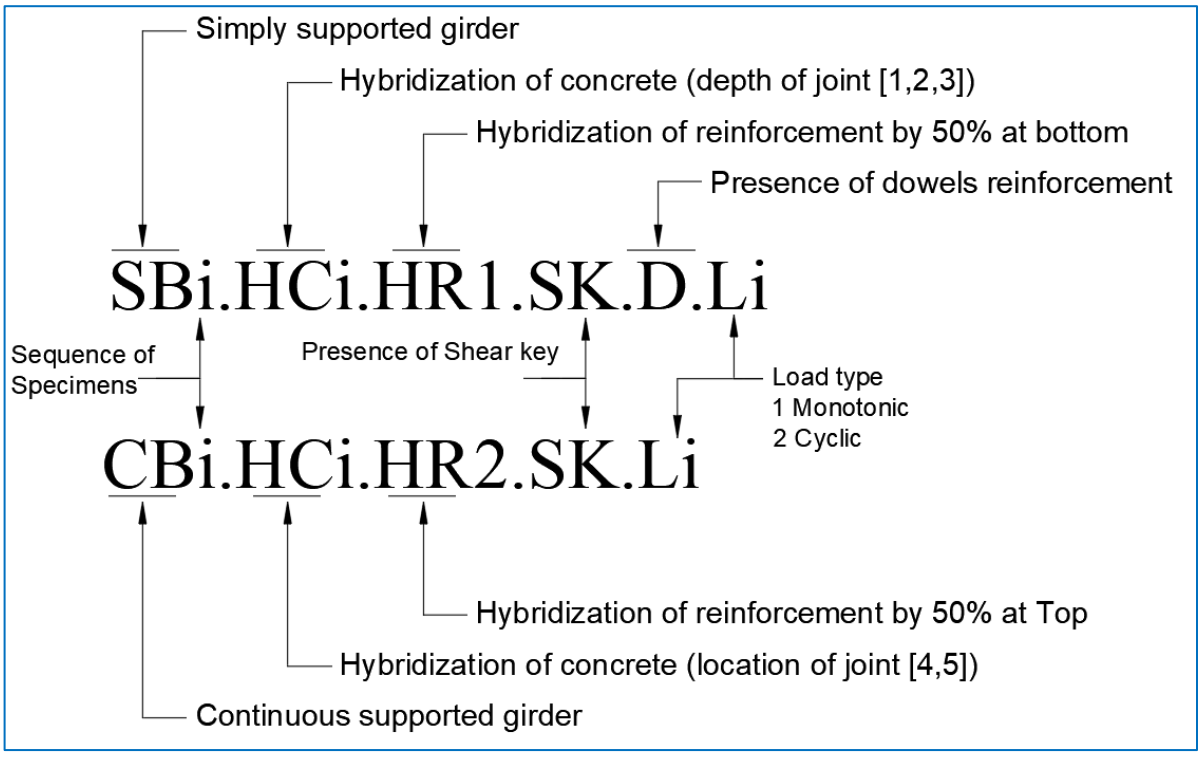

Figure 3-2: Description of symbol for specimens.

3-2-1 Simply supported girders

All girders of this group have total length 1700 mm, and supported length 1500 mm. The T shape cross-section and reinforcement will be shown in the next figures. The three-point load at mid span of girder was adopted for this group. Table 3-1 illustrates details of this group and variables adopted.

1- HC_1: Control girders were cast as one unit (without joint: deck of UHPC and web of NSC) and detailed as shown in Figure 3-3.
2- HC_2 and HC_2.SK: Girders with two joints, casting the web of NSC and deck of UHPC monolithically as precast unit. while, casting the joint region with UHPC for full depth. The first without shear key Figure 3-4 and other with shear key Figure 3-5 .
3- HC_3, HC_3.SK, HC_3.HR_1, HC_3.D: Girders with two joints, casting the web with NSC as precast unit. while, casting the joint region and deck of UHPC monolithically. The figures show the dimensions and reinforcement of this parameter such as without shear key Figure 3-6 , with hybrid reinforcement Figure 3-7,with shear key Figure 3-8, and with additional dowels Figure 3-9.

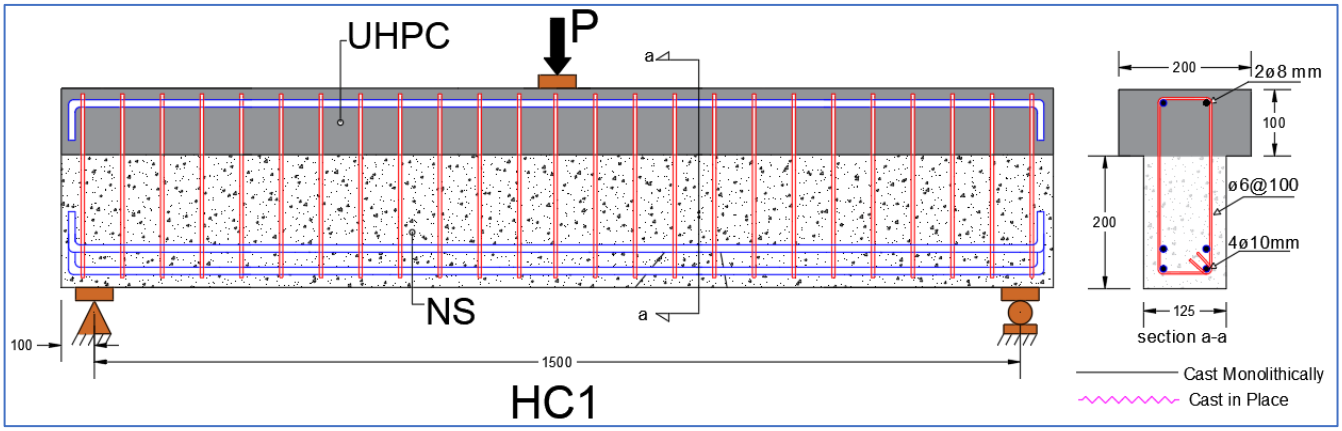

Figure 3-3: Details of control girders ($SB_1.HC_1.L_1$, $SB_7.HC_1.L_2$).

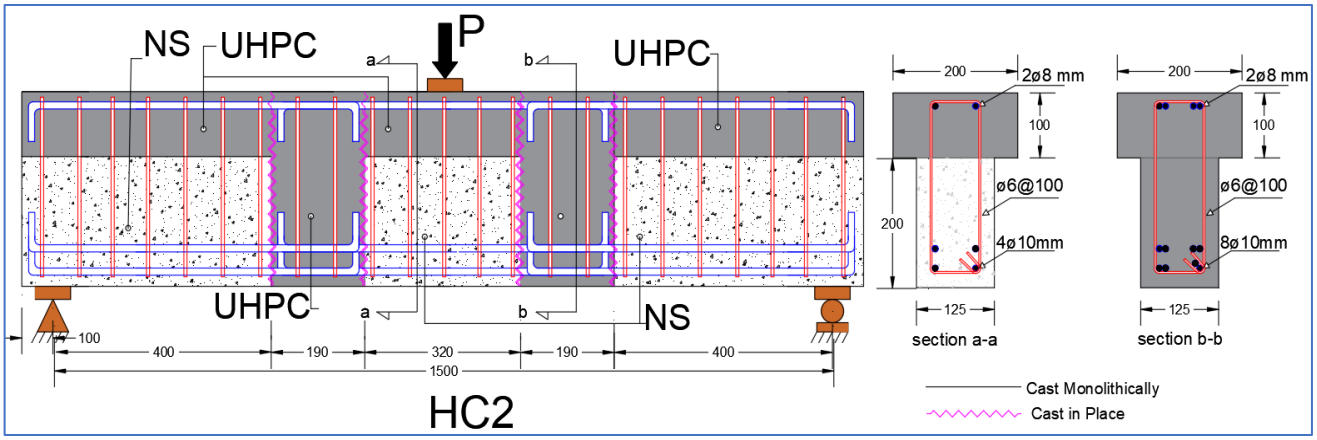

Figure 3-4: Details of full depth joint girders ($SB_2.HC_2.L_1$, $SB_8.HC_2.L_2$).

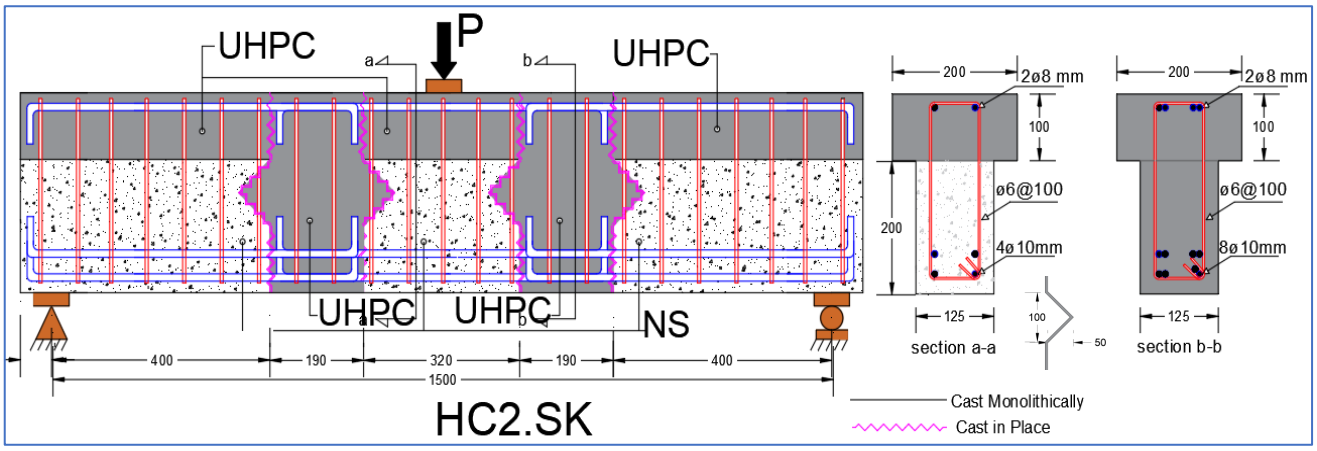

Figure 3-5: Details of full depth joint girders with shear key ($SB_5.HC_2.SK.L_1$, $SB_{10}.HC_2.SK.L_2$).

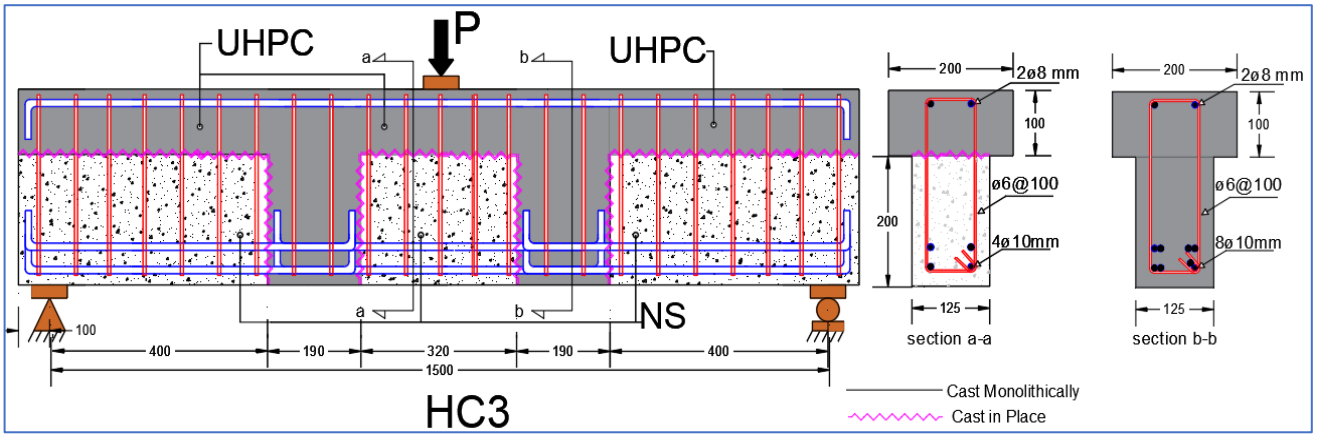

Figure 3-6: Details of partial depth joint girders ($SB_3.HC_3.L_1$, $SB_9.HC_3.L_2$).

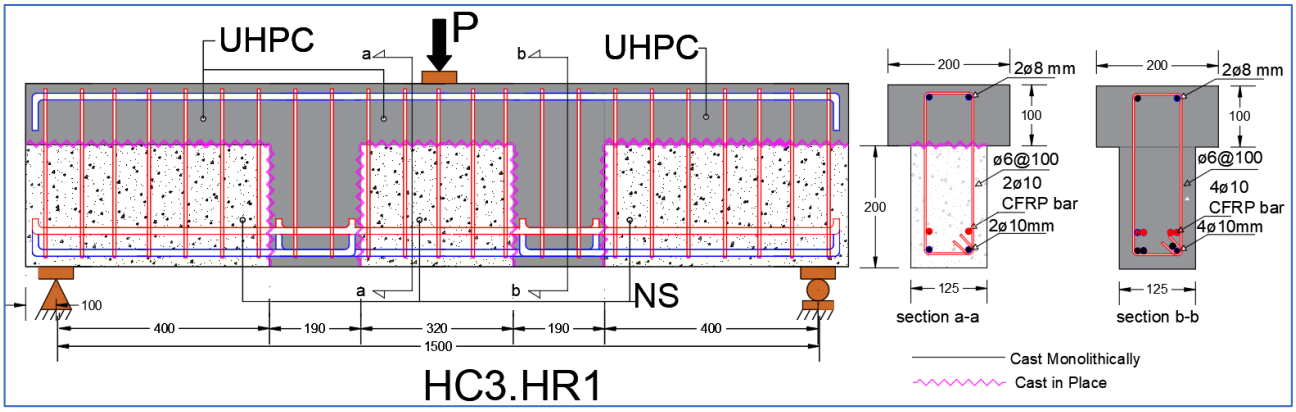

Figure 3-7: Details of partial depth joint girders with Hybridization of reinforcement ($SB_4.HC_3.HR1.L_1$).

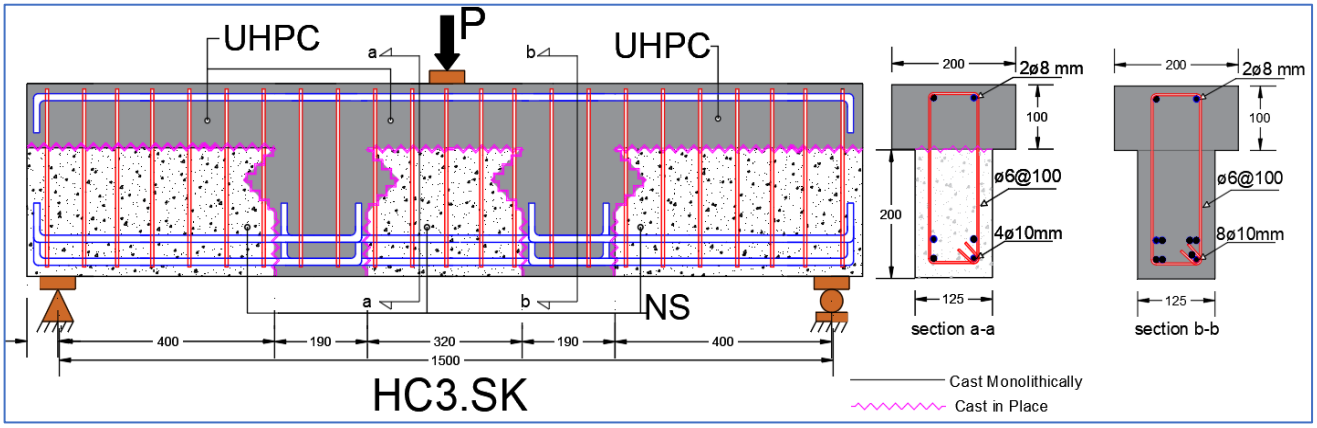

Figure 3-8: Details of partial depth joint girders with shear key ($SB_6.HC_3.SK.L_1$, $SB_{11}.HC_3.SK.L_2$).

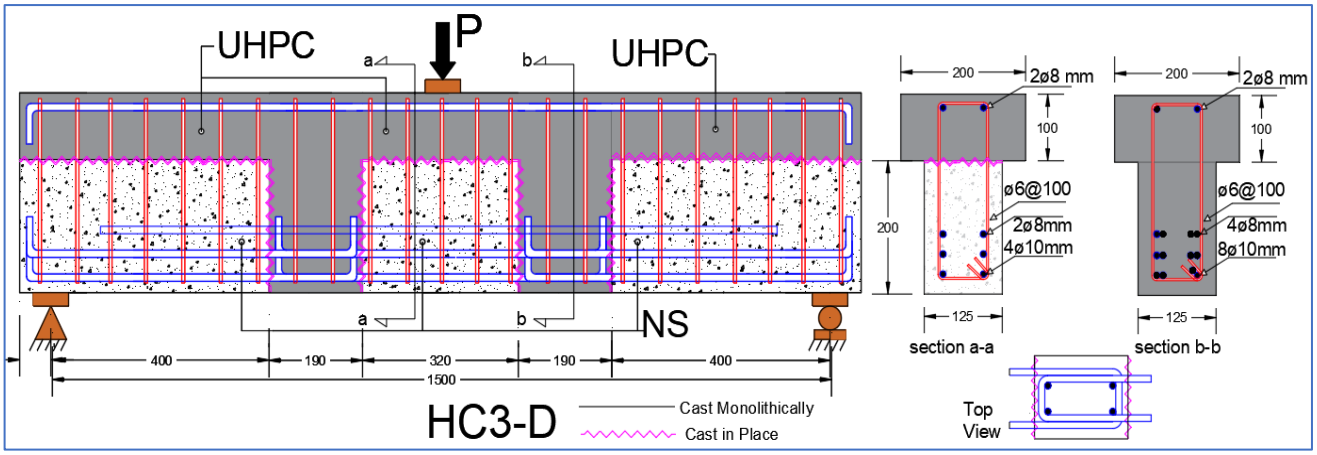

Figure 3-9:Details of partial depth joint girders with additional dowels ($SB_{12}.HC_3.D.L_1$).

Table 3-1: Symbol and details of simply supported girders.

Parameter (Variable)	Symbol	Type of Reinforcement	Shape of joint	Depth of vertical joint	Type of load
Reference (Control)	$SB_1.HC_1.L_1$	Steel 100%	No joint	No joint	Monotonic
	$SB_7.HC_1.L_2$	Steel 100%	No joint	No joint	Cyclic
Depth of Joint Region	$SB_2.HC_2.L_1$	Steel 100%	Flat	Full depth	Monotonic
	$SB_8.HC_2.L_2$	Steel 100%	Flat	Full depth	Cyclic
	$SB_3.HC_3.L_1$	Steel 100%	Flat	Partial depth (web)	Monotonic
	$SB_9.HC_3.L_2$	Steel 100%	Flat	Partial depth (web)	Cyclic
Hybrid Reinforcement	$SB_4.HC_3.HR1.L_1$	50% steel 50% CFRP bar	Flat	Partial depth (web)	Monotonic
Shear Key	$SB_5.HC_2.SK.L_1$	Steel 100%	Key	Full depth	Monotonic
	$SB_{10}.HC_2.SK.L_2$	Steel 100%	Key	Full depth	Cyclic
	$SB_6.HC_3.SK.L_1$	Steel 100%	Key	Partial depth (web)	Monotonic
	$SB_{11}.HC_3.SK.L_2$	Steel 100%	Key	Partial depth (web)	Cyclic
Dowel Action	$SB_{12}.HC_3.D.\ L_1$	Steel 100%	Flat	Partial depth (web)	Monotonic

3-2-2 Continuous girders

All girders of this group have two similar spans with total length 3200 mm and supported length 3000 mm, the T shape cross-section and their reinforcement will be shown in next figures. A point load at mid of each span of girder was adopted for this group. Table 3-2 illustrates this group with all details and variables.

1- HC_1: Control girders were cast web of NSC and deck of UHPC as one unit and detailed as shown in Figure 3-10

2- HC_4, HC_4.SK ,HC_4.HR2: Girders with one joint at support, cast the precast web with NSC. Then after that, casting the joint region and deck with UHPC monolithically. The figures show the dimensions and reinforcement of this parameter such as without shear key Figure 3-11, with shear key Figure 3-12 , and the hybridization of reinforcement Figure 3-13 .

3- HC_5 , HC_5.SK: Girders with two joints at inflection point, casting the precast web with NSC. Then after that, casting the joint rejoin and deck of UHPC monolithically. The figures show the dimensions and reinforcement of this parameter such as without shear key Figure 3-15 and with shear key Figure 3-15

Table 3-2: Symbol and details of continuous girders.

Variable	Symbol	Type of Reinforcement	Shape of joint	Number of joint(mm)	Type of load
Control	$CB_{13}.HC_1.L_1$	Steel 100%	No joint	No joint	Monotonic
	$CB_{19}.HC_1.L_2$	Steel 100%	No joint	No joint	Repeated
Location of Joint Region	$CB_{14}.HC_4.L_1$	Steel 100%	Flat	One joint	Monotonic
	$CB_{20}.HC_4.L_2$	Steel 100%	Flat	One joint	Repeated
	$CB_{15}.HC_5.L_1$	Steel 100%	Flat	Two joints	Static
	$CB_{21}.HC_5.L_2$	Steel 100%	Flat	Two joints	Repeated
Hybrid Reinforcement	$CB_{16}.HC_4.HR2.L_1$	50% steel 50% CFRP bar	Flat	One joint	Monotonic
Shear Key	$CB_{17}.HC_4.SK.L_1$	Steel 100%	Key	One joint	Monotonic
	$CB_{18}.HC_5.SK.L_1$	Steel 100%	Key	Two joints	Monotonic

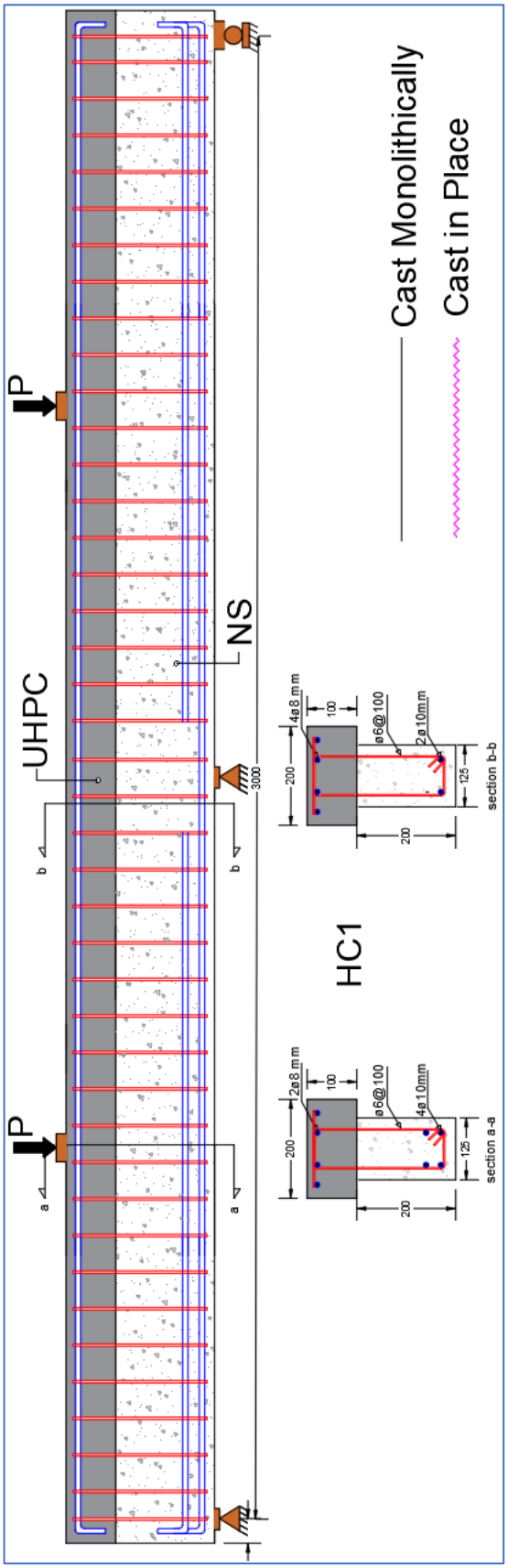

Figure 3-10: Details of control continuous girders ($CB_{13}.HC_1.L_1$, $CB_{19}.HC_1.L_2$).

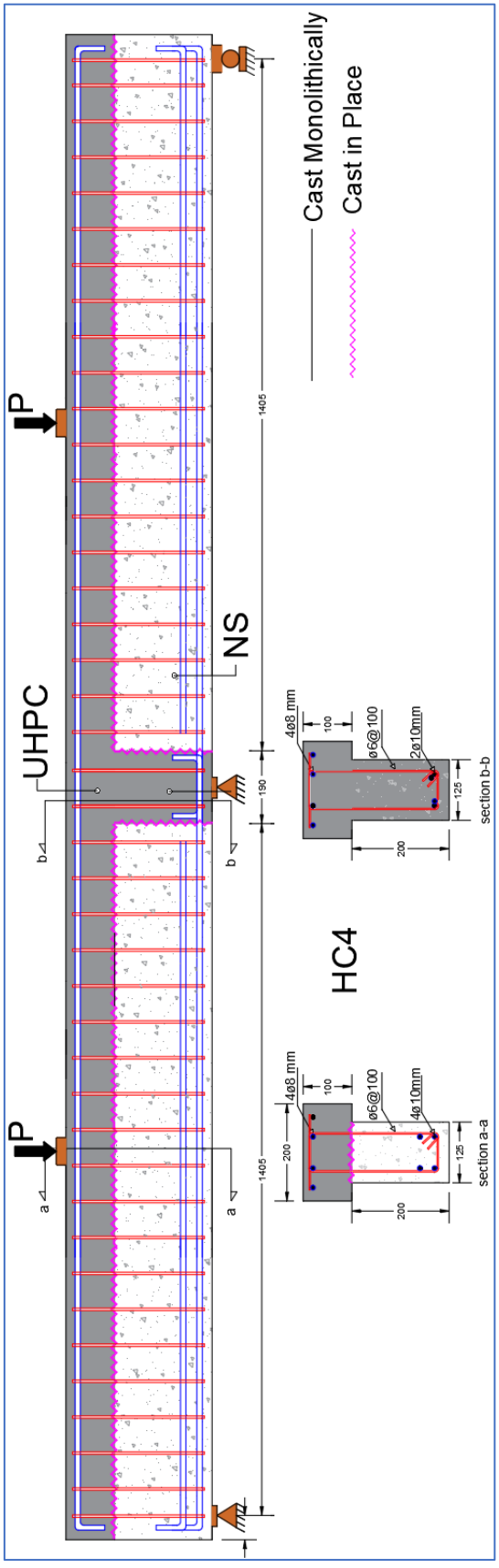

Figure 3-11: Details of continuous girders with joint at support ($CB_{14}.HC_4.L_1$, $CB_{20}.HC_4.L_2$).

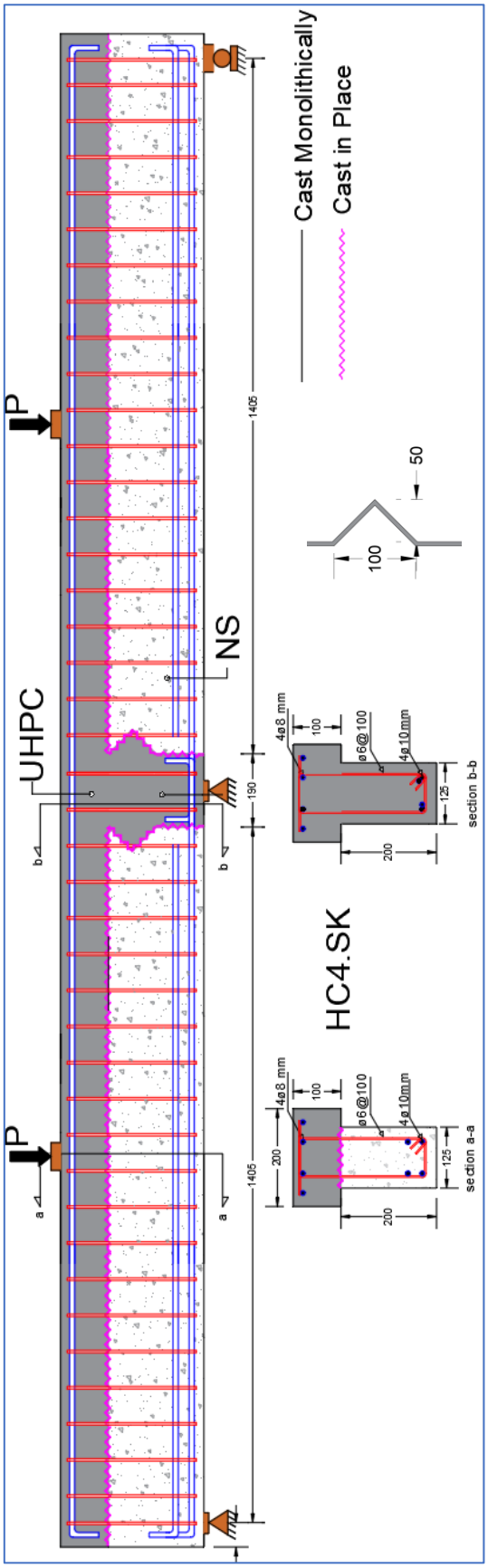

Figure 3-12: Details of girders with shear key joint at support ($CB_{17}.HC_4.SK.L_1$).

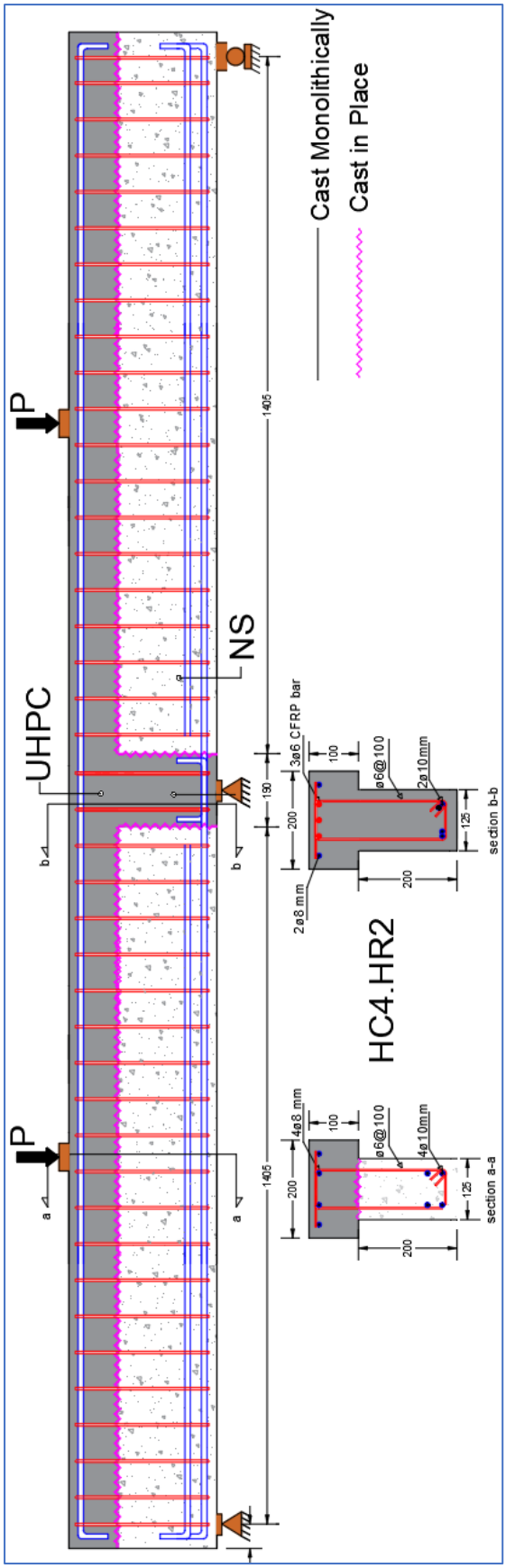

Figure 3-13: Details of girders with joint at support and hybridization of reinforcement ($CB_{16}.HC_4.HR2.L_1$).

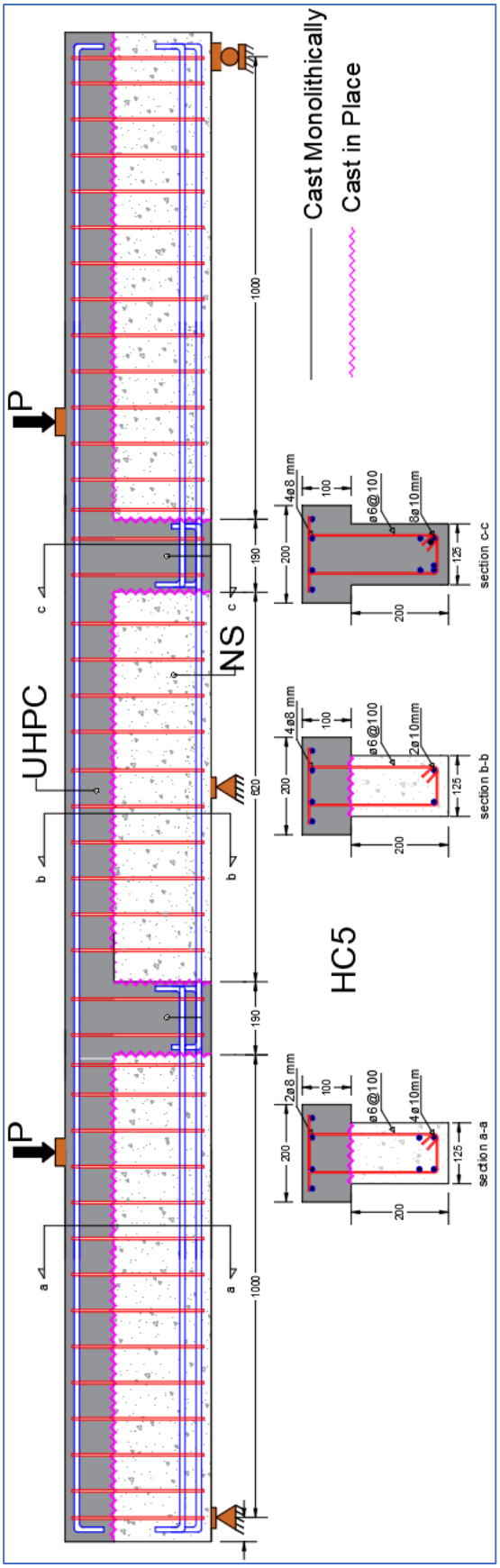

Figure 3-15: Details of continuous girders with joints at inflection point ($CB_{15}.HC_5.L_1$, $CB_{21}.HC_5.L_2$).

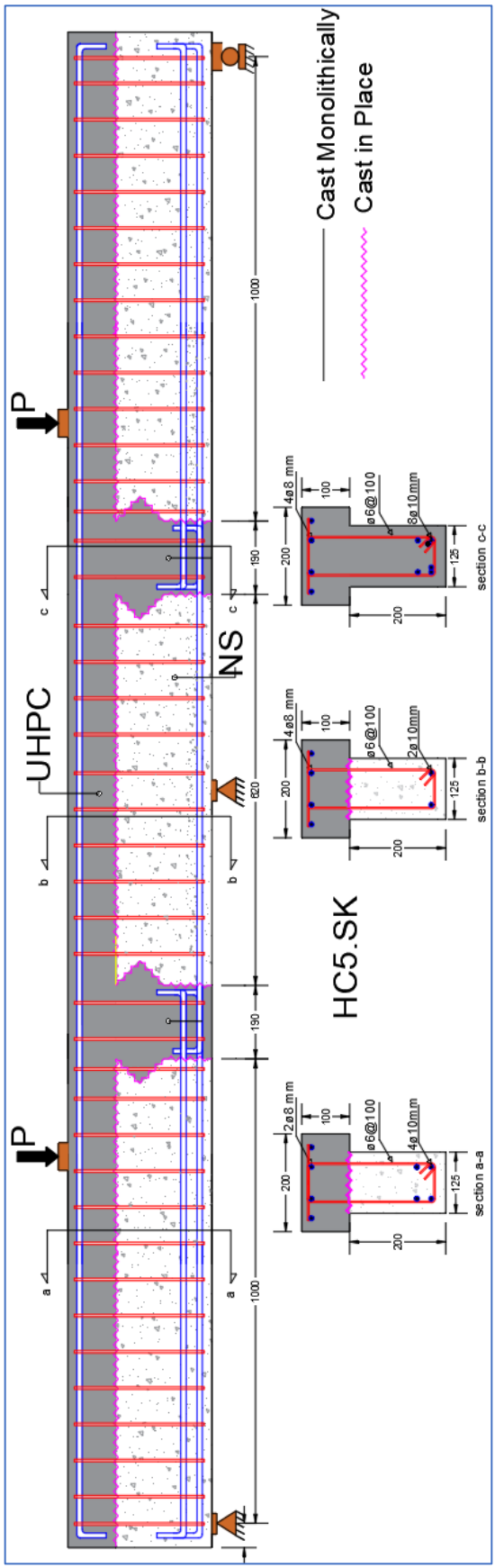

Figure 3-14: Details of girders with shear key joints at inflection point ($CB_{18}.HC_5.SK.L_1$).

3-3 Materials Properties

3-3-1 Cement

Sulphate resisting Portland cement (type v) was used in this work to produce the NSC and UHPC because it gives better compressive strength in trial mixes. This type of cement (Aljisir Cement) was produced in Sulaymaniyah factory-Iraq. This type was satisfied the limits of Iraqi specification No.5/1984. Test results of chemical and physical properties are shown in **Appendix B**.

3-3-2 Fine Aggregate

Natural sand was used in mixture of NSC. Very fine sand with largest size of granule (0.6 mm) was used for UHPC mixtures only. It was separated by sieve analysis for the natural sand by sieve (600 μm). Results of sieve analysis of the natural sand are shown in **Appendix B**, these results were compatible with the limits of Iraqi specification No.45/1984.

3-3-3 Coarse Aggregate

The gravel used was obtained from AL-Nibaai region in Iraq with a maximum size of (14 mm). The gravel was washed and cleaned by water, later it was left in air to dry before use. The gravel used conforms to the Iraqi specification **(**IQS, No.45:1984). The grading and other properties of this type of aggregate are shown in **Appendix B**.

3-3-4 Steel fiber

Micro steel fiber gold coated as shown in Plate 3-1,was used in mixing of UHPC. The properties of this material listed in Table 3-3. This type of steel fibers confirms the requirements of (ASTM A820M-04, 2004).

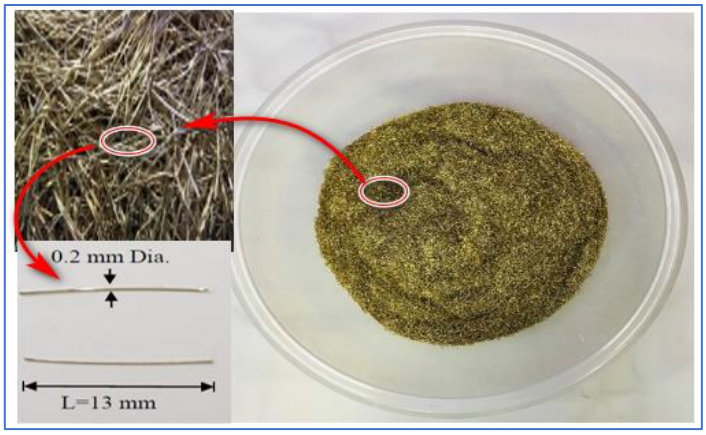

Plate 3-1: Micro steel fiber used in UHPC.

Table 3-3: Steel fiber properties.

Property*	Specification
Shape	straight
Diameter	0.22 mm
Length	13.1 mm
Tensile strength	3005MPa
Density	7800 kg/m3
Aspect ratio(L/D)	59

* supplied by the manufacturing company

3-3-5 Silica fume

A grey fine powder silica fume MasterRoc MS 610 from BASF chemical company was added to cement in production of UHPC, as shown in Plate 3-2. The constituent of this type of silica fume was listed in Table 3-4 . The results show that there was conformable with standard specification of **(ASTM C1240-15, 2015).**

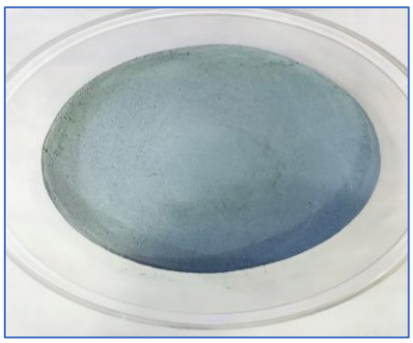

Plate 3-2: Silica fume used in UHPC.

Table 3-4: Technical data of silica fume.

Property*	Specification
Form	Powder
Color	Grey
Density	0.55 - 0.7 kg/l
Chloride content	<0.1%

* supplied by the manufacturing company

3-3-6 Super plasticizer

In mixing of UHPC, a high range water reducer named **MasterGlenium 54** was used to provide super strength and better flow for mix. It follows the (ASTM C494-15, 2015). Table 3-5 reports the major properties of **MasterGlenium 54.**

*Table 3-5: Properties of **MasterGlenium 54***

Property*	Specification
Form	Viscous liquid
Color	Whitish to straw
Relative density	1.07 gm/cmP3P @25PoPC
PH	5-8

* According to the certificate of conformity

3-3-7 Water

The tab water was used for mixing and curing all girder specimens and control samples.

3-3-8 Steel reinforcement

In this study, three different bar diameters were used for reinforcement of girders specimen as shown in figures from Figure 3-3 to Figure 3-15. The yield and ultimate stresses for these bars are listed in Table 3-6. Tensile tests on three specimens for each bar size according to (ASTM A615M-15, 2015) have been

carried out. This test has been carried out in the laboratory of Mechanical Engineering Department of Babylon University using tensile testing machine as shown in Plate 3-3. Bars 10 and 8-mm diameter were used in Bottom and Top longitudinal reinforcement respectively, as well as the bar 6 mm diameter was used for stirrups reinforcement as shown in Plate 3-4.

Table 3-6: Properties of Steel Reinforcement Bars

Nominal Diameter mm	Actual Diameter mm	Yield Stress (MPa)	Ultimate Stress (MPa)	Modulus of Elasticity* (GPa)
10	9.91	585	668	200
8	7.4	375	572	200
6	5.82	317	541	200

*Assumed

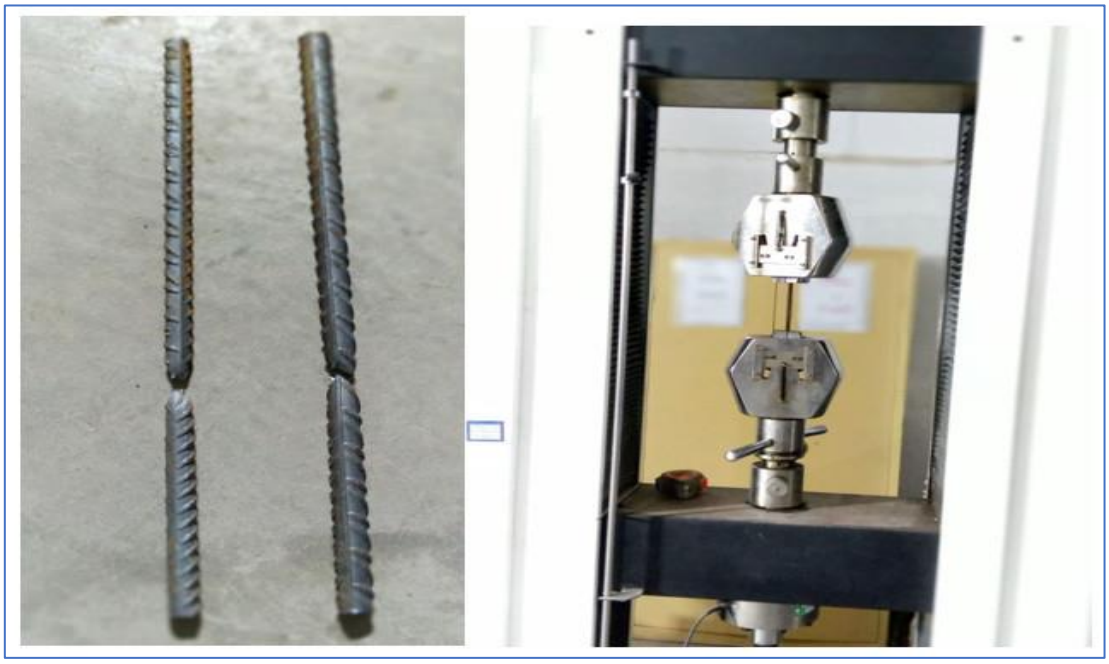

Plate 3-3: Test of steel reinforcement.

Plate 3-4:Steel reinforcement used in this work.

3-3-9 Carbon Fiber Reinforcement Polymers (CFRP) Bars

Sika CarboDur Rods CFRP bars with nominal diameter of (10 and 6 mm) sand coating have been used for embedded to reinforcement hybridization in the experimental work of this study. CFRP rebar, has high specific strength and excellent mechanical performance. It's had greatest tensile strength as compared with steel and GFRP bars as well as the weight of these bars was about 20 % of steel reinforcing bars. Table 3-7 shows properties of this type as supplied from the manufacture **(Appendix B).** The results were acceptable according to the standard specification (ASTM D7205M-06, 2011)(Standard Test Method for Tensile Properties of Fiber Reinforced Polymer Matrix Composite Bars **)**.

Table 3-7: Mechanical properties of CFRP bars.*

Nominal Diameter (mm)	Actual Diameter (mm)	Tensile strength (MPa)	Modulus of Elasticity (GPa)
10	9.53	1716	155
6	6.35	1755	155

*As per manufacturing data sheet

3-4 Formwork

The formwork of spliced girders used in this work made from ply wood with thickness 10 mm and supported the pieces by small steel nails. The joint region was separated by small part of same plywood had the cross section of the required model. The shear key was implemented by steel plate with a thickness 1 mm, cut and bent as required and fixed on the plywood partitions with small nails. Plate 3-5 illustrates formworks for spliced girders and shape of shear key.

Plate 3-5: Formwork of girders and shear key.

3-5 Concrete

3-5-1 Normal strength concrete (NSC)

The web of girders was cast with NSC by using mixer have capacity (0.15 m^3). The component of concrete mix was adequate to the standard characteristics of concrete material. Mix proportion used in this study as shown in (Figure 3-16). Samples were cast to estimate the mechanical properties of NSC such as cube with (150*150*150) mm, cylinders with 300 mm height and 150 mm diameter, and prisms with section (100*100) mm and length 400 mm. **Appendix C** shows the number of control samples and the method of calculation of each test type to estimate the mechanical properties.

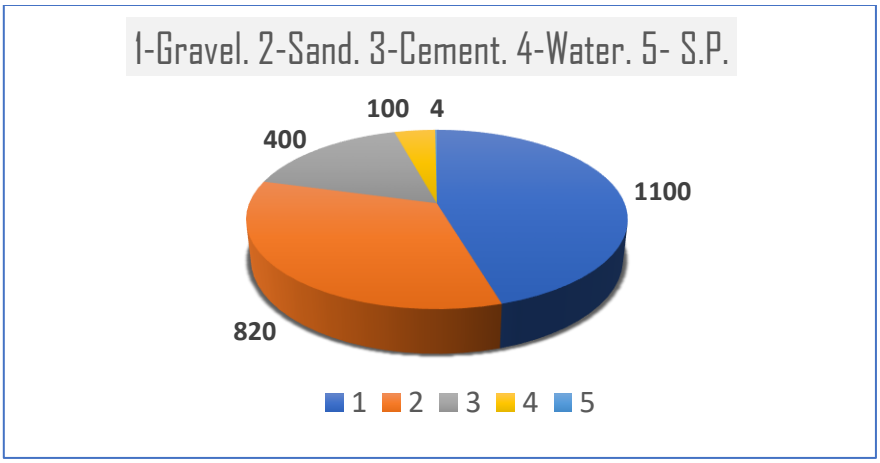

Figure 3-16: Mix proportion of NSC

3-5-2 Ultra High-Performance Concrete (UHPC)

The flange of girders and joint region for 21 girders were cast with UHPC only for all specimens. Many trial mixes were made to achieve the suitable mix that verified the requirement of strength and workability, Table 3-8 shows the details of trial mix for UHPC. Samples were cast to estimate the mechanical properties of UHPC such as cube with (50*50*50) mm, cylinders with 300,150 mm height and 150,100 mm diameter, and prisms with section (50*50) mm and length 200 mm. Appendix C shows the number of control samples and the method of calculation of each test type.

Table 3-8: Trial mix of UHPC

Trail No.	Cement kg/m^3	Micro Silica kg/m^3	Sand kg/m^3	Steel fiber kg/m^3	$w/binder$ %	Superplasticizer %	Flow %	Compressive strength @7-day Mpa	Compressive strength @28-day Mpa	Density kg/m^3
1 2/2/2021	853	214 Commix	1069 Pass from 4.75mm	157(2%)	18	1.5 Mag3000	82	63.5	91.2	2503
2 2/2/2021	853	214 Commix	1069 Pass from 4.75mm	157(2%)	17.5	2 Mag3000	144	51.82	86	2474
3 10/2/2021	950	210 Commix	1050 Pass from 0.6mm	157(2%)	16	4.5 Mag3000	105	74		2490
4 14/2/2021	856	214 PASF	1070 Pass from 4.75mm	157(2%)	16	3 GLENIUM 54	150	81.1	99.5	2567

Trail No.	Cement kg/m^3	Micro Silica kg/m^3	Sand kg/m^3	Steel fiber kg/m^3	$w/binder$ %	Superplasticizer %	Flow %	Compressive strength @7-day Mpa	Compressive strength @28-day Mpa	Density kg/m^3
5 14/2/2021	950	210 PASF	1050 Pass from 0.6mm	157(2%)	16	3 GLENIUM 54	130	84.19	104.75	2510
6 15/2/2021	860	215 PASF	1075 Pass from 4.75mm	157(2%)	15	3 GLENIUM 54	120	76.16	89.81	2546
7 1-3-2021	950	210	1050	157	15	3	220	83.62	101.5	2485 2538
8 1-3-2021	858	215	1077	157	15	3.5	220	69.84	93.6	2752
9 15-3-2021	960 KARASTA	240	1040	157	16	4 Pc200	220	87.28	96.87	2466.67
10 15-3-2021	950 KARASTA	210	1050	157	16	5 Pc200	240	78.9	112	2536
11 15-3-2021	950 **AL-JESR**	210	1050	157	16	5 Pc200	230	82.7	116.8	2490.6
12 16-3-2021	960 KARASTA	240**	1040	157	18	6 Pc200	No flow	fail		
13 16-3-2021	960 KARASTA	240	1040 90%0.6mm+ 10%0.075mm	157	16	5 Pc200	230	70	100.14	2453.33
14 17-3-2021	960 KARASTA	240	1040	157	16	5 sicka	240		110.675	
15 28-3-2021	960 AL-JESR	240 conmix	1040	157	16	5 PC200	240	89.7	114.25	2456
16 28-3-2021	960 AL-JESR	240 PASF	1040	157	16	2.5 Gilinume 54	250	91.53	123.26	2472
17 28-3-2021	960 AL-JESR	240 PASF	1040	157	15	5 PC200	240	89.3	127.485	2480
18 29-3-2021	960 AL-JESR	240 PASF	1040	157	14	3 Gilinume 54	190	104.5		2522.7
19 29-3-2021	950 **AL-JESR**	210	1050	157	15	2.5 Gilinume 54	200	114.16	132.81	2506.7
20 30-3-2021	950 **AL-JESR**	210 conmix	1050	157	15	5 Pc200	230	95.63	112	2525
21 30-3-2021	960 AL-JESR	240 PASV	1040	118	15	5 PC200	250	88.86	94	2525
22 30-3-2021	960 KARASTA	240 PASV	1040	157	15	5 PC200	240	89.1	100	2525
23 7-4-2021	950 **AL-JESR**	210	1050	157	15	3 Gilinume 54	195	108.63		
24 7-4-2021	950 **AL-JESR**	190	1050	157	16	3 Gilinume 54	200	109.4		
25 7-4-2021	950 **AL-JESR**	171	1050	157	16	3 Gilinume 54	210	108.316		
26 8-4-2021	950 **AL-JESR**	171	1050	118	16	3 Gilinume 54	190	103.53		
27 14/4/2021	950 KARASTA	210	1050	157	16	4 Gilinume 54	210	80.85		
28 27/4/2021	950 **AL-JESR sul.**	190	1050	157	15	4 Gilinume 54	230	104.82		

3-6 Mixing Procedure of Concrete

Both types of concrete used in this study (NSC and UHPC) were produced in same rotary mixer as shown in Plate 3-6 . NSC was produced by adding the water and S.P. together by about 2/3 of its quantity. During rotating the mixer, the other material gravel, sand, and cement were added, respectively. when These materials have full mixing together, the remain water and S.P. were added to complete mixture. UHPC was produced also by adding water and S.P. to gather by about 2/3 of its quantity. Then added sand, silica fume, and cement by whole quantity. Waiting the material to completely mixed, then added the remain water and S.P. Through rotating the mixer intel, the mixture was homogenous and integrated with suitable flow, steel fiber was added slowly by hand. When complete the quantity of fiber, remain about 3-5 minutes to settle then used.

Plate 3-6: Mixer used to produce NSC and UHPC.

3-7 Preparation of Joint Surface

The exposed aggregate system was used for all specimens to preparation the surface between NSC of web and the UHPC of joint. This method illustrated by coated the surface of partition with retarder by suitable dosage before placing of NSC in formwork as shown in Plate 3-7A. Then after opened the formwork, the surface of joint presence as shown in Plate 3-7B and finally, washed the surface by strong jet water to remove the un-hydrated cement to become as shown in Plate 3-7C**.** For full depth joint girders, the deck was cast with UHPC, so some of scratches were implement with depth (6 mm) in the deck horizontally when casting the joint.

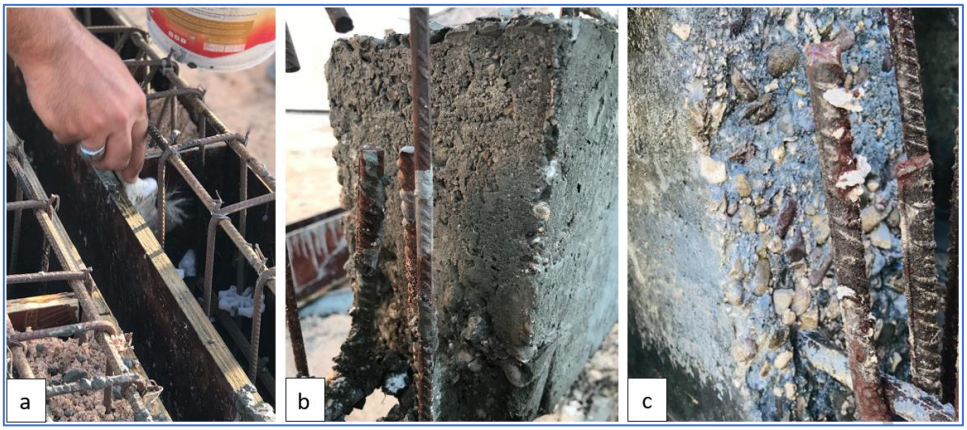

Plate 3-7: Working of exposed aggregate surface: a- coating the retarder on the formwork surface, b- remove the formwork, c- washing the surface to remove the un hydrated cement to expose the aggregate.

3-8 Placing of Concrete and Curing

The experimental work has two stages of casting, first one the casting of web of all specimens with NSC and the deck for control girders and also the decks of simply supported girders with full depth joint with UHPC as shown in Plate 3-8 . Then remove the molds and put the precast unit and the control specimens in place for exposure to curing as shown in Plate 3-9. After remaining the precast unit an enough duration exposed to curing. The precast unit placed in the same

mold and supported strongly to insure prevent the UHPC from seepage out the joint rejoin. The second stage of casting was cast the joints and decks of web joint girders with UHPC as shown in Plate 3-10. Then remove the molds and returned the girders to curing in same place and method.

Plate 3-8: Casting of web with NSC and the deck of control girder with UHPC.

Plate 3-9: Curing of the precast unit.

Plate 3-10: Second stage of casting with UHPC for joints and decks: a-placing the precast unit in the formwork, b-cast the joint, c-cast the deck, d- cast the full depth joint.

At all the stages of casting, the control samples were taken to give an understanding of the mechanichal properties of each type of concrete at different stage of castig.

3-9 Testing Equipment and Procedure

When the curing of all specimens completed, the preparations for testing were started. First of these processing are transport girders from the place of curing to place near from testing machine. Then, cleaning the girders must be done to remove dust, the bulges of concrete and another unwanted thing. After that painted the girders by white color to easy watch the cracking pattern and failure mode during test. Plate 3-11 shows the steps of preparations process.

Plate 3-11: Steps of preparations to testing girders: [a]cleaning and remove the dust, [b] transport the girders to test laboratory, [c] painted the specimens.

3-9-1 Specimens setup

Transporting the girder to test machine and setup as shown in Figure 3-17. The girder was placed under the test machine horizontally and supports in correct positions to ensure clear span 1500 mm. The deflection measurement was taken in mid span and joints regions, so the LVDT supported to provide this purpose. Then, the load was applied in mid spans as shown in Figure 3-17.

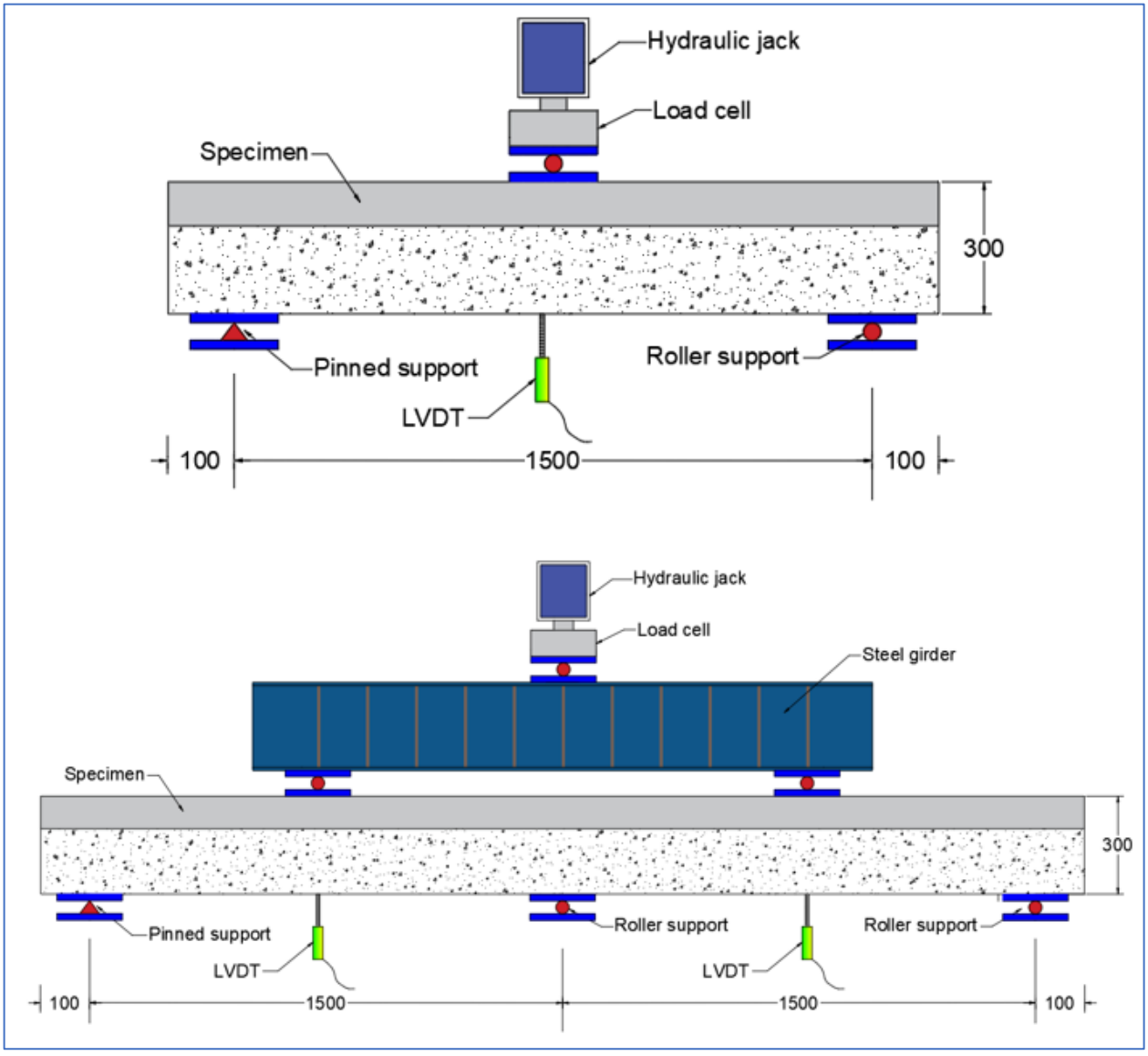

Figure 3-17: Setup of girders in test machine.

3-9-2 Instruments

Some of instruments must be used in this test to measure the structural parameters of tested girders. So, the electronic system was manufactured to adopt the test process and obtain on the details of structural members with high accuracy. The components of this system and other instrument were listed as following: see Plate 3-12

1- Load cell with capacity 500 kN to measure the applied load.
2- LVDT to measure the deflection.
3- Data logger to collect the data from the test.
4- Computer to show the output data.
5- Crack meter to measure the crack width.
6- Hydraulic jack for applying load.

3-9-3 Test procedure

There are two types of loads applied in this study which are static load and repeated load. The static load represented by applied constant load in mid span of girder with rate 1 kN/sec. up to failure. The repeated load represented by applied load in mid span of girder with rate 1kN/sec. (Takemura and Kawashima, 1997) examined six cyclic loading protocols, as shown in Figure 3-18 (A) on the behavior of identical RC bridge piers. It was found that the envelope curve of the tested specimens depended on the number of cycles, the amplitude of each cycle and the sequence of loading cycle. Figure 3-18 (B) presents the envelope curves of tested specimens. Since the behavior of tested specimens was approximately similar, and according to available equipment the cyclic load protocol adopted in this study was similar in TP05 used by Takemura and Kawashima, as shown in Figure 3-19.

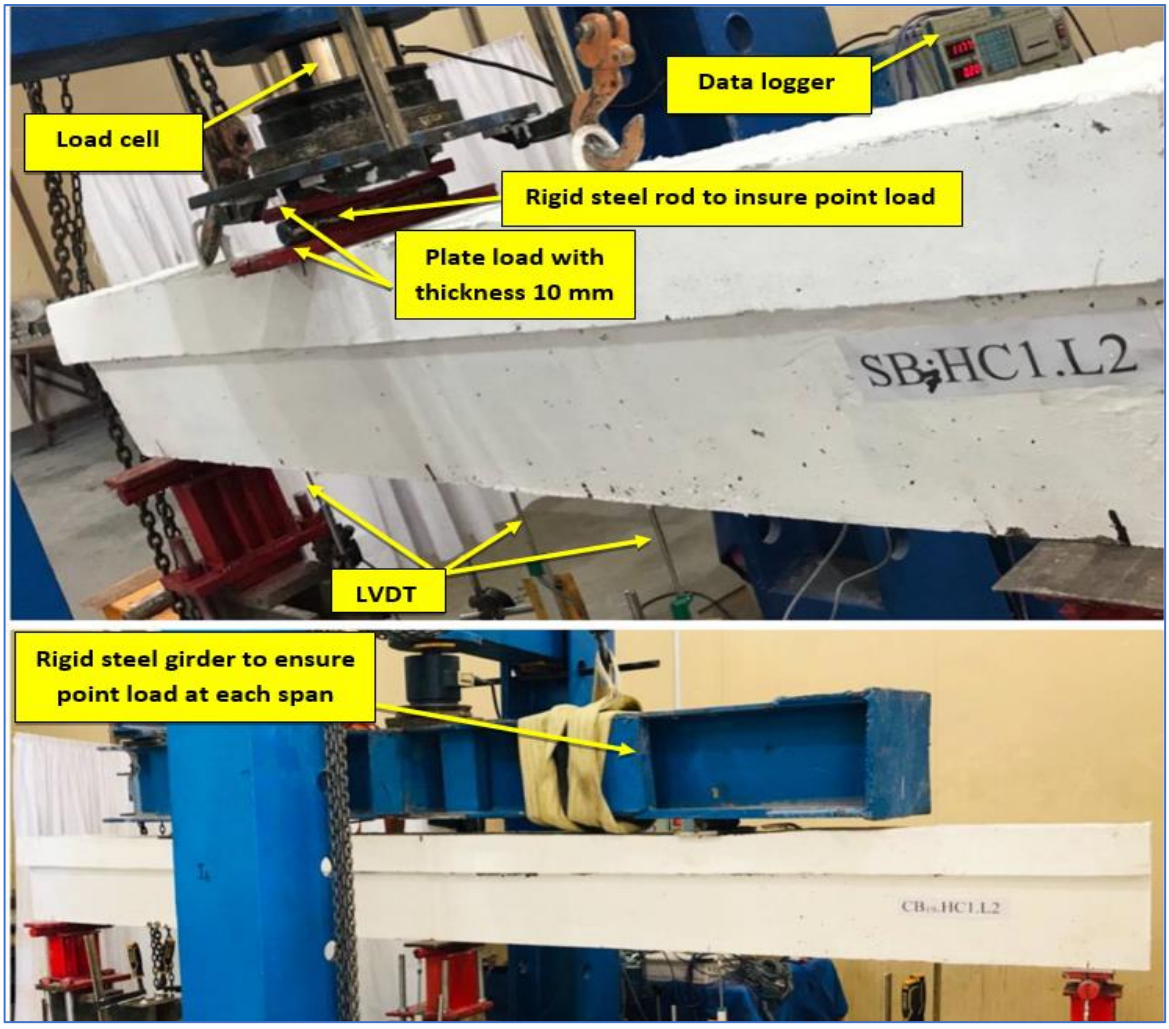

Plate 3-12: The instruments and tools used in the test process.

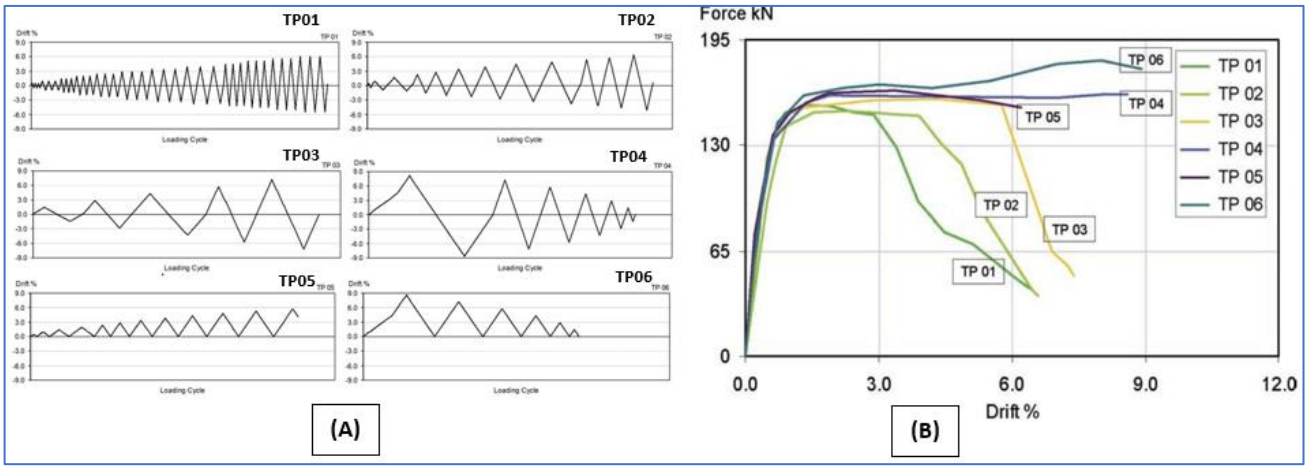

Figure 3-18: Cyclic response: A load cycle protocols B the envelope load-drift curve (Takemura and Kawashima, 1997).

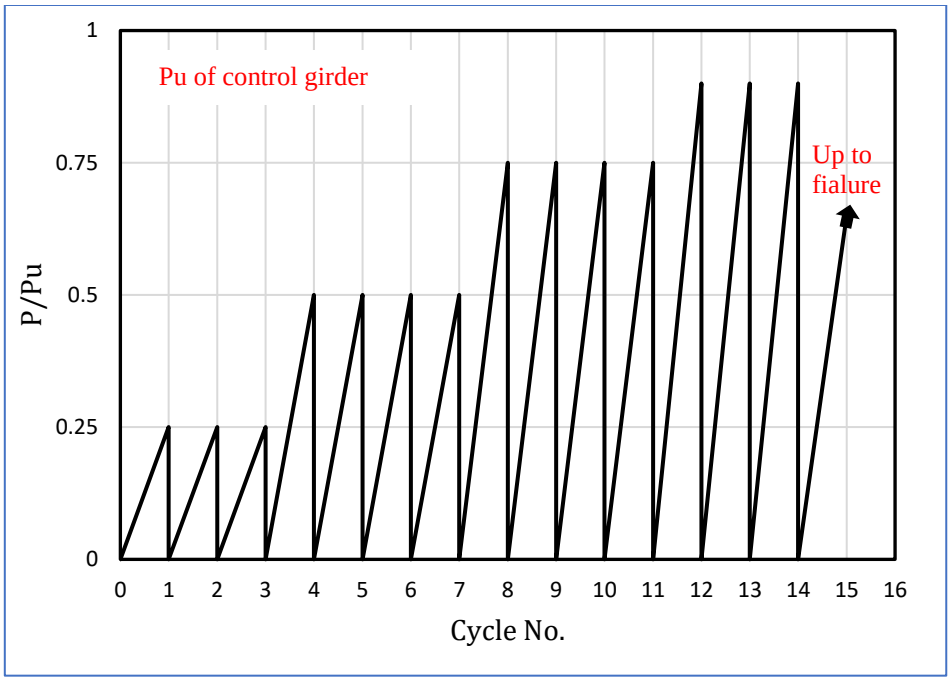

Figure 3-19:Cyclic load protocol used in this study.

Chapter Four

Experimental Results and Discussions

4-1 Introduction

The results of experimental work will be presented, analyzed, and discussed to give a good understanding about the variables referred to in chapter three. These variables were divided into two groups with respect to the support condition of the tested girder. Simply supported group have varying the depth of joint, presence of shear key, hybridization of reinforcement, addition steel reinforcement as dowel action, and type of load applied. Continuous supported group have varied the location of joint, presence of shear key, hybridization of reinforcement, and type of load applying.

The evaluation of tested girders will be presented depend on the results of ultimate loads, service deflection, mode of failure, load-deflection curve, crack pattern, cracking load, stiffness, ductility, and energy absorption.

4-2 Mechanical Properties of Concrete Control Samples

Control samples such as cubes, cylinders, and prisms were taken as mentioned in chapter three, and tested as described previously. These control samples of NSC and UHPC were tested in saturated surface dry condition (ASTM C1856, 2017) and at 28 days. The results of tested samples listed in (Table 4-1)for NSC and in (Table 4-2) for UHPC, where:

$E = 4700\sqrt{\acute{f}c}$ (MPa) …… (4-1) (ACI-318, 2019) for NSC

$E = 3840\sqrt{\acute{f}c}$ (MPa) ……..... (4-2) (Graybeal, 2007) for UHPC

Table 4-1: Results of control samples for NSC.

Group	Compressive Strength (MPa)(cube)*	Compressive Strength (MPa)(cylinder)**	Indirect tension strength Splitting (MPa)**	Modulus of Elasticity (MPa)
I Control and precast unit	50.4	39.32	5.36	24073
II Precast unit	52.6	43.4	5.24	25297
III Precast unit	55.1	45.3	5.21	25846

*Average of six samples for each group, **Average of three samples for each group

Table 4-2: Results of control samples for UHPC.

Group	Compressive Strength (MPa)(cube)*	Indirect Tension strength Splitting (MPa)**	Modulus of Elasticity (MPa)
I Control	134.25	14.65	54407
II Precast unit	165.16	14.31	60373
III Deck and joint	152.02	12.72	57946

*Average of nine samples, **Average of three samples

4-3 General Behavior of Tested Girders

The results of tested girders would be presenting in two series according to their support condition.

4-3-1 Simply supported girders

4-3-1-1 General behavior

This group were consisted of twelve simply supported girders. Two of these girders were cast monolithically as one unit referring to the control specimen to be one of them for monotonic and other for cyclic. Other girders had two joints in the same location and length with some of variables in these joints. These variables are the depth of joint, hybridization of reinforcement, presence of shear key, and present of additional reinforcement as dowels action. Seven of them were applied to monotonic load and others tested under repeated load. The results of this group were listed in Table 4-3, and the behavior of each specimen will be described in the coming sections. From the result, the mode of failure of all girders were flexural failure (i.e., Tension controlled) due to adequate shear reinforcement and good bond for vertical and horizontal joints. The flange region gives high stiffness without any crushing except some of simple vertical cracks near the point load.

- **$SB_1.HC_1.L_1$**

The control girder of simply supported group, cast monolithically (without joint) for NS in web and UHPC in flange. This specimen was reference to compare with other spliced girders to study the items of its structural behavior**.** SB_1 was tested under static three-point load up to failure. The deformations were developed with increasing the applied load, where the load increased in high range due to high stiffness of this girder during elastic range.

Table 4-3: Summary of results for simply supported girders.

Girder symbol	*Cracking load* P_{cr} *(kN)*	*Ultimate load* P_{ul} *(kN)*	*Deflection* Δ_{ul} *(mm)*	*Failure mode*
$SB_1.HC_1.L_1$	60	198.45	23.26	Tensile Flexural
$SB_2.HC_2.L_1$	61	189.13	22.8	Tensile Flexural
$SB_3.HC_3.L_1$	53	183.2	22.45	Tensile Flexural
$SB_4.HC_3.HR1.L_1$	78	208.3	21.84	Shear- Flexural
$SB_5.HC_2.SK.L_1$	88	193.95	20.9	Tensile Flexural
$SB_6.HC_3.SK.L_1$	65	187.73	22.3	Tensile Flexural
$SB_7.HC_1.L_2$	45/ cyc. 3	187.27 /cyc. 15	19.7	Tensile Flexural
$SB_8.HC_2.L_2$	57 /cyc.5	175.45 /cyc. 15	22.83	Tensile Flexural
$SB_9.HC_3.L_2$	47 /cyc.5	164.5/ cyc. 12	23.04	Tensile Flexural
$SB_{10}.HC_2.SK.L_2$	67 /cyc.6	178.18 /cyc. 15	23.14	Tensile Flexural
$SB_{11}.HC_3.SK.L_2$	61 /cyc.1	174.84/cyc. 15	21.16	Tensile Flexural
$SB_{12}.HC_3.D.\ L_1$	83	191.26	17.42	Tensile Flexural

At load 60 kN appeared the first crack at mid span region (vertically under point load), then with increasing applied load the cracks were spread at all mid span and crept toward the support region at load 135 kN. These cracks initiated at the bottom of girder and with increased the load penetrate during the section to the top of web girder. The cracks reached to the flange at load 165 kN, this means the UHPC started to ductile stage with loose its very high stiffness when reached the crack to point load. After that, the deformations continued to increase with simple increasing in the load until the failure of specimen at 198.45 kN. Figure 4-1 show the load –deflection response of SB_1. The failure and crack pattern were explained in Plate 4-1.

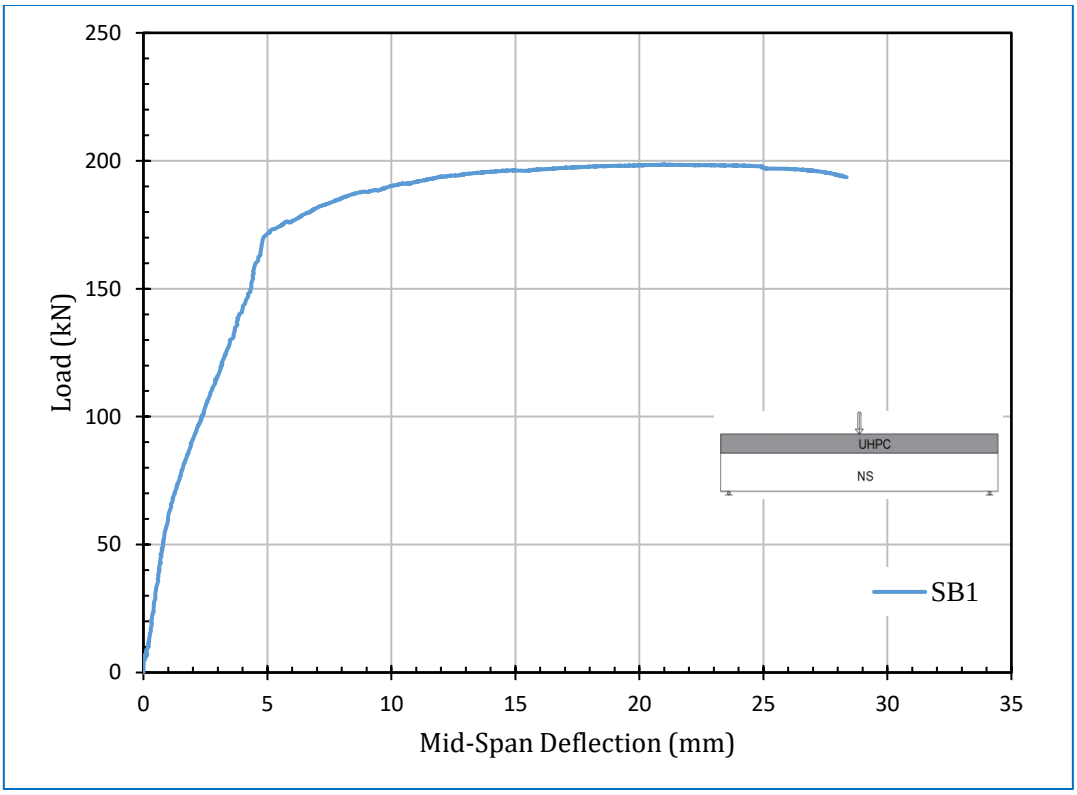

Figure 4-1:Load-mid-span deflection curve of $SB_1.HC_1.L_1$.

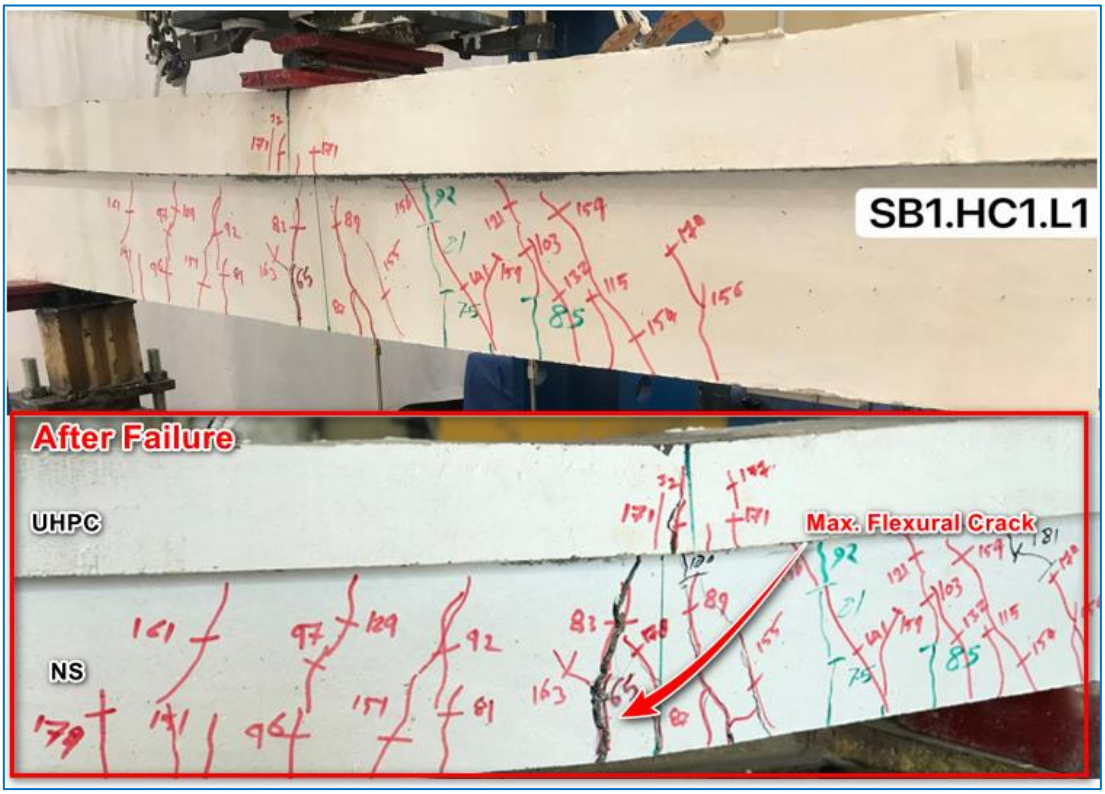

Plate 4-1: Cracks and mode fialure of girder $SB_1.HC_1.L_1$.

- **$SB_2.HC_2.L_1$**

This girder was consisted of three precast segments spliced together with UHPC joint. For precast segments, the web cast with NSC and flange with UHPC at same time, then cast full depth of joint (web and flange) with UHPC. Static three-point load was applied on this girder. First crack appeared at the interface region at load 37 kN at side of middle segment. The deformations increased at mid span zone and crack appeared at mid span under point of loading after load 61 kN, then become clear and start to develop towards the top layer (compression zone) with increasing the load. The cracks become too appears at end segments at load 132 kN after passing through joint region. Joints give good bond with precast segment with some of no significant cracks at the interface. While, the cracks at mid span developed and become wider with increasing load. The joint zone gives a high stiffness during the load, where wide cracks or deboned did not observed at the interface. After that the girder starts to plastic stage and give high ductility until the failure at load 189.13 kN. The load deflection response shows a great similarity in structural behavior with control girder with some difference in ultimate load values about (4.7 %), as shown in Figure 4-2. The cracks pattern at failure explained at Plate 4-2.

Plate 4-2: Cracks and mode fialure of girder $SB_2.HC_2.L_1$.

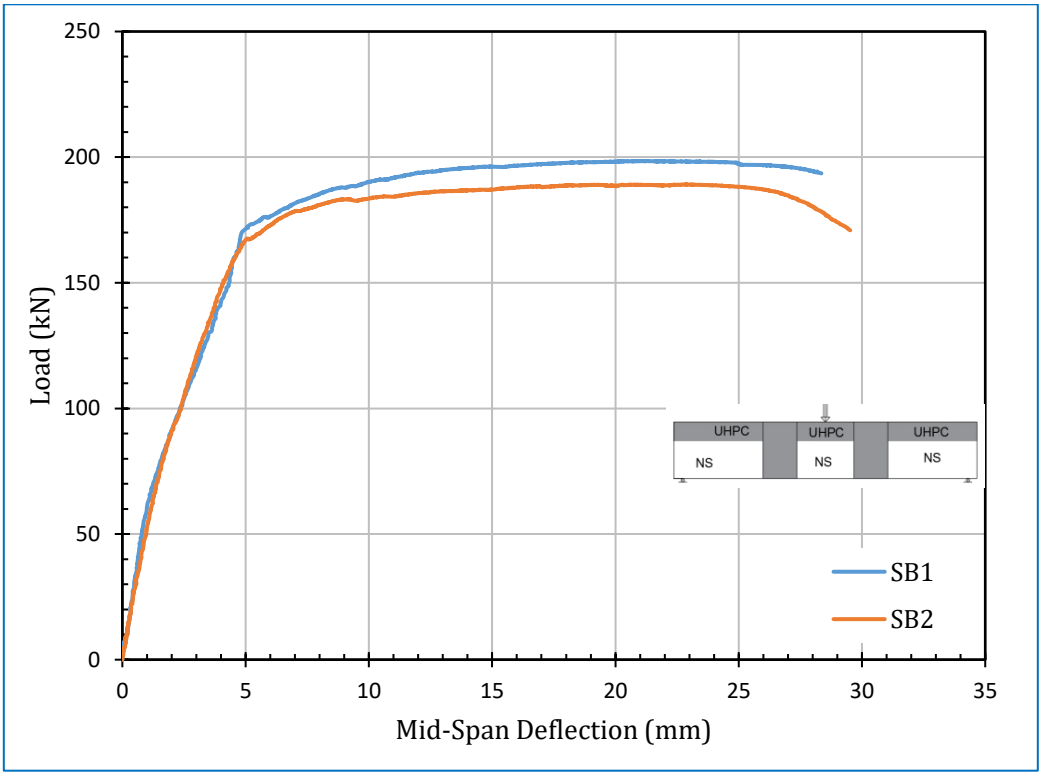

Figure 4-2: Load-mid-span deflection curve of $SB_2.HC_2.L_1$.

- **$SB_3.HC_3.L_1$**

This girder was consisted of three precast segments spliced together with UHPC joint. For precast segments, its web only (rectangular section) cast with NSC, then cast the joint and flange of girder at the same time by UHPC. Static three-point load was applied on this girder. First crack appears at the interface region at load 35 kN in side the middle segment as a very simple crack. The deformations increased at mid span zone and appear crack at mid span under point of loading after load 53 kN, then become clear and start to developed towards the top layer (compression zone) with the increasing the load. The cracks separated to appears at end segments at load 149 kN after passing the joint region. Joints give full bond with precast segment with some no significant cracks at interface. While, the cracks at mid span developed and become wider with increasing the load. The joint zone gives a good stiffness during the load, where wide cracks or deboned did not appear at interface. The flange cracked at load 119 kN under point load from bottom and continued to penetrate all depth of flange. This crack appeared at load less than in previous specimen due to the presence of horizontal joint between flange and precast segments leading to finding more a weakly zone. After that the girder start to plastic stage and give high ductility until the failure at load 183.2 kN. The load deflection response shows a great similarity in structural behavior with control girder with some difference in ultimate load values about (7.6 %) as shown in Figure 4-3. The cracks pattern at failure illustrated in Plate 4-3.

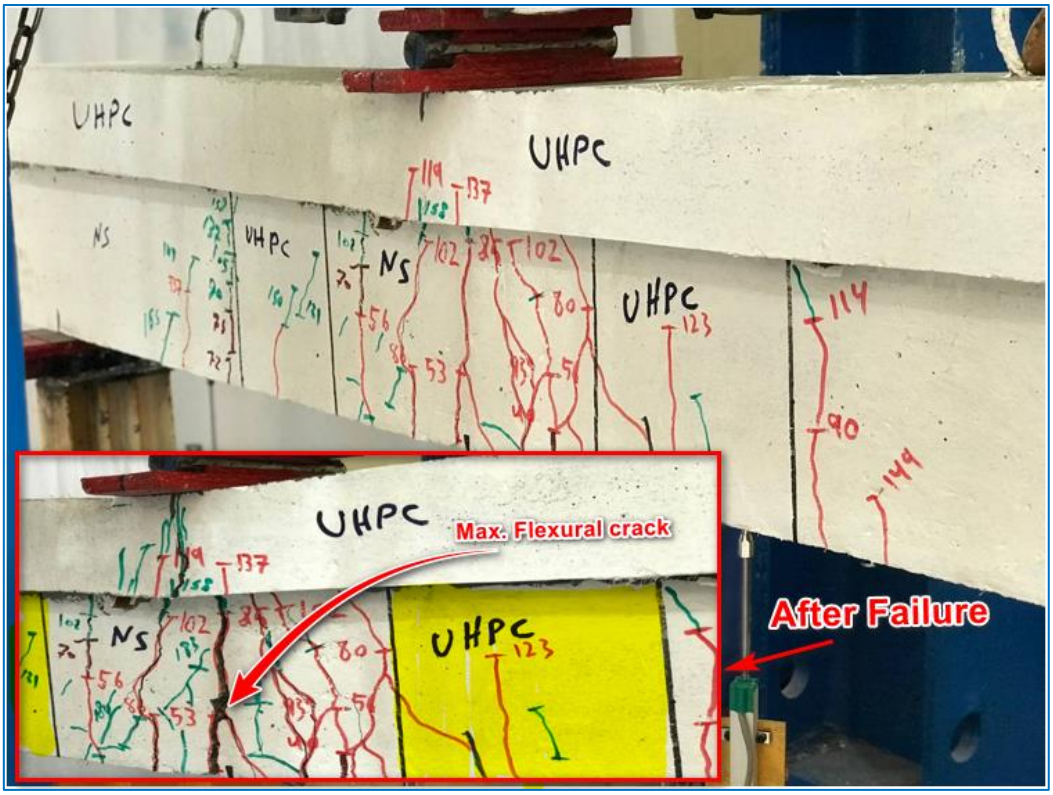

Plate 4-3: Cracks and mode fialure of girder $SB_3.HC_3.L_1$.

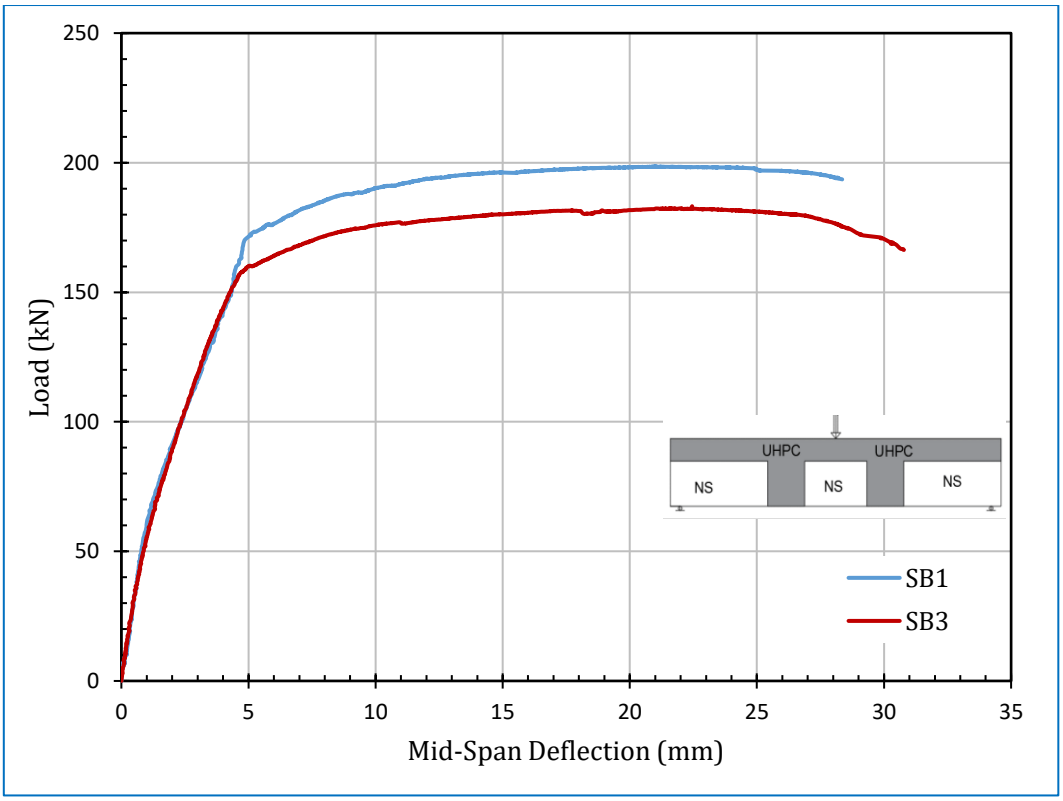

Figure 4-3: Load-mid-span deflection curve of $SB_3.HC_3.L_1$.

- **$SB_4.HC_3.HR1.L_1$**

This girder was consisted of three precast segments spliced together with UHPC joint. For precast segments, its web only (rectangular section) cast with NSC, then cast the joint and flange of girder at same time by UHPC. The reinforcement of this girder was hybrid by replace 50% of steel reinforcement by CFRP bar Static three-point load was applied on this girder. First crack appears at the interface region at load 40 kN at side of middle segment. The deformations increased at mid span zone and crack appeared at mid span under point of loading after load 78 kN, then become clear and start to developed toward top layer (compression zone) with increasing the load. The cracks separated to appears at end segments at load 90 kN after passing the joint region. Joints give full bond with precast segment with some of no significant cracks at interface. While, the cracks at mid span developed and become wider with increasing load. The joint zone gives a good stiffness during the load, where wide cracks or debone did not show at interface except some simple crack after load 140 kN. The flange cracked at load 118 kN under point load from bottom and continued to penetrate all depth of flange. The load deflection response shows a difference in the behavior of control and spliced specimens, where did not give a ductility before failure and did not show a clear plastic stage during tracing the curve. At load 208.3 kN , the CFRP bar reinforcement was slip due to bond failure (debond) of the splice technique leading to fail the girder and reduction in load, then its comeback to increase the load up to 202 kN also, cutting the remain steel reinforcement. The cracks pattern at failure illustrated in Plate 4-3 show that middle segment not had wide cracks compared in SB_3.

Plate 4-4: Cracks and mode fialure of girder $SB_4.HC_3.RH1.L_1$.

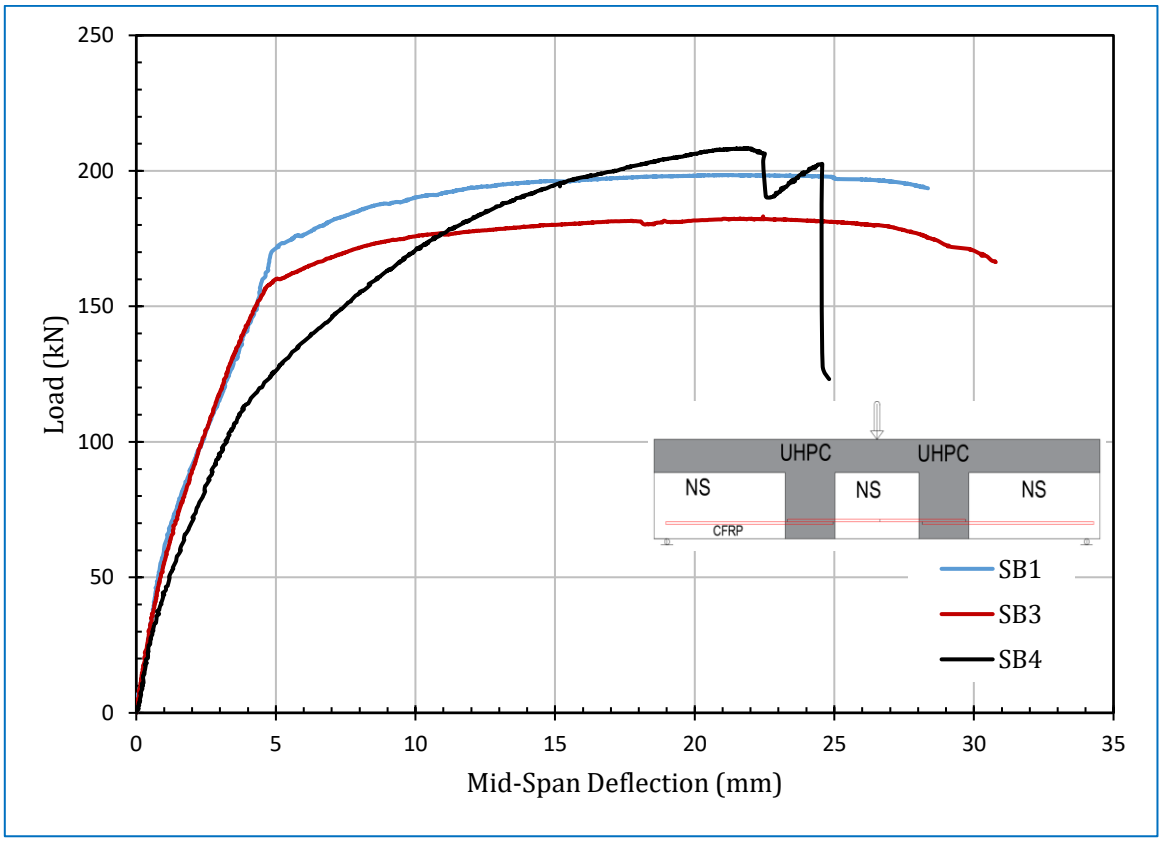

Figure 4-4: Load-mid-span deflection curve of $SB_4.HC_3.HR1.L_1$.

- **$SB_5.HC_2.SK.L_1$**

This specimen has the same properties of girder SB2 with addition shear key in the UHPC vertical joints. In the test of girder approached similar behavior of SB_2 with some difference in the value of crack and ultimate load as shown in Figure 4-5. First crack was developed in the mid span near to joint (in the interface) at load 43 kN, crack in mid span at load 88 kN, and the crack in flange at load 165 kN. The cracks pattern after failure at load 193.95 kN illustrated in Plate 4-5 . Presence of shear key added a simple improvement in the cracking and ultimate loads, also lead to more spared of cracks after the joint region with similar general mode of failure. The challenge properties of UHPC and good bond of joint with shear key may lead to no significant difference between spliced and control girders after presence of shear key.

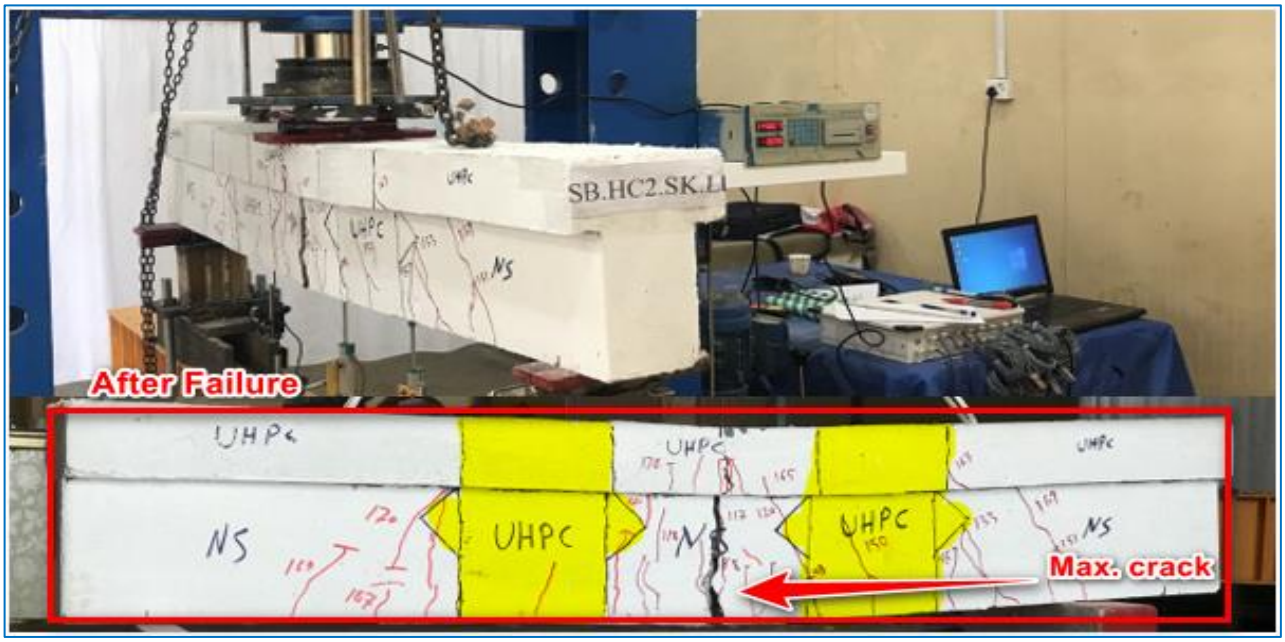

Plate 4-5: Cracks and mode failure of girder $SB_5.HC_2.SK.L_1$.

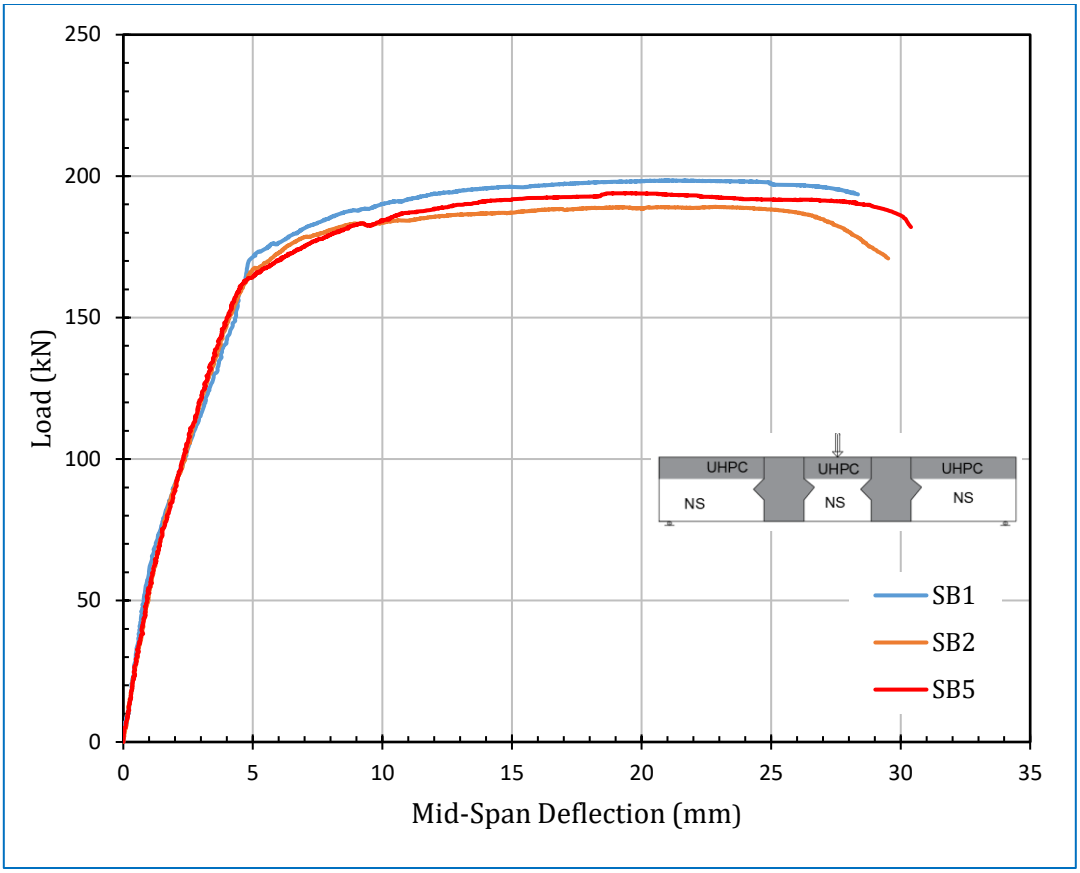

Figure 4-5: Load-mid-span deflection curve of $SB_5.HC_2.SK.L_1$.

- **$SB_6.HC_3.SK.L_1$**

This specimen has the same properties of girder SB_3 with addition shear key in the UHPC vertical joints. In the test of girder approached similar behavior of SB_3 with some difference in the value of cracking and ultimate load as shown in Figure 4-6. First crack was show in the mid span near to joint (in the interface) at load 39 kN, crack in mid span at load 65 kN, and the crack in flange at load 163 kN. The cracks pattern after failure at load 187.37 kN illustrated in Plate 4-5 . Presence of shear key added a slightly improvement in the cracks and ultimate loads, also lead to more spared of cracks after the joint region with same general mode of failure. The good properties of UHPC and full bond of joint may cause no significant difference in girders after presence of shear key.

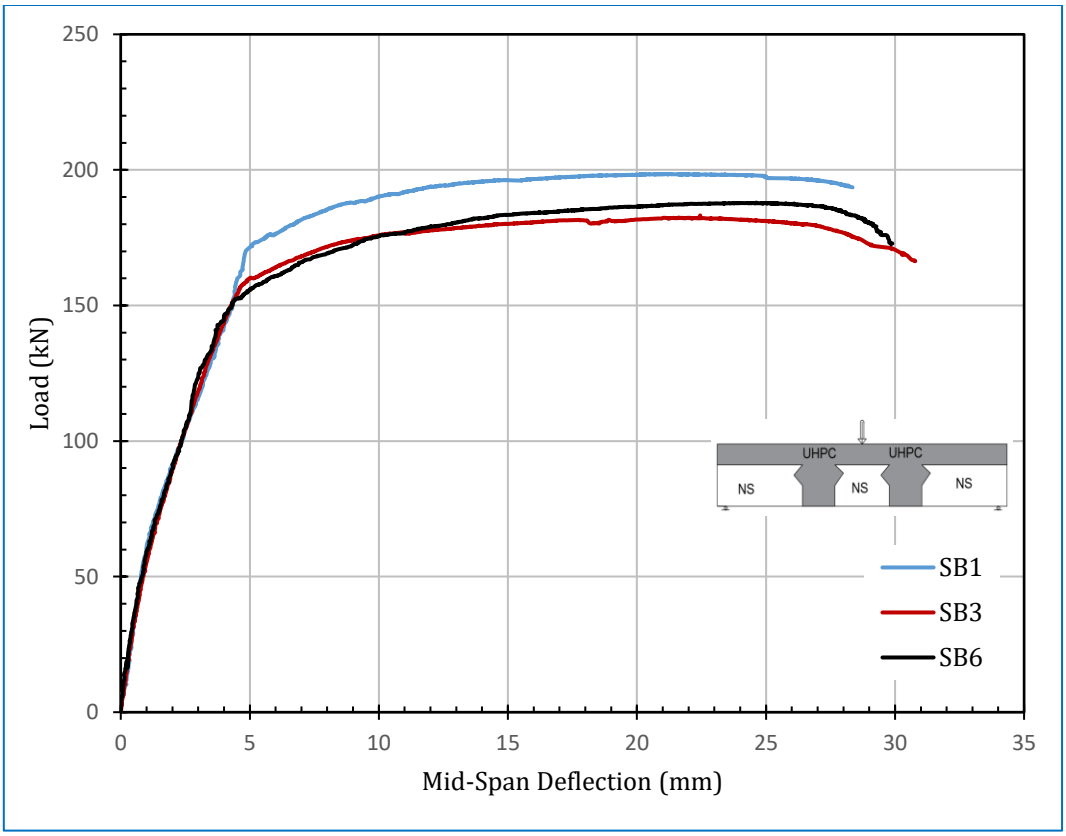

Figure 4-6: Load-mid-span deflection curve of $SB_6.HC_3.SK.L_1$.

From the test, the very important finding that the girder at the last stage of loading and after the failure, the bottom reinforcement was cut as shown in Plate 4-6. This refer to the full bond between steel reinforcement and UHPC at joint zone (the zone at which the reinforcement was spliced). In other word, that the spliced length of reinforcement in joint were adequate.

Plate 4-6: Cracks and mode failure of girder ***$SB_6.HC_3.SK.L_1$***.

- **$SB_7.HC_1.L_2$**

This girder has same geometric properties of control girder (SB_1). But, it was tested under three-point repeated load with the protocol as shown in chapter Three item (3-10-3). The first crack at mid span of specimen appeared at load 45 kN in third cycle, then continued the loading by specified intensity. In 11^{th} cycle, the flange was cracked under point load at load 165 kN. The cycles of loading continued for completed 14^{th} cycles then started in last cycle (failure cycle) and in this stage the girder reached to ultimate load at 187.27 kN. Load- deflection curve show a similar behavior approximately to SB_1 as illustrated in Figure 4-7,where the repeated load with this low number of cycles did not give a significant effect on the general behavior of specimen. Mode of failure was

maintained as in girder SB_1 with more intensity of cracks and spread of cracks near to supports as shown in Plate 4-7.

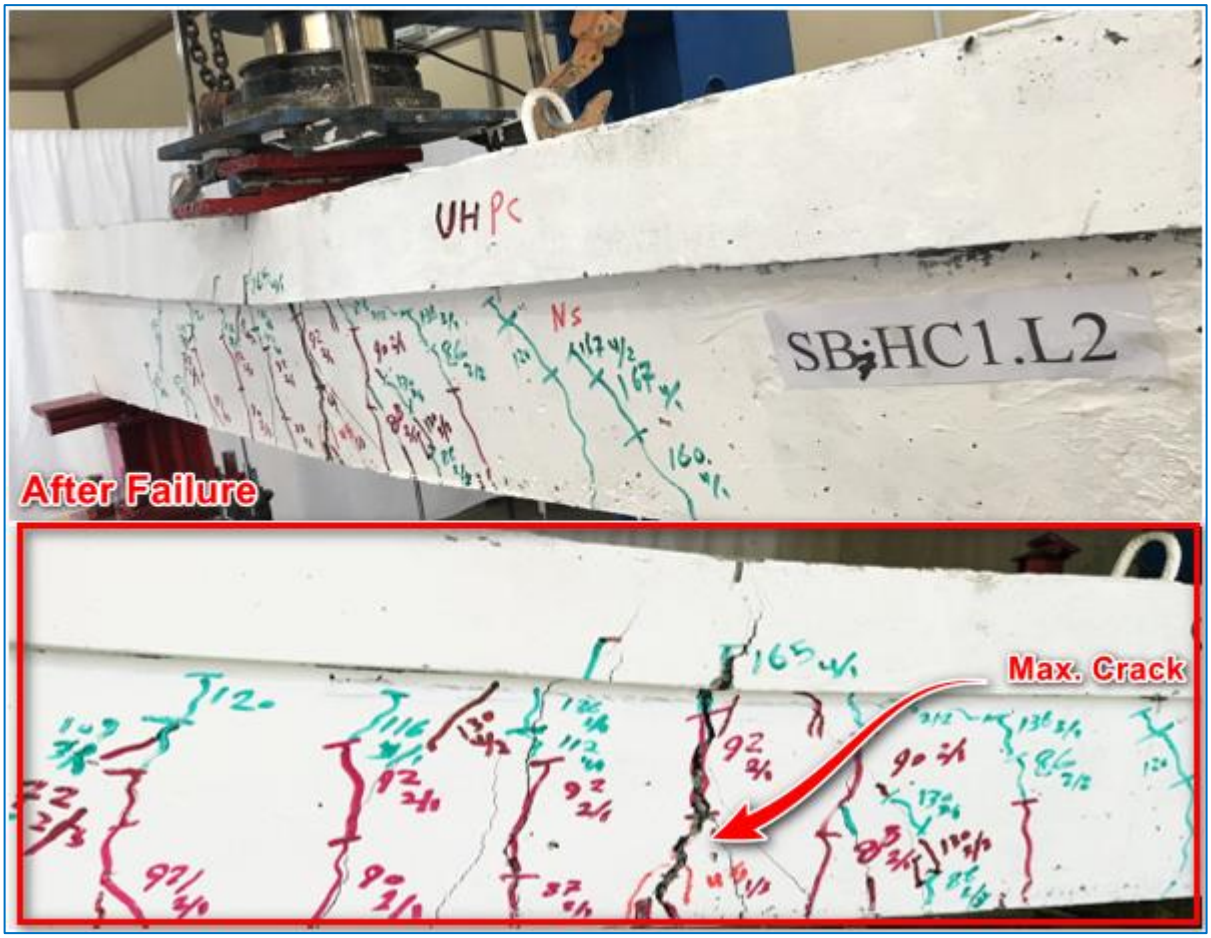

Plate 4-7: Cracks and mode failure of girder $SB_7.HC_1.L_2$.

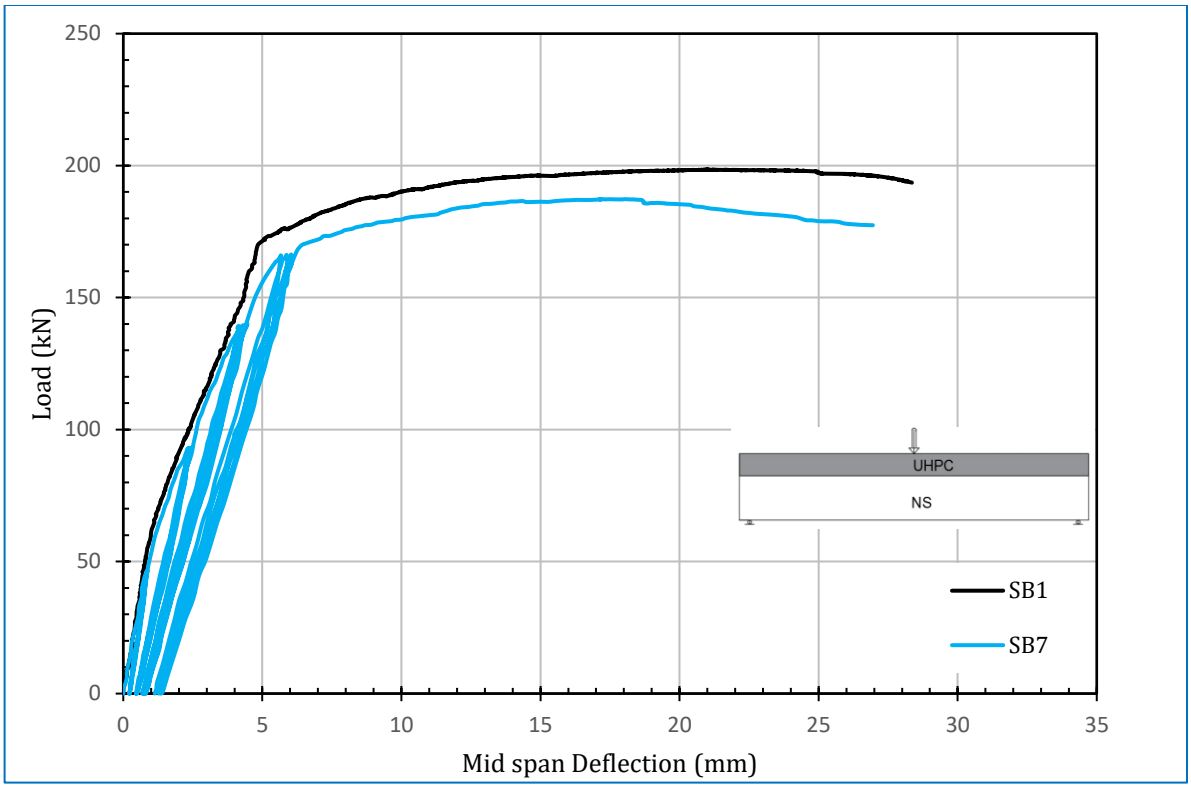

Figure 4-7: Load-mid-span deflection curve of $SB_7.HC_1.L_2$.

- **$SB_8.HC_2.L_2$**

This girder has same geometric properties of spliced girder (SB_2) with test under three-point repeated load. The first crack at mid span of specimen appears at load 36 kN in first cycle, then continued the loading by specified intensity. In 11^{th} cycle, the flange was cracked under point load at load 165 kN. The cycles of loading continued for completed 14^{th} cycles then started in last cycle (failure cycle) and in this stage the girder reached to ultimate load at 175.45 kN. Load-deflection curve show a similar behavior approximately to SB_2 as illustrated in Figure 4-8, at last cycle the girder inters in the plastic stage before 165 kN and give high ductile behavior due to a high efficiency of UHPC in the joints and full bond with precast segments. Mode of failure was maintained as in girder SB_2 and spread of cracks near to supports as shown in Plate 4-8.

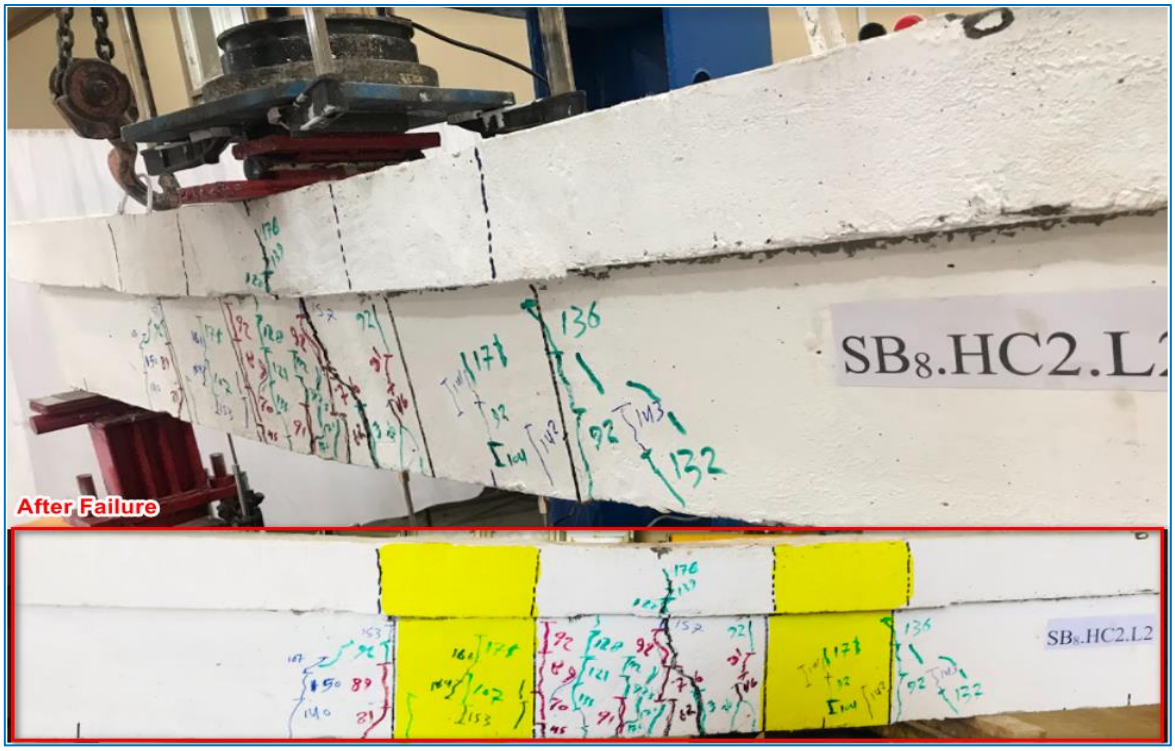

Plate 4-8:Cracks and mode failure of girder $SB_8.HC_2.L_2$.

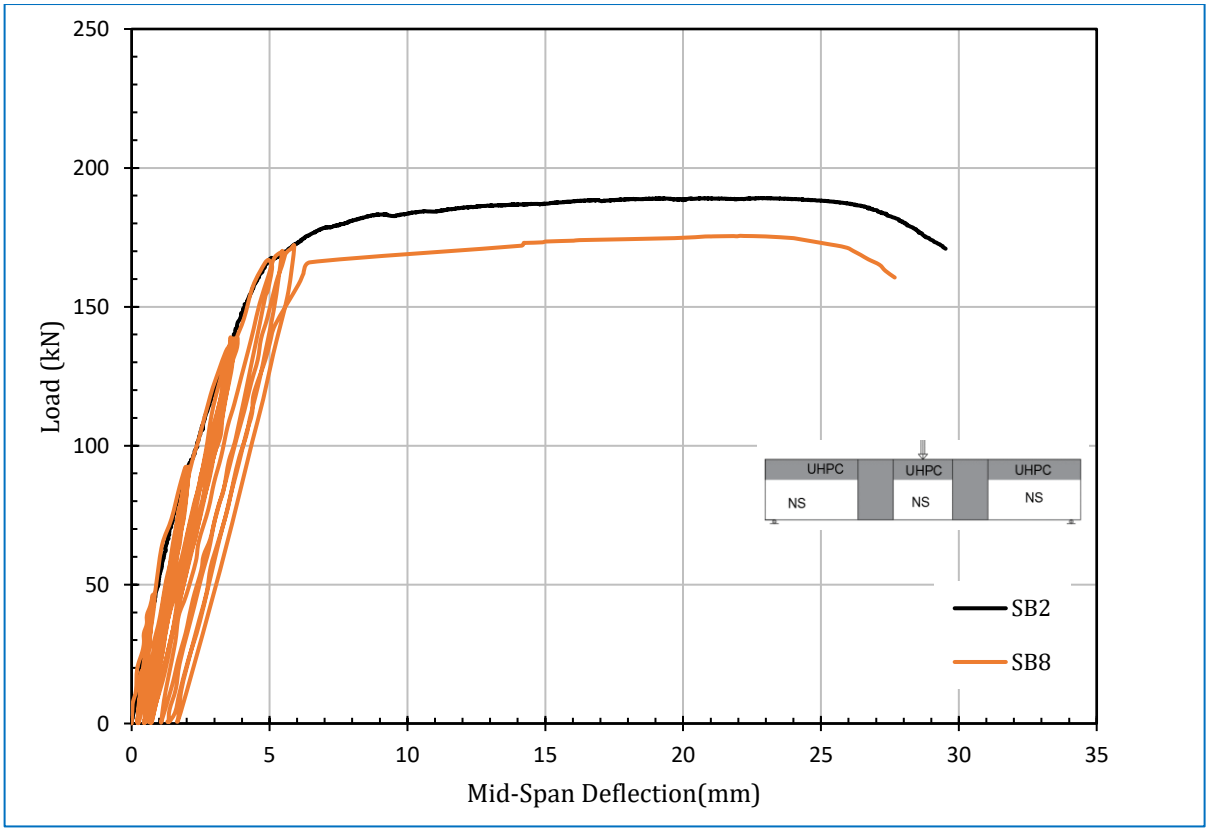

Figure 4-8:Load-mid-span deflection curve of $SB_8.HC_2.L_2$.

- **$SB_9.HC_3.L_2$**

This girder has same geometric properties of spliced girder (SB_3) with test under three-point repeated load. The first crack at mid span of specimen appears at load 36 kN in first cycle, then continued the loading by specified intensity. In 8th cycle, the flange was cracked under point load at load 136 kN. The cycles of loading continued for completed 10th cycles then started in 11th cycle, but the girder reached to plastic stage until to failure load at 164.5 kN. Load- deflection curve show a similar behavior approximately to SB_3 as illustrated in Figure 4-9, at last cycle the girder gives high ductile behavior due to a high efficiency of UHPC in the joints and full bond with precast segments. Mode of failure was maintained as in girder SB_3 and spread of cracks after joints with hair line cracks in joint zone as shown in Plate 4-9.

Plate 4-9:Cracks and mode failure of girder $SB_9.HC_3.L_2$.

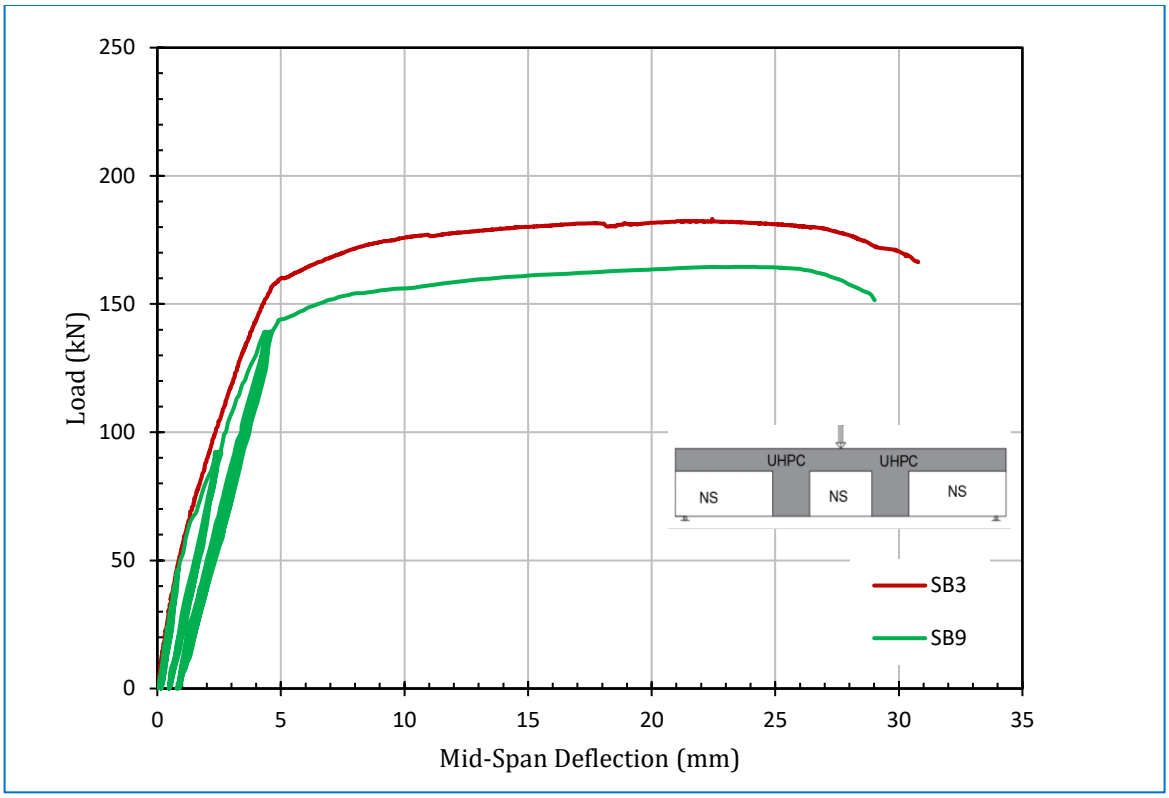

Figure 4-9:Load-mid-span deflection curve of $SB_9.HC_3.L_2$.

- **$SB_{10}.HC_2.SK.L_2$**

This girder has same geometric properties of spliced girder (SB_5) with test under three-point repeated load. The first crack at mid span of specimen appears at load 40 kN in first cycle, then continued the loading by specified intensity. In 10^{th} cycle, the flange was cracked under point load at load 139 kN. The cycles of loading continued for completed 14^{th} cycles then started in last cycle (failure cycle) and in this stage the girder reached to ultimate load at 178.18 kN. Load-deflection curve show a similar behavior approximately to SB_5 as illustrated in Figure 4-10. The presence of shear key led to a slightly increase in the first crack and ultimate load due to a high efficiency of UHPC in the joints and good bond with precast segments without shear key, for thus, the mid span of interior precast segment was controlled the failure mode as shown in Plate 4-10.

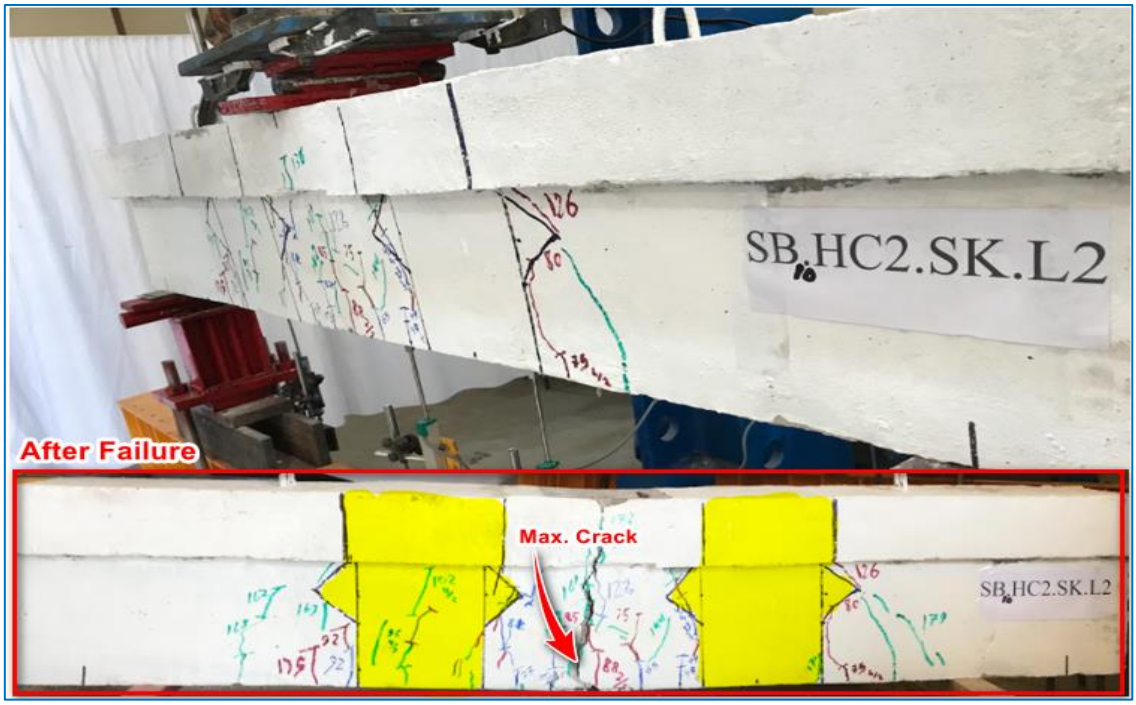

Plate 4-10:Cracks and mode failure of girder $SB_{10}.HC_2.SK.L_2$.

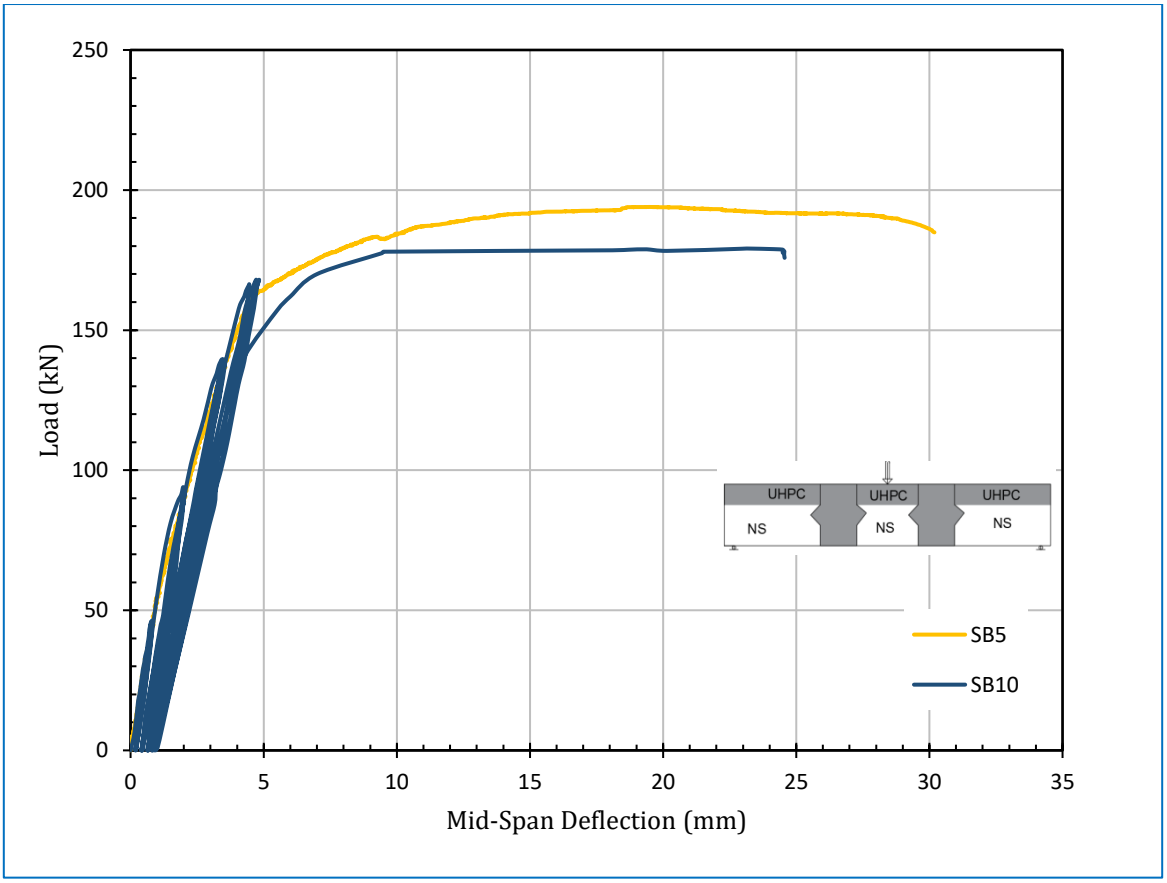

Figure 4-10:Load-mid-span deflection curve of $SB_{10}.HC_2.SK.L_2$.

- **$SB_{11}.HC_3.SK.L_2$**

This girder has same geometric properties of spliced girder (SB_6) with test under three-point repeated load. The first crack at mid span of specimen appeared at load 36 kN in first cycle, then continued the loading by specified intensity. In 9th one, the flange was cracked under point load at load 130 kN. The cycles of loading continued to complete 10th cycles then started at 11th cycle, but the girder reached to yield stage, where the deformations became stilling clear in spite of remove the load to complete 14 cycles then started in last cycle up to failure at 175.5 kN. Load- deflection curve show a high similarity in structural behavior to SB_6 as illustrated in Figure 4-11, at last cycle the girder gives high ductile behavior due to a high efficiency of UHPC in the joints and full bond with precast segments. Mode of failure was maintained as in girder SB_6 and spread of cracks after joints with hair line cracks in joint zone as shown in Plate 4-11. In this plate, the development of interface cracks did not pass through shear key due to good properties of UHPC, while it's inclined to continue in NSC to reach the flange. The presence of shear key added a good stiffness to girder and improve the ultimate load of specimen.

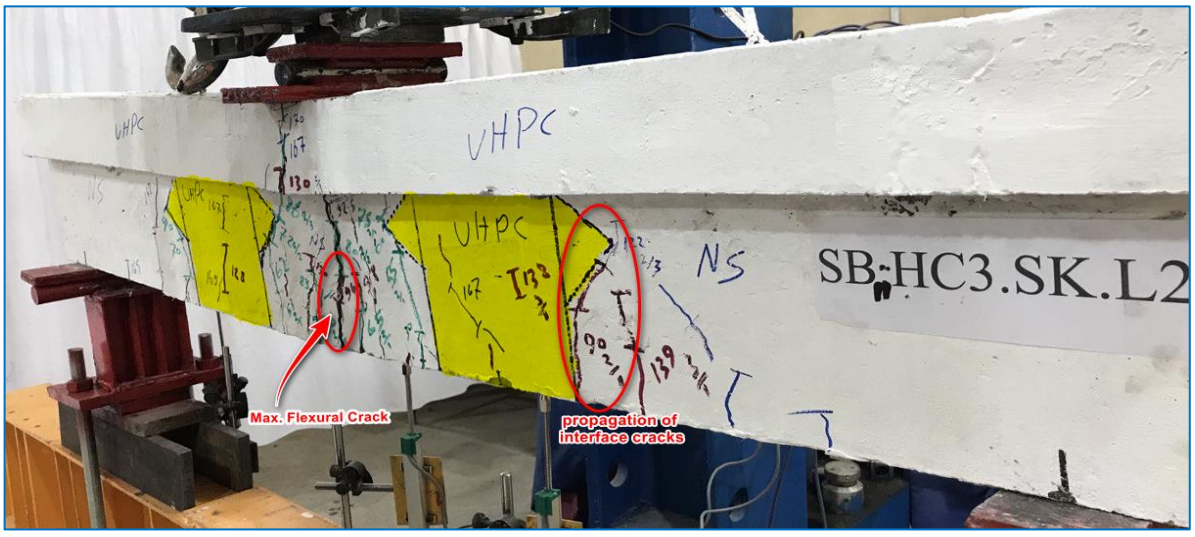

Plate 4-11:Cracks and mode failure of girder $SB_{11}.HC_3.SK.L_2$.

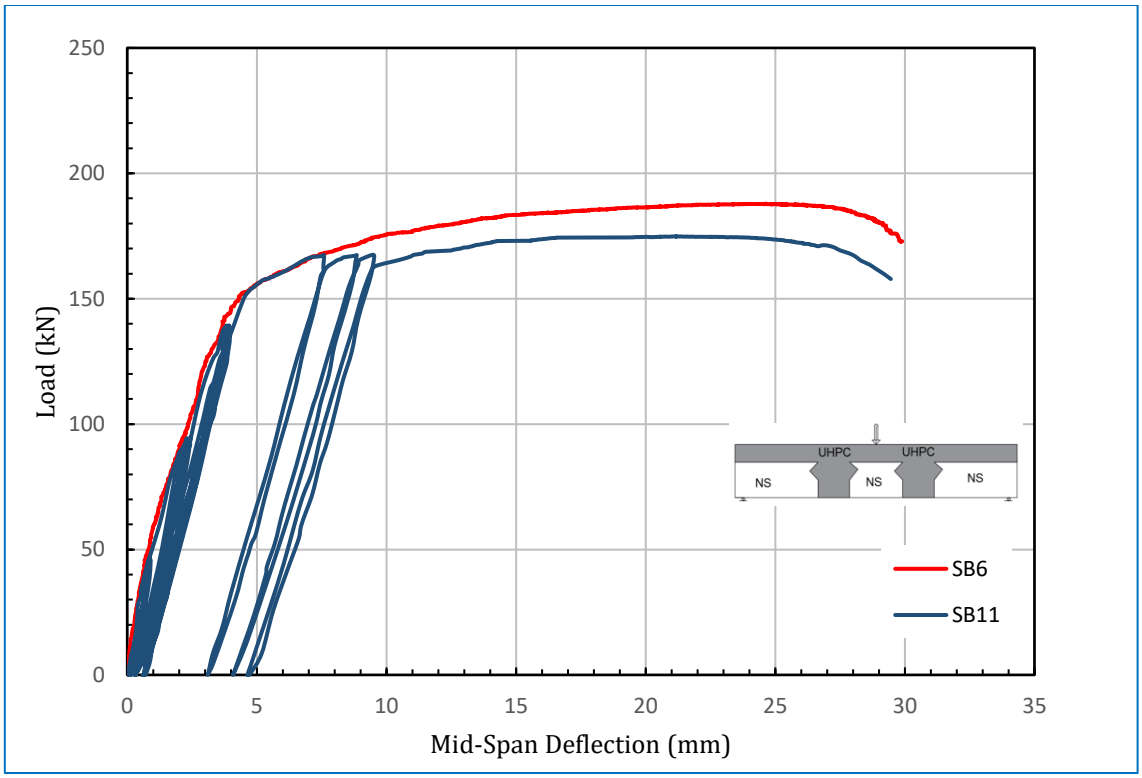

Figure 4-11: Load-mid-span deflection curve of $SB_{11}.HC_3.SK.L_2$.

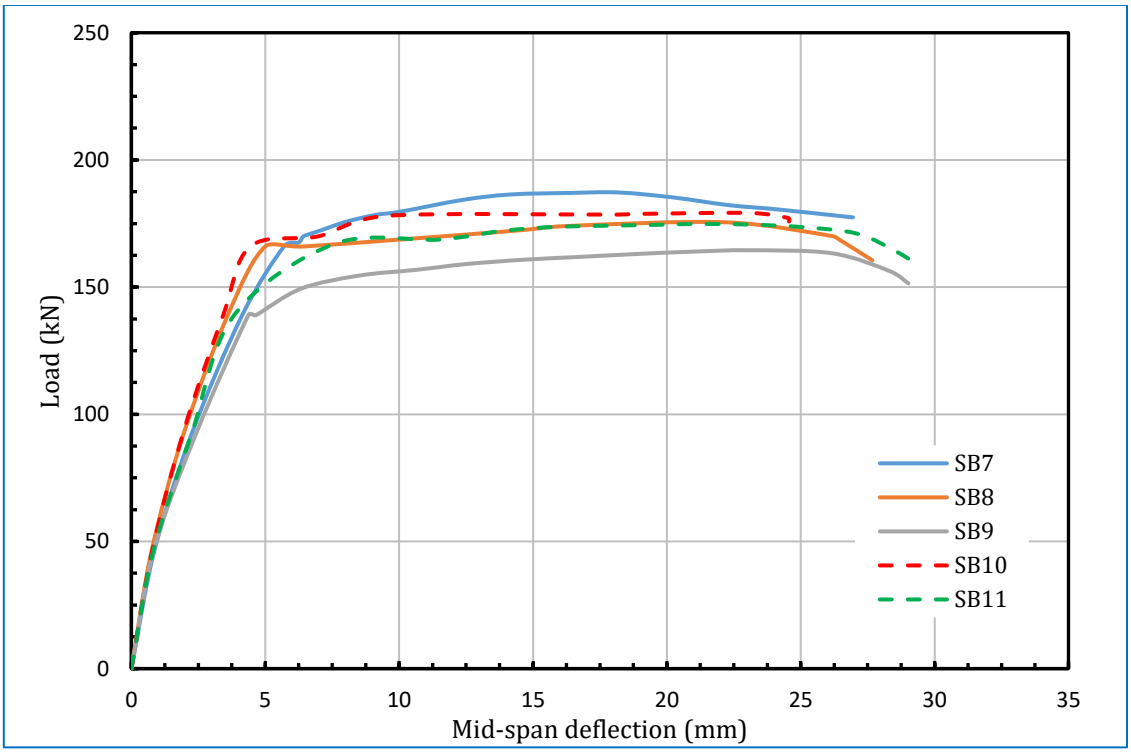

Figure 4-12: The envelope load deflection response for specimens tested with cyclic loading.

Figure 4-12 shows the load-deflection responses in the mid-span section of all test specimens. All specimens experienced similar behavior with a linear load-deflection response before flexural cracking. After that, some of the differences in the yielding stage of girders. Where the girder SB_9 shows the little yield load. All the girders have good ductile responses before the collapse stage. For girder, SB_{11} notices the last three cycles have sustained high deflection because of the specimen inter the plastic stage. The full-depth girders have approximately similar load-deflection responses due to the good bond strength of the joints with the precast segment.

- **$SB_{12}.HC_3.D.\ L_1$**

This girder has the same properties of girder SB_3 with addition steel reinforcement as a dowel to increase the bond strength of joint. This reinforcement embedded through the interior precast segment. In the test of girder gave similar behavior of SB_3 with some difference in the value of crack and ultimate load as shown in Figure 4-13. First crack was initiated at the mid span near to joint (in the interface) at load 33 kN and the crack in flange at load 160 kN. The cracking pattern after failure occur at load 191.26 kN illustrated in Plate 4-12 . The good properties of UHPC and active bond of joint may reflect non-significant difference in overall behavior of girders with presence of dowels. But, there was an increased in the ultimate load, and that may resulting from increase reinforcement ratio in the mid span zone, and reduced the cracks at interface plane of joint and precast segment.

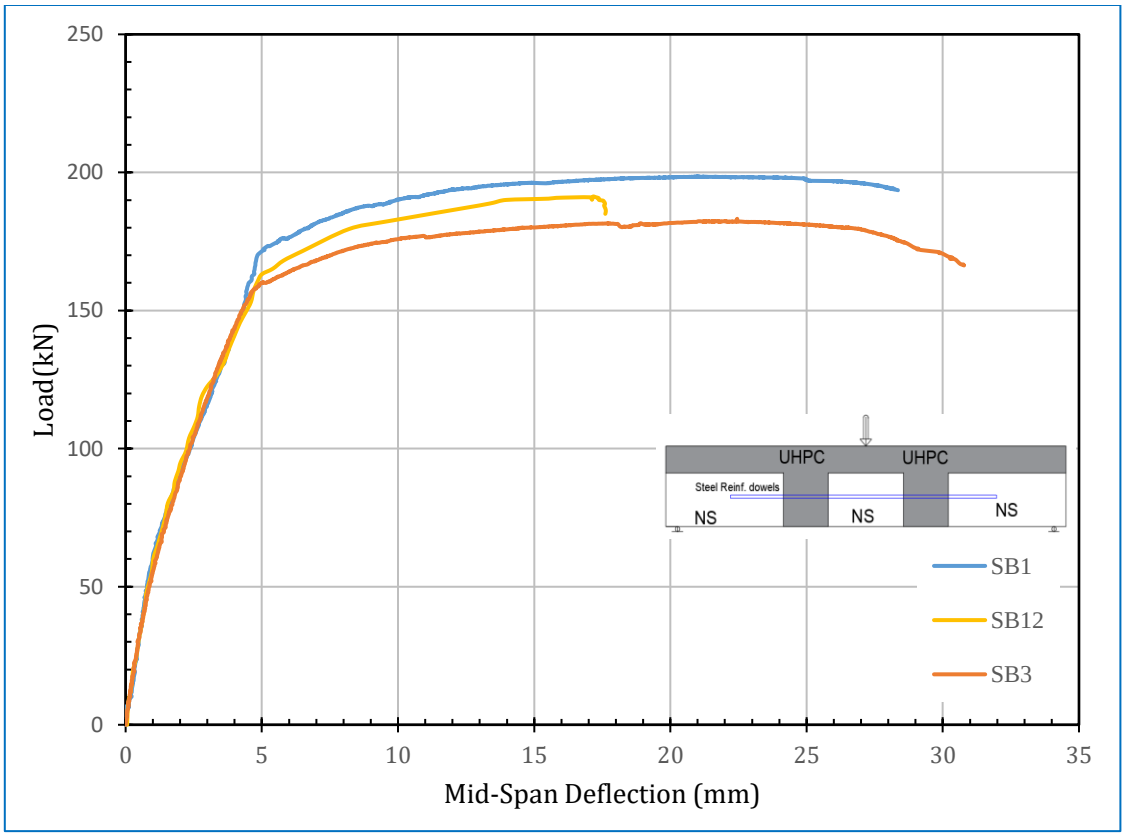

Figure 4-13:Load-mid-span deflection curve of $SB_{12}.HC_3.D.\ L_1$.

Plate 4-12:Cracks and mode failure of girder $SB_{12}.HC_3.D.\ L_1$.

4-4-1-2 Effect of Considered Variables

The effect of variables that studied in experimental program such as (depth of joint, hybridization of reinforcement, presence of shear key, addition of steel reinforcement as dowel action, and type of loading) will be discussed to addition more understanding of the overall behavior of this group.

I. Cracking load and cracking pattern

The presences of joints were led to decrease the cracking load and location for all spliced girder as compared with control (monolithically) girder.

The spliced girders were appeared the first flexural crack at or close to the interface region between precast segment and UHPC joint as hair line crack then transport the cracks to the mid span zone in more developing state. While the control specimen has first crack at mid span zone were location of maximum bending moment. In the same field, the presence of flat joint has slight effect on the first flexural cracking load for full depth and partial depth (web depth) joint, as compared with control girder.

Adding the shear key to spliced girder for both case of joint depth improved the cracking load by increasing first flexural crack load to 44.3% for full depth joint and 22.6% for partial depth joint as compared with spliced girder of flat joints. Cracking pattern of girder stay as in flat joint specimens except the interface cracking did not propagate vertically to reached the flange. These cracks inclined when reached the UHPC shear key toward the precast segments and continue to the flange then did not observe.

Replacement 50% of steel reinforcement by CFRP bar were caused a slight increasing in first flexural crack load, where increased by 47.2 % compared to partial depth flat joint. The propagation of cracks was similar approximately to

girder $SB_3.HC_3.L_1$ with little crack intensity. Shear crack initiated after about 0.75Pu and developed with increasing the load. At UHPC joint did not occur any splitting cracks, while a splitting crack was visible in precast segment at final stage of loading (more than 0.95Pu).

Adding more steel reinforcement as dowel action in joint had high enhancement for the first flexural cracking load by about 56.6 % compared to partial depth flat joint. Some of shear crack appeared after about 0.75Pu at top of web and propagated to flange zone after 0.9Pu, meanwhile that did not observe any splitting cracks.

In case of cyclic load, the location of first flexural cracks and the development of it were similar to same specimen tested under monotonic load with more intensity. In general, the first crack load was less than in monotonic load because the effect of cycles of loading and unloading. In control girder decreased the cracking load by 25%, while the spliced girder with full depth flat joint gives 6.5% deceased than same girder with monotonic load. In case of spliced girder with partial depth, also the decreased in cracking load about 11.3 % than same girder with monotonic load. When addition of shear key in cyclic loading, also the decreasing in the first flexural crack become about (23.8 and 6.2) % as compared with girder tested under monotonic load.

For all spliced girders, the UHPC joint zone had limited cracks. Those cracks had not propagated and no increased width with increasing the load. The same finding in (Maya and Graybeal, 2017). Meanwhile, the splitting cracks did not observed in UHPC joint due to adequate spliced length of reinforcement, the presence of stirrups in that joint, and the confinement provided by steel fiber in UHPC (Maya and Graybeal, 2017).

All those cracks were referred to visible crack that ranged by width (0.02–0.05) mm (Qiu et al., 2020). Then propagated with increase the load and reached to width about 4 mm at peak load.

II. Ultimate load and mode of failure

In general, the ultimate load of tested girders did not appear high differences in the load that caused failure of specimens. This fact was due to the high performance of joint and activity of bond mechanism of spliced girders, as well as, the adequate splice length of reinforcement and hooked encouragement. These reasons led to reduction effect of exist joint and transformation of forces (flexure and shear) through this joint with efficient mechanism. What proves this is the appearance of cracks after the joint zone and the stability of the deflected shape for all spliced girders during loading and the absence of wide cracks at interface of joint. Figure 4-14, illustrates the percentage of ultimate loads of girders compared with control girder.

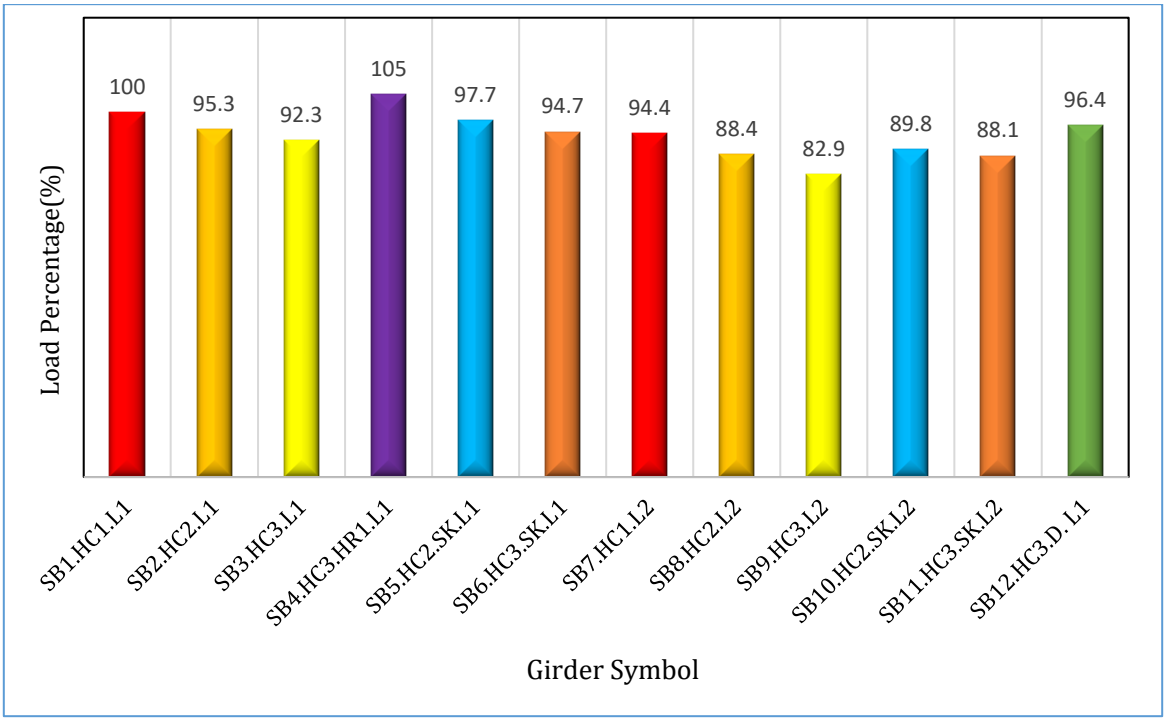

Figure 4-14: Load percentage of simply supported girders.

The existing of joint gives a reduction in ultimate load by about 4.7 and 7.7 % with respect to control girder, for full depth joint ($SB_2.HC_2.L_1$) and partial depth joint ($SB_3.HC_3.L_1$), respectively. This splicing did not affect the mode of failure (flexural failure) were that controlled. The length of interface joint that occur vertical only in HC_2 pattern of splicing girders was caused this better result in stiffness of girder and a slightly more ultimate load compared with HC_3.

In (Al-Tameemi, 2015), the decreasing of the ultimate load when used one NSC joint in mid span with full length development splicing were about 3% with Interface crack opening and splitting mode of failure. Also for (Hassoon, 2021), when used NSC joint with full length development reduced the ultimate load by 24.1% and close to reference beam when used SFC in that joint.

Replacement of 50% of steel reinforcement by CFRP bar in girder ($SB_4.HC_3.HR_1.L_1$) achieve a good performance for splicing girder. Where it is provided increasing in ultimate load by 5% compared with control specimen. Meanwhile, the presence of CFRP bar gives an increasing in the ultimate load by 13.7% when compared with ($SB_3.HC_3.L_1$) this result also observed by (Cao et al., 2017). In spite of this increment in ultimate load of girder SB_4, however, the joint did not appear bond failure or large wide cracks in those joints. Due to high applied load without any strengthening for shear strength of specimen, this girder showed a shear crack with addition to flexural crack leading to change the mode of failure from pure flexural failure to combined shear-flexure failure.

The presence of shear key in joints provide challenge effect of ultimate load close to that of control and by about 2.4% when compared with flat joint girder for both case of joint depth. In the same hand, shear key did not change or effect on the mode of failure of girder.

Adding of steel reinforcement as dowel action in girder ($SB_{12}.HC_3.D.\ L_1$) led to improve the ultimate load of specimen close to that of control where the reduction 3.6 %, while as that was 7.7% in ($SB_3.HC_3.L_1$). Mode of failure did not change (i.e. flexural failure) were controlled.

Duo to the adverse effect of the loading and unloading in cyclic load, the ultimate load of girder was reduced. In control specimen, reduction in ultimate load achieved about 5.6%. the reduction in girder ($SB_8.HC_2.L_2$, $SB_9.HC_3.L_2$, $SB_{10}.HC_2.SK.L_2$, *and* $SB_{11}.HC_3.SK.L_2$) about 7.2, 10.2, 8.1, and 7 % compared with same girder tested monotonically. Mode of failure still as in monotonic loading with more deterioration for specimen.

III. Cracks width

From testing of girders, the initiated cracks during loading process such as flexural, interface, and shear cracks observed and meagered its width with load increment by crack meter instrument as listed in Table 4-4. All splice girders have interface crack started at bottom layer where maximum tension stresses and propagated toward top layer with increase loading. But those cracks did not develop or penetrate the girder section due to high bond strength of UHPC joint with precast segment. So, it has crack width range by (0.02- 0.1) mm during the increasing of load. Also, the development of flexural cracks at mid span and give more width with load increment led to restrained the interface cracks from having wider.

Maximum flexural crack occurred at mid span zone where the maximum bending moment was applied. Figure 4-15 shown the variation of flexural cracks width with applied load for simply supported girders. From Table 4-4, the presence of joint did not affect on the crack width at service load. While, when

addition shear key for spliced girder gives reduction in crack width by about 25 and 16.7 % for girders $SB_5.HC_2.SK.L_1$ and $SB_6.HC_3.SK.L_1$, respectively.

On the other hand, the presence of CFRP bar in $SB_4.HC_3.HR_1.L_1$ girder did not gives any enhancement to service crack width. It is important to say that shear and splitting cracks that appeared at last stage of loading was a visible cracks had width ranged by (0.02- 0.07) mm.

Due to the adverse effect of loading and unloading process of cyclic load, the flexural crack width at service load increased by about 7.1% for control girder, and 16.7% for both case of depth joint in spliced girder with flat joint, 11.1% for girder has full depth joint with shear key, and 20 % for girder of partial depth joint with shear key. These results were compared with same girder tested monotonically. Also, these girders showed more deterioration and intensity of cracks separation during the cycles of load and unload. This results was confirmed by (Maya and Graybeal, 2017);(Qiu et al., 2020);(Hassoon and Aljanabi, 2020).

The results of flexural cracks showed that all spliced girders did not exceeded the limits of crack width in service stage according to ACI-code requirement (ACI-318, 2019). The interface cracks in all spliced girder did not develop with increased the load, thus these cracks were no direct significant in the failure prosses of spliced girders.

While for research of (Al-Tameemi, 2015) and (Hassoon, 2021), the wide cracks occurred in the interface of joint that causing the failure of beams. These interface cracks were exceeded the limits of cracks in service stage according to ACI-code requirement (ACI-318, 2019).

Table 4-4: Flexural crack width values of girders at service load.

Girder Symbol	Service load, *Ps* (kN)	Crack width at service load (mm)
$SB_1.HC_1.L_1$	129.0	0.14
$SB_2.HC_2.L_1$	122.9	0.12
$SB_3.HC_3.L_1$	119.1	0.12
$SB_4.HC_3.HR1.L_1$	135.4	0.24
$SB_5.HC_2.SK.L_1$	126.1	0.09
$SB_6.HC_3.SK.L_1$	122.2	0.1
$SB_7.HC_1.L_2$	121.7	0.15
$SB_8.HC_2.L_2$	114.0	0.14
$SB_9.HC_3.L_2$	106.9	0.14
$SB_{10}.HC_2.SK.L_2$	115.8	0.1
$SB_{11}.HC_3.SK.L_2$	113.6	0.12
$SB_{12}.HC_3.D.\ L_1$	124.3	0.1

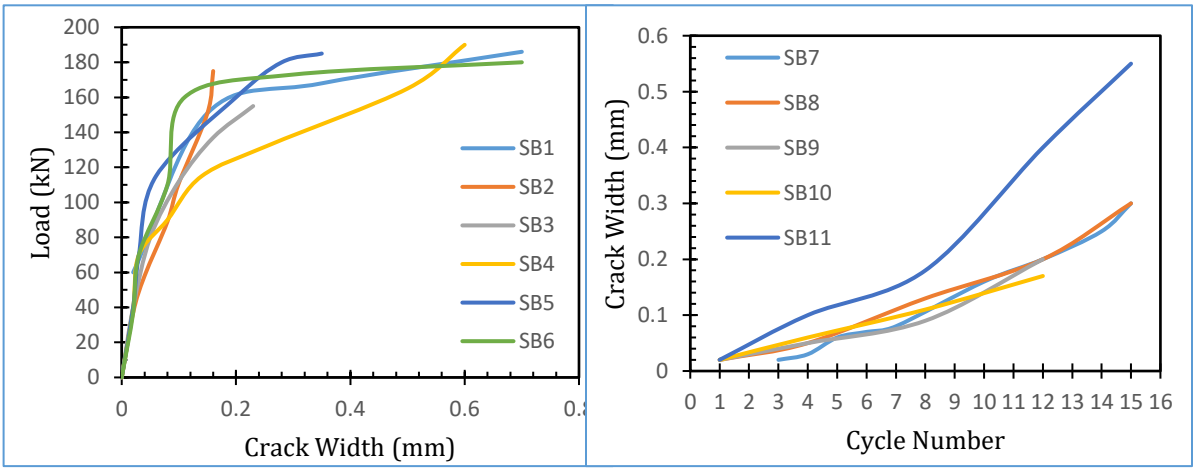

a- *Flexual crack width verses applied load for girder tested statically.*

b- *Flexual crack width verses cycle number for girder tested with cyclic loading.*

Figure 4-15:Relationship of crack width with load for simply supported girder.

IV. Initial stiffness

Stiffness is the deflection caused by the applied load at service stage. Initial stiffness can be determine from the slope of load-deflection curve at service load stage (0.65 *Pu*) (Al-Quraishy, 2012),(AL-Khafaji et al., 2018). Elastic stiffness also can be determined from the ratio of cracking load to the deflection at this load (Qiu et al., 2022). Table 4-5 show the results of secant stiffness of this group.

The good properties of UHPC in joint and the high bond strength for UHPC joint with NSC of precast segments caused the increasing in the initial stiffness of splice girders. High modulus of elasticity of UHPC may cause more stiffness for specimen. Girder ($SB_2.HC_2.L_1$ and $SB_3.HC_3.L_1$) included increasing in stiffness by about 7.6 and 6.6 % respectively, with respect to control girder. The splice girder with full joint depth appears more stiffness due to absence of horizontal cold joint between web and flange.

Hybridization of reinforcement did not achieve addition stiffness for spliced girder as resulted by (Song et al., 2021).

When addition of shear key for spliced girders provides some improvement in stiffness of these girders by 2.5% for ($SB_5.HC_2.SK.L_1$) and 5.7% for ($SB_6.HC_3.SK.L_1$) when compared with same girder having flat joint.

Also, addition of steel reinforcement to increase the dowel action of joint led to slight increasing in stiffness.

In the cyclic load, the stiffness of girders was decreasing due to the adverse effect of load and unload process as result to cumulative residual stresses. Where that the control girder showed decreasing in stiffness about 7%. while the spliced girder gives decreasing in stiffness by 4.1 and 6.2% for girder ($SB_8.HC_2.L_2$ and

$SB_9.HC_3.L_2$) respectively. Notice that the partial depth joint appeared more deterioration than full depth joint girder. Shear key in full depth girder has reduction in stiffness by 1.8% as result to cyclic load, while the partial depth joint has reduction about 8.8 % for same reason.

Table 4-5: Initial stiffness of simply supported girder.

Girder Symbol	*Service load, P_s (kN)*	*Deflection Δ_s (mm)*	Stiffness, K (kN/mm)
$SB_1.HC_1.L_1$	129	3.5	36.9
$SB_2.HC_2.L_1$	122.9	3.1	39.7
$SB_3.HC_3.L_1$	119.1	3.03	39.3
$SB_4.HC_3.HR_1.L_1$	135.4	5.7	23.8
$SB_5.HC_2.SK.L_1$	126.1	3.1	40.7
$SB_6.HC_3.SK.L_1$	122.2	2.94	41.5
$SB_7.HC_1.L_2$	121.7	3.55	34.3
$SB_8.HC_2.L_2$	114.0	3	38.0
$SB_9.HC_3.L_2$	106.9	2.9	36.9
$SB_{10}.HC_2.SK.L_2$	115.8	2.94	39.9
$SB_{11}.HC_3.SK.L_2$	113.6	3	37.9
$SB_{12}.HC_3.D.\ L_1$	124.3	3.15	39.5

V. Ductility index

Ductility is the ratio of displacement caused by peak load $\Delta_{\max or\ u}$ to the yield displacement Δ_y as illustrated in Figure 4-16. It is referred to the ability of structural member to resist load and give more displacement without descending in the load carrying capacity. The yield displacement Δ_y of girder can be

predicted as shown in Figure 4-17. While $\Delta_{\max or\ u}$ suggesting by many researchers that refer to displacement corresponding to 80% of peak load after reduce the load on load-deflection curve((Saghafi et al., 2019) ,(Chidambaram and Agarwal, 2015), and (Qiu et al., 2020)). On the other hand, many of researchers defined this term on that the displacement corresponding to peak load((Song et al., 2021),(Cao et al., 2017),(Yoo and Yoon, 2015),(Yang et al., 2010), and (Qi et al., 2020) (Qiu et al., 2022)).

In the present study, the last definition of $\Delta_{\max or\ u}$ was adopted and the results of ductility index are listed in Table 4-6. The spliced girders were achieving more ductility than control girder by about 16.8% for full depth joint and 17.3% for partial depth joint. The presence of UHPC with good bond to precast segment gives this high ductility for spliced girders. The monolithic connection of UHPC joint with flange were added improvement to ductility.

Girder ($SB_4.HC_3.HR1.L_1$) was appeared reduction in ductility due to the presence of CFRP bars which have brittle response, agree with that of (Song et al., 2021).

The presence of shear key did not added improvement in ductility. It reduces by 10.1 and 2.65 % for ($SB_5.HC_2.SK.L_1$ and $SB_6.HC_3.SK.L_1$) respectively, when compared with same girders having flat joints, but larger than control.

When added steel reinforcement to joint in order to support the dowel action, the reinforcement ratio was increased and leading to decrease the ductility by about 14.2% when compared with control girder in spite of the presence of UHPC joint (Hasgul et al., 2018).

In the cyclic load, the control girder was appearing reduction in the ductility by about 6.6% as compatible with (Hassoon, 2021). While in the spliced girder, the ductility was increased in cyclic loading by (1.9, 3, 24.1, and 1.8) % when compared with same girders with monotonic load and (27.1, 29.3, 39.5, and 15.9)

% when compared with control girder with cyclic load, for girders ($SB_8.HC_2.L_2$, $SB_9.HC_3.L_2$, $SB_{10}.HC_2.SK.L_2$, and $SB_{11}.HC_3.SK.L_2$) respectively.

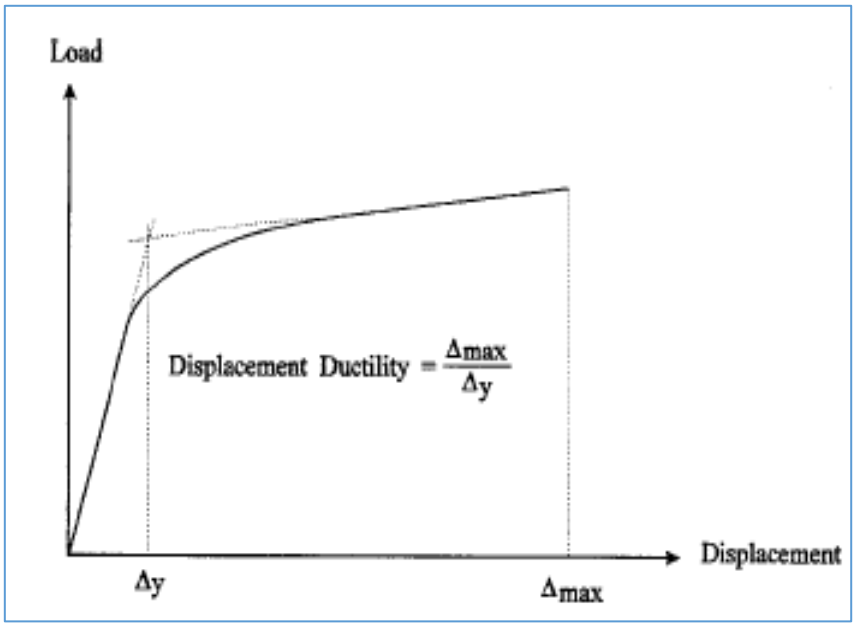

Figure 4-16:Method of calculation ductility index (Azizinamini et al., 1999)

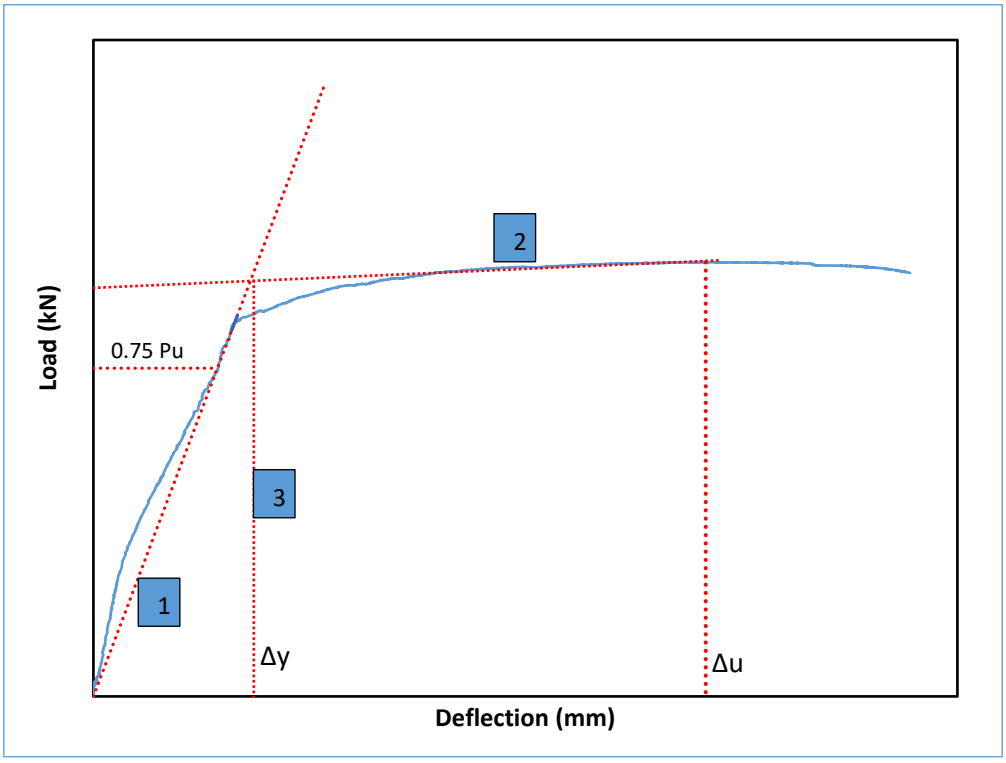

Figure 4-17:Example to determine the ductility index for girders.

Table 4-6: Results of ductility index for simply supported girders.

Girder Symbol	Ultimate disp. Δu (mm)	Yield disp. Δy (mm)	Ductility index μ
$SB_1.HC_1.L_1$	22.26	5.7	3.91
$SB_2.HC_2.L_1$	22.8	5	4.56
$SB_3.HC_3.L_1$	22.45	4.9	4.58
$SB_4.HC_3.HR1.L_1$	21.84	10.8	2.02
$SB_5.HC_2.SK.L_1$	20.9	5.1	4.10
$SB_6.HC_3.SK.L_1$	22.3	5	4.46
$SB_7.HC_1.L_2$	19.7	5.4	3.65
$SB_8.HC_2.L_2$	22.83	4.7	4.84
$SB_9.HC_3.L_2$	23.07	5.1	4.52
$SB_{10}.HC_2.SK.L_2$	23.14	4.55	5.09
$SB_{11}.HC_3.SK.L_2$	21.16	5	4.23
$SB_{12}.HC_3.D.\ L_1$	17.42	5.2	3.4

VI. Energy absorption

Energy absorption was calculated by the sum of area under load-deflection curve limited by failure load. It was significant parameter describing the post yielding response of structural member (Chidambaram and Agarwal, 2015). The results of energy absorption calculation were illustrated in Figure 4-18.

For the spliced girders, the full depth joint girder gave very close energy absorption to control girder because it was resisted more deflection at plastic stage before failure. On the other hand, the partial depth girder included reduction (6%) in the energy absorption due to the reduction in the strength capacity.

In the hybridization of reinforcement, the energy absorption was reduced by 3.6% when compared with girder having full steel reinforcement. This reduction due to the shear behavior of girder in the advanced stage of loading and this provided in the ductility results. As introduced by (Song et al., 2020).

The energy absorption of girders with shear key were very close together. The girder ($SB_5.HC_2.SK.L_1$) was achieve reduction by about 6.5% when compared with flat joint girder. Meanwhile, the girder ($SB_6.HC_3.SK.L_1$) reduced by 1.8% with respect to flat joint girder. These result insured in the ductility index results.

For girder ($SB_{12}.HC_3.D.\ L_1$), the energy absorption was reaching the lower value of this group due to the non-ductile behavior of this girder caused by addition of reinforcement.

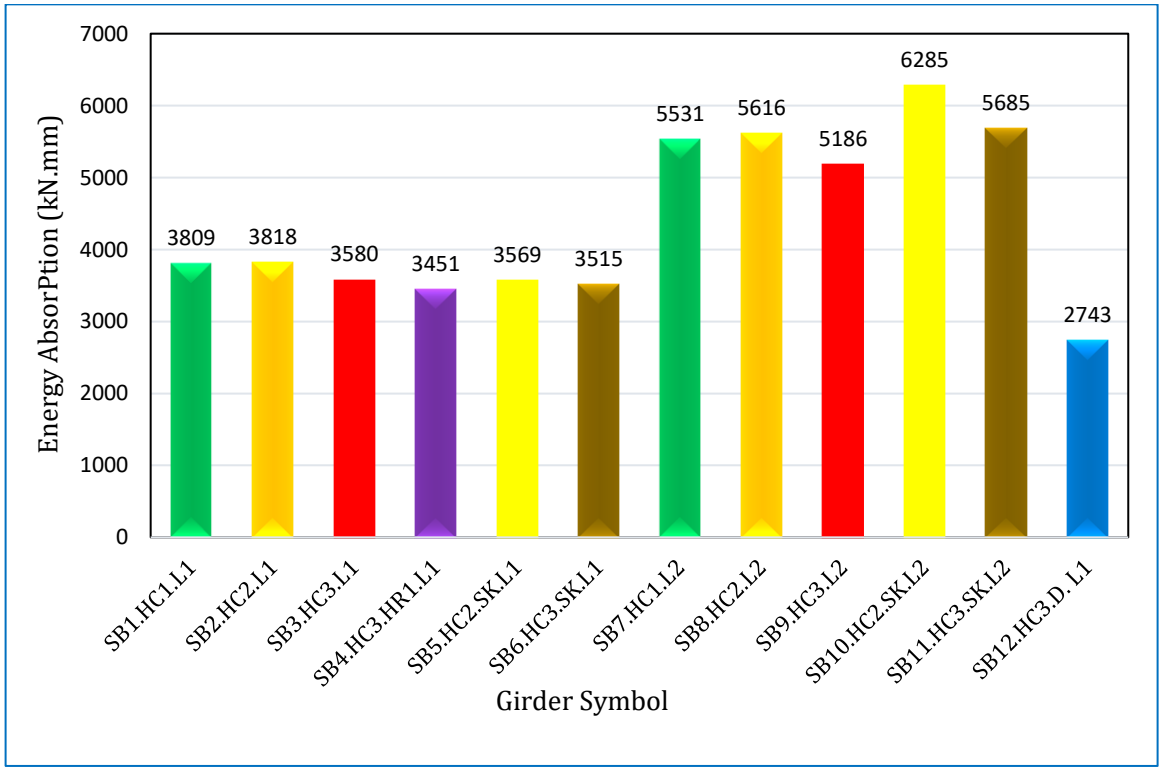

Figure 4-18: The variation of energy absorption of simply supported girders.

In the girders that tested under cyclic loading, the cumulative energy absorption was measured to having more understanding on the post yield response of tested girders. The cumulative energy absorption equal to the sum of area under load-deflection curve for each load cycle (Song et al., 2020);(Cao et al., 2017). Figure 4-19 explained the cumulative energy absorption of cyclic loading girders.

For control girder, the energy absorption was increased by 45.2% when compared with control girder tested monotonically.

When existing of joints in the girders, the energy absorption was increased 47.1% for specimen ($SB_8.HC_2.L_2$) and 44.9% for specimen ($SB_9.HC_3.L_2$) when compared with same girders tested statically. In the same hand, the girder ($SB_8.HC_2.L_2$) was reach to increasing the energy absorption by 1.5% on the girder ($SB_7.HC_1.L_2$) owing to the good performance of UHPC joint in absorbing the energy and resisting the deflection without failure. While, the girder ($SB_9.HC_3.L_2$) showed reduction in the energy absorption by 6.2% respected to ($SB_7.HC_1.L_2$).

The presence of shear key in the girder tested with cyclic load was led to increase the energy absorption. This increasing was reached to (76.1 and 61.7) % with respect to same girder tested statically and (11.9 and 9.6) % with respect to flat joint girder tested under cyclic load, these result for ($SB_8.HC_2.SK.L_2$ and $SB_9.HC_3.SK.L_2$) respectively.

From Figure 4-19,The primary cycles of loading include close value of energy absorption in all girder and become different after 11^{th} cycle.

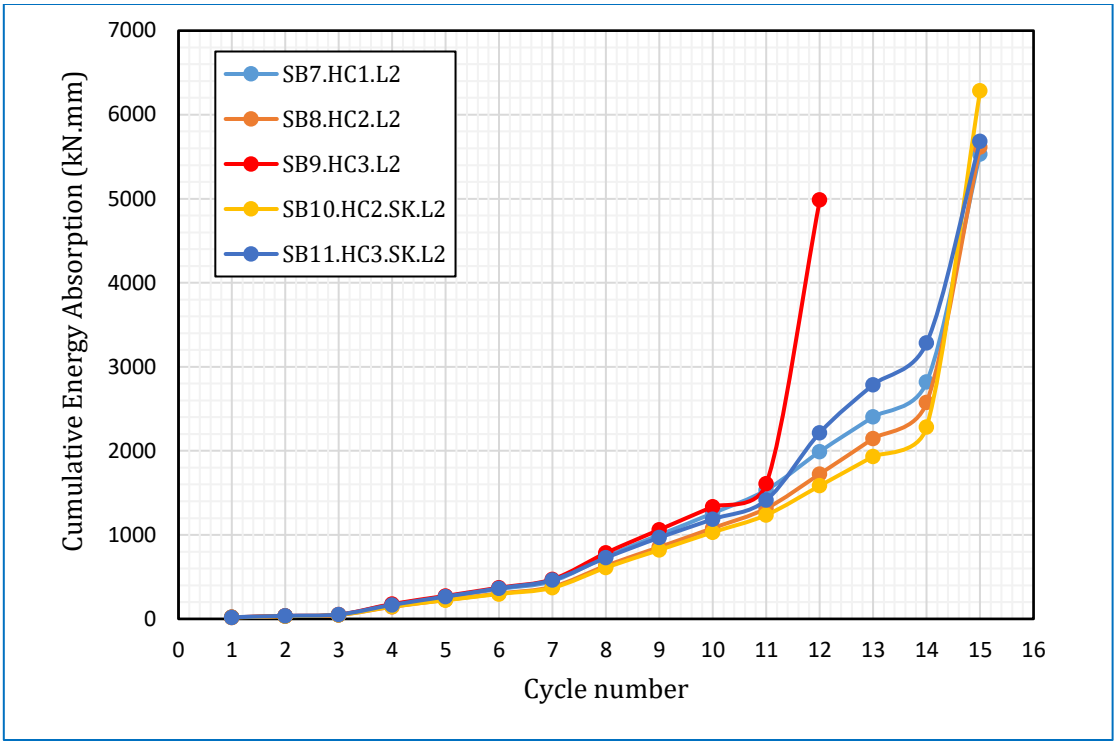

Figure 4-19: The cumulative energy variation of simply supported girders tested under cyclic load.

VII. Damage Index

This index was calibrated to be used in comparison of the damages in the structural members exposed to cyclic load(Villemure and Ventura, 1995).

Damage index [DI] vary from zero to 1, so that zero indicates no damage and 1 indicates a complete damage and the among this value illustrated in Table 4-7.

Table 4-7: Indications of damage index value (Saghafi et al., 2019)

Value of DI	Indication of damage
0 < DI < 0.2	non-damage
0.2 < DI < 0.4	minor damage
0.4 < DI < 0.6	moderate damage
0.6 < DI < 0.8	serious damage
DI > 0.8	complete damage

$DI = \frac{\Delta_c}{\Delta_u} + \frac{\beta}{F_y.\Delta_u} E_i$ …… *(4-14)* (Chidambaram and Agarwal, 2015)

Where:Δ_c is the maximum displacement of each cycle, Δ_u is the maximum displacement after complete loading, F_y is the peak load of each cycle, β is the degradation parameter equal to 0.1 according to (Villemure and Ventura, 1995), and E_i is the energy absorption for each cycle.

The results of damage index that calculated for this group were explained in Figure 4-20. The control girder interred the minor damage state after 7 cycles of loading. While the spliced girders interred this stage after 11 cycles. The girder ($SB_{11}.HC_3.SK.L_2$) exceeded minor damage after 12 cycles to inter in moderate stage and give clear damage indication with each cycle.

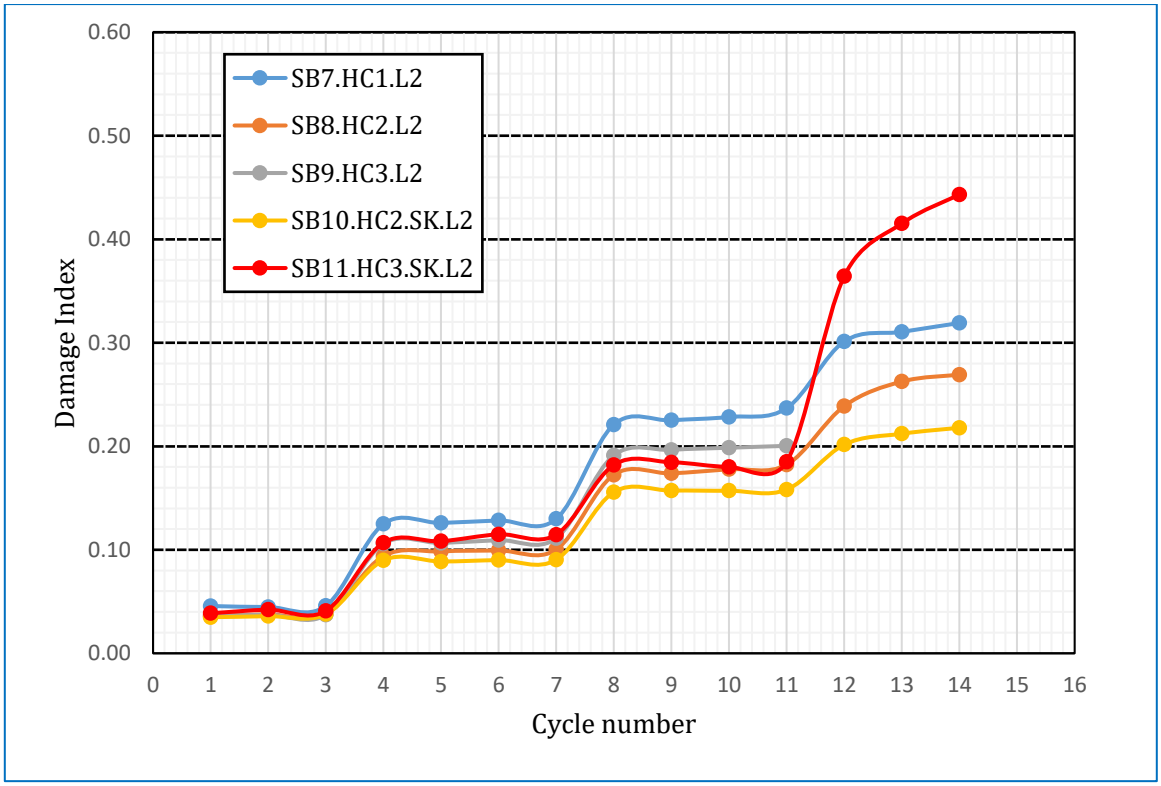

Figure 4-20: The damage index value with cycle no. of simply support girder.

4-4-2 Continuous Girders

4-4-2-1 General behavior

This group were consisting of nine continuous supported girders. Two of these girders were cast monolithically as one unit to refer the control specimen. Other girders divided to subgroup according to the location of joint, three of them had two joints at inflection point and four girders had one joint at interior support. All girders have same length, section, and length of joint, with some of variables such as the location of joint, hybridization of reinforcement, and presence of shear key. Six of them were applied to static load and others tested under repeated load by the previous adopted protocol. The results of this group were listed in Table 4-8, and the behavior of each specimen will be described in sections below.

Table 4-8:Summary the results of continuous supported girders.

Girder Symbol	*Cracking load* P_{cr} *(kN)*	*Ultimate load* P_{ul} *(kN)*	*Deflection* Δ_{ul} *(mm)*	*Mode of failure*
$CB_{13}.HC_1.L_1$	174	481.85	18.4	Flexural
$CB_{14}.HC_4.L_1$	162	398.8	12.4	Shear Flexural
$CB_{15}.HC_5.L_1$	170	454.6	11.3	Flexural
$CB_{16}.HC_4.HR2.L_1$	160	491	12.16	Shear Flexural
$CB_{17}.HC_4.SK.L_1$	109	413.1	13.6	Shear Flexural
$CB_{18}.HC_5.SK.L_1$	110	460.5	13.8	Flexural
$CB_{19}.HC_1.L_2$	170 /cyc.4	469.3 /cyc. 15	18.7	Flexural
$CB_{20}.HC_4.L_2$	135 /cyc.4	389.1 /cyc.12	16	Shear Flexural
$CB_{21}.HC_5.L_2$	120 /cyc.3	450.9/cyc. 15	17.3	Flexural

- **$CB_{13}.HC_1.L_1$**

The control girder of continuous supported group, cast monolithically (without joint) for NSC in web and UHPC in flange. This specimen is very important to compare with other spliced girder to study the details of its structural behavior**.** CB_{13} tested under static five-point load up to failure. The deformations were developed with increasing the applied load, where the load increased in high range due to high stiffness of this girder during elastic range. At load 174 kN, the first crack appeared at mid span region (under point load), then remain load in increasing with a little crack at mid span and at load 184 kN show the first crack at flange of interior support. The cracks at this region continued to develop and transported to bottom zone (web) with increasing the load and the extension of crack at mid span. From the observation of test process, show that after load about 375 kN, become the crack develop at flange of interior support are large and the steel fiber start to splitting from the paste, but the girder still absorbed the load and the crack at mid span region were become clean and rapidly expanding. This condition persisted until failure at load 481.85 kN on two spans. Figure 4-21 show the average load –deflection response of CB_{13} and shape of failure and crack pattern were explained in Plate 4-13.

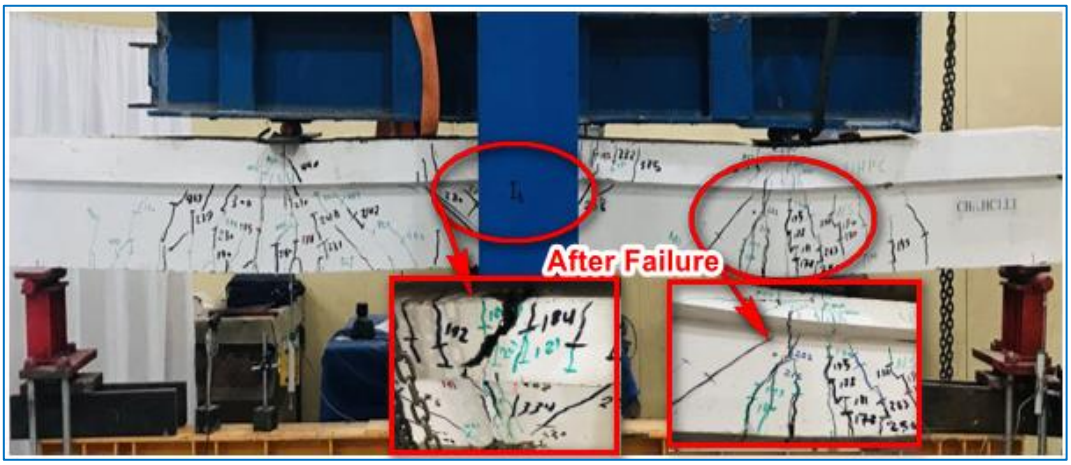

Plate 4-13: Cracks and failure mode of girder $CB_{13}.HC_1.L_1$.

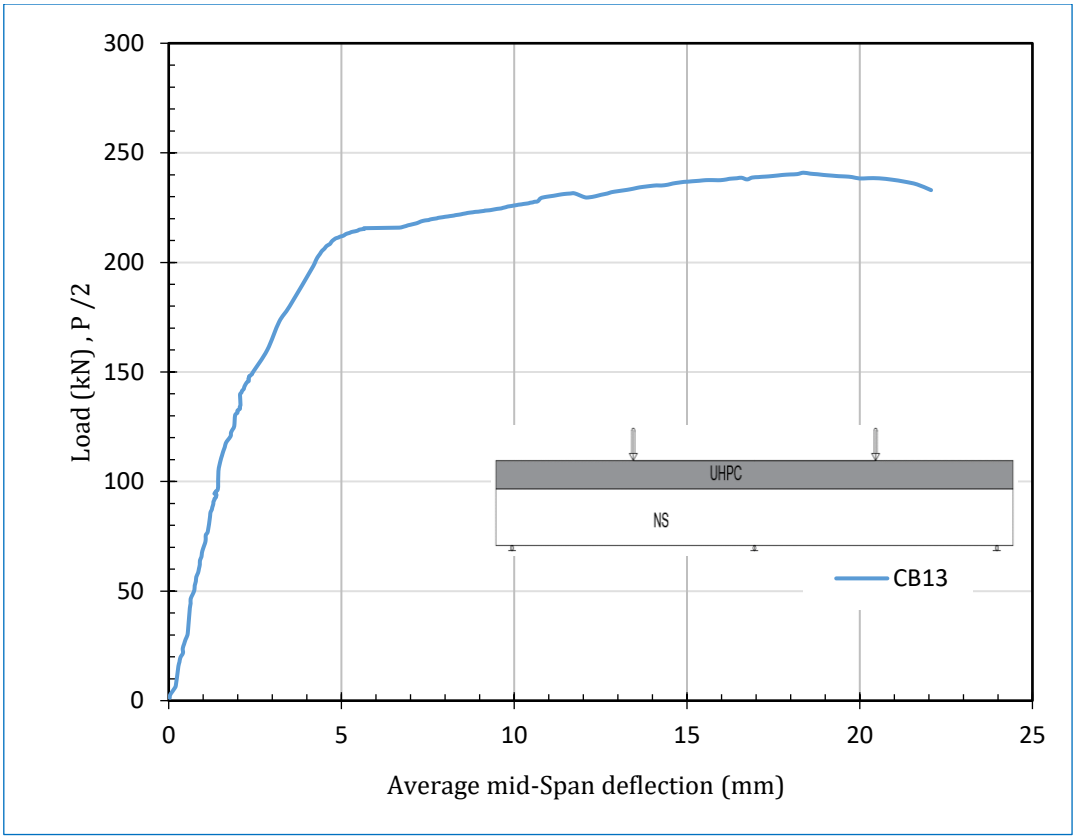

Figure 4-21: Load-Average mid span deflection curve of $CB_{13}.HC_1.L_1$.

- **$CB_{14}.HC_4.L_1$**

This girder was consisting of two precast segments having rectangular section (web only) made by NSC connected together by joint cast simultaneously with flange of UHPC. This joint located on the interior support exactly, so it's would be exposed to maximum moment and shear during the test. Static five-point load was adopted for testing this specimen. From tracking the test, the first crack was appearing at mid span of load about 160 kN then the first crack appeared in flange (of interior support) after load 190 kN. The deformations remain in development with increase the load for both region (mid span and interior support). After that, the crack being more separation at joint region and interface

due to direct shear of support and maximum negative moment. Vertical crack at joint between web and flange was initiated after load 243 kN, this crack started at interface between precast segment and UHPC joint from top layer to bottom at support with inclined path then developed to interface between web and flange horizontally. At support, where the maximum moment was occurred, the flexural cracks were smaller and has a slightly effect throughout the loading test due to the high performance and effect of steel fiber in UHPC in joint zone. So, shear crack initiated at support zone to being its adequate at failure mode by load about 398.8kN as shown in Plate 4-14. The average load-deflection behavior illustrated in Figure 4-22 and showed the difference with control specimen.

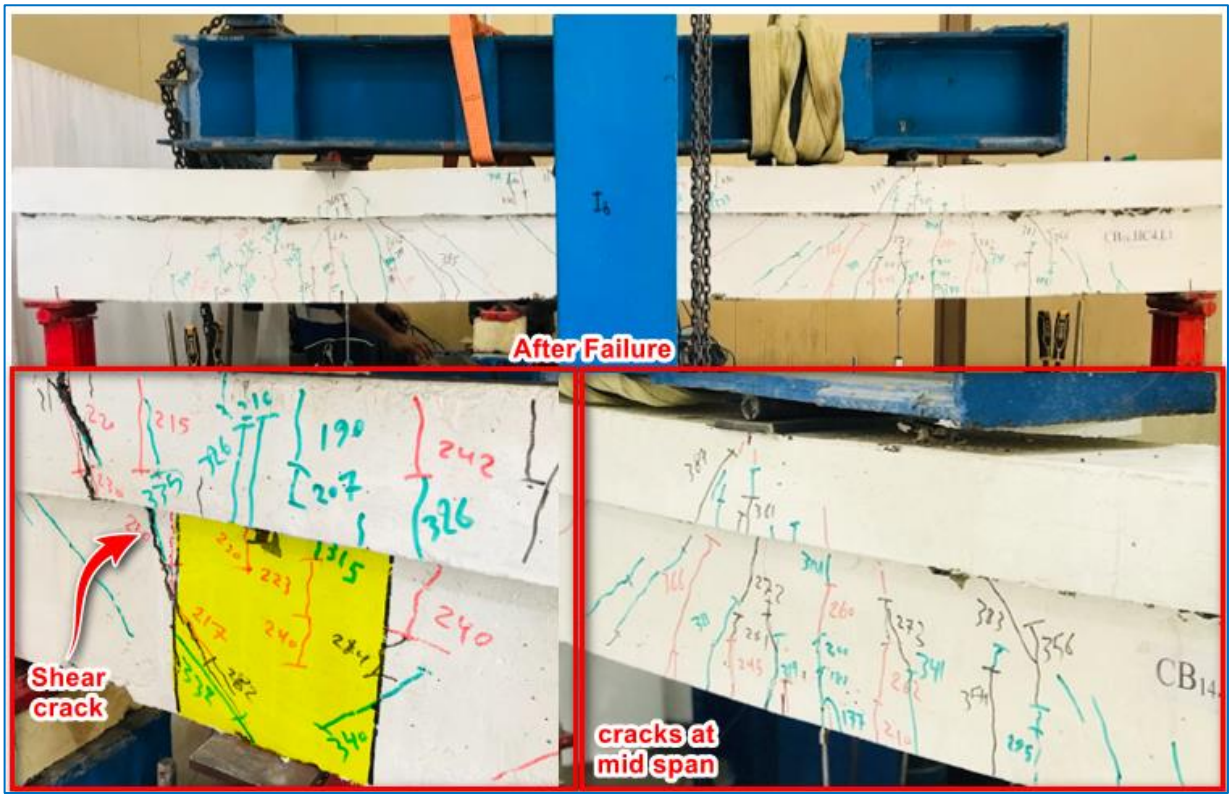

Plate 4-14: Cracks and failure mode of girder $CB_{14}.HC_{4}.L_{1.}$

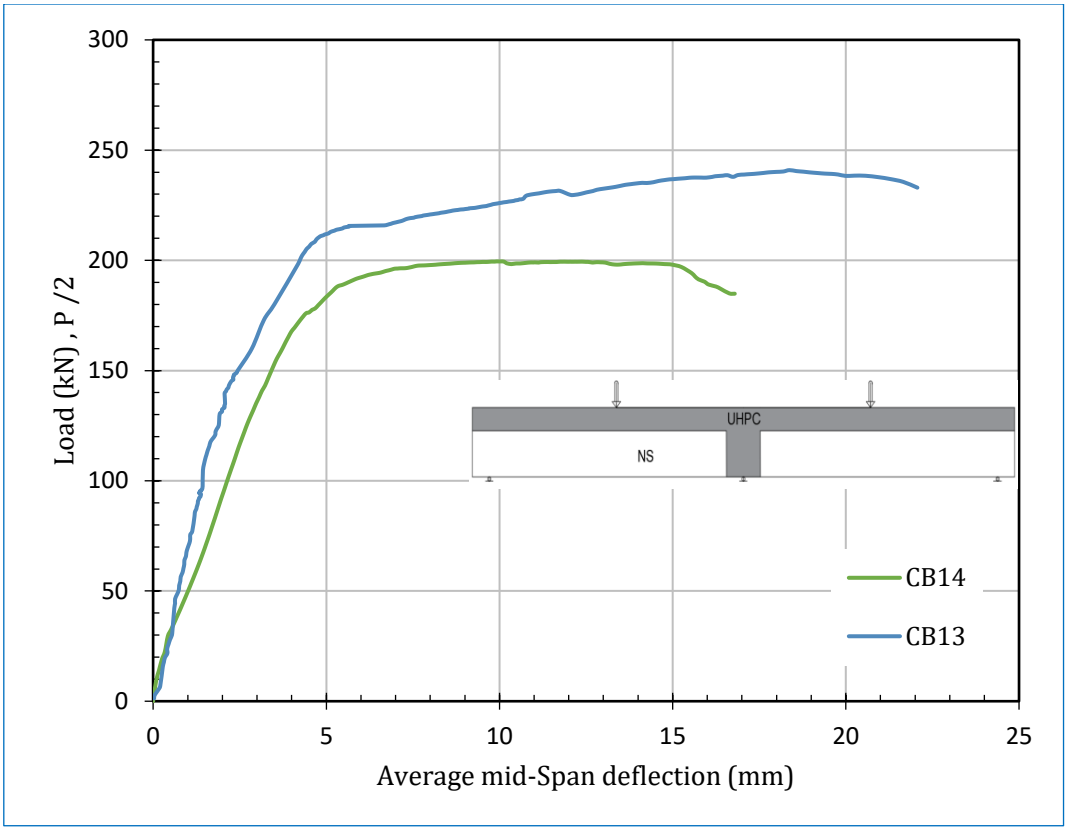

Figure 4-22:Load-Average mid span deflection curve of $CB_{14}.HC_4.L_1$.

- **$CB_{15}.HC_5.L_1$**

This girder was consisted of three precast segments having rectangular section (web only) made by NSC connected together by two joints cast simultaneously with flange of UHPC. Static five-point load was adopted for testing this specimen. From tracking the test, the first crack was appearing at mid span of load about 160 kN then the first crack appeared in flange (of interior support) after load 210 kN. The deformations continue to development with increase the load for both region (mid span and interior support). The crack reaches the bottom layer of interior support at load about 440 kN and at same load value the crack in mid span penetrates the flange completely. As happened in control

specimen, the deformations after load 400 kN included the flange was completely separated and splitting the steel fiber from the paste, then the crack rapidly developed at mid span with slowly development at support region in this stage. The joint region were remain in good state with some hair line cracks due to positive properties of UHPC and location of joint at inflection point. The crack pattern at failure load 454.6 kN was illustrated in Plate 4-15 and showed that the cutting in reinforcement at bottom in mid span and at top at interior support. This is referring to a good splice length of reinforcement in UHPC joints. The average load-deflection curve of this girder shown a great match in general behavior with control specimen as shown in Figure 4-23.

Plate 4-15: Cracks and failure mode of girder $CB_{15}.HC_{5}.L_{1}$.

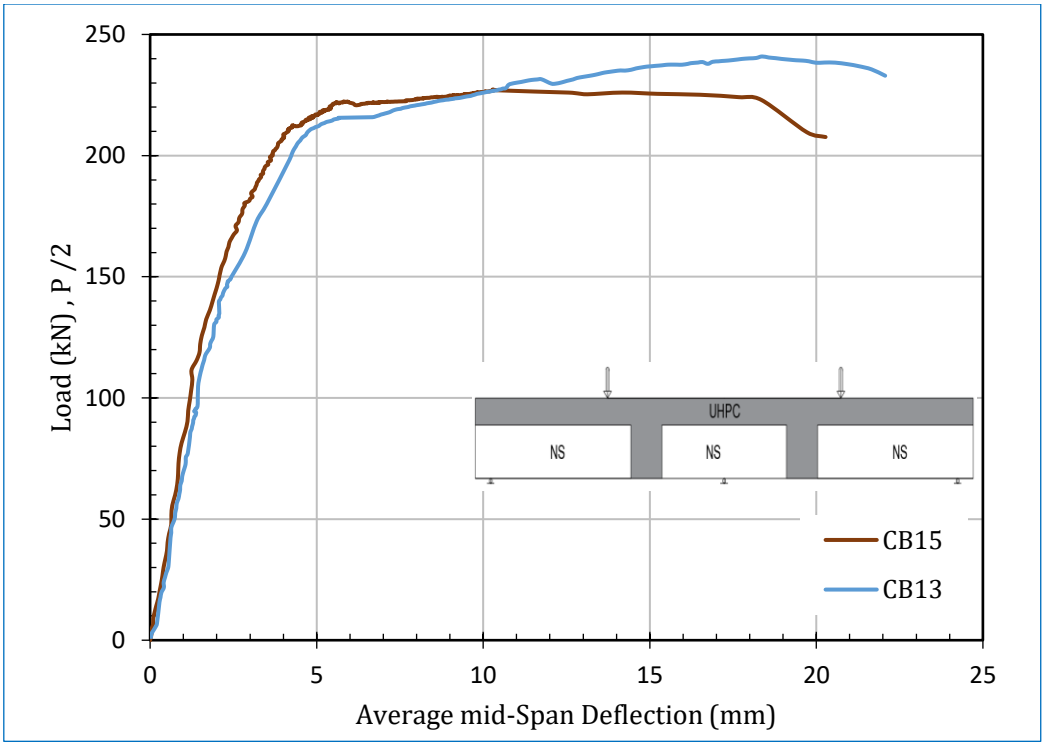

Figure 4-23:Load-Average mid span deflection curve of $CB_{15}.HC_5.L_1$.

- **$CB_{16}.HC_4.HR2.L_1$**

This girder has the same geometric properties of girder CB_{14} , as well as condition of testing with replacement of 50% of steel reinforcement by CFRP bar. Frist cracks and other general state of this girder were approximately similar to girder CB_{14} with some difference in load values. First crack load at mid span and interior support (flange) were 160 kN and 217 kN, respectively. CFRP was increase the stiffness of the girder at support flange. This led to maintain flange without large deformation of increasing crack width until to failure of girder by shear in joint at support, as shown in Plate 4-16. The ultimate load of girder was exceeded the control specimen to reach 491 kN with same mode of failure of CB_{14}. Average load deflection curve of this girder Figure 4-24 show the role of CFRP bar in improvement the behavior of girder.

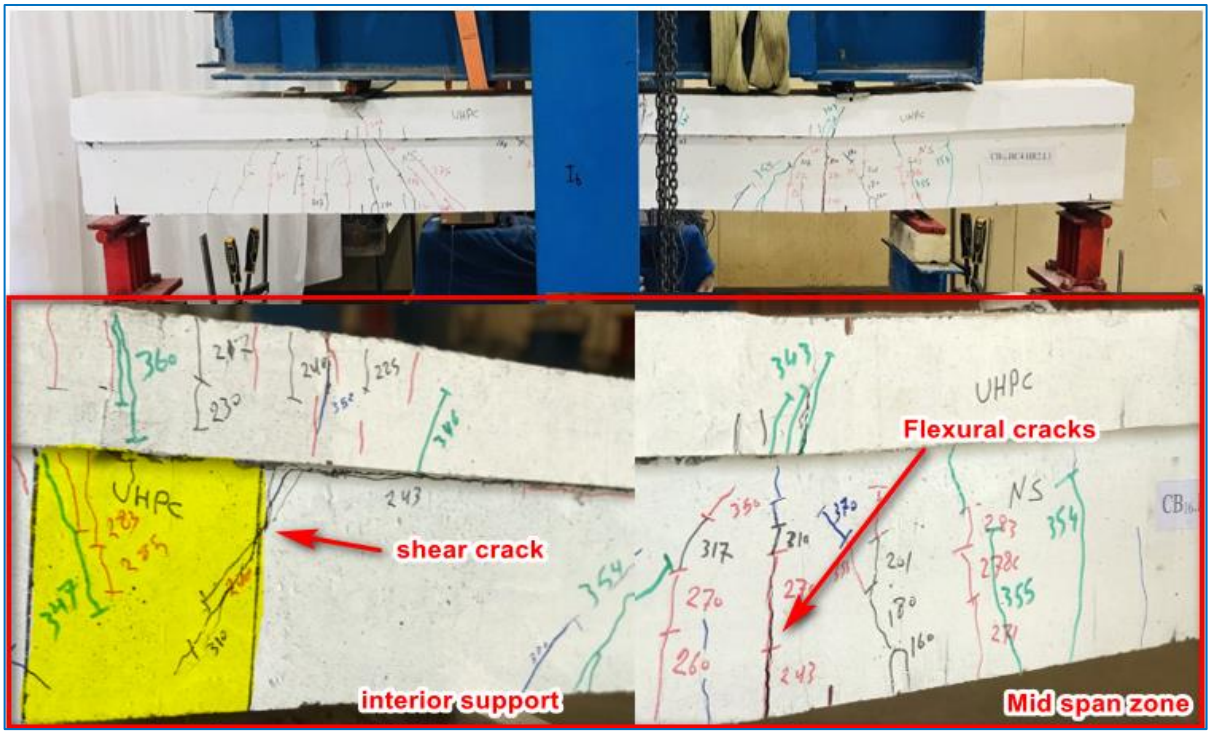

Plate 4-16: Cracks and failure mode of girder $CB_{16}.HC_4.HR2.L_1$.

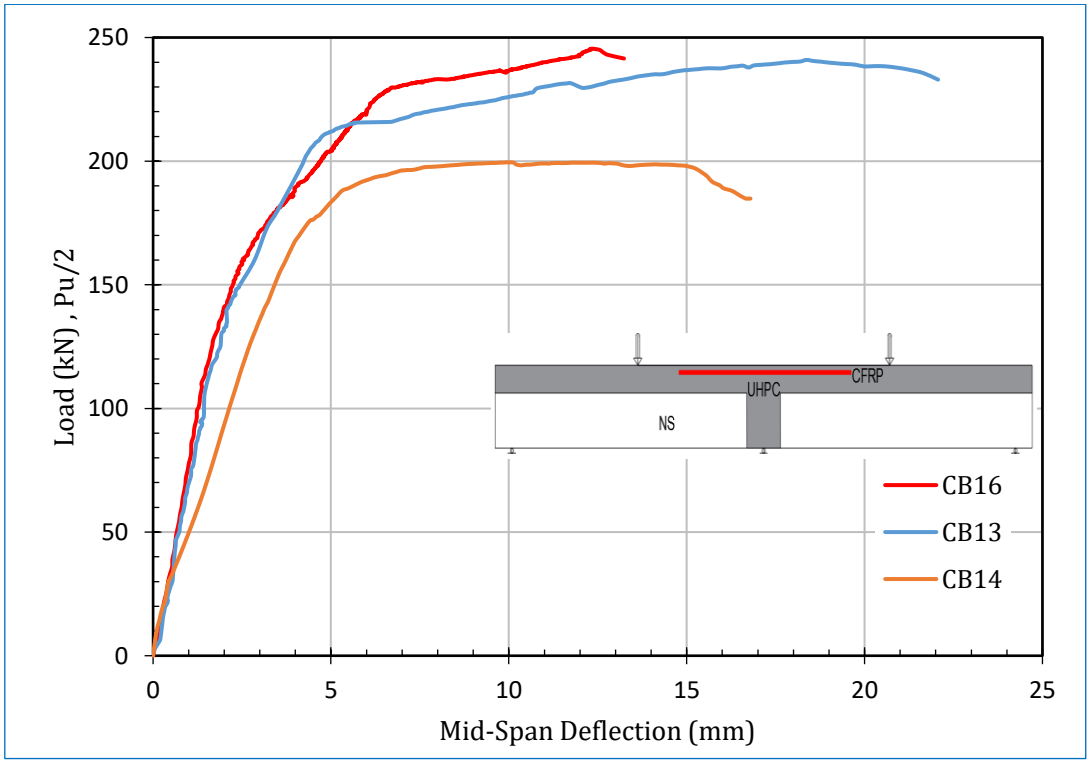

Figure 4-24:Load-Mid span deflection curve of $CB_{16}.HC_4.HR2.L_1$.

- **$CB_{17}.HC_4.SK.L_1$**

This girder has the same geometric properties of girder CB_{14}, as well as condition of testing with addition shear key at UHPC joint. First crack appeared of load 109 kN at mid span zone then, the deformations continued to developed multi cracks at this zone. After that, the interior support cracked at flange by load 250 kN and developed to reach the UHPC joint. The interface plane cracked vertical crack up to shear key then inclining toward the precast segment and continued to spread between web and flange. This situation occurred at load (270-320) kN. The mode of failure remains as in specimen CB_{14} as shown in Plate 4-17, that illustrated the cracks and failure mode at load 413.1 kN. Load-deflection curve explained in Figure 4-25 and shown the effect of shear key by increase the stiffness of girder.

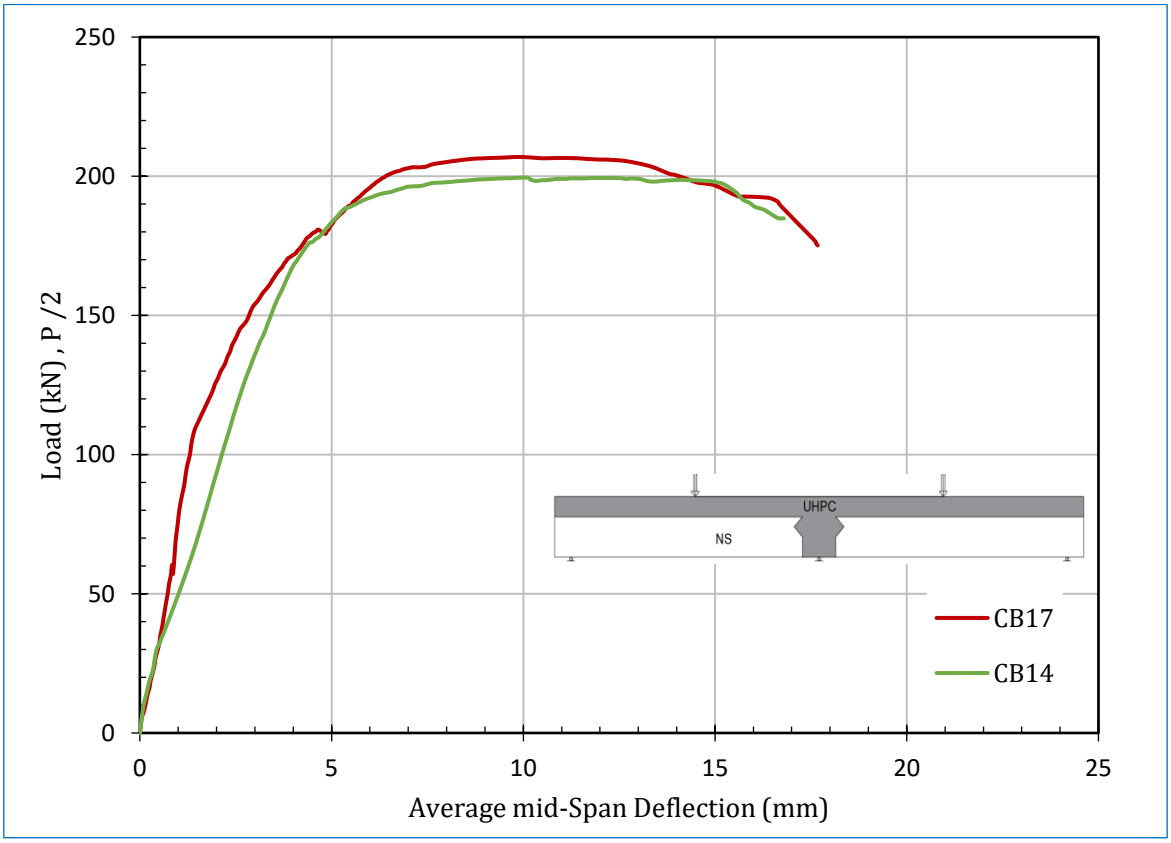

Figure 4-25:Load-Average mid span deflection curve of $CB_{17}.HC_4.SK.L_1$.

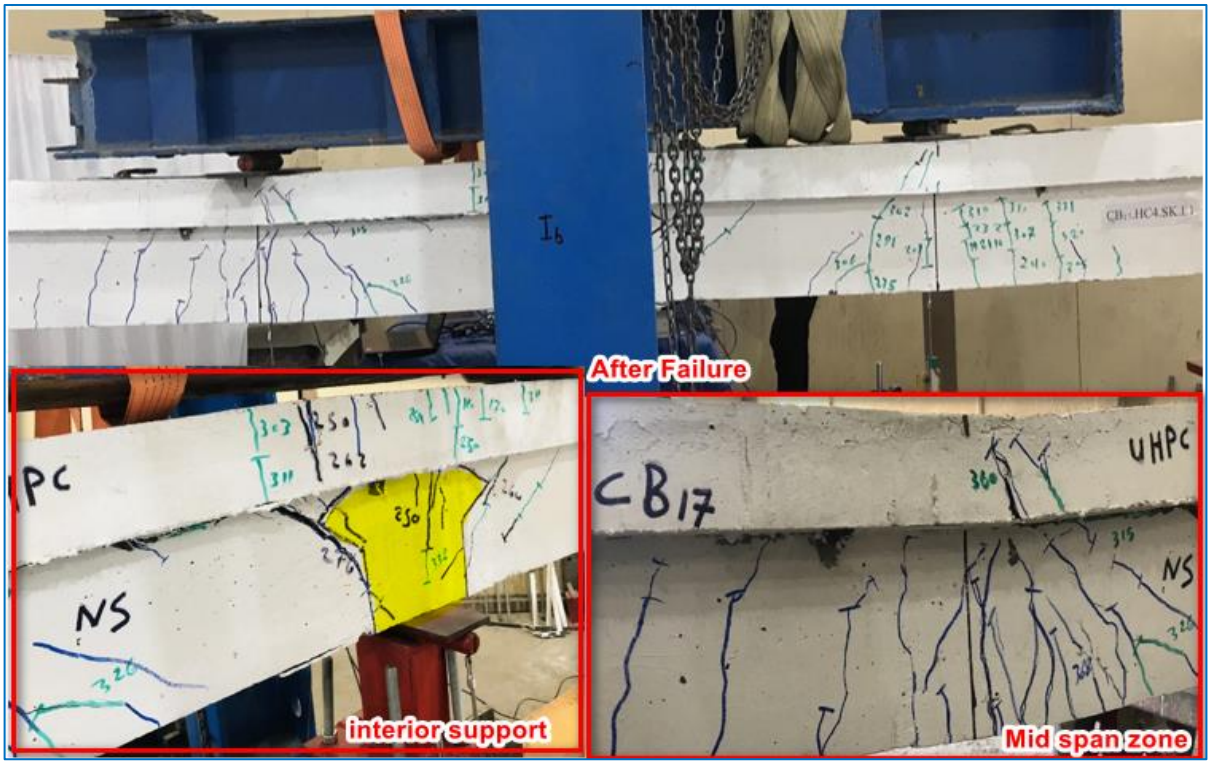

Plate 4-17: Cracks and failure mode of girder $CB_{17}.HC_4.SK.L_1$.

- **$CB_{18}.HC_5.SK.L_1$**

This girder has the same geometric properties of girder CB_{15}, as well as condition of testing with addition shear key at UHPC joint. From tracking the test of girder, girder showed a high similarity behavior of specimen CB_{15} according to mode of failure, cracks propagation, and the load deflection curve as shown in and Figure 4-26. Cracks started in mid span zone of load 110 kN then, cracks appear at interior support in flange of load 159 kN and developed to reach the web vertically to penetrate all section (flexural crack) at load about 382 kN. Mid span zone has many flexural cracks and reached to top of flange by load 420 kN. After that, the girder has a ductile behavior until failure at load 460.5 kN. A little hair line cracks occurred at UHPC joint and shear key did not give a significant effect because the joint shows a full bond with precast segment due to location of joint and high efficiency of UHPC.

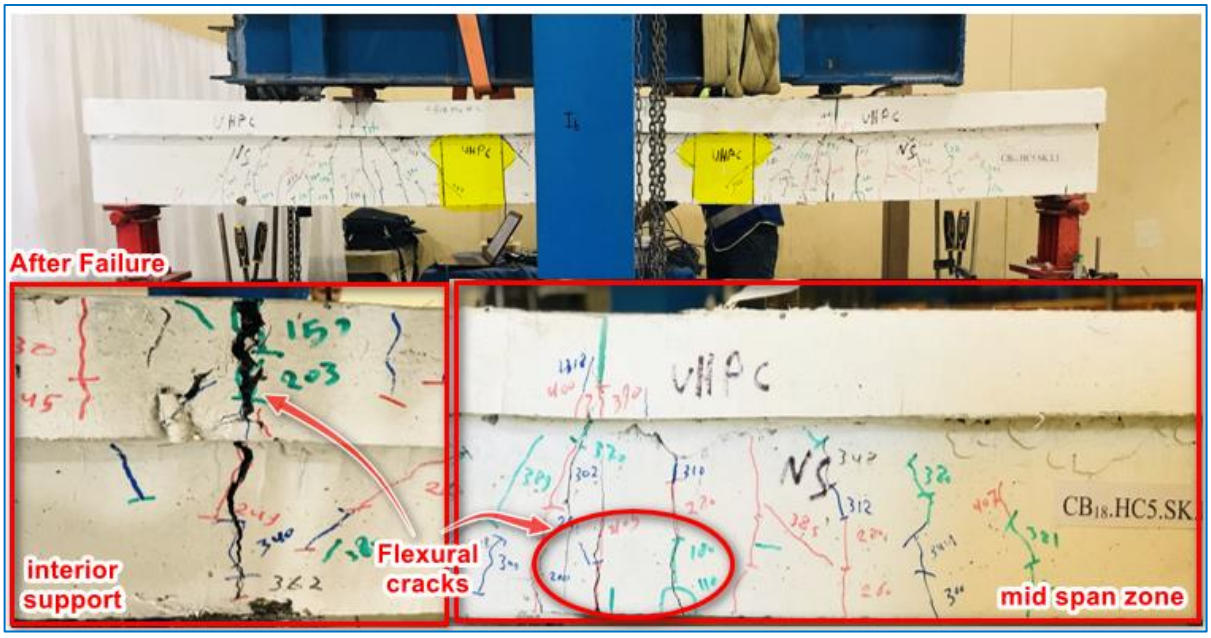

Plate 4-18: Cracks and failure mode of girder $CB_{18}.HC_5.SK.L_1$.

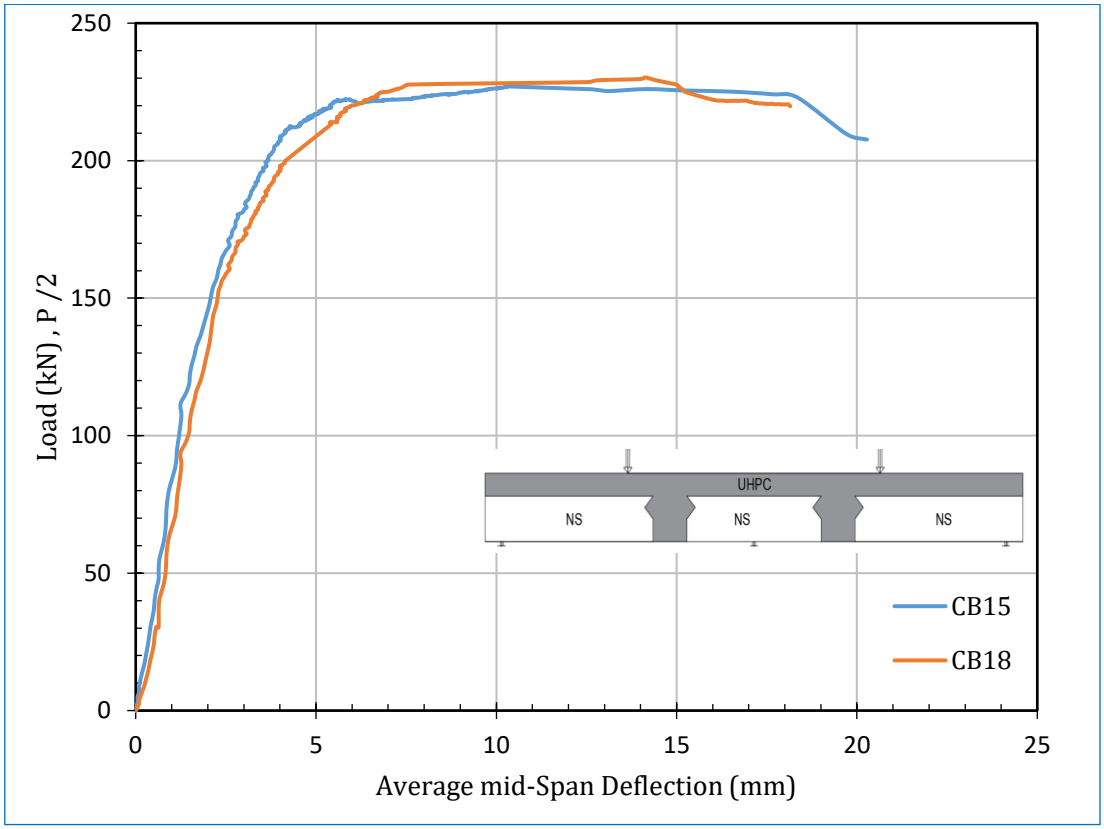

Figure 4-26:Load-Average mid span deflection curve of $CB_{18}.HC_5.SK.L_1$.

➢ **$CB_{19}.HC_1.L_2$**

This girder was cast monolithically as control specimen of one unit for hybrid section (web and flange). The testing of this girder was cyclic load (Repeated) with same protocol of simply supported group. First crack appeared at mid span after 4th cycle of load 170 kN, then, the flange cracked at interior support zone by load 213 kN. Cycles of loading continued on girder with specified intensity of loads and caused development of deformations and formation of cracks in highly separation through the tested girder especially at mid span and interior support zone. General behavior of girder approved a high similarity to control girder CB_{13} with some difference of load and gave more deflection, as shown in Figure 4-27. Cracking pattern and mode of failure are illustrated in Plate 4-19, at failure load 469.3 kN after 15th load cycle.

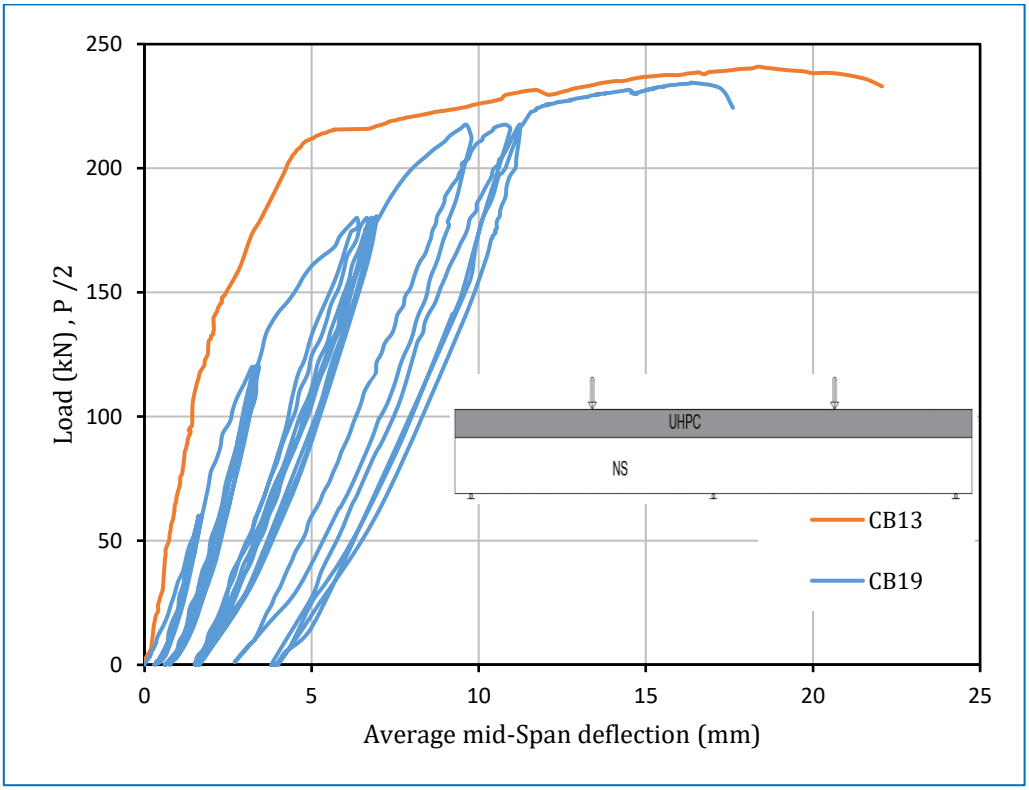

Figure 4-27:Load-Average mid span deflection curve of $CB_{19}.HC_1.L_2$.

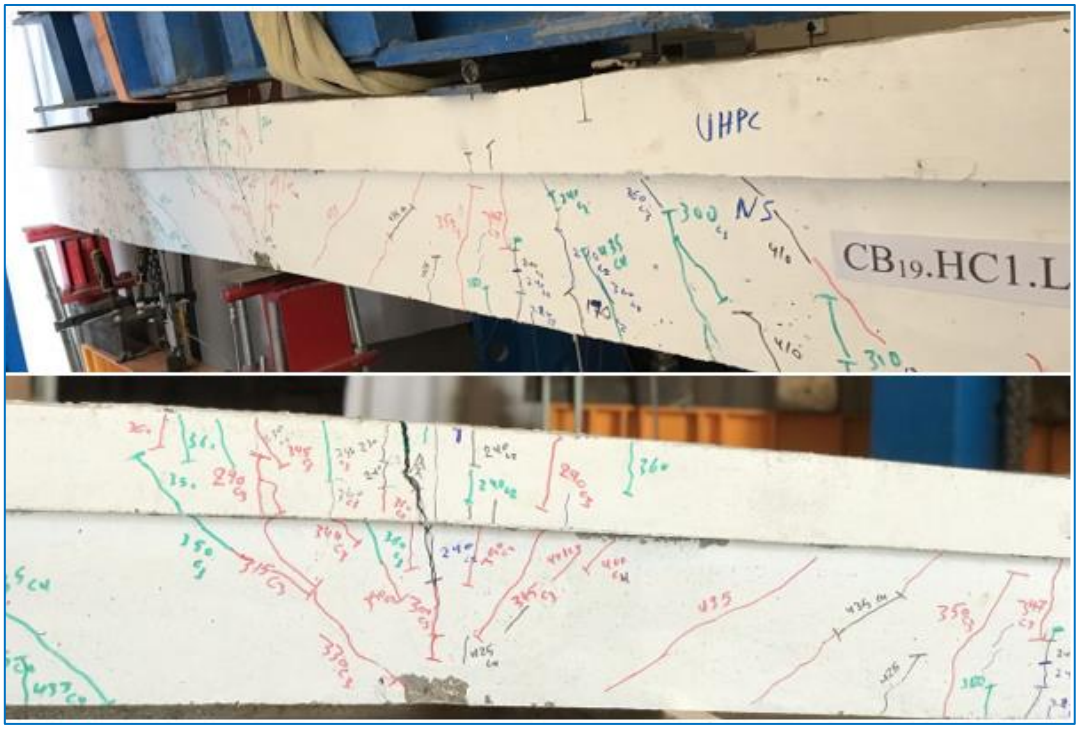

Plate 4-19: Cracks and failure mode of girder $CB_{19}.HC_1.L_2$.

- **$CB_{20}.HC_4.L_2$**

This girder was similar to CB_{14} exactly in geometric properties and reinforcement. The testing of this girder was cyclic load (Repeated) with same protocol of previous girder. First crack develops at mid span after 4th cycle of load 135 kN then, the flange cracked at interior support zone by load 150 kN. Cycles of loading caused development of deformations and cracks appear in highly separation through the tested girder especially at mid span and interior support zone. UHPC joint had interface crack propagated to support and inclined to separate between web and flange. General behavior of girder approved a high similarity to girder CB_{14} with some difference of load and give more deflection, as shown in Figure 4-28. Cracking pattern and mode of failure are illustrated in Plate 4-20, after failure of girder by load 389.1 kN due to 12th load cycle.

Plate 4-20: Cracks and failure mode of girder $CB_{20}.HC_4.L_2$.

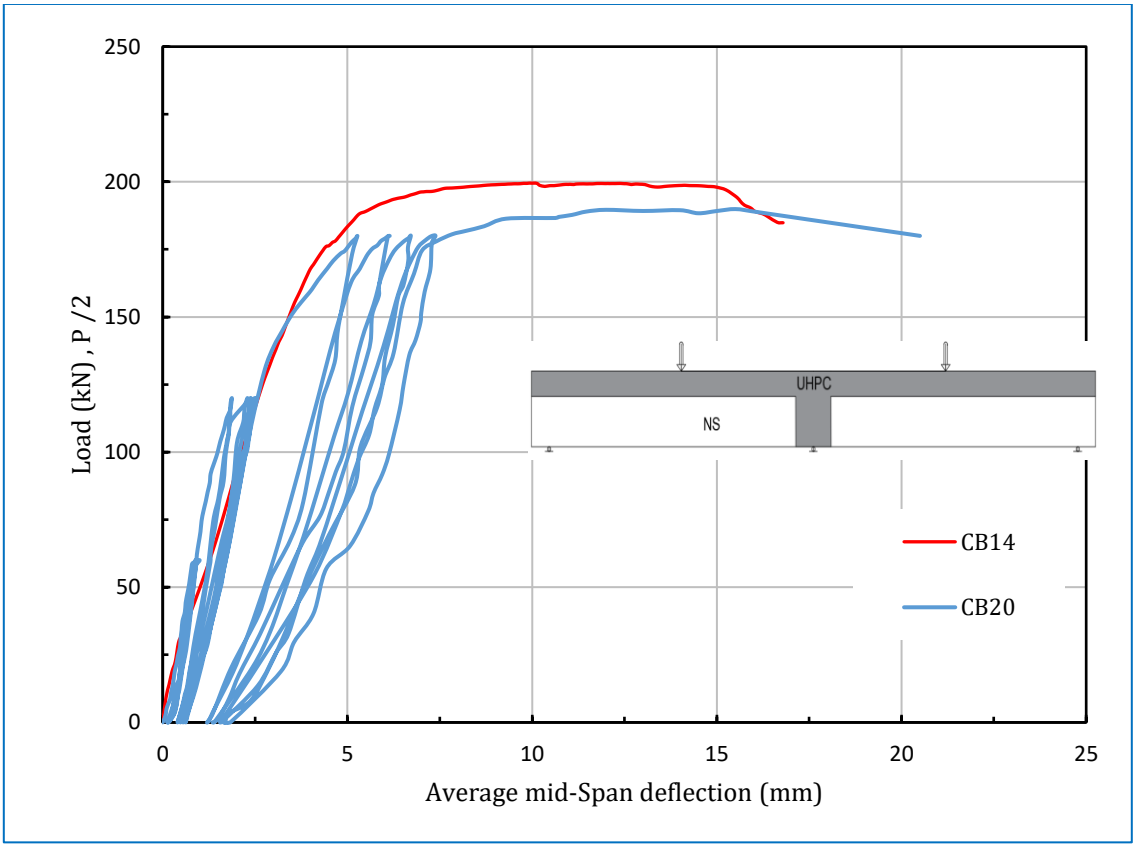

Figure 4-28:Load-Average mid span deflection curve of $CB_{20}.HC_4.L_2$.

- **$CB_{21}.HC_5.L_2$**

This girder was similar to CB_{15} exactly in geometric properties and reinforcement. The testing of this girder was cyclic load (Repeated) with same protocol of previous girder. First crack appeared at mid span after 4^{th} cycle of load 120 kN, then, the flange cracked at interior support zone by load 163 kN. Cycles of loading caused development of deformations and cracks appeared in highly separation through the tested girder especially at mid span and interior support zone. UHPC joint had a very little cracks after many cycles of load and these cracks did not control in failure proses. This girder showed high convergence with girder CB_{15} due to location of joint have approximately zero moment and UHPC suitable to resist the shear stresses. Figure 4-29 explained the load deflection relationship of tested girder. Cracks pattern and mode of failure illustrated in Plate 4-21, after failure of girder by load 450.9 kN due to 15^{th} load cycle.

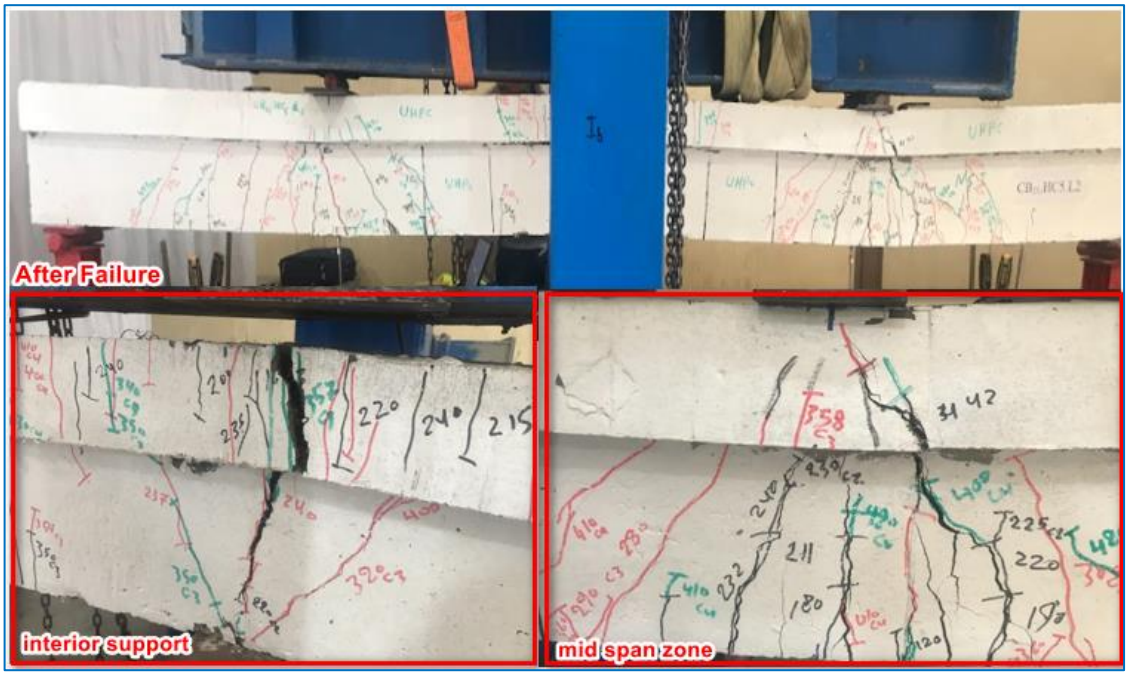

Plate 4-21: Cracks and failure mode of girder $CB_{21}.HC_5.L_2$

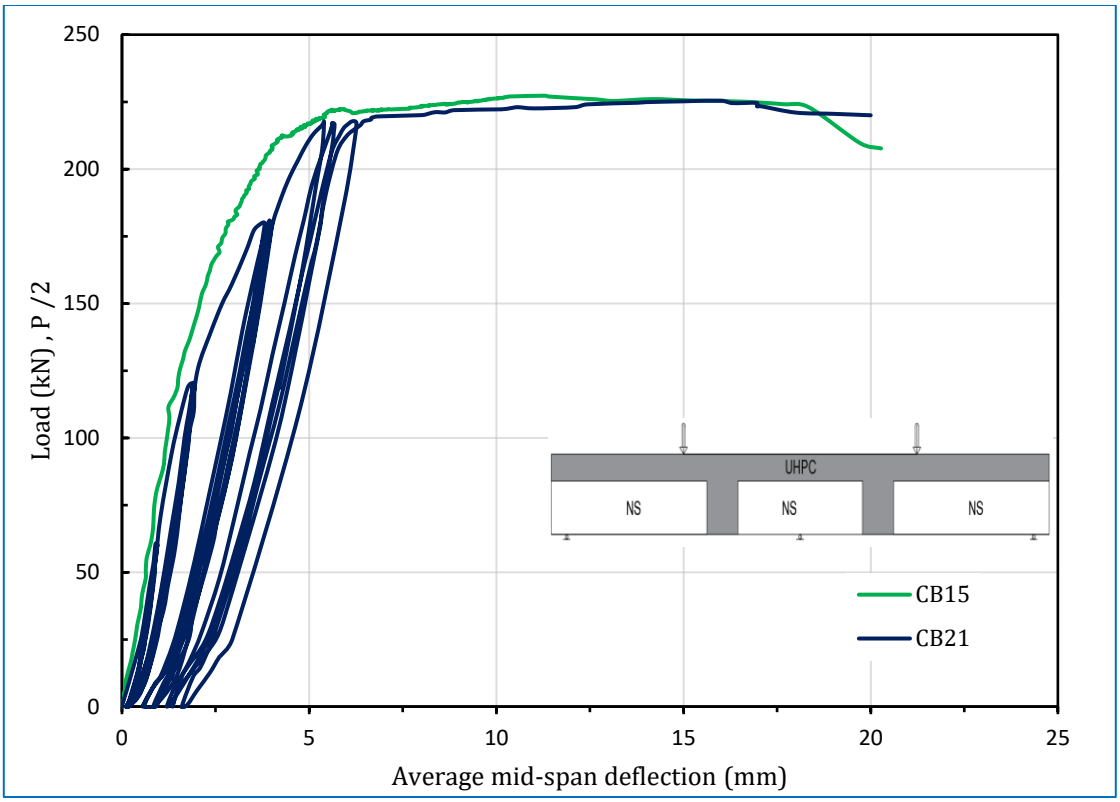

Figure 4-29:Load-Average mid span deflection curve of $CB_{21}.HC_5.L_2$.

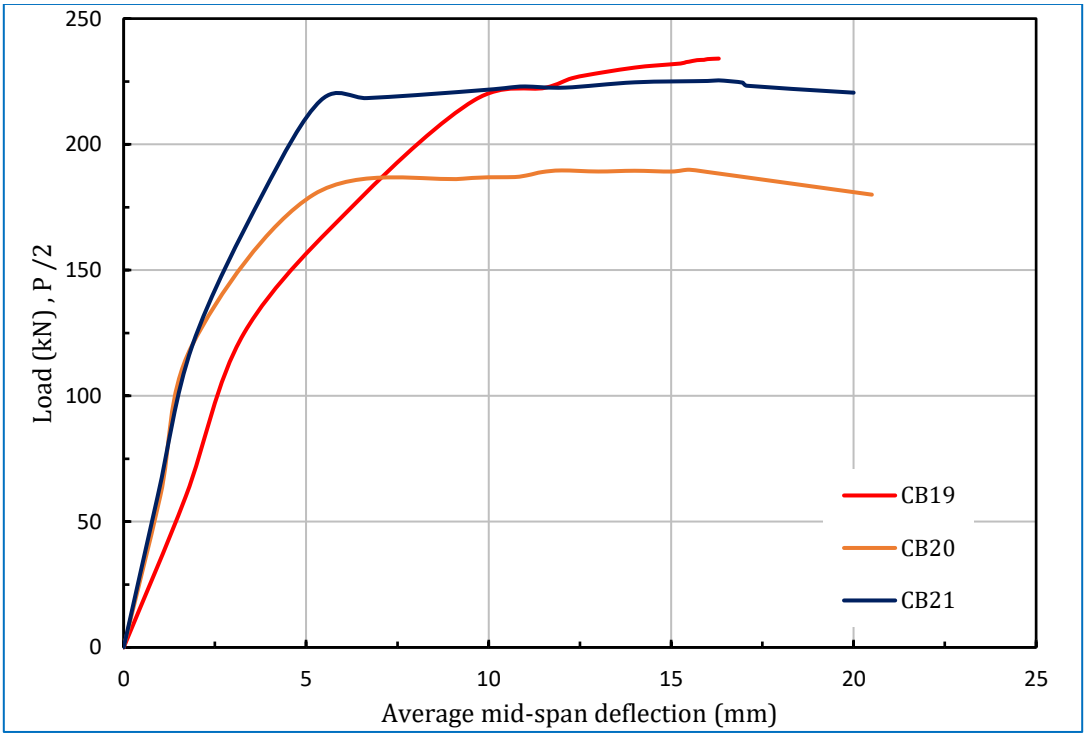

Figure 4-30: The envelope load deflection response for continuous specimens tested with cyclic loading.

Under the cyclic loading, the specimens present same behavior of monotonic loading with more deflection after the first crack loading, as shown in Figure 4-30. The girder (CB_{20}) reaches to plastic stage and collapse after 12^{th} cycle, while the girders (CB_{19}), (CB_{21}) complete a 15^{th} cycle to enter this state.

4-4-2-2 Effect of Considered Variables

The effect of variables that studied in experimental program such as (depth of joint, hybridization of reinforcement, presence of shear key, and type of loading) will be discussed to addition more understanding to overall structural behavior of this group.

I. Cracking load and cracking pattern

The general behavior of cracking propagation was initiated first as flexural crack at mid span zone where the maximum positive moment is occurred. After that the cracks observed at internal support zone where the maximum negative moment is provided. The reason of delaying the presence of first crack at interior support was the active properties of UHPC in flange. All girders were characterized by flexural cracks firstly then initiate some of shear cracks at interior support region and in a little separation in mid span zone, those cracks started to appear after load about 0.7Pu.

The first crack load of control girder gives the general above behavior exactly, where the cracking load was 174 KN at bottom layer of girder then propagated with load increment. When the interior support cracked and the crack penetrate the flange, the propagation and develop the crack width of crack in mid span zone were reduced or restricted. On the other hand, the propagation and width

of cracks increased with load increment until the plastic hinge occurred, then the consternation of cracks development at the mid span.

The presence of joint in girder led to decease the cracking load. In both cases of joint location except for girder CB_{16}, the first crack load decreased by about 6.9 and 8 % with respect to control girder for interion support joint and inflection point joints, respectively.

Replacement of 50% of steel reinforcement at interior support by CFRP bar provided increasing in first crack load by about 4.6% over the $CB_{14}.HC_4.L_1$ girder. Also, the cracks in flange zone appeared delaying and remained visible cracks without high development or increment in crack width to the limit that can be caused pullout of steel fiber from matrix of UHPC of flange.

Addition of shear key for continuous girder were not provide any enhancement in cracking load for both case of joint location.

For girder tested under cyclic loading, the first crack load was decreased due to the effect of loading and un loading causing reduction of stiffness of girder. Girder that cast monolithically had reduction in first crack load by about 2.3% as compared with girder tested statically. In the same hand, the splice girders were gives reduction in first crack load by about 16.7 and 25 % for interior support joint ($CB.HC_4$) and inflection point joint ($CB.HC_5$), respectively. The situation of crack propagation stays same of static tested girders with more cracks separation and deteriorating of large zone in girder. The other crack such as first crack in flange at interior support, also observed with early loads than monotonic loading.

II. *Ultimate load and mode of failure*

This group included some differences in the ultimate load and mode of failure of girders. Figure 4-31 illustrates the different load percentages of tested girders.

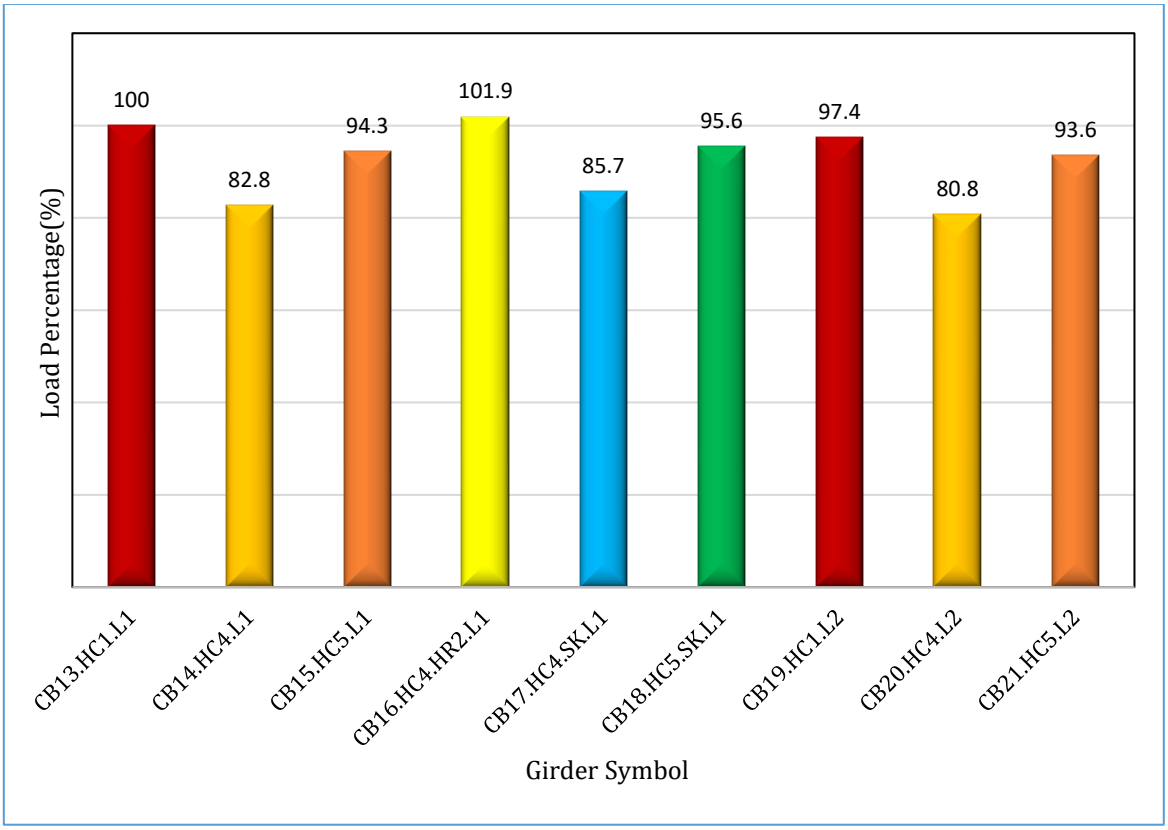

Figure 4-31: Ultimate load percentage of continuously supported girders.

For the control girder, the ultimate load achieved a good performance by reaching 481.85kN applied on two spans. That means the ultimate load of one span of the girder was 240.9kN to provide an increment 17.6% when compared with the control girder of simply support group ($SB_1.HC_1.L_1$). The flexural and shear-flexure mode of failure were controlled the process of failure in this girder. Where the plastic hinge occurred at the interior support then transports the strength of stresses to mid-span until development another plastic hinge to fails the girder.

The joints in the girder decrease the ultimate load by about 17.2 and 5.7 % for one joint at interior support ($CB_{14}.HC_4.L_1$) and two at inflection points ($CB_{15}.HC_5.L_1$) girders, respectively. The girder CB_{14} significantly reduced ultimate load because the joint was exposed to maximum direct shear from support. Thus, it could be concluded that using UHPC joints changed the failure mode from flexural failure to shear failure. The high tensile strength of UHPC increased the flexural capacity of the cross-section at the maximum moment (over the support), which corresponds to (Arafa et al., 2016). While the girder CB_{15} has less reduction in ultimate load because the location of the joint allows it to resist only shear stress (less than of shear on the joint in CB_{14}), the girder did not appear to shear failure on the joint. Also, the good bond and the confinement provided by steel fiber of UHPC in joint share reduce the ultimate load of this girder. Mode of failure remained as in control girder (flexural failure).

In (Hassoon, 2021), the reduction in the ultimate load when used spliced joint in the inflection point about 33% for NSC joint and 24.8% for SFC. Meanwhile, (Al-Tameemi, 2015) was used NSC in spliced joint at inflection points and resulting the reduction in the ultimate load about 36.1%. In both researches, the failure mode was direct shear, while in this study, the flexural failure was happened in spliced girder with UHPC at inflection points. That was indicated the UHPC joint in inflection points giving positive performance in splicing for ultimate load and failure criteria.

In girder ($CB_{16}.HC_4.HR2.L_1$), where the presence of CFRP bar with a ratio 50% of top reinforcement, the ultimate load has been reached 491kN (i.e., it exceeded the control girder). Also, it increased ultimate load by about 23.1% when compared to the same girder but has 100% steel at reinforcement (CB_{14}). This

hybridization in reinforcement did not change the mode of failure to stay the shear failure was controlled.

The presence of a shear key at the joint added some increment in the ultimate load of the girder by about 3.6 and 1.3 % for girder ($CB_{17}.HC_4.SK.L_1$) and ($CB_{18}.HC_5.SK.L_1$), respectively, when compared with the same girder with flat joints. Notice that the presence of the shear key gives more improvement in ultimate load in ($CB_{17}.HC_4.SK.L_1$) due to the high effect of the shear key in increasing the shear strength. The shear key did not give change in the mode of failure from the girder with the flat joint.

In the cyclic load, the ultimate load appeared to be a reduction in the tested girder due to loading and unloading. The ultimate load was reduced by about 2.4, 2.6, and 0.8 % for the girder ($CB_{19}.HC_1.L_2$, $CB_{20}.HC_4.L_2$, *and* $CB_{21}.HC_5.L_2$), respectively, when compared with the same girder tested monotonically. Also, the mode of failure did not change due to cyclic loading.

III. Cracks width

In continuous girders, it were observed that the crack width by crack meter with load increment. Always the first cracks initiated at the mid span in the bottom surface, then propagate to top surface with increasing load. The measured flexural crack at the mid span zone. In general, for all continuous girders did not appears splitting cracks due to adequate splice length in case of splice girder. Shear crack at mi span did not exceed (0.02-0.05) mm during the loading process.

The presence of joint at the interior support did not effect on the service crack width due to observed shear crack at interior support lead to decrease the stiffness of girder at early load. While the presence of joints at infection point

gives some of improvement at service crack width about 14.3%, this case owing to the good properties and high bond strength of UHPC joint.

When replace 50% of steel reinforcement by CFRP bar in girder (*CB_{16}.HC_4.HR2.L_1*) was showed enhancement on crack width as shown in Figure 4-32. But when its compare service crack width found that increase crack width by about 14.3% with respect to CB_{14} specimens with difference in load by about 23.5% increment.

Adding of shear key in girders (*CB_{17}.HC_4.SK.L_1*) and (*CB_{18}.HC_5.SK.L_1*) led to decrease the service crack width by 28.6 and 25 % respectively when compared with same girders having flat joint. This improvement in service crack width due to increase the stiffeners from addition UHPC shear key.

In cyclic load, the control girder gives same service crack width comparing with control girder tested statically. On the other hand, the cyclic loading caused increase in service crack width in (*CB_{20}.HC_4.L_2, and CB_{21}.HC_5.L_2*) by about 7.1 and 8.3% compared with girders tested statically. The above results explained in Table 4-9 for all girder of this group.

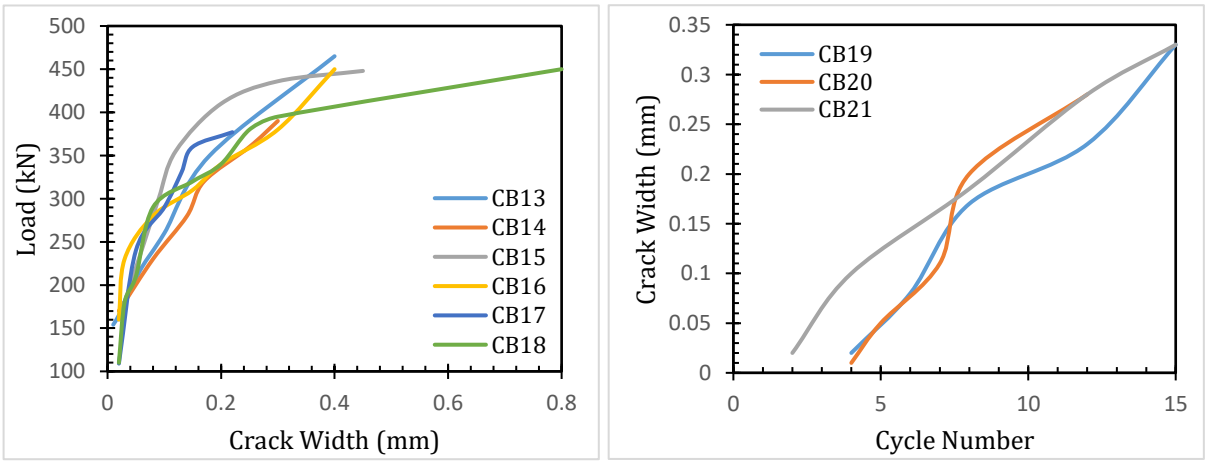

a- Flexual crack width verses applied load for girder tested statically.

b- Flexual crack width verses cycle number for girder tested with cyclic loading.

Figure 4-32: Relationship of crack width with load for continuous girders.

Table 4-9: Service crack width of continuous girders.

Girder Symbol	*Ps (kN)*	*Service Crack Width (mm)*
$CB_{13}.HC_1.L_1$	313.2	0.14
$CB_{14}.HC_4.L_1$	259.22	0.14
$CB_{15}.HC_5.L_1$	295.49	0.11
$CB_{16}.HC_4.HR2.L_1$	319.15	0.16
$CB_{17}.HC_4.SK.L_1$	268.52	0.1
$CB_{18}.HC_5.SK.L_1$	299.33	0.09
$CB_{19}.HC_1.L_2$	305.04	0.14
$CB_{20}.HC_4.L_2$	252.91	0.15
$CB_{21}.HC_5.L_2$	293.1	0.13

The results of flexural crack width above showed that all spliced girders did not exceeded the limits of cracks in service stage according to ACI-code requirement (ACI-318, 2019). The interface cracks in all spliced girder did not develop with increased the load, thus these cracks were no direct significant in the failure prosses of spliced girders.

While for research of (Al-Tameemi, 2015) and (Hassoon, 2021), the wide cracks occurred in the interface of joint that causing the failure of beams. These interface cracks were exceeded the limits of cracks in service stage according to ACI-code requirement (ACI-318, 2019).

IV. Stiffness criteria

Stiffness of this group was calculated by same method mentioned in first group. The results of stiffness were illustrated in Table 4-10. In the splice girder, stiffness was increased by about 4.4% for girder (*$CB_{14}.HC_4.L_1$*) and 11.1% for girder (*$CB_{15}.HC_5.L_1$*). This increment was provided owing to the presence of UHPC joints with high modulus of elasticity and these joints showed high interface bond strength to limiting that did not disturb the stiffness of girder during service stage.

When addition CFRP bar in girder (*$CB_{16}.HC_4.HR2.L_1$*) led to improvement in stiffness by 3% when compared with same girder without CFRP.

The presence of shear key gives an increase in stiffness by 1.2 and 1.3 % for girders (*$CB_{17}.HC_4.SK.L_1$* and *$CB_{18}.HC_5.SK.L_1$*) respectively, when compare with same girders have flat joints.

In cyclic load, the adverse effect of loading and unloading process have been cleared. Where the control girder gives decreasing in stiffness by about 62%. Meanwhile, the splice girders were gives decreasing in stiffness by about 55.9% for (*$CB_{20}.HC_4.L_2$*) and 39.7 % for girder (*$CB_{21}.HC_5.L_2$*) when compared with same specimens tested monotonically. These results mean that the cyclic load caused more deterioration in girders and more displacement during service stage.

V. Ductility index

Ductility in this group determined same as in the previous group. The spliced girders have reduced in the ductility by 31.1% for girder (*$CB_{14}.HC_4.L_1$*) due to the shear failure that effect on the behavior of girder. Meanwhile, the girder (*$CB_{15}.HC_5.L_1$*) has reduction in the ductility about 16.9% due to adverse effect of the presence of horizontal and vertical joints with precast segment.

Table 4-10: Initial stiffness of continuous girder.

Girder Symbol	*Service load, P_s (kN)*	*Deflection, Δ_s (mm)*	*Stiffness, K (kN/mm)*
$CB_{13}.HC_1.L_1$	156.60	2.65	59.09
$CB_{14}.HC_4.L_1$	129.61	2.1	61.71
$CB_{15}.HC_5.L_1$	147.75	2.25	65.66
$CB_{16}.HC_4.HR2.L_1$	159.58	2.51	63.57
$CB_{17}.HC_4.SK.L_1$	134.26	2.15	62.44
$CB_{18}.HC_5.SK.L_1$	149.66	2.25	66.51
$CB_{19}.HC_1.L_2$	152.52	6.8	22.42
$CB_{20}.HC_4.L_2$	126.46	4.65	27.19
$CB_{21}.HC_5.L_2$	146.54	3.7	39.60

For girder ($CB_{16}.HC_4.HR2.L_1$), ductility was reduced by 10.8% when compared with girder ($CB_{14}.HC_4.L_1$) due to the presence of CFRP bar at the top reinforcement. From that, the strength was increased by CFRP and the ductility was increased by steel reinforcement. This result was agree well with the finding in (Qin et al., 2017).

The presence of shear key was provided improvement in the ductility of spliced girders by about 20.4 and 3.8 % for girder ($CB_{17}.HC_4.SK.L_1$and $CB_{18}.HC_5.SK.L_1$) respectively, when compared with same girder having flat joints. From result, notice that the direct effect of shear key more in case of joint in the interior

support where the joint exposed to direct shear force. This fact was insuring the good performance of UHPC shear key to obstruction of failure line.

In the cyclic loading, the prosses of loading and unloading was owing to decrease the ductility of girders. Ductility of control girder reduced by 44% in the cyclic load due to deterioration of specimen and high intensity of cracks. The splice girders, the ductility of ($CB_{20}.HC_4.L_2$) was reduced by 10.7% and girder ($CB_{21}.HC_5.L_2$) reduced by 2.2%. this high reduction percent in ductility of girder ($CB_{20}.HC_4.L_2$) ensure the more influence of cyclic load on the general behavior of this specimen where it was collapse at cycle 12th of loading process. This results were give good agreement with (Hassoon, 2021).

Table 4-11: Results of ductility index for continuous girders.

Girder Symbol	Ultimate disp. Δu (mm)	Yield disp. Δy (mm)	Ductility index μ
$CB_{13}.HC_1.L_1$	18.4	4.6	4.00
$CB_{14}.HC_4.L_1$	12.4	4.5	2.76
$CB_{15}.HC_5.L_1$	11.3	3.4	3.32
$CB_{16}.HC_4.HR2.L_1$	12.16	4.95	2.46
$CB_{17}.HC_4.SK.L_1$	13.6	4.1	3.32
$CB_{18}.HC_5.SK.L_1$	13.8	4	3.45
$CB_{19}.HC_1.L_2$	18.7	8.35	2.24
$CB_{20}.HC_4.L_2$	16	6.5	2.46
$CB_{21}.HC_5.L_2$	17.3	5.32	3.25

VI. *Energy Absorption*

For this group, the method of calculation the energy absorption as referred in the first group. Figure 4-33 shown the energy absorption values of this group. The existing of joint led to decreased the energy absorption by about (42.4 and 35.3) % for ($CB_{14}.HC_4.L_1$ and $CB_{15}.HC_5.L_1$) respectively.

The hybridization of reinforcement caused improvement in the energy absorption by 15.5% compared with ($CB_{14}.HC_4.L_1$) due to remaining the behavior of girder with increasing in the strength capacity. This result has well agreement with finding in (Hassoon, 2021).

Meanwhile, the presence of shear key led to increasing the energy absorption by about (4 and 9.6) % for girders ($CB_{17}.HC_4.SK.L_1$ and $CB_{18}.HC_5.SK.L_1$) respectively, when compared with same girder having flat joint.

In the case of cyclic loading, also the cumulative of each load cycle was calculated and illustrated in Figure 4-34. The process of load-unload was caused more energy absorption for the tested girders. Where this girder has increasing in the energy absorption by (110, 114.7, and 141.9) % for girder ($CB_{19}.HC_1.L_2$, $CB_{20}.HC_4.L_2$, and $CB_{21}.HC_5.L_2$) respectively compared with same girder tested monotonically. Also, it showed that the splicing of girder decreasing by about 41.1% for girder ($CB_{20}.HC_4.L_2$) and 25.5% for girder ($CB_{21}.HC_5.L_2$) . the splice girder gives close value of energy absorption until to 7^{th} cycle, but after that shown the differentiated in energy absorption capacity. From these results can be conclude that the girder spliced by UHPC were adequate for ductility response when exposed to cyclic load.

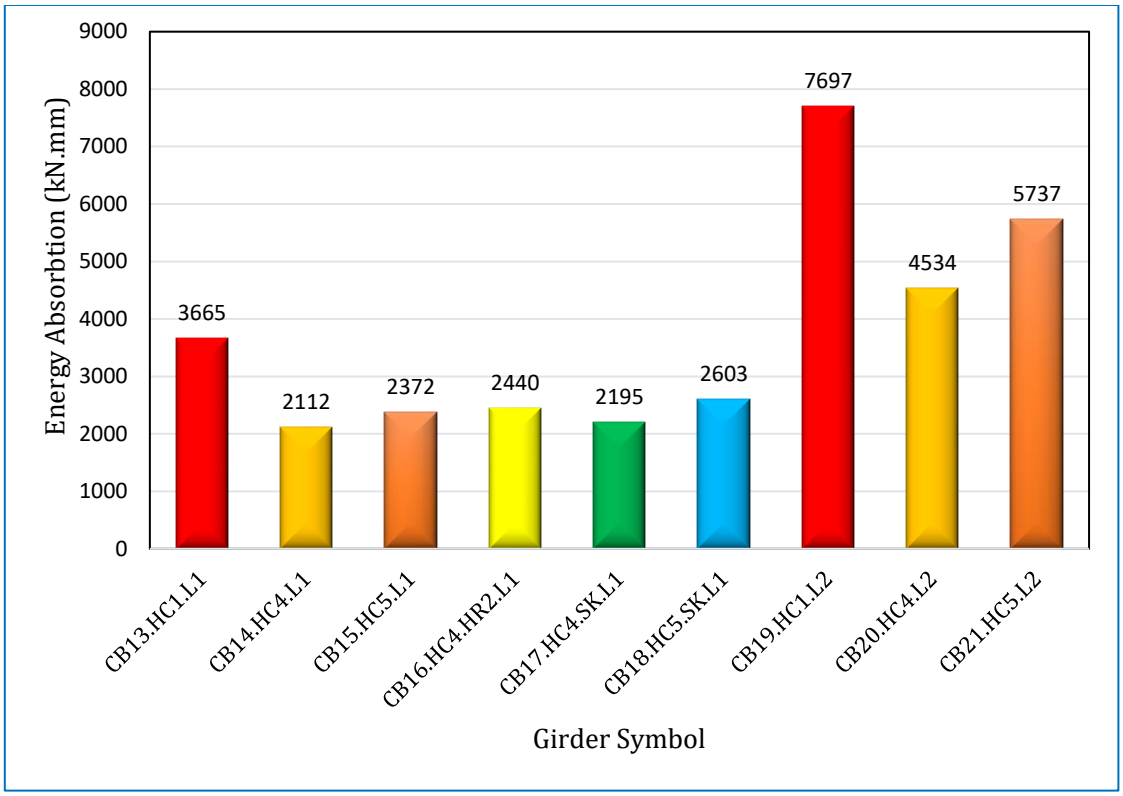

Figure 4-33: The variation of energy absorption of continuous girders.

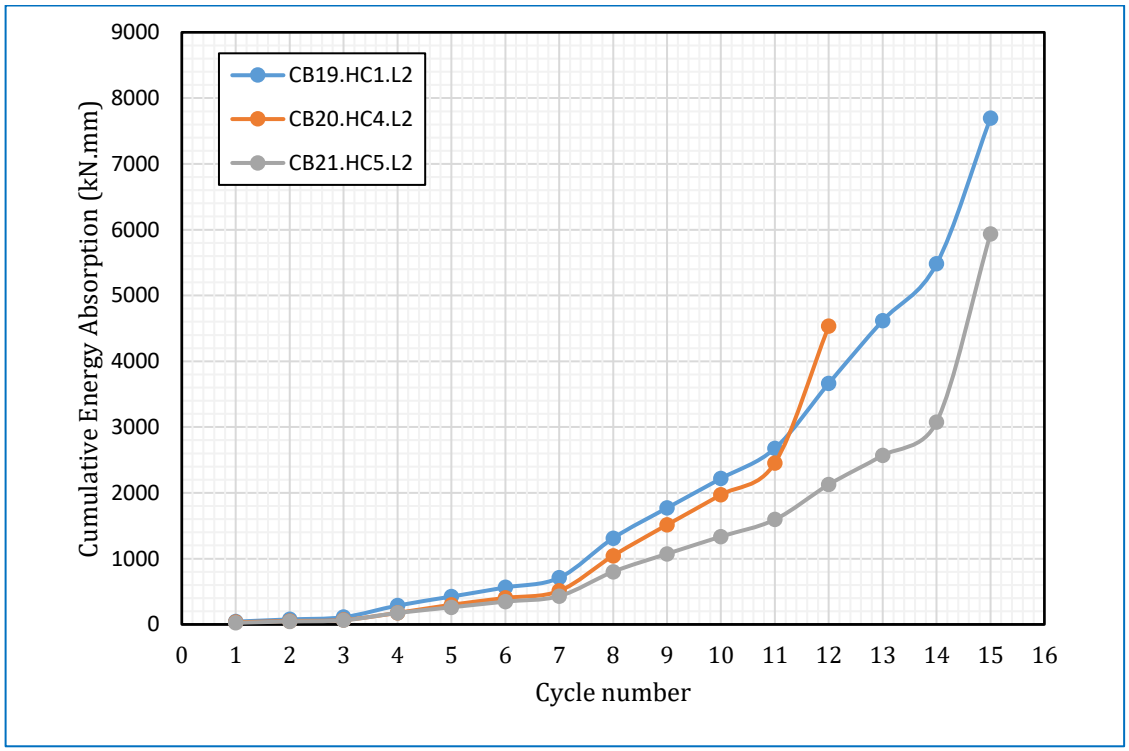

Figure 4-34: The cumulative energy variation of continuous girders tested under cyclic load.

VII. Damage Index

As mentioned for this field in the first group, the results of calculating the damage index for this group were illustrated in Figure 4-35. For firstly 7 cycles, the damage index of the girders range in no damage stage. Then the girders interred the minor damage stage in 8th cycle. The control girder was interred the moderate damage state after 11th cycle and continuo in damaged to reaches the serious damage stage. Girder ($CB_{20}.HC_4.L_2$) was exceeded the minor stage in 9th cycle to reached the moderate stage and collapsed in this stage. While, the girder ($CB_{21}.HC_5.L_2$) stay in minor damage stage up to cycle 14th. The fast girder in reach to moderate stage was girder ($CB_{20}.HC_4.L_2$), so that refer to the early failure of this specimen by shear in the joint at interior support.

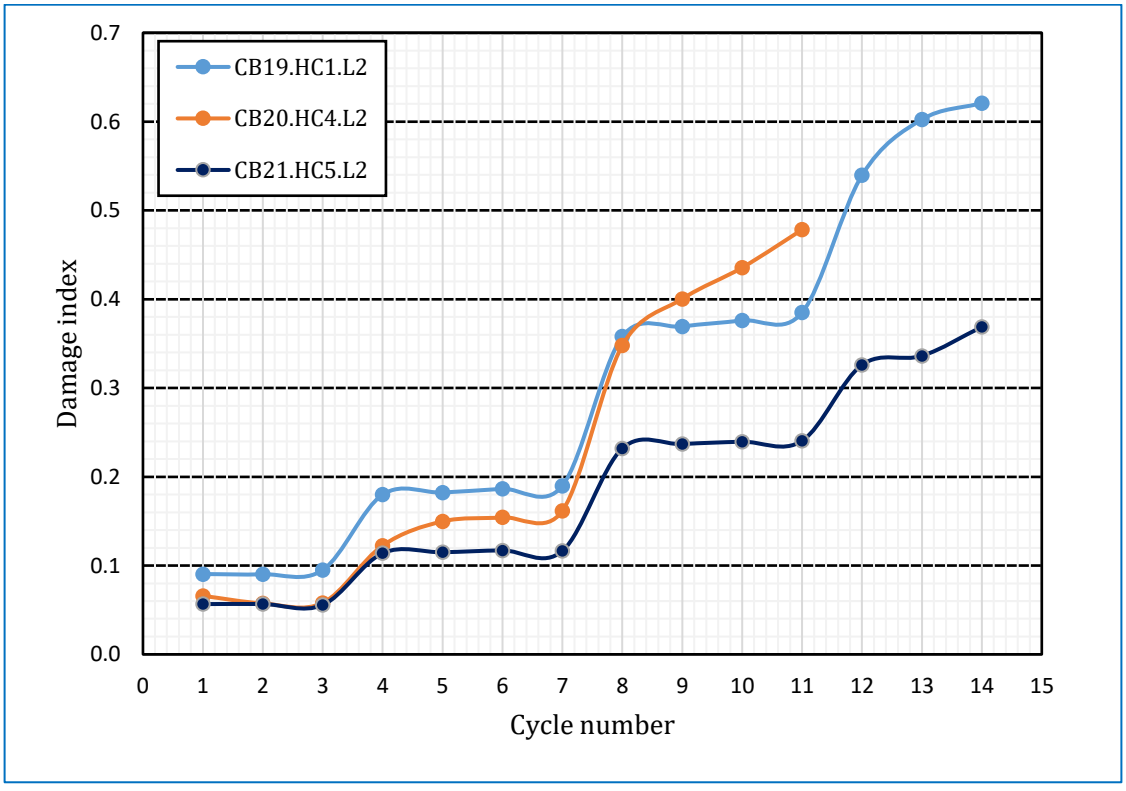

Figure 4-35: The damage index value with cycle no. of continuous girder.

Chapter Five

Finite Element Method

5-1 Introduction

The most reliable way to evaluate the actual performance of structural elements is through experimental testing. However, conducting experiments is often impractical due to their cost and time-consuming nature. Therefore, alternative methods that consider the anisotropic behavior of concrete, including the impact of tensile cracks, are required. One of the most efficient and versatile techniques for structural analysis is the finite element method. The accuracy of this method is primarily dependent on the types of elements chosen to represent the problem, appropriate modeling of material properties, and the application of suitable boundary conditions.

5-2 Numerical Modelling

In this chapter, the Finite Element Method was used to simulate a model has similar or close properties of the tested experimental specimens. This model was validated with the results of the experimental test and then used this model to study the other parameters that could not studied experimentally. For this purpose, the computer program **ABAQUS** was used. This software package was adopted in this study to ensure adequate modeling for beams involving: material properties, elements-type, real constant, and convergence study.

5-3 Material Modelling

The concrete damaged plasticity (CDP) model was used for modeling concrete (NSC and UHPC). It assumes that the main two failure mechanisms of concrete are tensile cracking and compressive crushing (SIMULIA 2014). The CDP model is provided by Abaqus 6.11 code to present the plastic behavior of concrete in both compressive and tensile conditions, namely, cracking under tension and crushing under compression.

The CDP model can be used in applications where concrete is subjected to either static or cyclic loading (Shamass et al. 2017). For steel reinforcement used elastic perfect plastic model and elastic model for simulation the plate load and plate support. More details about material modelling explained in Appendix D.

The simulation of specimen by ABAQUS performed with the following steps.

5-3-1 Part and Assembly

The assembly of the parts, that were utilized in modelling these beams and the details about the steel reinforcement are shown in Figure 5-1. Quarter size of girders were used in simulation due to the symmetry of girders in two directions to reduce the solution matrices and speed the analysis time.

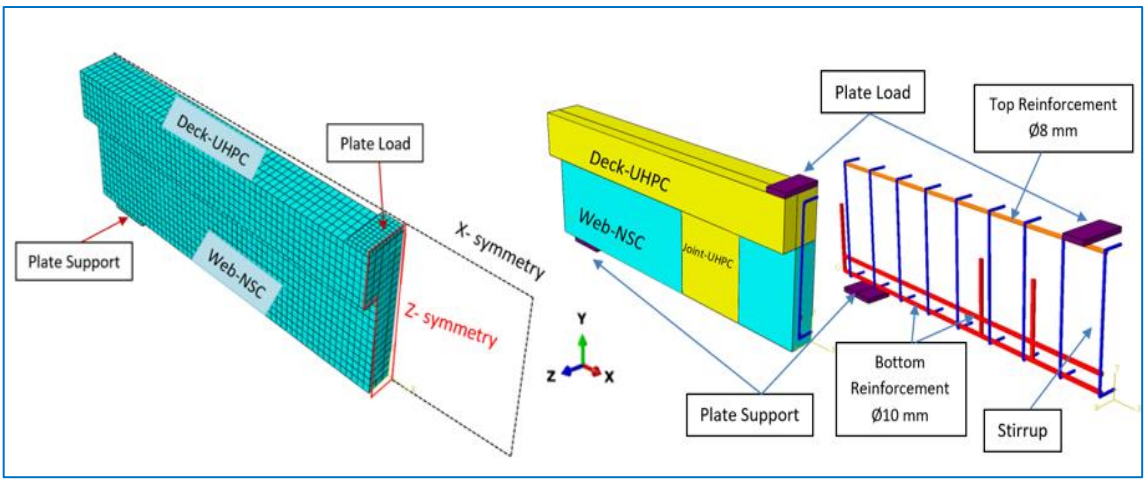

Figure 5-1: The assembly of parts for girder.

5-3-2 Mesh and elements type

A significant step in the modelling of finite elements is to choose the mesh size. Previous to the numerical analysis, an adequate pre-analysis of various mesh sizes was done to choose the best size which gives the necessary accuracy until an expansion in the size of the mesh has a negligible influence on the results. Hence, in the current model different element sizes of 10,15, 20, 30, and 40 mm were examined as shown in Figure 5-2. It can observe from Figure 5-3, that the variation of load-deflection curve can be ignored in case of the size is enlarged from (10) mm to (20) mm. Also, the curve of load-

displacement is more precise with experimental results. Hence, 15 mm element size was chosen for the mesh size, which ensures a good alteration between the stability of the numerical solution and the size of the elements.

The elements used in the representation of the adopted specimens and geometrical properties in this model can be summarized by:

1. C3D8R; 8 node brick element, reduced integration used to represent the beams, supporting and loading plates.

2. T3D2; 2 nodes 3 D truss element which were used to represent the steel bars.

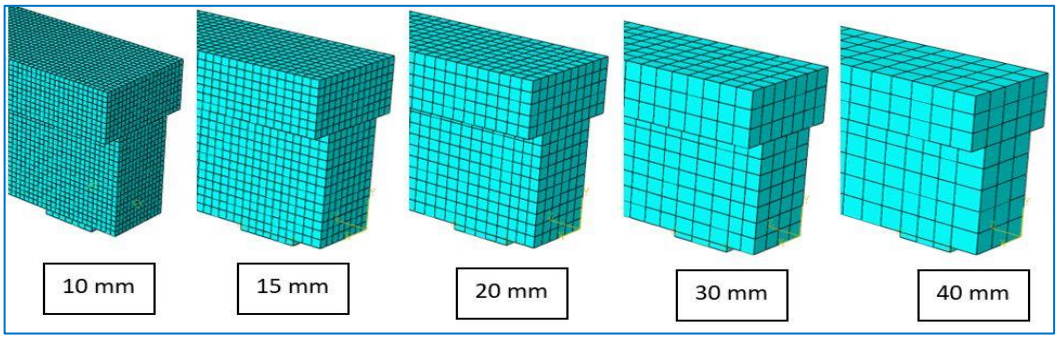

Figure 5-2: The mesh sizes that analyzed in mesh sensitivity test.

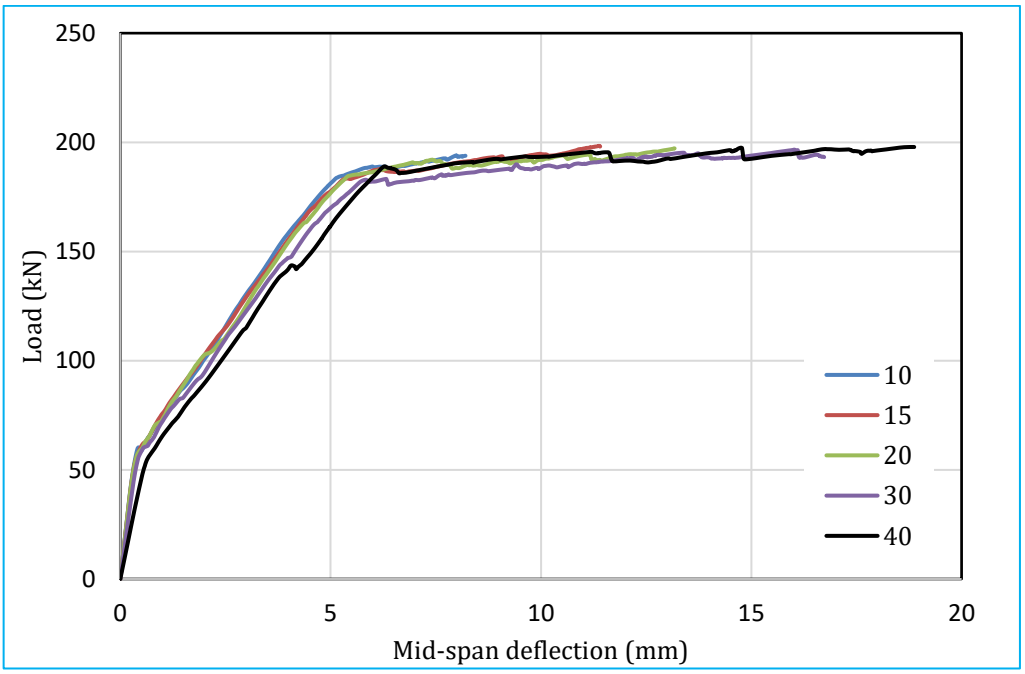

Figure 5-3: The results of load-deflection response for the mesh size element of SB_1 girder.

5-3-3 Loading and boundary conditions

The experimental test loaded by three-point load, so the model of FEM must be loaded by similar method as shown in Figure 5-4. Meanwhile, the boundary condition of the end of girder are pin-roller support as a line in the middle of bearing plate. So, in the FEM model represent the boundary as pin-roller support. To applied these supports, in pin support must be restrain the displacement in the direction of (x, y, and z), and restrain the rotation in the direction of (z and z). Also, symmetry boundary conditions were applied to all symmetry surfaces. Specifically, in the x-direction, ABAQUS constrains displacement in the x-direction and rotation in both the y and z directions. Meanwhile, in the z-direction, ABAQUS constrains displacement in the z-direction and rotation in both the y and x directions.

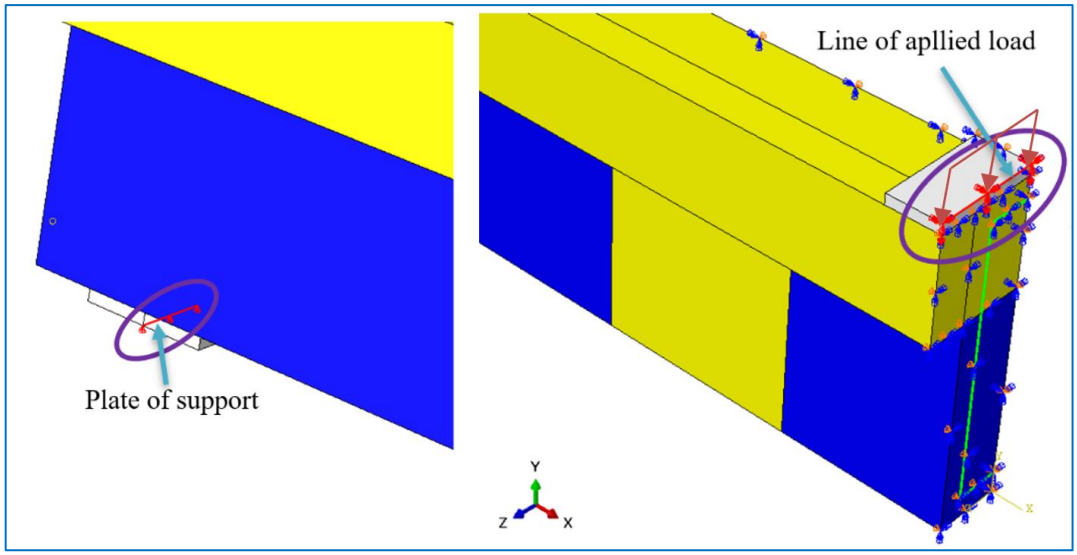

Figure 5-4: The load and boundary condition of specimen.

5-3-4 Interaction

To ensure the model works as a complete composite section, the interaction between the assembled parts must be done according to the state of the parts in the experimental test as following:

1- Embedded region: used for the interaction between the concrete and steel reinforcement bar.

2- Tie: used for the interaction between the parts that did not have any slip between them, such as the plate load - deck, and plate support -web.
3- Surface to surface: used to the interaction between the precast concrete unit and the cast in place joint. This contact type was defined by "hard contact" in normal behavior and "penalty" in the tangent direction with the friction coefficient equals 1.44 .(Zhang et al., 2022),(Kadhim et al., 2021).

5-4 Stress-Strain of Concrete

The compression and tension stress-strain curves of both types of concrete (NSC and UHPC) were provided in this item according to formula and previous researches achieve the purpose as following.

5-4-1 **Normal strength concrete**

The curves of NSC drawing depended on the mechanical properties of concrete that obtained from tested samples imputed in driven formulas.

5-4-1-1 Compression

The average stress-strain curve of concrete in compression is shown in Figure 5-5and is expressed as:

$$\sigma_c = \xi\, f'_c \left[2\left(\frac{\epsilon_{cu}}{\xi\,\epsilon_{c1}}\right) - \left(\frac{\epsilon_{cu}}{\xi\,\epsilon_{c1}}\right)^2\right] \text{ if } \frac{\epsilon_{cu}}{\xi\,\epsilon_{c1}} \leq 1 \text{... (5-1) (Wang and Hsu, 2001)}$$

$$\sigma_c = \xi\, f'_c \left[1 - \left(\frac{\frac{\epsilon_{cu}}{\xi\,\epsilon_{c1}} - 1}{\frac{2}{\xi} - 1}\right)^2\right] \text{ if } \frac{\epsilon_{cu}}{\xi\,\epsilon_{c1}} > 1 \text{ ..... (5-2) (Wang and Hsu, 2001)}$$

and

$$\epsilon_{c1} = 0.0014[2 - exp(-0.024\, f_c) - exp(-0.14\, f'_c)] \text{ ..... (5-3)}$$

$$\epsilon_{cu} = 0.004 - 0.0011\,[1 - exp(-0.0215\, f'_c)] \text{ ..... (5-4)}$$

Where: coefficient ξ representing the reduction in compressive stress taken as 1, f'_c is the cylinder compressive strength of concrete (MPa), ϵ_{c1} concrete strain at maximum compressive stress, and ϵ_{cu} is ultimate strain of concrete.

The above equations from Eq. 5-1 to Eq.5-4 expressed by (Wang and Hsu, 2001)

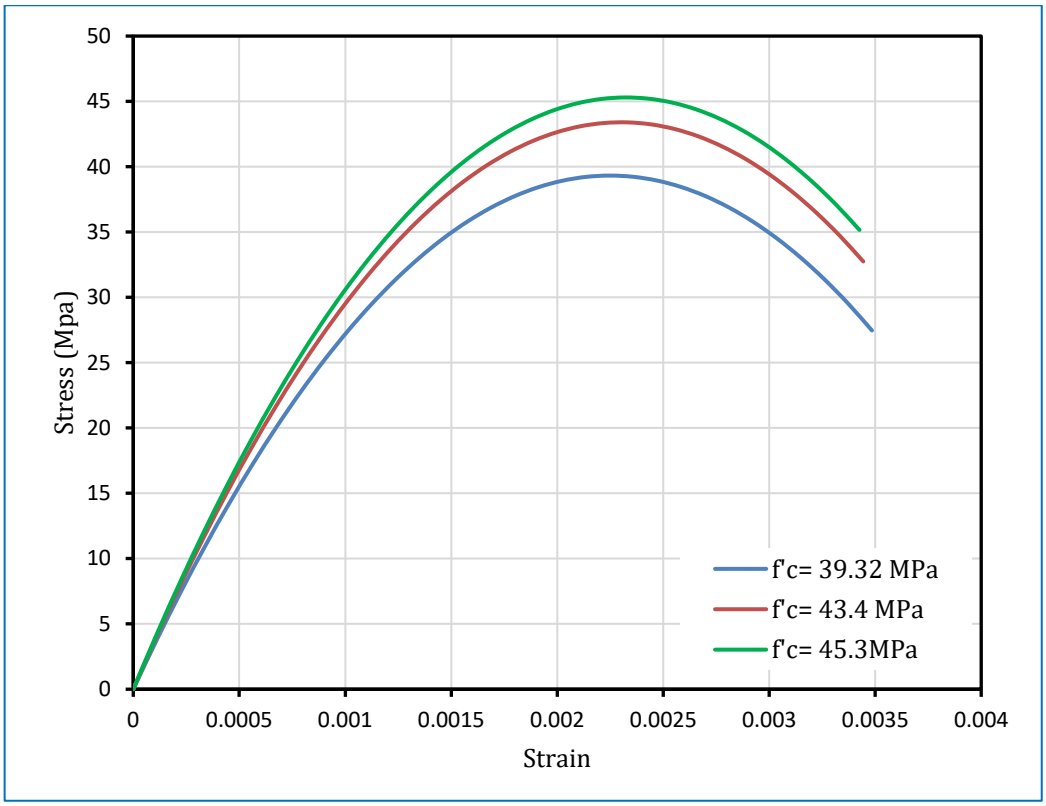

Figure 5-5: Stress-strain curve for NSC in compression.

5-4-1-2 Tension

The tensile strength of concrete under uniaxial stress is seldom determined through a direct tension test because of the difficulties involved in its execution and the large scatter of the results. Indirect methods, such as sample splitting or beam bending, tend to be used (BS EN 1992-1-1, 2004).

The average stress- strain curve of concrete in tension is shown in Figure 5-6, where the ascending and descending branches are given as:

$$\sigma_t = E_c\, \epsilon_t \text{ if } \quad \epsilon_t \leq \epsilon_{cr} \quad \text{.....(5-5)}$$

$$\sigma_t = f_{cr}\left(\frac{\epsilon_{cr}}{\epsilon_t}\right)^{0.4} \quad \text{if} \quad \epsilon_t > \epsilon_{cr} \ldots\ldots\ldots\ldots(5\text{-}6)$$

And

$$f_{cr} = 0.31\sqrt{f'_c}(\text{MPa}) \ldots\ldots\ldots\ldots\ldots\ldots\ldots\ldots\ldots\ldots\ldots\ldots\ldots\ldots\ldots(5\text{-}7)$$

Where: E_c is modulus of elasticity of concrete (MPa); f_{cr} is cracking stress of concrete (MPa), f'_c is the cylinder compressive strength of concrete (MPa), ϵ_t tension strain , and ϵ_{cr} is cracking strain of concrete taken as 0.00008.

The above equations from Eq. 5-5 to Eq.5-7 expressed by (Wang and Hsu, 2001)

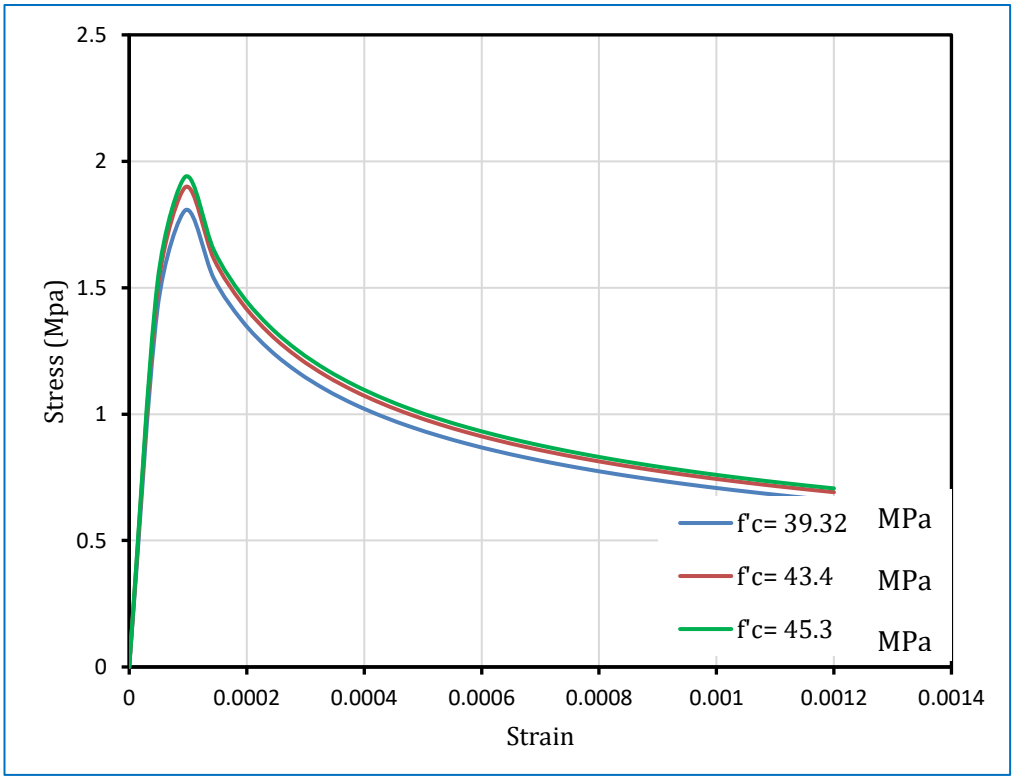

Figure 5-6: Stress-strain curve for NSC in tension.

5-4-2 **Ultra high-performance concrete**

For UHPC, the stress strain data for compression and tension obtained depending on the formulation modeled by (Graybeal and Russel, 2013) by input the data that obtained from tested samples in driven formulas.

5-4-2-1 Compression

The stress-strain of UHPC in compression was formulated as clarified in Equ. (5-8 to 5-10) and for tension as shown in Equ. (5-11) see Figure 5-7.

$$\sigma_c = E_c\,\epsilon_c \text{ if } \sigma_c \le 0.5 f_c \quad \ldots\ldots\ldots (5\text{-}8)$$

$$\sigma_c = E_c\,\epsilon_c\,(1-\alpha) \text{ if } \sigma_c > 0.5 f'_c \quad \ldots\ldots (5\text{-}9)$$

And $$\alpha = (0.001 * e^{\frac{E_c\,\epsilon_c}{0.243 * f_c}}) - 0.001 \quad \ldots\ldots\ldots (5\text{-}10)$$

Where: σ_c is compressive stress; ε_c is concrete strain; α is a coefficient relating to the deviation of the actual stress–strain curve from the linear trend.

5-4-2-2 Tension

The following formula was adopted to evaluate the model of stress-strain curve of UHPC in tension as clarified in Equ. (5-11) and shown the result in Figure 5-8

$$\sigma_t = 0.55\sqrt{f_c}(\text{MPa}) \ldots\ldots\ldots\ldots\ldots (5\text{-}11)$$

Where: σ_t is the tension stress; ε_c is concrete strain taken as 0.05.

This technique of UHPC in tension response was developed by (Shafieifar et al., 2017);(Kadhim et al., 2021).

5-5 Numerical Analysis Results (Validation Study)

The previously mentioned experimental results are compared with the corresponding FE results to validate the modeling approach. The comparison depended on the load-deflection curve of both simply supported and continuous girders.

5-5-1 Simply supported girders

The result of numerical analysis of the simply supported girder was listed in Table 5-1. The comparison of result with experiment were consisted of the load deflection response, cracking pattern, and the failure mode as shown in Figure 5-9 to Figure 5-24.

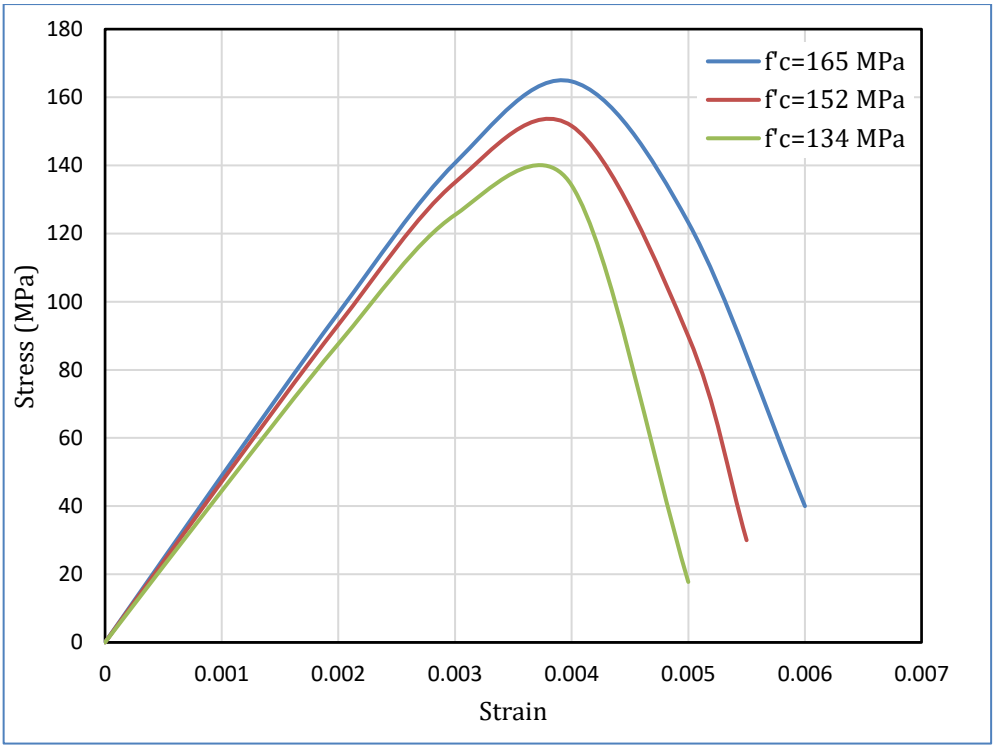

Figure 5-7: Stress-strain curve in compression of UHPC.

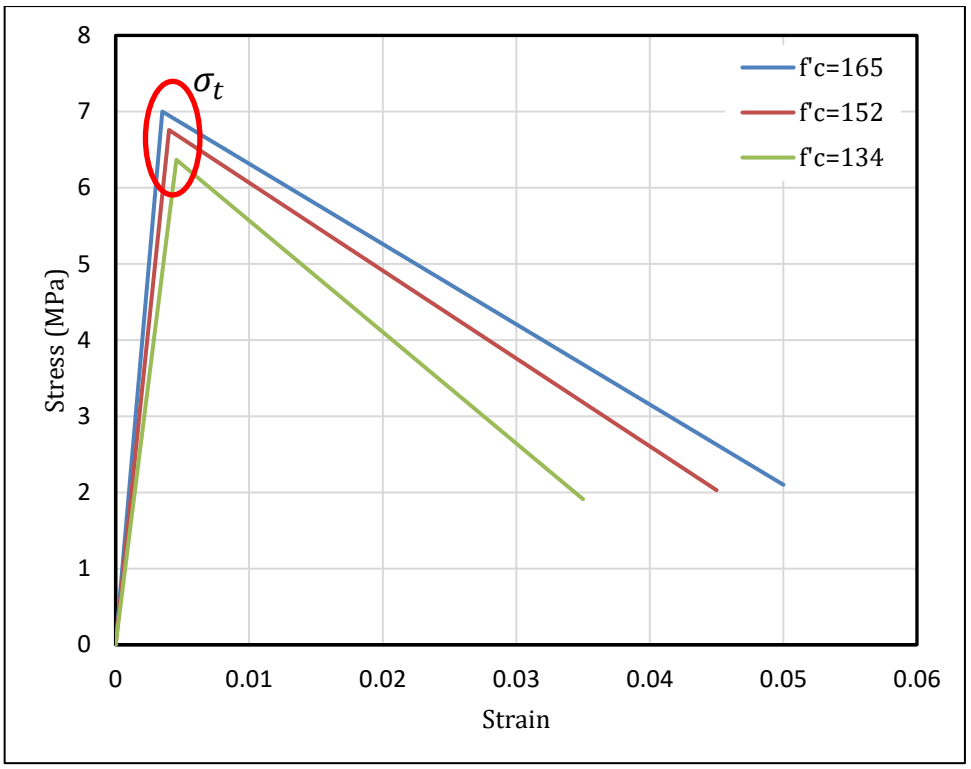

Figure 5-8: Stress-strain curve in tension of UHPC.

Table 5-1: The results of the validations of simply supported specimens.

Girder Symbol		***Cracking load P_{cr} (kN)***	***P_{cr} FE / P_{cr} Exp***	***Ultimate load P_{ul} (kN)***	***P_{FE}/P_{exp}***	***Deflection Δ_{ul} (mm)***	***Δ_{FE}/Δ_{Exp}***
$SB_1.HC_1.L_1$	Exp	60	1.1	198.45	1.04	23.26	0.8
	FE	65.7		206.4		18.5	
$SB_2.HC_2.L_1$	Exp	37	1.35	189.13	1.02	22.8	0.71
	FE	50		193.03		16.1	
$SB_3.HC_3.L_1$	Exp	35	1.23	183.2	1.01	22.45	0.86
	FE	43		184.8		19.3	
$SB_5.HC_2.SK.L_1$	Exp	43	1.2	193.95	1.01	20.9	0.72
	FE	50		196.8		15	
$SB_6.HC_3.SK.L_1$	Exp	39	1.28	187.73	0.99	22.3	0.7
	FE	50		187		15.1	
$SB_7.HC_1.L_2$	Exp	45		187.27	1.01	19.7	1.03
	FE	….		189.9		20.2	
$SB_8.HC_2.L_2$	Exp	36		175.45	1.03	22.83	1.04
	FE	….		180.15		23.8	
$SB_9.HC_3.L_2$	Exp	36		164.5	1.02	23.04	0.98
	FE	….		168.1		22.78	

➢ **$SB_1.HC_1.L_1$**

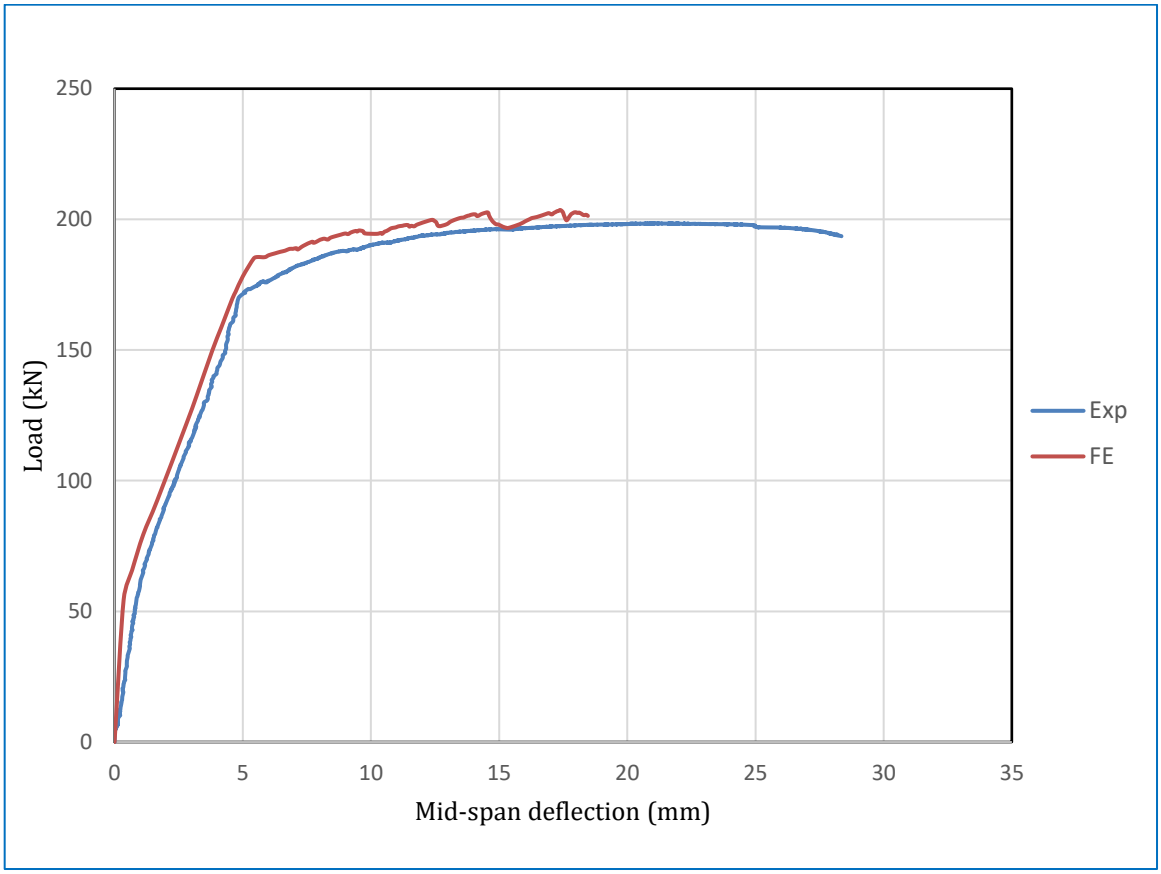

Figure 5-9: Load- mid-span deflection response of $SB_1.HC_1.L_1$

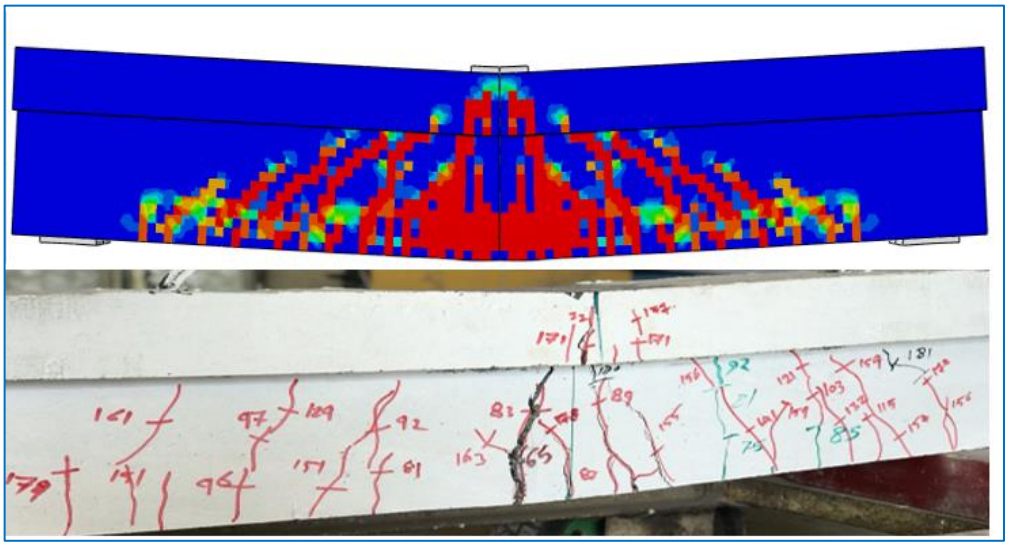

Figure 5-10:Failure mode and crack pattern of $SB_1.HC_1.L_1$

- **$SB_2.HC_2.L_1$**

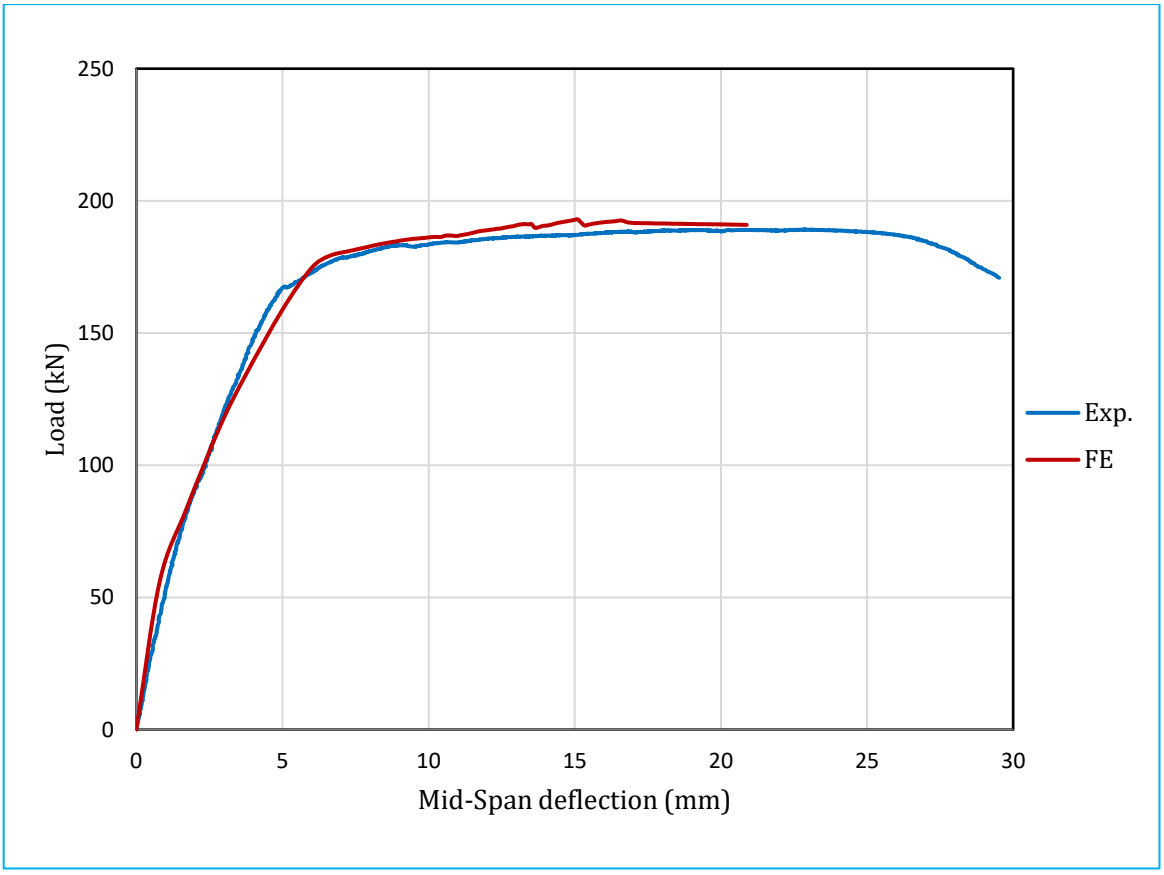

Figure 5-11 : Load- mid-span deflection response of $SB_2.HC_2.L_1$

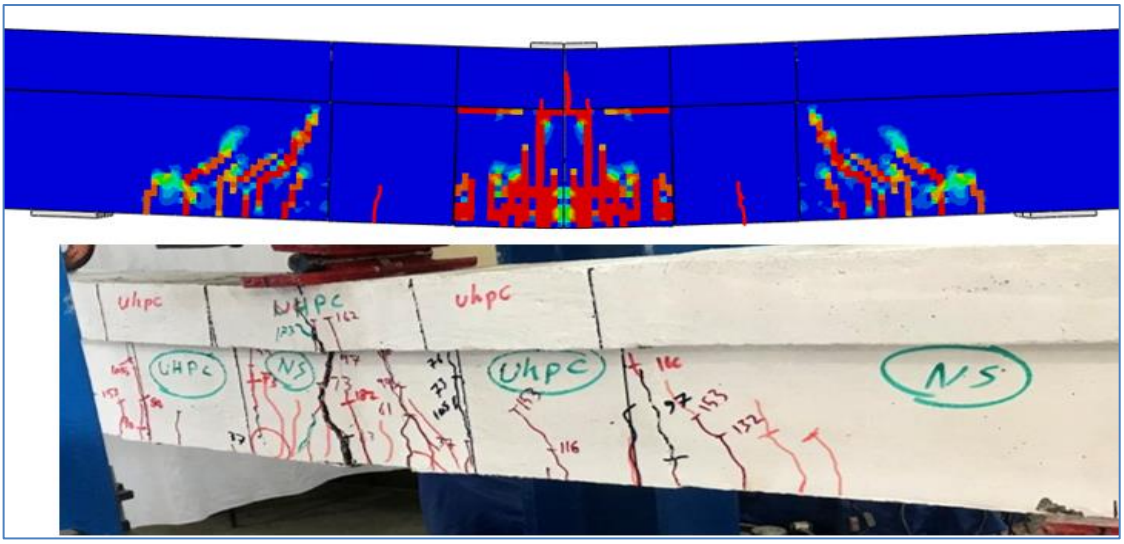

Figure 5-12: Failure mode and crack pattern of $SB_2.HC_2.L_1$

- **$SB_3.HC_3.L_1$**

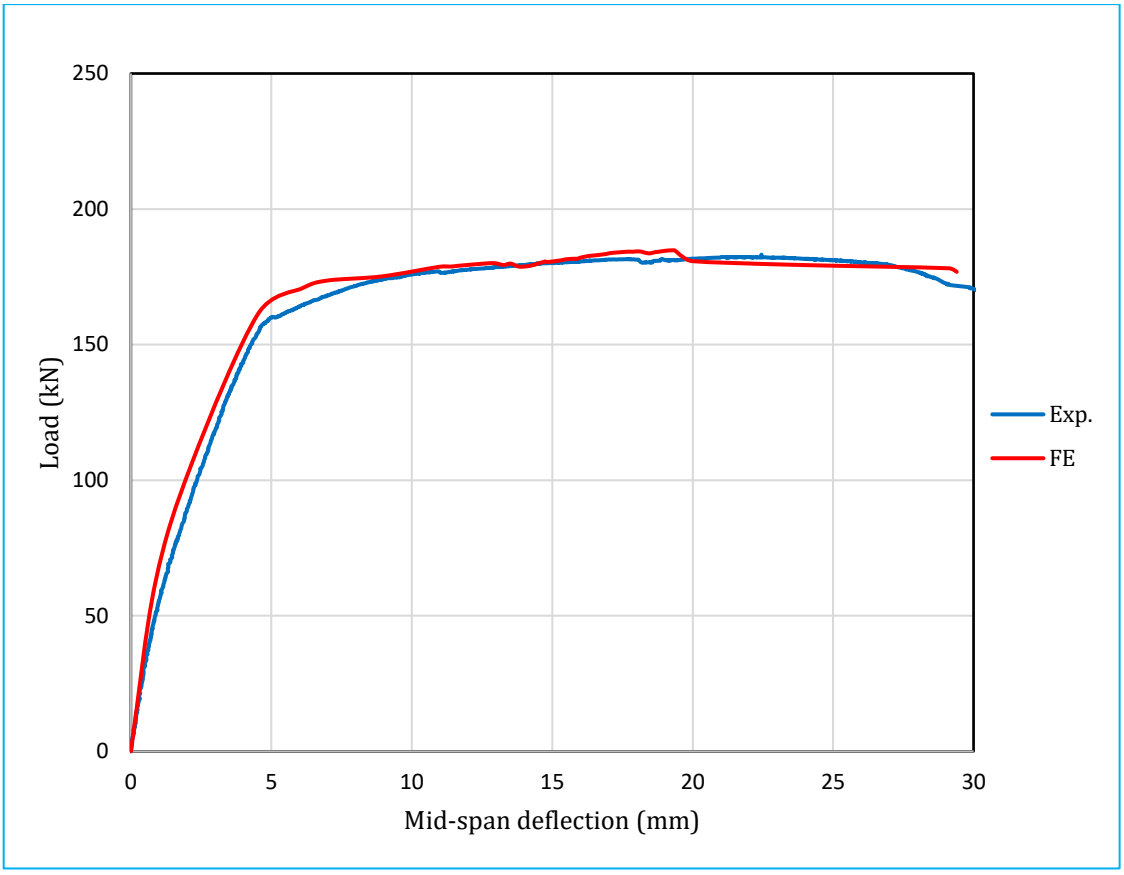

Figure 5-13:Load- mid-span deflection response of $SB_3.HC_3.L_1$

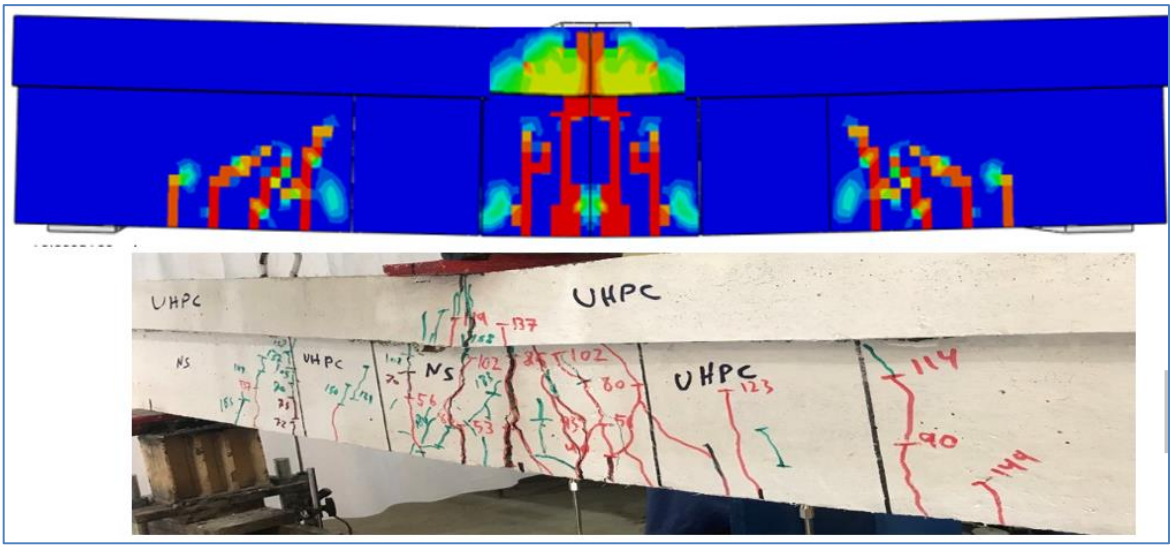

Figure 5-14: Failure mode and crack pattern of $SB_3.HC_3.L_1$

- **$SB_5.HC_2.SK.L_1$**

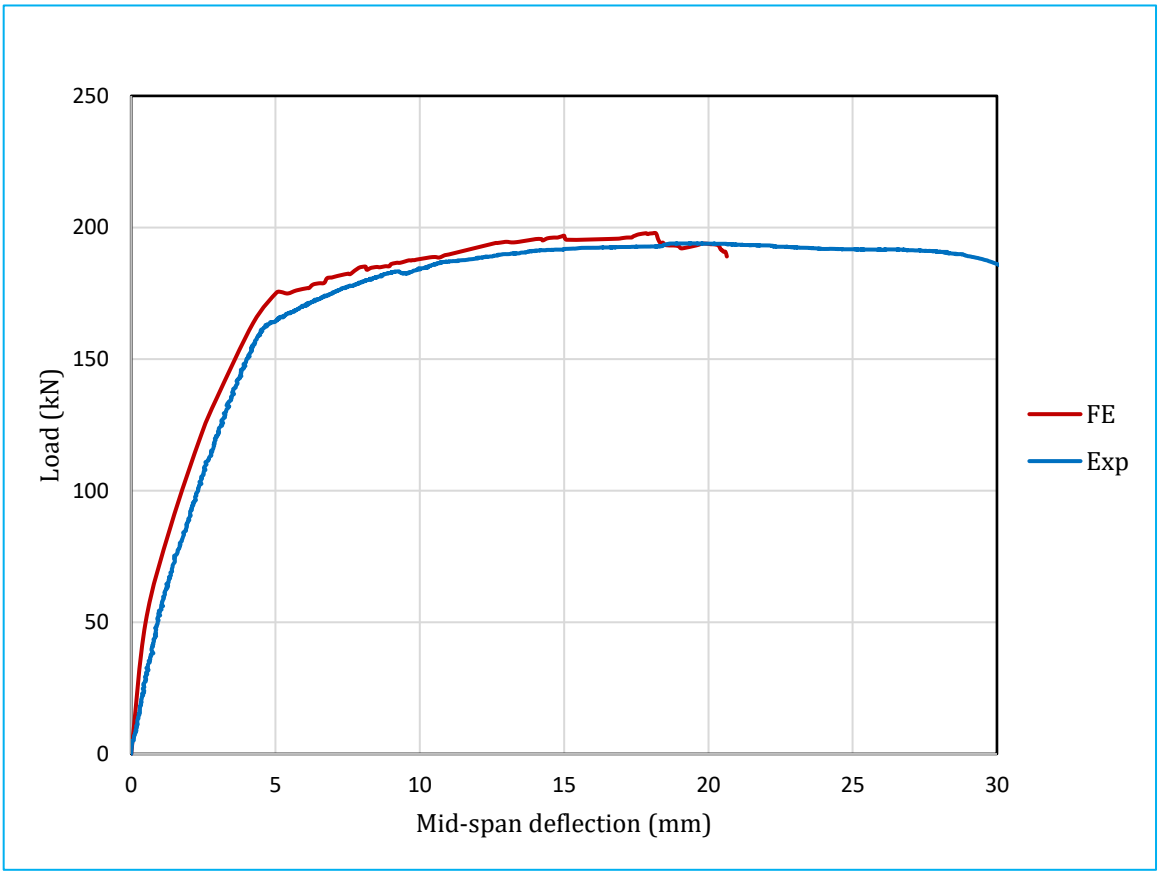

Figure 5-15:Load- mid-span deflection response of $SB_5.HC_2.SK.L_1$

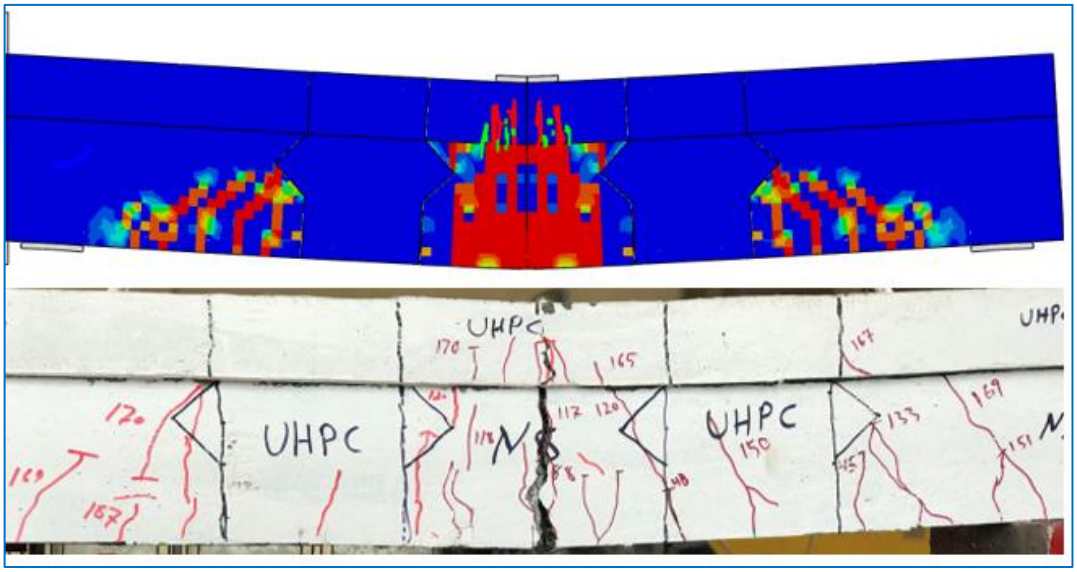

Figure 5-16: Failure mode and crack pattern of $SB_5.HC_2.SK.L_1$

- **$SB_6.HC_3.SK.L_1$**

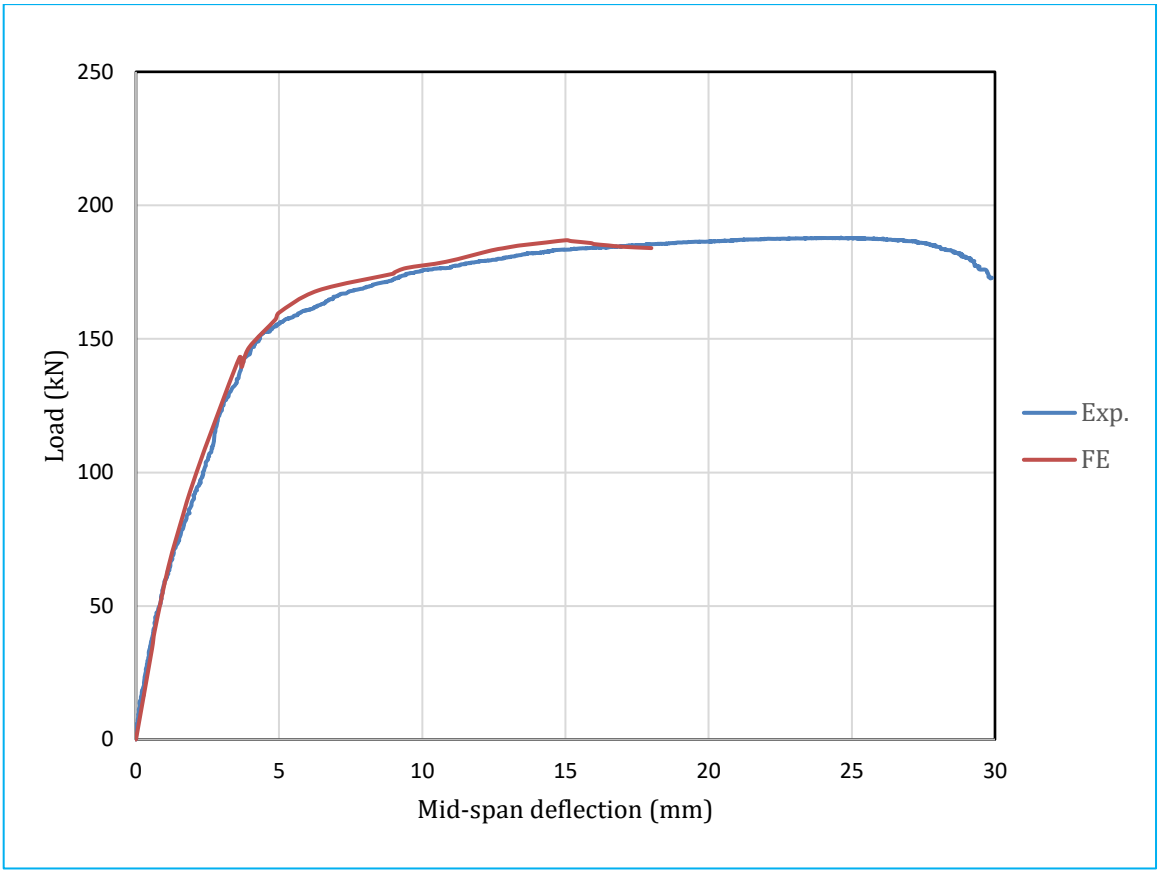

Figure 5-17: Load- mid-span deflection response of $SB_6.HC_3.SK.L_1$

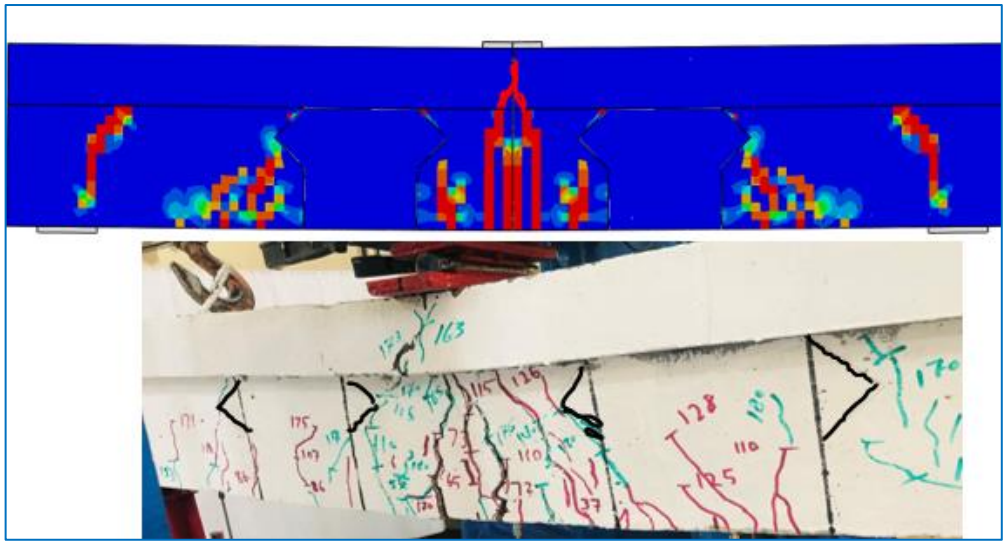

Figure 5-18: Failure mode and crack pattern of $SB_6.HC_3.SK.L_1$

- **$SB_7.HC_1.L_2$**

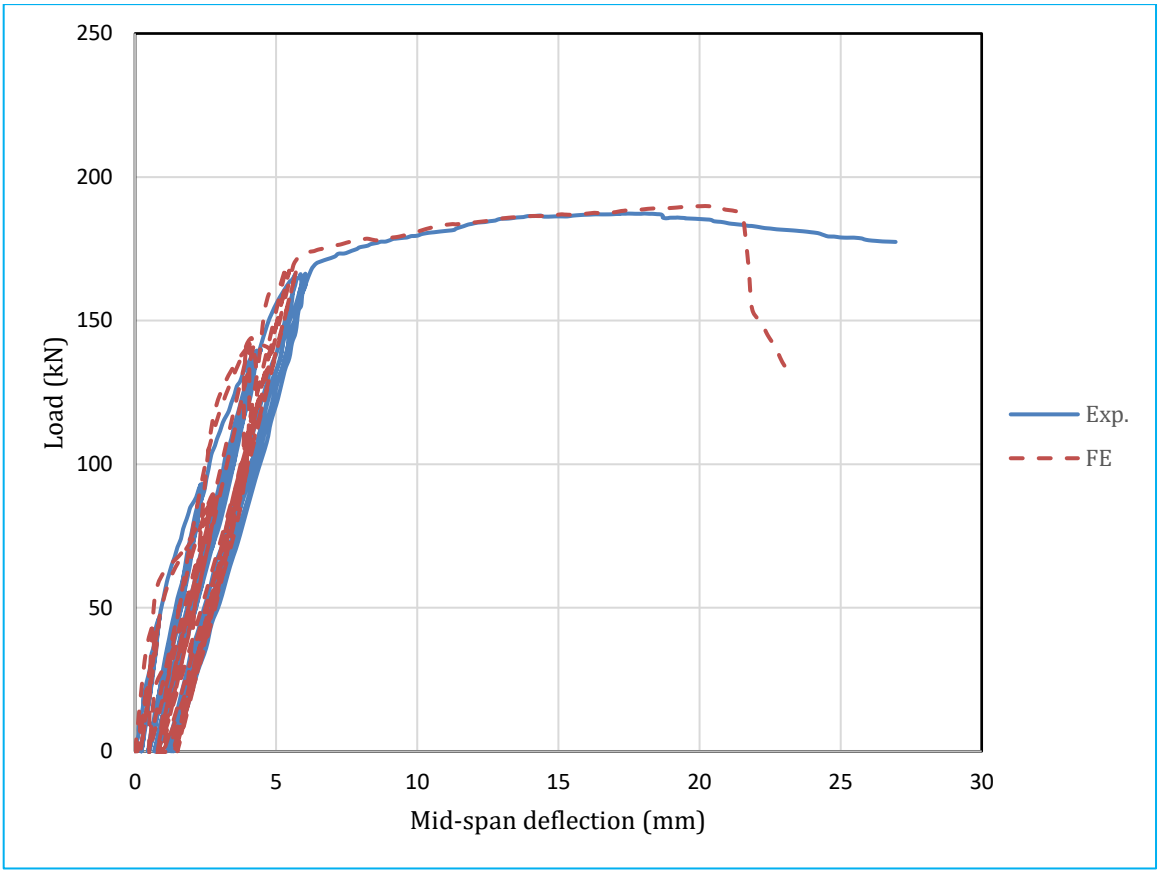

Figure 5-19: Load- mid-span deflection response of $SB_7.HC_1.L_2$

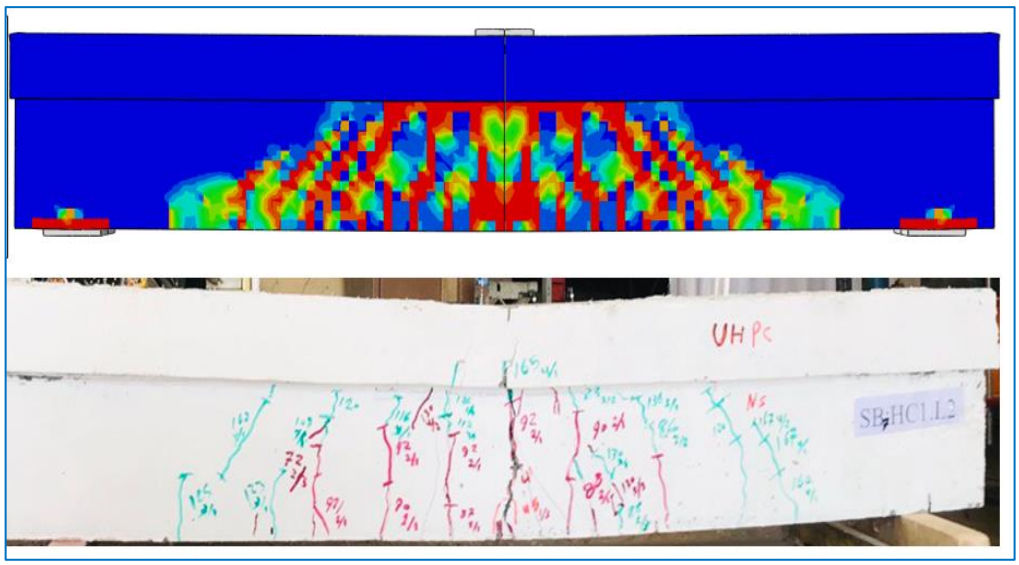

Figure 5-20: Failure mode and crack pattern of $SB_7.HC_1.L_2$

- **$SB_8.HC_2.L_2$**

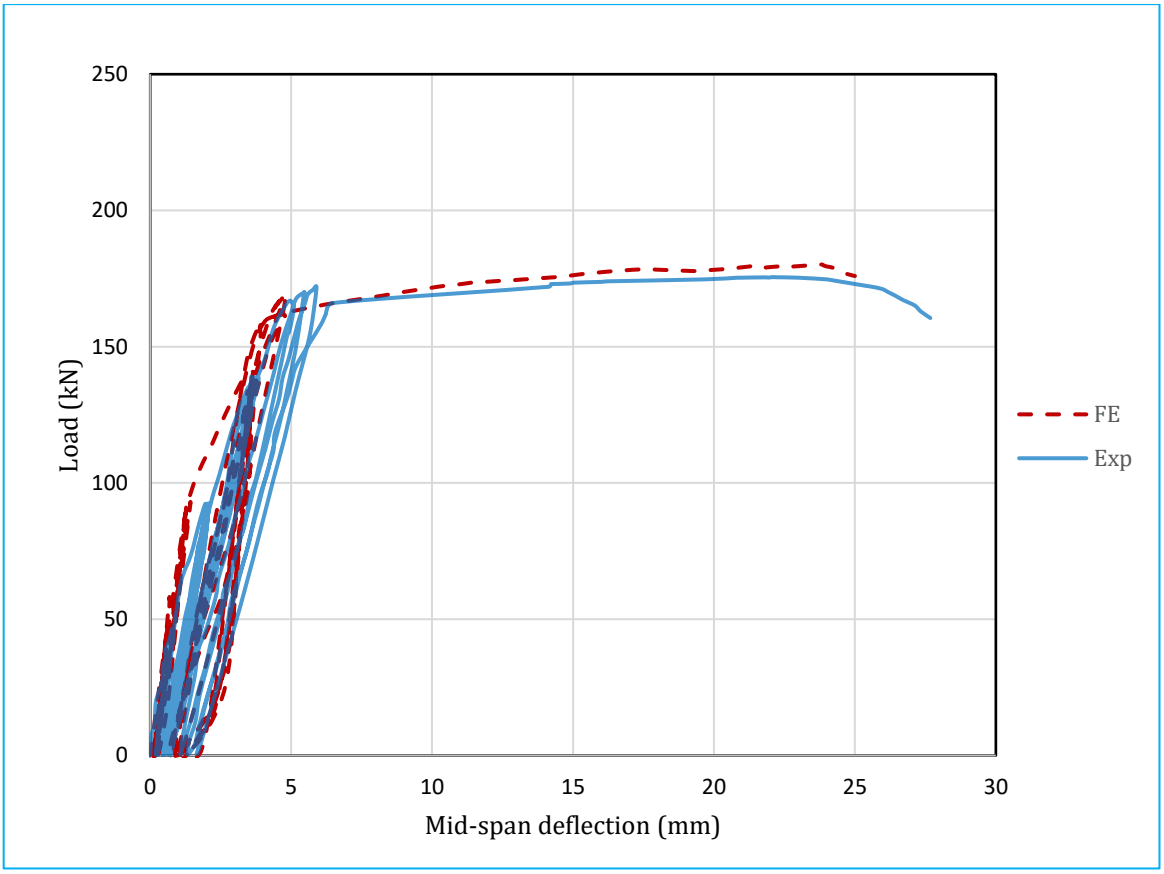

Figure 5-21: Load- mid-span deflection response of $SB_8.HC_2.L_2$

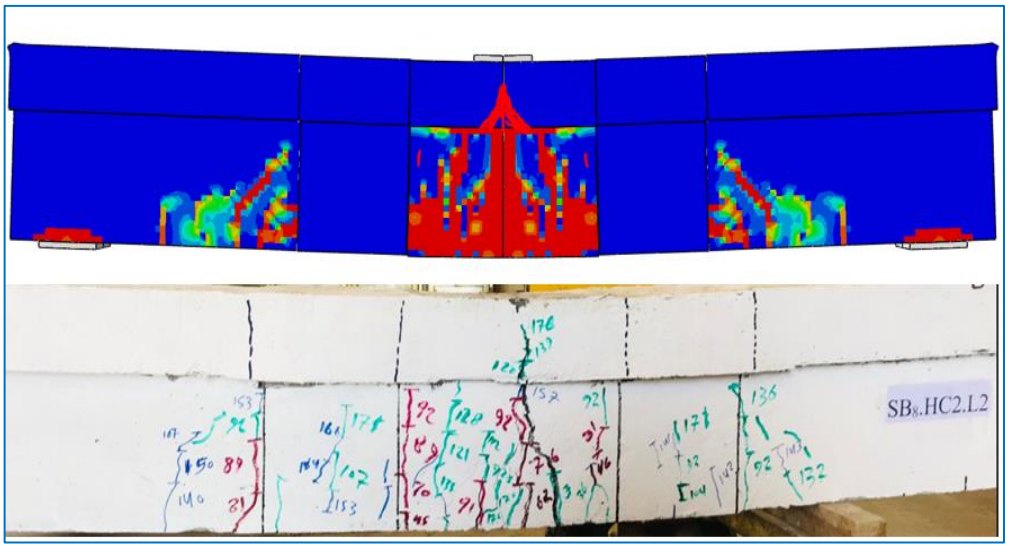

Figure 5-22: Failure mode and crack pattern of $SB_8.HC_2.L_2$

- **$SB_9.HC_3.L_2$**

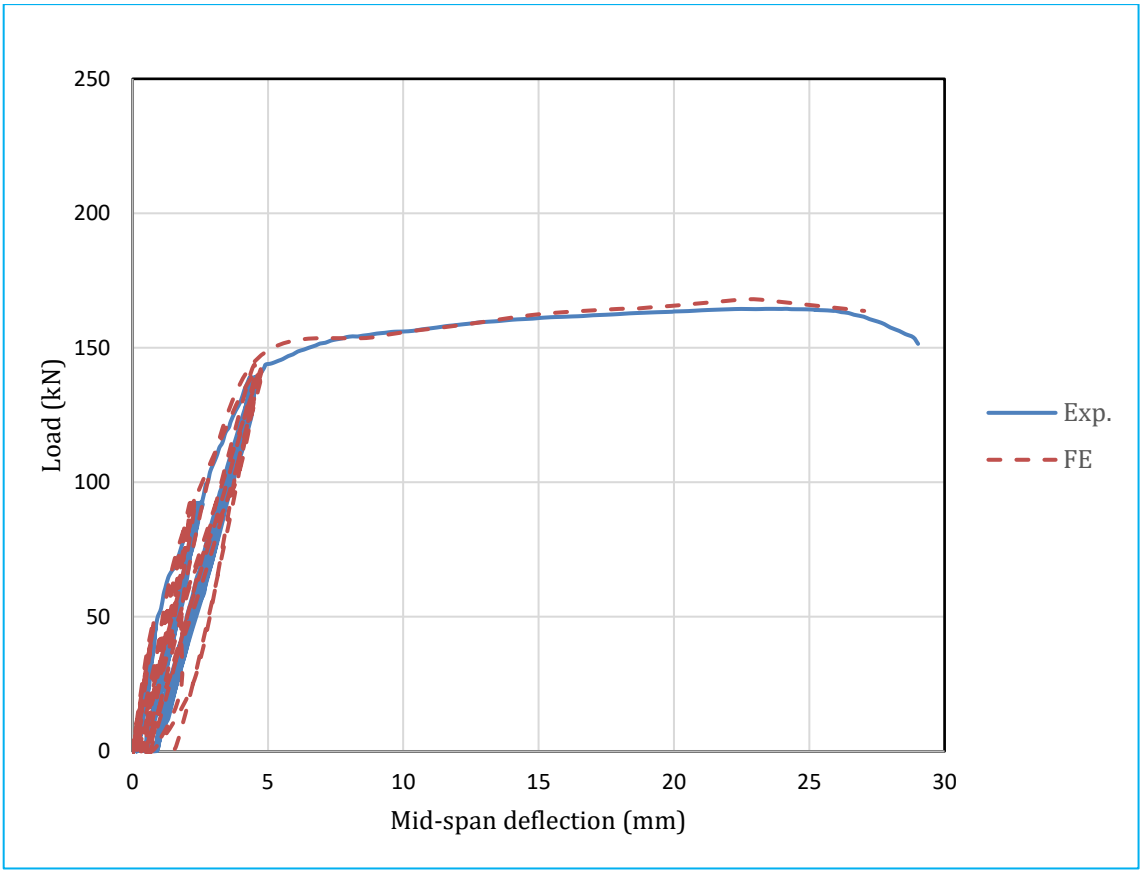

Figure 5-23: Load- mid-span deflection response of $SB_9.HC_3.L_2$

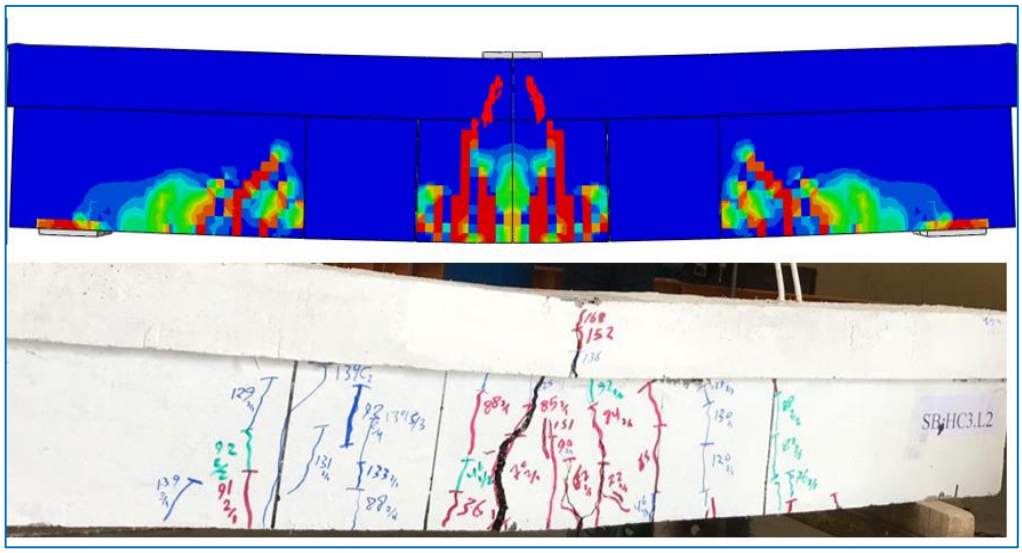

Figure 5-24: Failure mode and crack pattern of $SB_9.HC_3.L_2$

5-5-2 Continuous girder

The result of analysis of the continuous girder was listed in Table 5-2. The comparison of result with experimental data were consisted of the load deflection response and the failure mode as shown in Figure 5-26 to Figure 5-30.

Table 5-2: The results of the validations of continuous specimens

Girder Symbol	*Cracking load P_{cr} (kN)*		*P_{exp}/P_{FE}*	*Ultimate load P_{ul} (kN)*	*P_{exp}/P_{FE}*	*Deflection Δ_{ul} (mm)*	*Δ_{FE}/Δ_{Exp}*
$CB_{13}.HC_1.L_1$	Exp	174	1.04	481.85	1.02	18.4	0.83
	FE	181		491.4		15.3	
$CB_{14}.HC_4.L_1$	Exp	162	1.07	398.8	1.03	12.4	0.79
	FE	174		409.2		9.8	
$CB_{17}.HC_4.L_1$	Exp	109		413.1	1.03	13.6	0.78
	FE	...		426.2		10.6	

- **$CB_{13}.HC_1.L_1$**

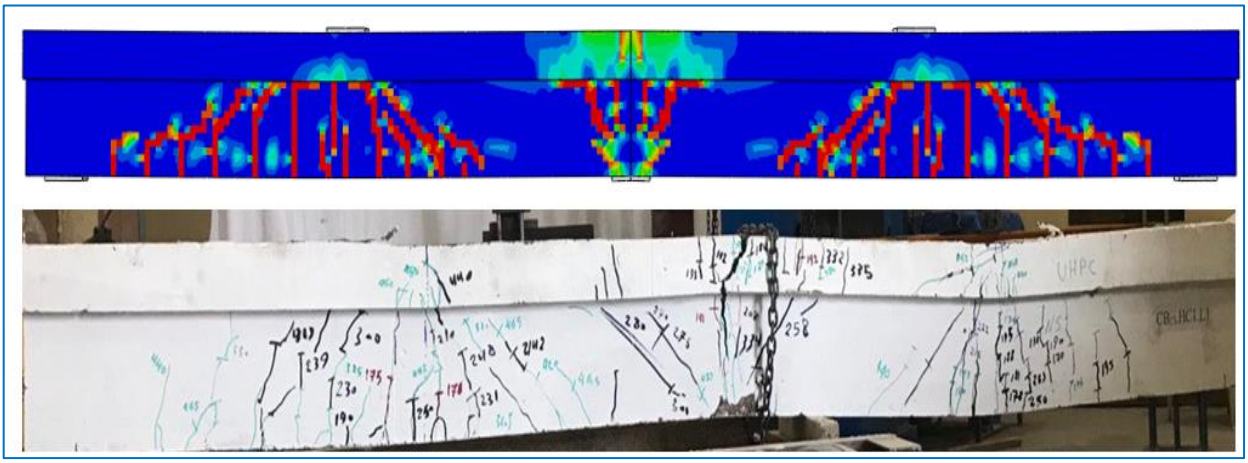

Figure 5-25: Failure mode and crack pattern of $CB_{13}.HC_1.L_1$

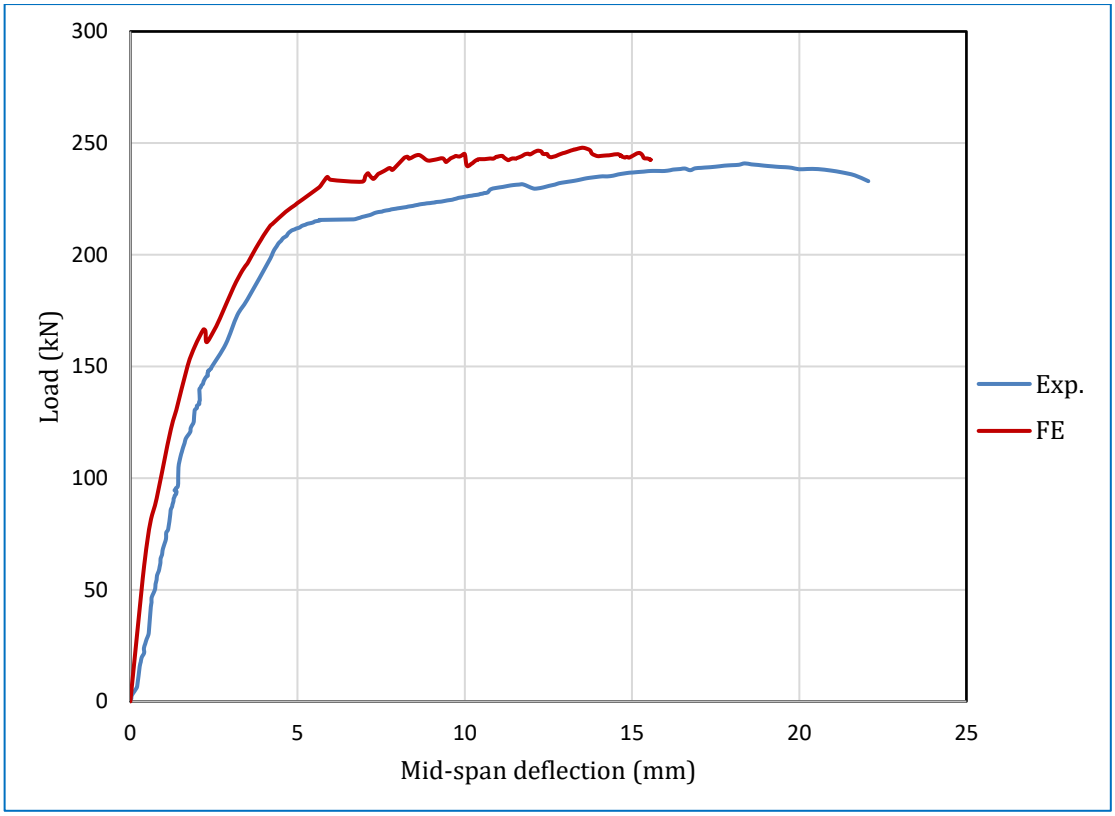

Figure 5-26: Load- mid-span deflection response of $CB_{13}.HC_{1}.L_{1}$

- **$CB_{14}.HC_{4}.L_{1}$**

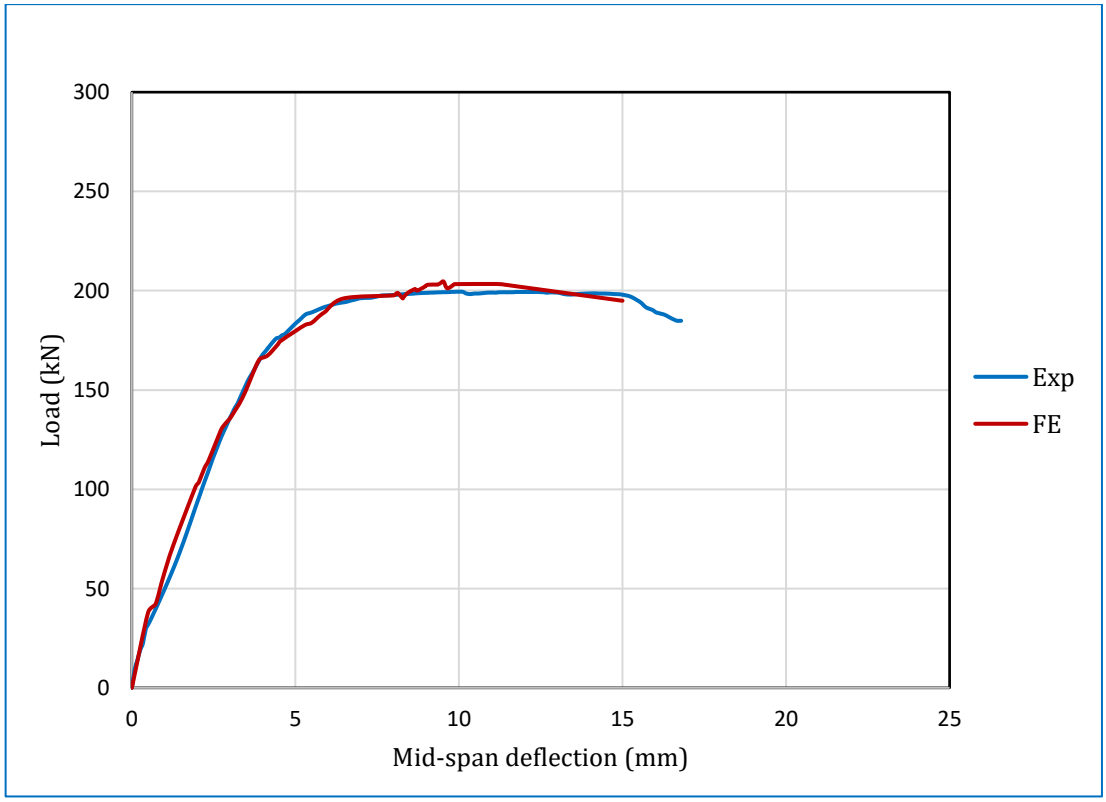

Figure 5-27:Load- mid-span deflection response of $CB_{14}.HC_{4}.L_{1}$

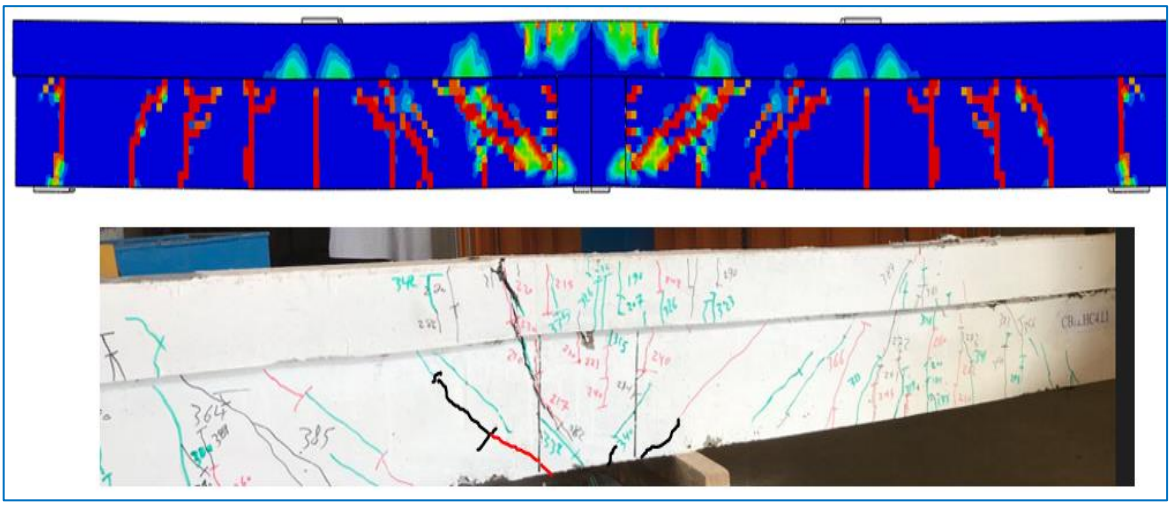

Figure 5-28: Failure mode and crack pattern of $CB_{14}.HC_4.L_1$

- **$CB_{17}.HC_4.SK.L_1$**

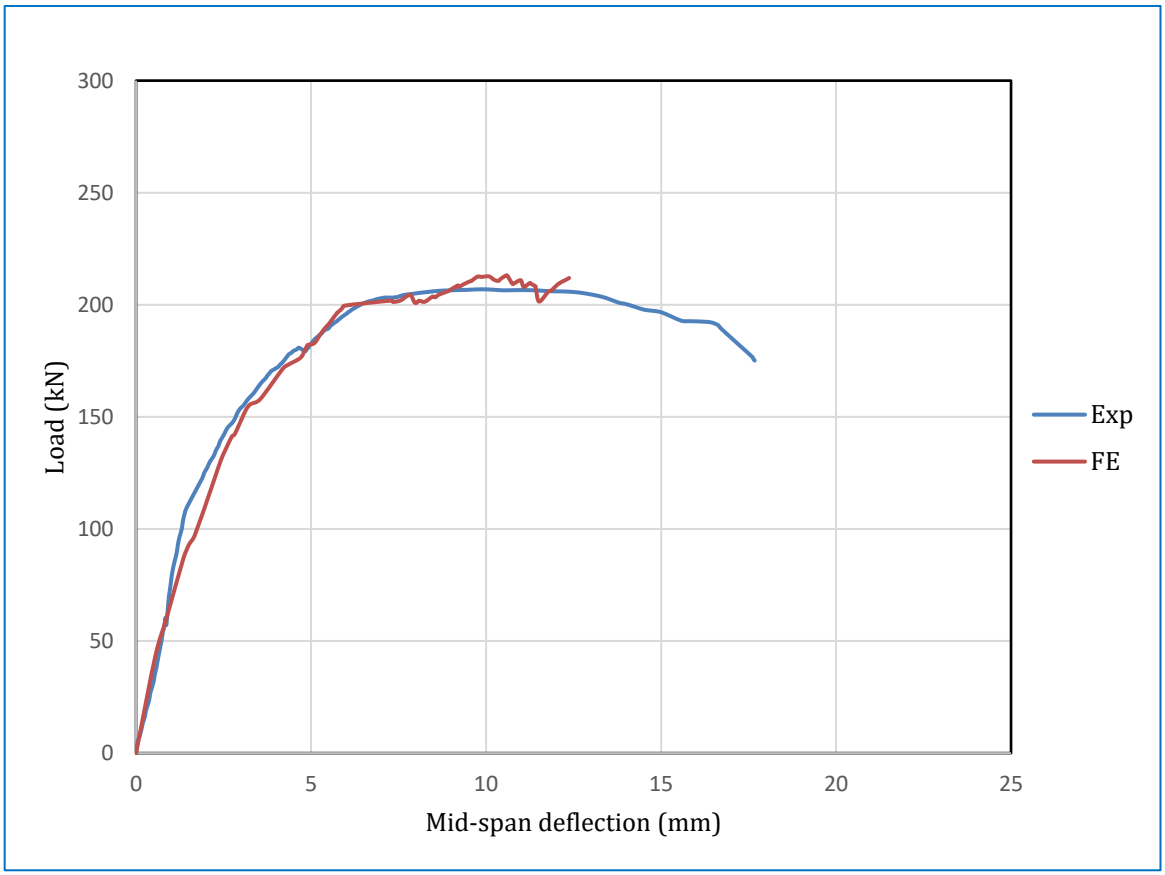

Figure 5-29: Load- mid-span deflection response of $CB_{17}.HC_4.SK.L_1$

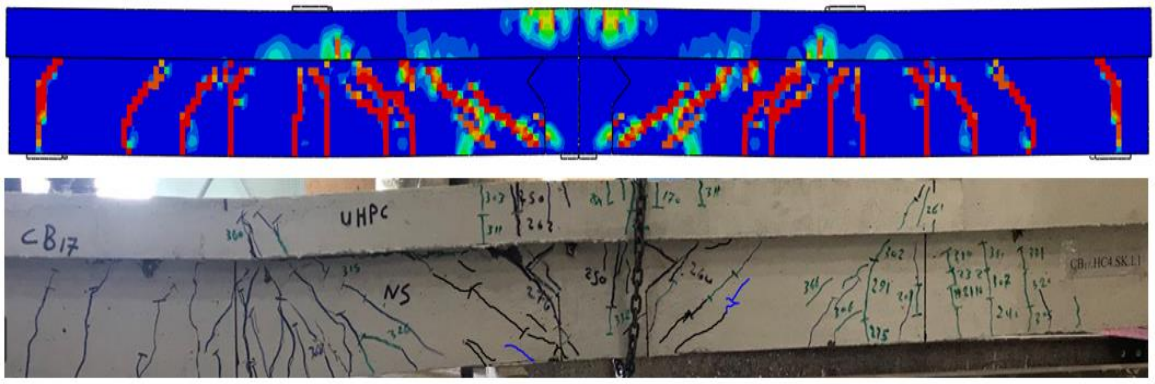

Figure 5-30: Failure mode and crack pattern of $CB_{17}.HC_4.SK.L_1$

5-6 Parametric Study of Simply Supported Girders

This part was included the important cases that did not studied in the experimental part. For simply supported girder would test the effect of reverse cyclic load, thickness of deck, the type of interface preparation, and the reinforcement ratio.

5-6-1 Cyclic reverse load

Figure 5-31 shows the history of reverse cyclic load adopted in the FE analysis, it was similar to the protocol mentioned in chapter Three (3.9.3) Figure 3-18 ,TP01 (Takemura and Kawashima, 1997) . This load was applied to the control and splice girders.

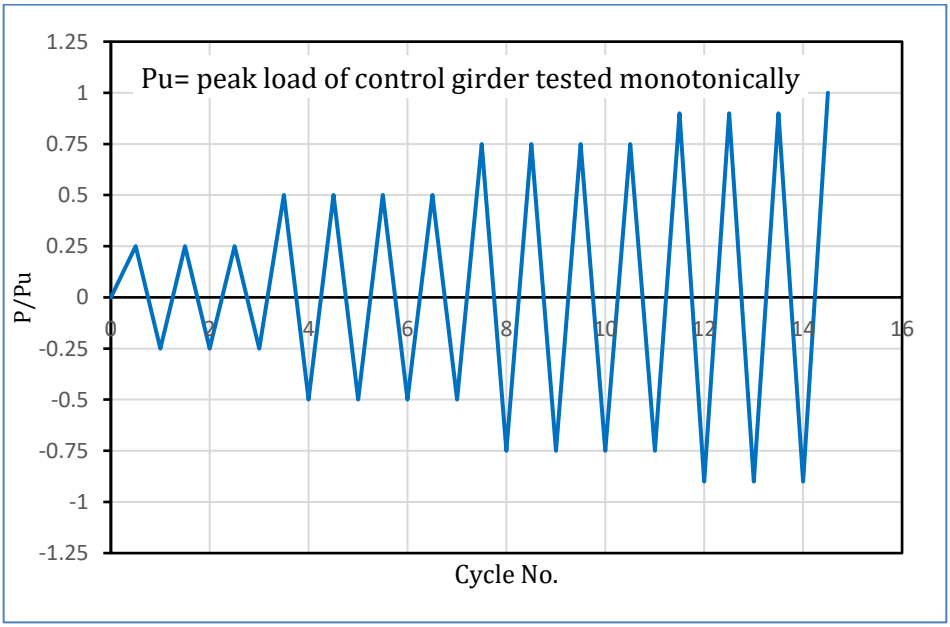

Figure 5-31: The history of reverse cyclic load.

The reverse cyclic loading was affected on the deterioration of stiffness of the girders. From Figure 5-32 shown that yielding the control girder under load less than the yield load in the repeated load, also this fact was applied on the partial depth spliced girder as shown in Figure 5-33. The ultimate load was reduced by about 33.4 % and 28.6 % for control girder in monotonic and repeated loading respectively. Meanwhile, the ultimate load in the spliced girder was reduced by about 34.4 % and 27.9 %for monotonic and repeated loading respectively. In spite of the reverse cyclic load had a high effect on the overall behaviors of girders, but it did not change the mode of failure or cause debonding in the joint (i.e., the UHPC joint was presence high performance even under reverse cyclic load) see Figure 5-34.

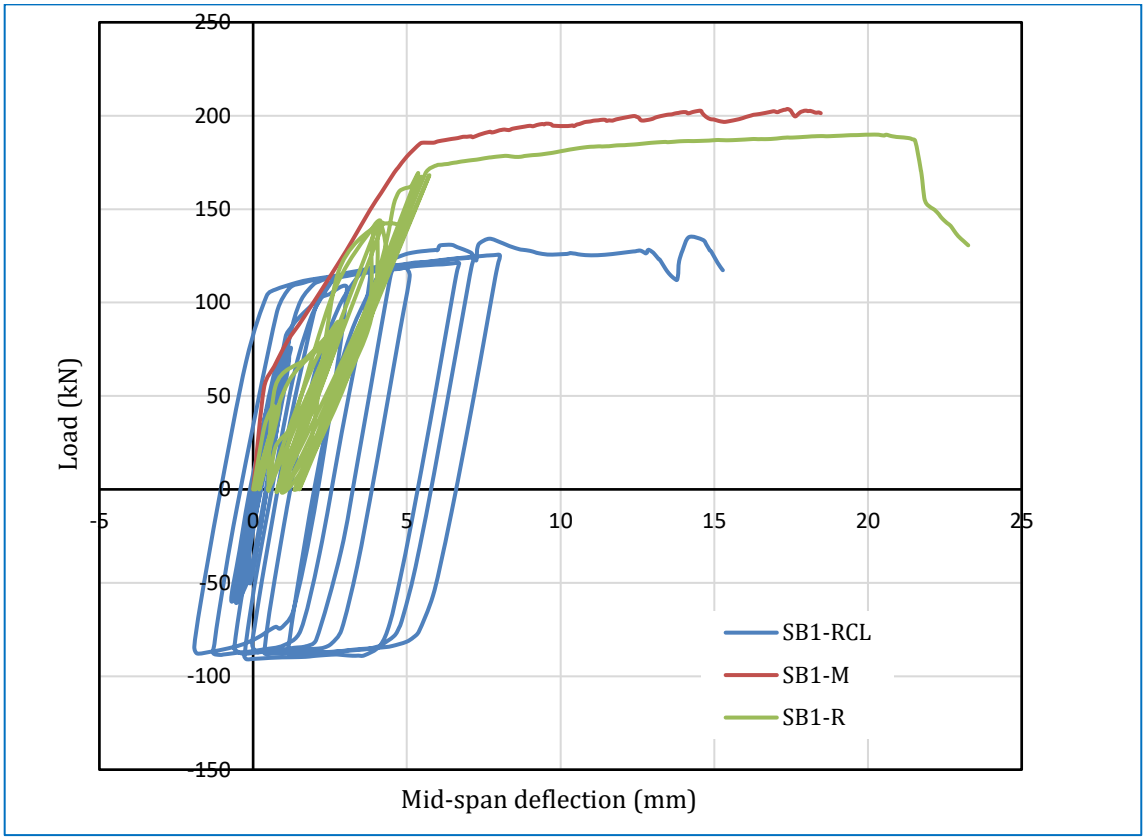

Figure 5-32: Load-mid span deflection response for reverse cyclic load of control girder.

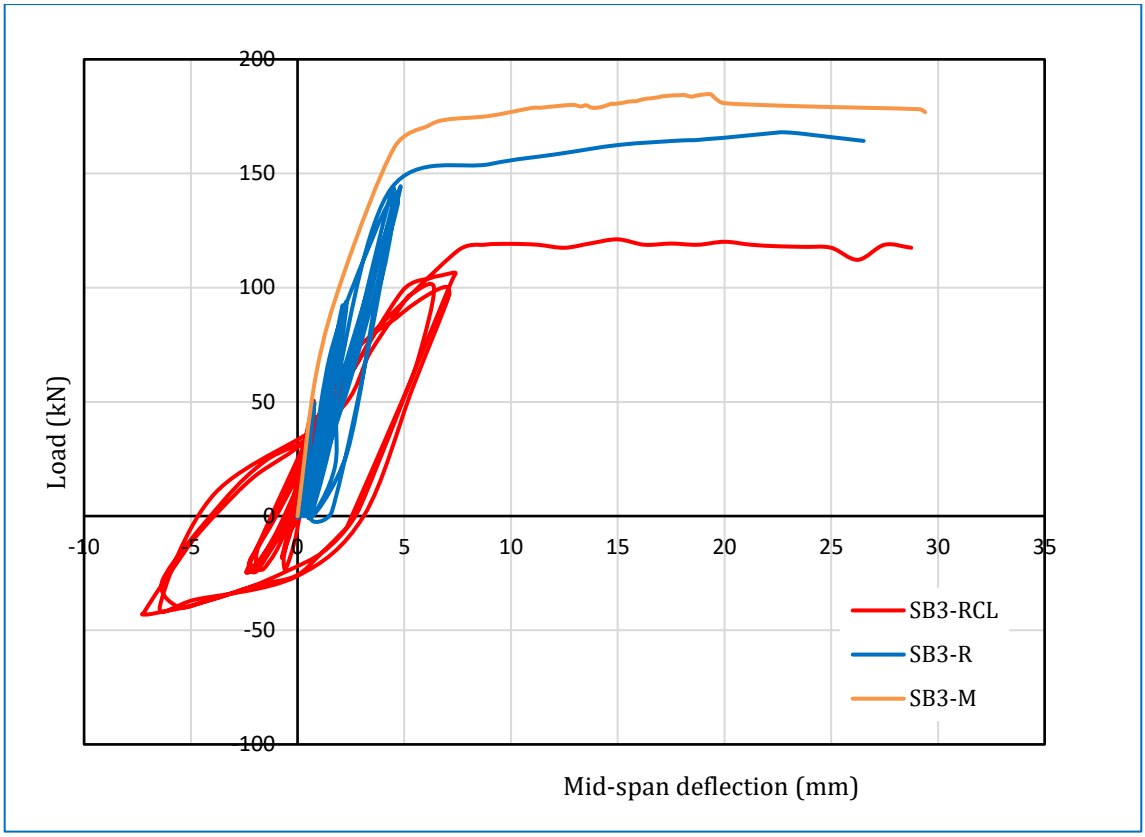

Figure 5-33: Load-mid span deflection response for reverse cyclic load of partial depth spliced girder.

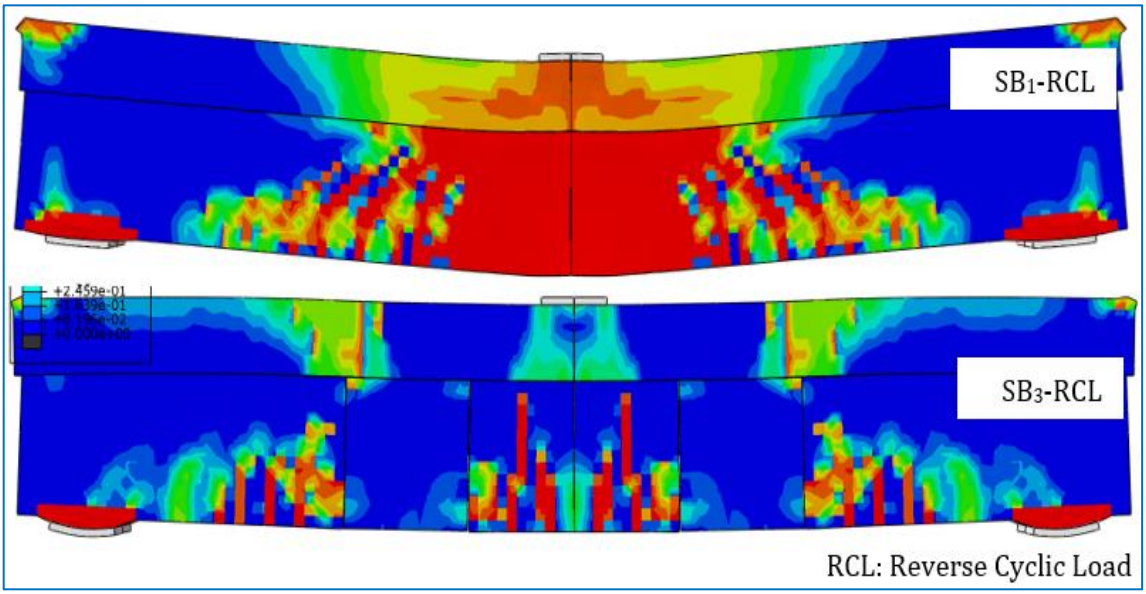

Figure 5-34: Failure mode and cracks pattern for the girder exposed to reverse cyclic load.

5-6-2 Thickness of deck

In experimental test was used 100 mm for thickness of the UHPC deck. This depth had high effect in the carrying out the load applied on the girder. Thus, in the FE study would study the variation of decreasing the deck thickness for 75 mm and 50 mm spliced girder with remain the total height of girder. The analysis results were showed that the reduction in the UHPC thickness of the deck led to decreasing in the ultimate load and stiffness of the spliced girder by about 3.4 and 64.7 % for 75- and 50-mm thickness respectively as illustrated in Figure 5-35. The large percentage of reduction for 50 mm deck thickness due to the high depth of web joint and increased the tensile stress in the bottom surface cause separation in the joint and yield the reinforcement then collapse the girder, as shown in Figure 5-36.

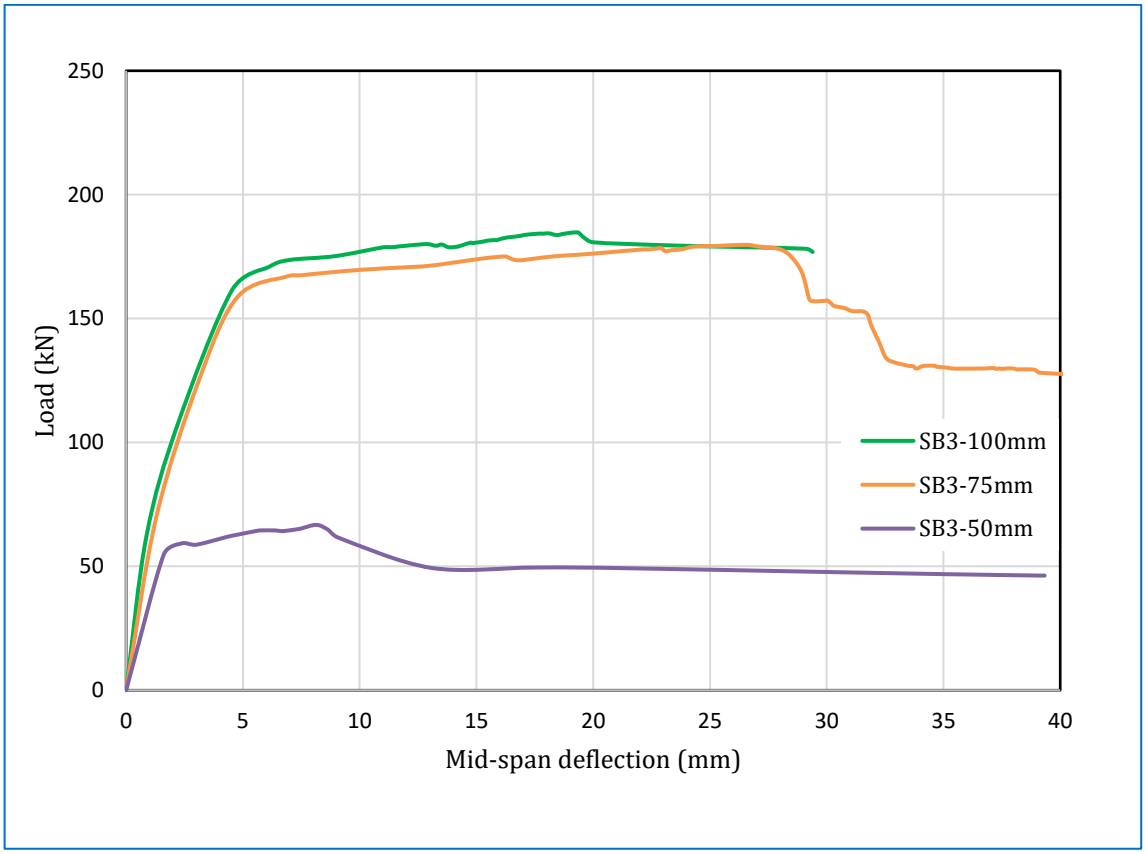

Figure 5-35: Load-mid span deflection response for the deck thickness variation of SB_3 girder.

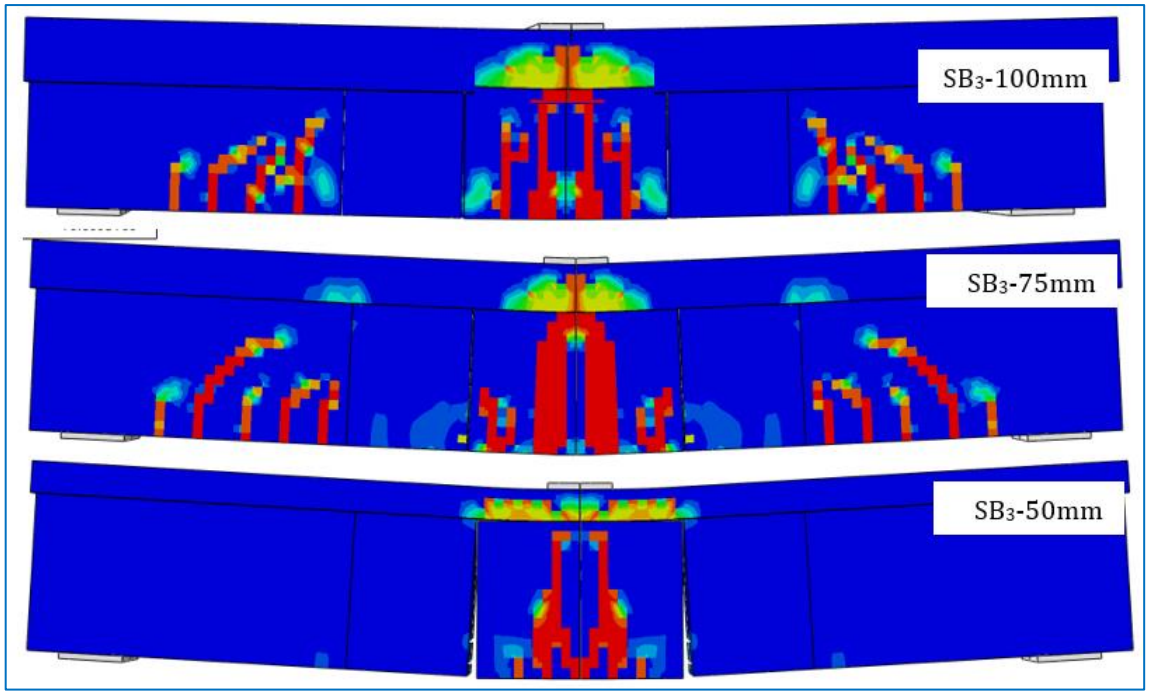

Figure 5-36: Failure mode and cracks pattern for the deck thickness variation of SB_3 girder.

5-6-3 Type of interface preparation

In the experimental work was used the exposed aggregate surface preparation system was used to ensure a good bond between the precast unit and the cast-in-place UHPC concrete. The FE model adopted the coefficient of friction equal to 1.44 to simulate the contact in the state of exposed aggregate according to (Kadhim et al., 2021);(Tayeh et al., 2012);(Hussein et al., 2016). Also, the parametric study would use the coefficient of friction as 1.3 for smooth surface (as cast surface) and 1.31 for Mid-Rough surface treated by sandblasting.

The results of analysis prove that the full depth joint specimen had high bond strength even the preparation surface would smooth or mid rough. Also, the reduction in the ultimate load was 2.9 and 3.4 % for mid rough and smooth surface respectively, with little increase in the ultimate deflection with decreasing the coefficient of friction, see Figure 5-37 and Figure 5-38.

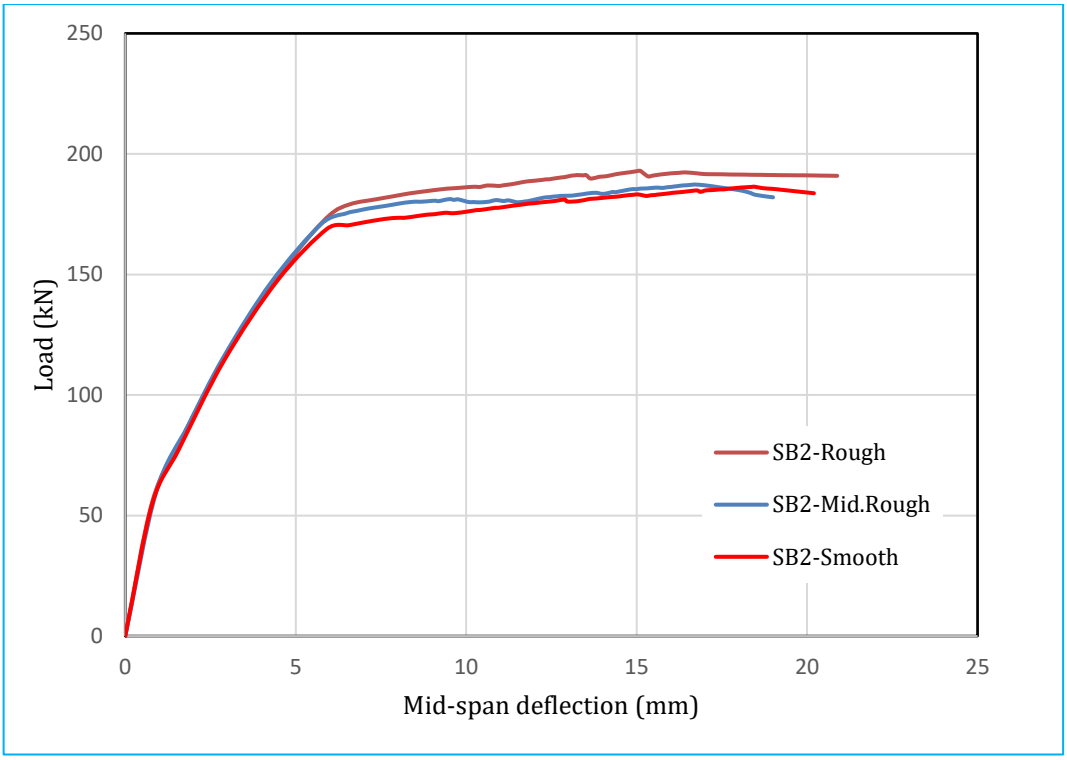

Figure 5-37: Load-mid span deflection response for the surface preparation variation of SB_2 girder.

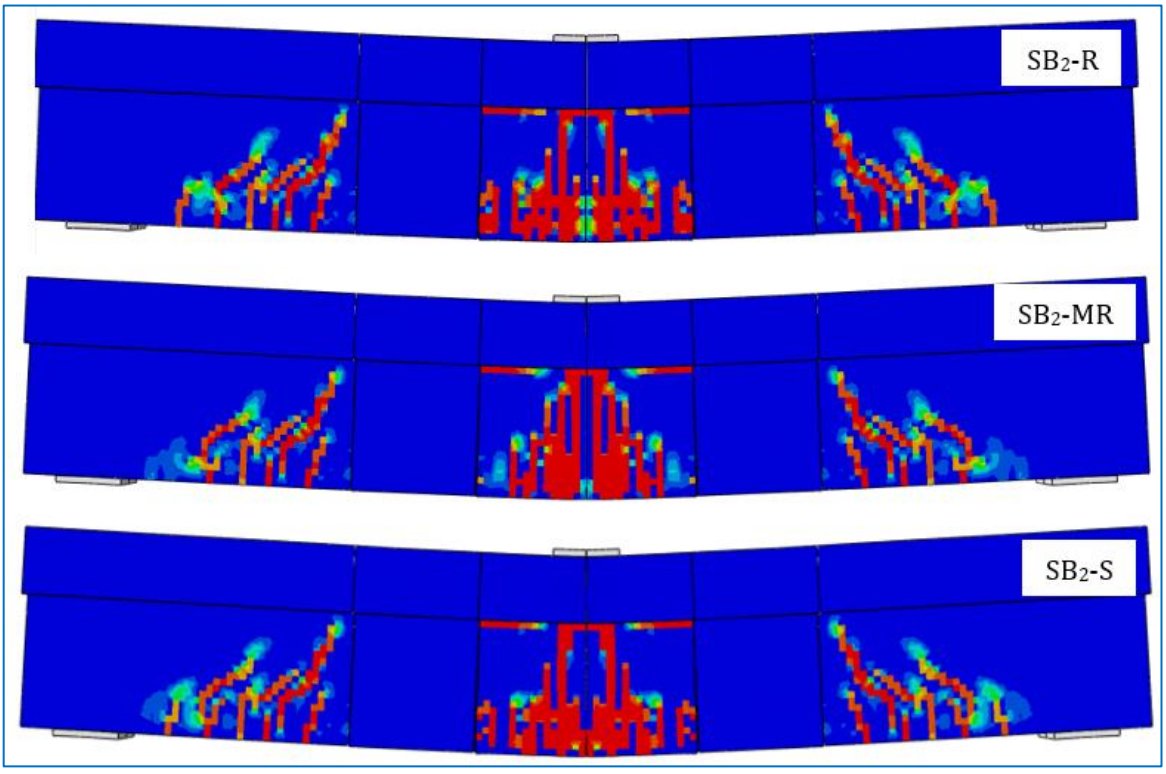

Figure 5-38: Failure mode and cracks pattern for the surface preparation variation of SB_2 girder.

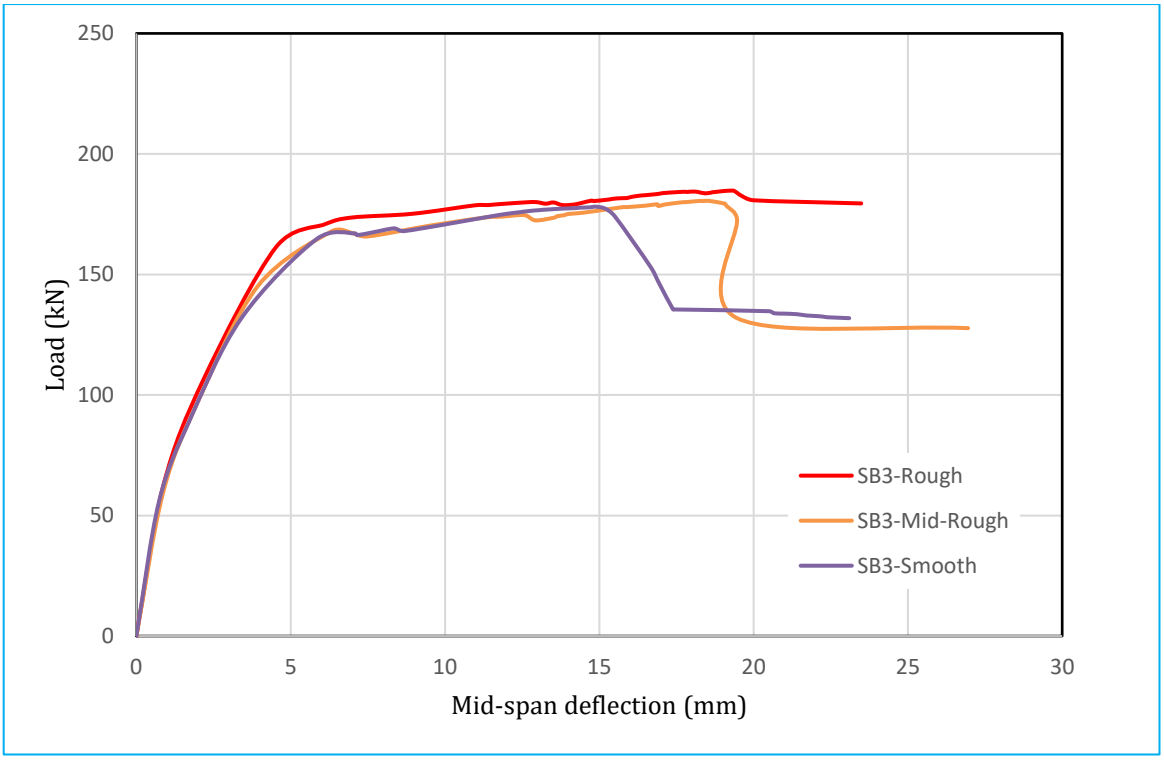

Figure 5-39: Load-mid span deflection response for the surface preparation variation of SB_3 girder.

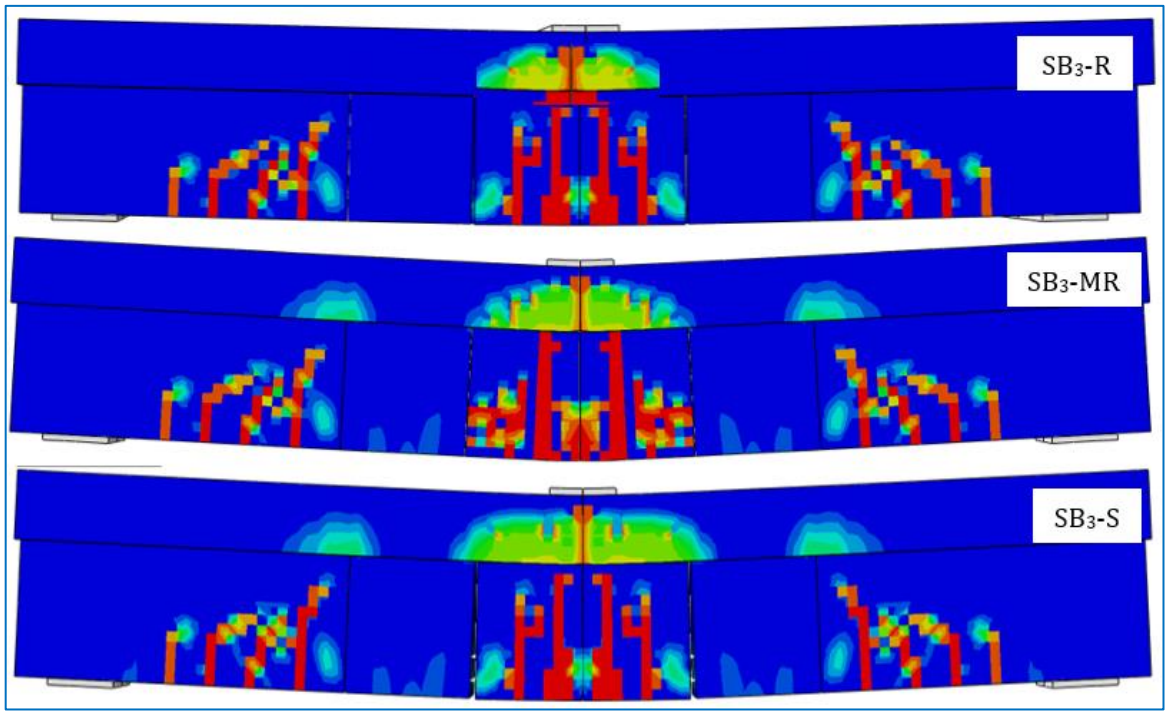

Figure 5-40: Failure mode and cracks pattern for the surface preparation variation of SB_3 girder.

Also, for the partial depth girder, the reduction in the ultimate load was about 2.2 and 3.5 % for mid rough and smooth surface respectively, with separation of the joint in smooth surface, see Figure 5-39 and Figure 5-40.

5-6-4 Reinforcement ratio

For the flexural members, the reinforcement ration was main factor that controlled the behavior of girder. The steel reinforcement ratio used in experimental test was 0.006 for control and spliced girder to provided flexural failure. In order to have more understand on the effect of reinforcement ratio would study the ratio 0.003(min. ratio) and 0.012. Doubling the reinforcement ratio led to increase the ultimate load by about 82.1% with improvement in the overall stiffness of girder and remain the ductile behavior and flexural failure. Also, the reduction of the reinforcement ratio to the half caused a decreased in the ultimate load by about 55% and stiffness of the spliced girder with flexure failure as shown in Figure 5-41 and Figure 5-42. This result compared to girder of 0.006 ratio.

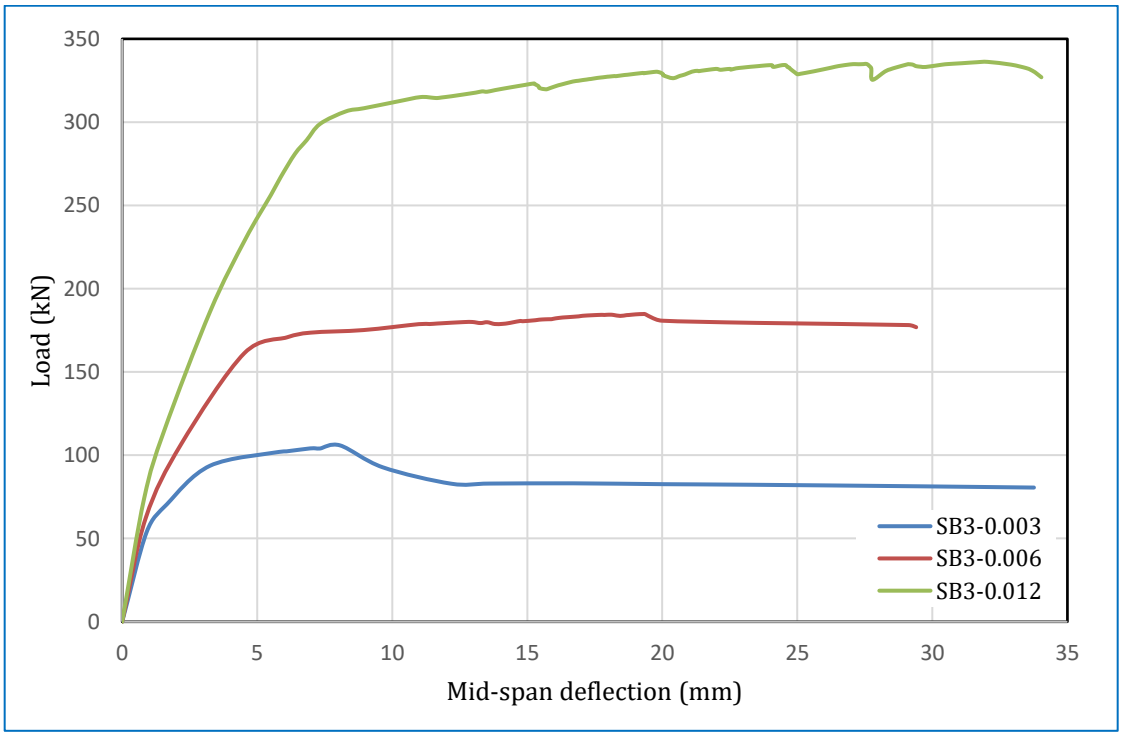

Figure 5-41: Load-mid span deflection response for the reinforcement ratio variation of SB_3 girder.

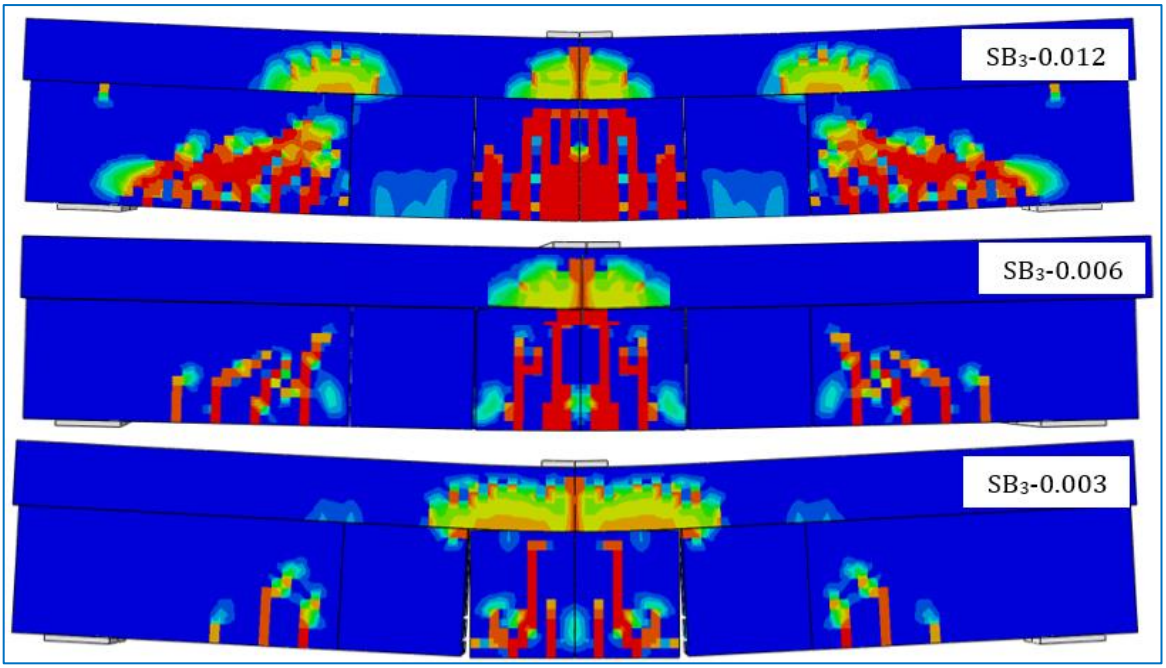

Figure 5-42: Failure mode and cracks pattern for the reinforcement ratio variation of SB3 girder.

5-7 Parametric Study for Continuous Girders

In the continuous girder, the girders have joints on the interior support that got in shear failure due to the high flexural capacity provided by UHPC in the joint at maximum negative moment. For this reason, the parametric study of continuous girders concentrated on the interior joint to increase the shear capacity and the flexural capacity.

5-7-1 Length of joint

The length of joint (L_j) was effect on the failure mode and bond mechanism activity of the girder by passing the failure line to the support. The length of the joint used in the experimental test that 190 mm, so in the FE parametric study was used $1.5L_j$ (285mm) and $2L_j$ (380 mm) of the length of the experimental test. The length of the joint 285 mm was given some of increasing in the stiffness of the girders with slight improvement in the ultimate load, but no changed in the shear failure. The length of the joint 380 mm increased the stiffness of the girder and the ultimate load by about 14% of the girder with original length of joint, as shown in Figure 5-43. Also, the

mode of failure for the girder had the length of joint 380 mm, joint that showed less shear crack compared with the flexural cracks, as illustrated in Figure 5-44.

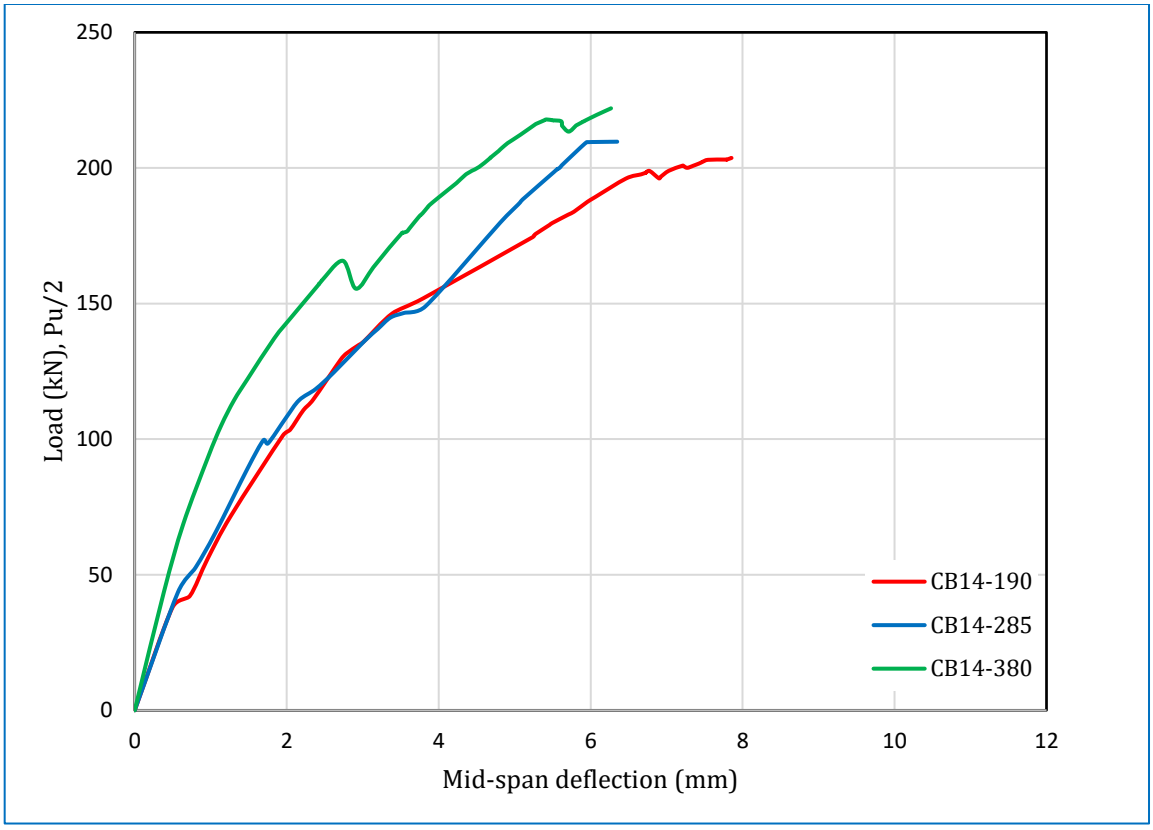

Figure 5-43: Load-mid span deflection response for the length of joint variation.

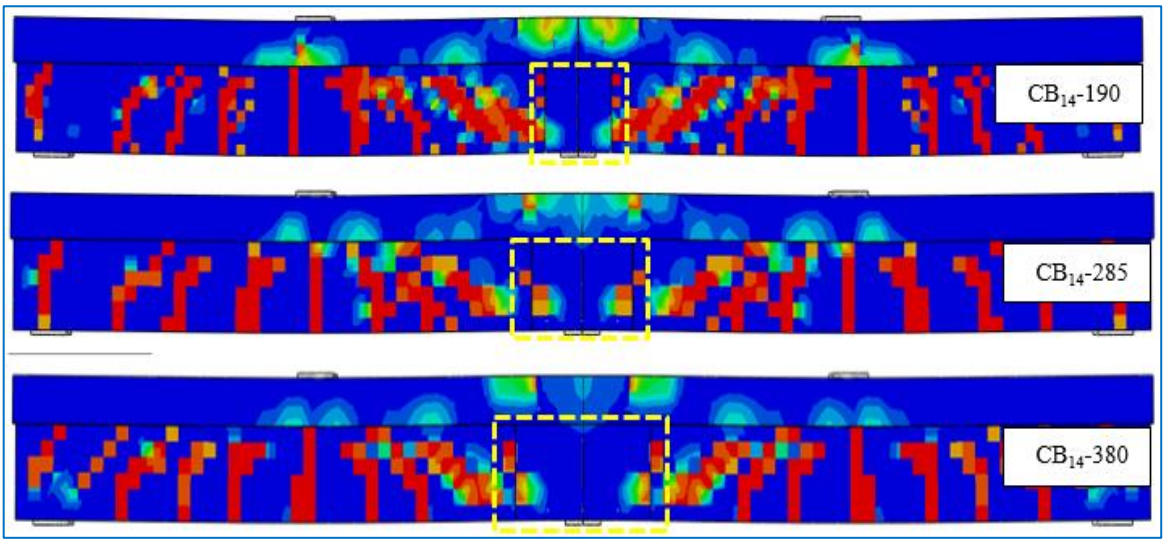

Figure 5-44: Failure mode and crack pattern of the spliced girder for the length of joint variation.

5-7-2 Number of shear key

The continuous girder had a joint at the interior support was reached to failure stage due to shear flexure failure as observed in the girder CB_{14} and CB_{17} (i.e., flat and one shear key joint). So, the two-shear key of UHPC in the joint was studied to understand the effect of the shear key in the joint.

From the analysis results, the use of two shear keys did not have a high effect on the general behavior of spliced girder in spite of slightly increasing the ultimate load about 1.9%. This result was observed because the girder was exposed to shear-flexural failure and that have less effected by the shear key as compared with direct shear failure, as clarified in Figure 5-45 and 5-46 .

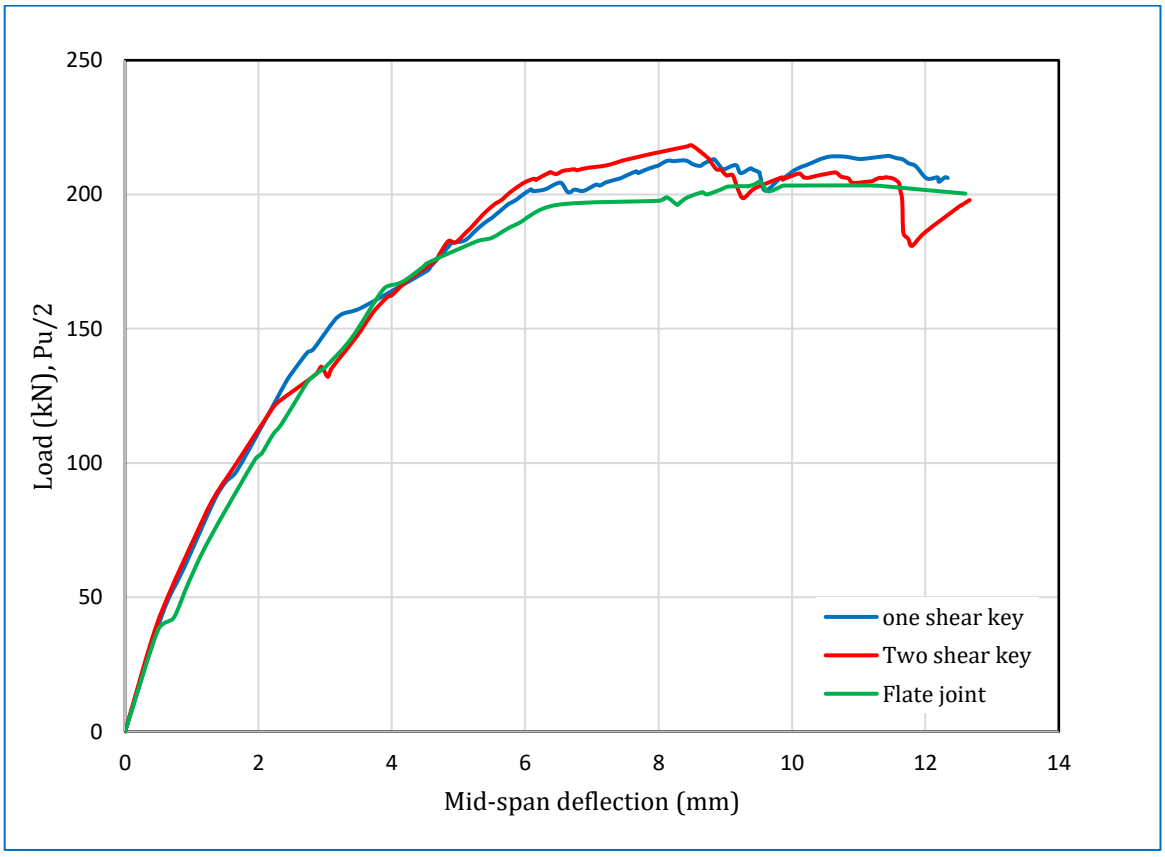

Figure 5-45: The load-mid span deflection response for shear key variation.

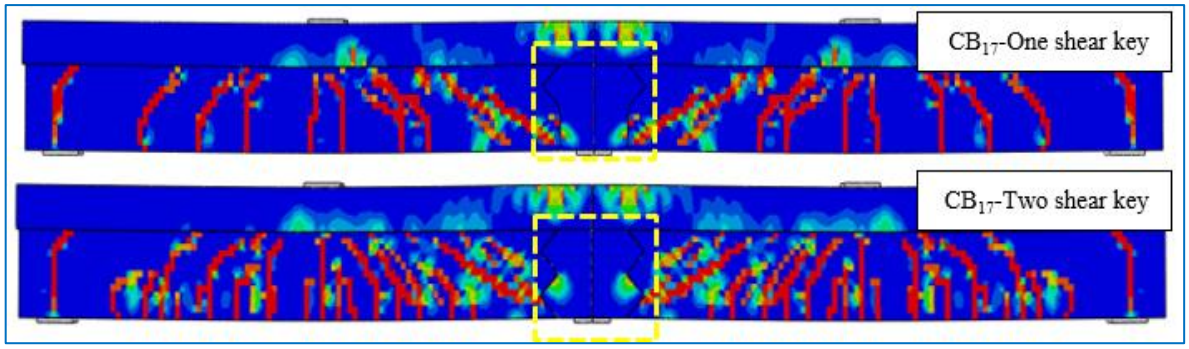

Figure 5-46: Failure mode and crack pattern of the spliced girder for shear key variation.

5-7-3 Number of interior supports

The maximum shear stress was applied to the interior support of the continuous girder. Two interior supports on the both side of the joint were used in the FE study to decreased the shear stress through this region. The ultimate load was increased by about 13% when used two interior supports. The stiffness of girder was increased in overall behavior of girder as clarified in Figure 5-47. The mode of failure was remains as shear failure, but the cracks were fared out from the UHPC joint as shown in Figure 5-48.

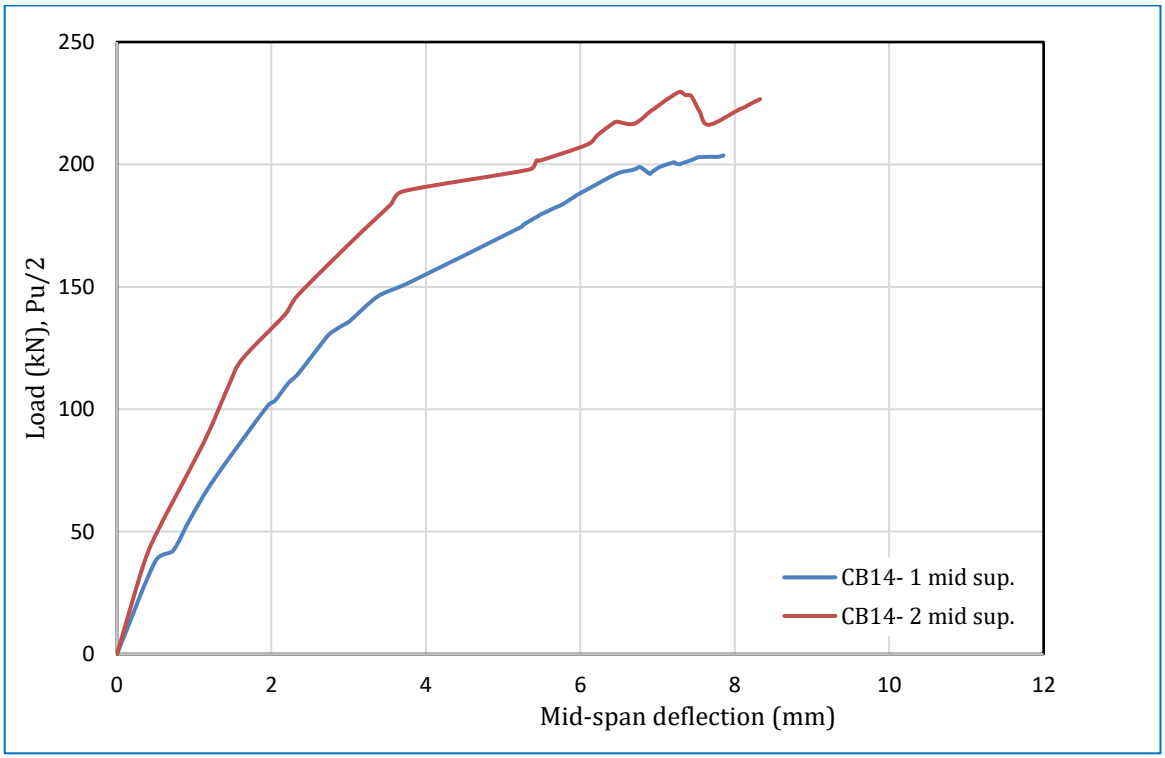

Figure 5-47: The load-mid span deflection response for type of interior support variation.

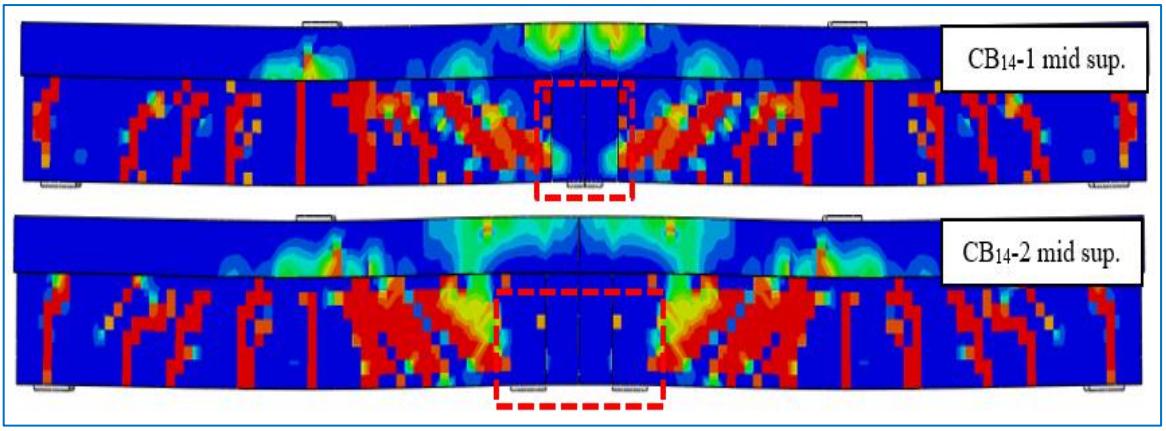

Figure 5-48: Failure mode and crack pattern of the spliced girder for interior support variation.

5-7-4 Spacing of shear reinforcement

Increasing the shear reinforcement led to an increase in the shear capacity of the girder. Thus, decreasing the spacing of stirrups from 100 mm to 50 and 75 mm was used in FE study to treat the shear failure of spliced girder. From the analysis result, the stiffness of girder was improved with reducing the spacing of stirrups, as shown in Figure 5-49. The ultimate load of girder was increased by about 9% and 6.5 % when decreased the spacing for 50 and 75 mm respectively. Figure 5-50 showed the crack pattern for spacing variation and clarified that the shear crack in the mid support region were become less than the state of girder had 100 mm spacing of stirrups.

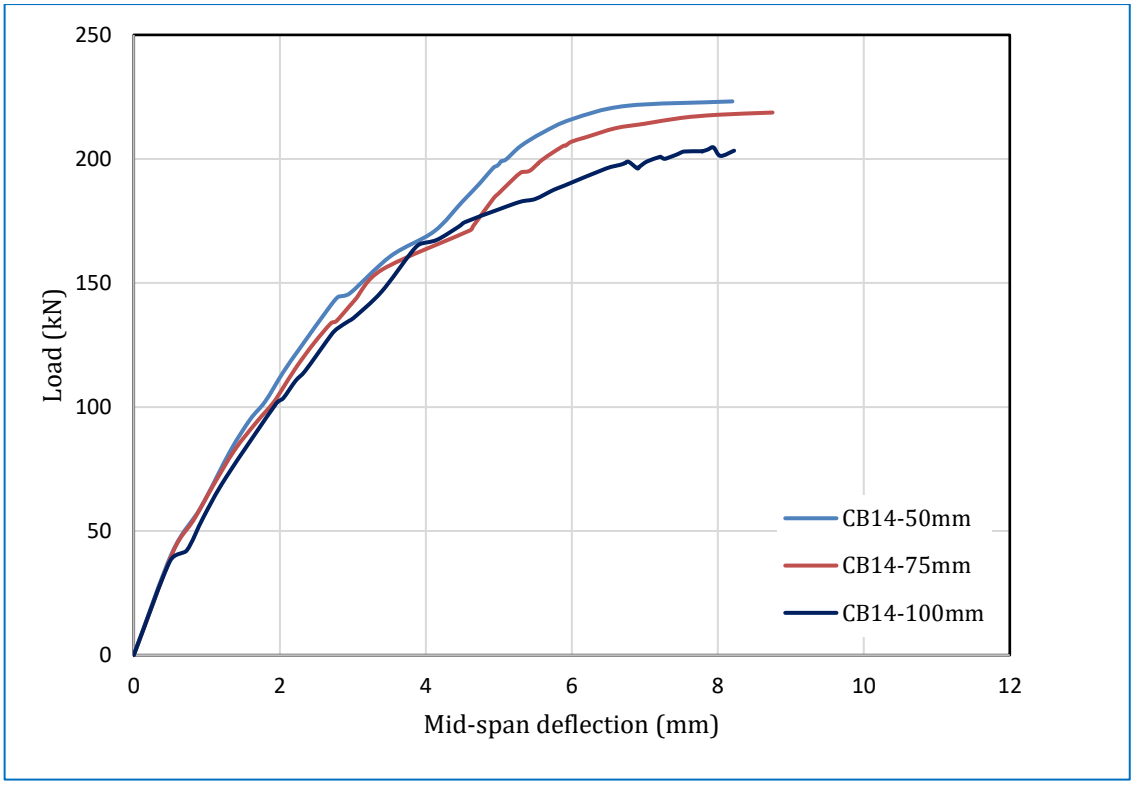

Figure 5-49: The load-mid span deflection response for shear reinforcement spacing variation.

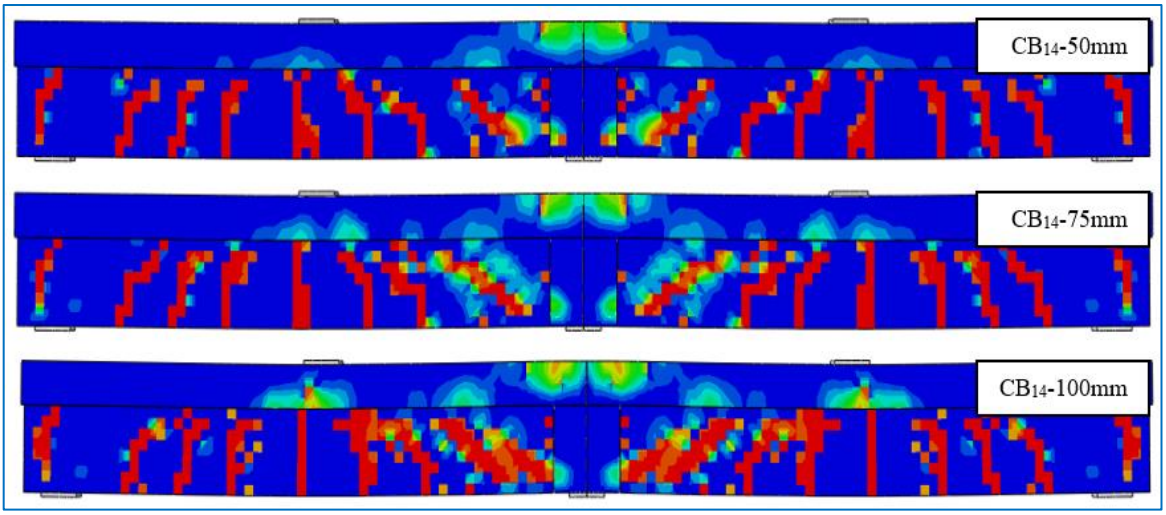

Figure 5-50: Failure mode and crack pattern of the spliced girder for shear reinforcement spacing variation.

Chapter Six

Conclusions and Recommendations for Future Research

6-1 Introduction

An experimental and numerical study has been performed to investigate the structural behavior of reinforced hybrid concrete spliced deck girders under effect of static and cyclic loads. The conclusions which can be drawn from the experimental and numerical outcomes of this study as well as some recommendations and suggestions for future works, are illustrated below.

6-2 Conclusions of Experimental Results

Several points can be concluded from the experimental study of considered hybrid spliced deck girders under the effect of static and cyclic loads.

6-2-1 Conclusions of Simply Supported Girders

The following points are essential and optimized from the test data of this group.

1- The exposed aggregate surface preparation system was very suitable to use in congested dowel reinforcement joints. This system gives a good bond strength of the interface between the precast segment and UHPC.

2- UHPC showed a high property with V_f=2% to resist the bending moment and shear stress. The results of the tested girder show that the UHPC joint exceeded the applied stresses without failure, except some of the hairline cracks do not cause the failure of the joint. The presence of deformations out

3- of the joints toward the supports refers to the success of the joint in transporting the stresses between the precast segment.

4- The concrete splitting at the joint does not happen at any girder due to enough splice length (15 d_b) with 90^o hooked encouragement of reinforcement in the UHPC joint with hook encouragement under both static and cyclic load.

5- All simply supported girders' failure mode is controlled as flexural failure (tension failure) except the girder with hybridization of reinforcement failed by shear-flexural mode. The high activity of UHPC joints and adequate shear strength of the girder caused this.

6- The full depth of the joint showed more overall stiffness and ultimate load than the partial depth joint because good bond for both cases and the presence of horizontal and vertical joints in the second case.

7- Replacement of 50% of steel reinforcement by CFRP bar leads to an increase in the ultimate load of the spliced girder by about 5% compared with the control specimen. But there was no improvement in the serviceability requirement, stiffness, ductility, and energy absorption.

8- The presence of a shear key improves the ultimate load by about (1.5-5.8)% without a change in the failure mode. This is a little significant for the shear key due to the good performance of the joint and bond with the precast segment.

9- Adding reinforcement in the joint as dowel action causing improvement in ultimate load by about 4.1% with remaining same behavior and mode of failure.

10- Cyclic (Repeated) load is gives no significant effect on the general behavior of spliced girder due to few cycles in one direction (compression only) and the high performance of joints and deck.

11- The presence of UHPC in the joint led to the crack width of all girders did not override the maximum limit in the service load stage (ACI-318, 2019).

12- The stiffness of the girders gives a simple increase in the spliced girder due to the presence of UHPC in the joint, except the girder has hybridization in the reinforcement by 50% CFRP bar, which gives a reduction in the stiffness about 35.5% less than the control girder.

13- The ductility of all girders with full steel reinforcement showes a fully ductile response. In contrast, the girder has a hybridization of reinforcement located in the zone of restricted ductile response.

14- From the results of the ultimate load, a reduction factor can be used when estimating the capacity of simply supported spliced girders by about (3-24.1)% for the NSC joint and (2.4-7.7)% for the UHPC joint.

6-2-2 Conclusions of continuous girder support

The following points are important and optimized from the test data of this group.

1- Splice joint at interior support is exposed to maximum moment and shear, so cracks occurred in the joint and changed the failure mode to shear failure and separation at the web and flange. The Splice joint in the inflection point was given very high stiffness without significant cracks at the interface due to high properties of UHPC. **Thus, in the case of a design spliced continuous girder is preferable to execute the splice joint at the inflection point.**

2- Replacement 50% of steel reinforcement by CFRP bar at the splice region increased the ultimate load of spliced girder by about 1.9% compared with the control girder.

3- The presence of the shear key at spliced region led to good performance in the ultimate load for the interior support specimen. In contrast, the splice joint at the inflection point did not optimize the advantage of the addition shear key.
4- Cyclic (Repeated) load is gives no significant effect on the general behavior of spliced girder due to the high performance of UHPC at spliced joints and deck.
5- The crack width of the continuous girder was close to each other for all the girders in the service load stage.
6- Stiffness was increased by about 4% for the girder with the joint in the interior support, and 11 % for the girder had splice joints at the inflection point, with a slight increase when the presence of the shear key.
7- Ductility of a continuous girder is more than the ductility of simply supported girder by about 2.3%, whereas the control girder is described as a fully ductile response. In comparison, the spliced girders are located in the zone of restricted ductile response.
8- From the results of ultimate load, a reduction factor can be used when estimated the capacity of continuous spliced girders by about (33-36.1)% for the NSC splice joint, (24.8)% for the SFC joint, and (4.4-17.2)% for UHPC splice joint.

6-3 Conclusions of the Numerical Results

Several points can be concluded from the FE study of hybrid spliced deck girder under the effect of static and cyclic load with different parameters.

6-3-1 Conclusions of simply supported girders

1- The developed model in FEM by Abaqus computer program provided good simulation depending on the comparison with experimental results of load-deflection response, ultimate load, cracking pattern, and mode of failure. Where, the average percentage of difference between the experimental and numerical results were about 2.7% for the ultimate load.
2- For the reversed cyclic load, the ultimate load was reduced by about 33 % and 28 % for the control girder in monotonic and repeated loading, respectively. Meanwhile, the ultimate load in the spliced girder was reduced by about 34 % and 27 %for monotonic and repeated loading, respectively. It was not changing the mode of failure or cause debonding in the joint.
3- Reducing of deck thickness from 100 mm to to 75mm with same depth section had no significant effect on the overall behavior, while a thickness 50 mm resulting a reduction in ultimate load about 64 % with separation in the joints.
4- The type of preparation of interface surface had no significant influence on the ultimate load, deflection, and the mode of failure. This result was provided due to the high bond performance of UHPC.
5- The reinforcement ratio had high effect on the behavior of spliced girder. The ultimate load decreased to 55% when reduced the ratio to half with separation in the joint. While it increased by about 82% when doubled, the ratio with the remaining flexural failure was controlled.

6-3-2 Conclusions of continuous girders

1- The developed model in FEM by Abaqus computer program provided good simulation depending on the comparison with experimental results of load-

deflection response, ultimate load, cracking pattern, and mode of failure. Where, the average percentage of difference between the experimental and numerical results were about 3 % for the ultimate load.

2- The length of the joint 285 mm (1.5 L_j) was given some of increasing in the stiffness of the girders with slight improvement in the ultimate load, but no changed in the shear failure. The length of the joint 380 mm (2 L_j) increased the stiffness of the girder and the ultimate load by about 14% of the girder with original length of joint. Also, the mode of failure for the girder has the length of joint 380 mm, joint that shows less shear crack compared with the flexural cracks.
3- The use of two shear keys did not have a high effect on the general behavior of spliced girder in spite of slightly increasing the ultimate load about 1.9% with same mode of failure.
4- The ultimate load was increased by about 13% when used two interior supports. The stiffness of girder was increased in overall behavior of girder with remains the mode of failure as shear failure.
5- The ultimate load of girder was increased by about 9% and 6.5 % when decreased the spacing for 50 and 75 mm respectively. When reducing the spacing of stirrups, the shear crack in the mid support region were become less than the state of girder had 100 mm spacing of stirrups.

6-4 Recommendations and Suggestions for Future Researches

In the spliced girder, many studies may be investigated to reached the suitable method and parameters to performed the spliced girder according to structural performance, cost, and time of construction.

1- Study the effect of different type of surface preparation system on different type of concrete used in the joint to connected the precast units.

2- Utilizing the CFRP bar to increase the flexural capacity, also using a laminate to enhance the shear strength and increase the bond mechanism of the longitudinal CFRP bars.
3- Study different splice lengths of reinforcement bars to investigate the length of the UHPC joint to obtain the optimal length to achieve good structural response.
4- Study the performance of transforming the multi-simple span to a continuous span with different parameters to connect the segment and strengthen the spliced region.
5- Study the horizontal curve reinforced concrete spliced girder under the effect of monotonic and cyclic load.

List of Content

Chapter One

Chapter Two

Chapter Three

Chapter Four

Chapter Five

List of Tables

List of Figures

List of Plates

List of Plates

Abbreviations

AASHTO: American Association of State Highway and Transportation Officials
ACI: American Concrete Institute
ANSYS: Analysis System Program (package)
ASTM: American Society for Testing and Materials
ASTM: American Society for Testing and Materials
BFRP: Basalt Fiber Reinforced Polymer
BS: British Standards
C3D8R: 8 node brick elements, reduced integration
CC: Conventional Concrete
CDP: concrete damaged plasticity
CFRP: Carbon Fiber Reinforced Polymer
CIP: Cast-In-Place
EC: Expansive Concrete
EPS: Externally Prestressed Segmental
EXP.: Experimental
FEM: Finite Element Method
FRP: Fiber Reinforced Polymer
GFRP: Glass Fiber Reinforced Polymer
GPa: Giga Pascal (GN/m2)
HPM: High-Performance Mortar
HSC: High Strength Concrete
HSFRC: High Strength Fiber Reinforced Concrete
IQS: Iraqi Specification Standard
LRFD: Load Resisting Factor Design
LWC: Light Weight Concrete
MPa: Mega Pascal (N/mm^2)
NSC: Normal Strength Concrete
NSM: Near Surface Mounted
PCSB: Precast Concrete Segmental Bridge
PSC: Prestress Concrete
PTMS: Posttensioned Metal Straps
RC: Reinforced Concrete
RCL: Reverse cyclic load
RPC: Reactive Powder Concrete
S.P.: Superplasticizer
SFC: Steel Fiber Concrete
SFRC: Steel Fiber Reinforced Concrete
SSD: Saturated Surface Dry
T3D2: 2 nodes 3 D truss element
UHPC: Ultra High-Performance Concrete
UHSC: Ultra-High-Strength Concrete
W/b: Water to binder ratio

W/C: Water to Cement ratio
Notation
Af :Area of one FRP bar (mm2)
As :Area of steel (mm2)
db :Diameter of reinforcement bar (mm)
DI: Damage index
dt: Tension damage parameter
Ec :Modulus of elasticity of concrete (MPa)

Ef :Modulus of elasticity of steel fibers or CFRP bars (MPa)

Es :Modulus of elasticity of steel (MPa)
ET :Strain hardening modulus of elasticity of steel (MPa)
fcr: cracking stress of concrete (MPa)
fcu :Cube compressive strength of concrete (MPa)
fr :Flexural strength of concrete (modulus of rupture) (MPa)
ft :Ultimate uniaxial tensile strength of concrete (MPa)
fu :Ultimate strength of steel (MPa)
fy :Yield strength of steel (MPa)
K: Stiffness criteria
L :Total length of splice

ldh :Standard development length of 90º hook according to (ACI 318-19)
le: Effective length
Lj: length of joint
Mn :Nominal moment capacity (kN.m)
Ps: Service load (kN)
Pu :Ultimate load (kN)
$Pu_{EXP.}$:Ultimate load obtained from the experimental tests (kN)
$Pu_{FE.}$:Ultimate load obtained with finite element analysis(kN)
U :Displacement
u, v, w :Displacement components (in x, y, and z-direction)
Ux :Displacement in x-direction
Uy :Displacement in y-direction
Uz :Displacement in z-direction
Vf :Volume fraction of steel fibers

Vn :Nominal shear capacity (kN)
α : a coefficient relating to the deviation of the actual stress–strain curve of UHPC from the linear trend.
β : degradation parameter
β1 : Factor used to determine the stress block in ultimate
Δs :Service deflection (mm)
Δu :Ultimate deflection (mm)
Δy : yield deflection (mm)

ε :Concrete compressive strain (mm/mm)
εcu :Ultimate compression strain of concrete (mm/mm)
εo :Compressive strain at peak stress (mm/mm)
μ : Ductility index
ρ min. :Minimum steel reinforcement ratio
ρ: Steel reinforcement ratio
σ: Concrete compressive strength (MPa)
υ: Poisson's ratio
φ: Reduction factor
$f'c$: Cylinder compressive strength of concrete (MPa)
$\epsilon c1$:concrete strain at maximum compressive stress
ϵ_{cr} : cracking strain of concrete
ϵcu : ultimate strain of concrete
ϵ_t :tension strain

References

ACI Committee 440.1R-15. 2015. *Guide for the Design and Construction of Structural Concrete Reinforced with Firber-Reinforced Polymer (FRP) Bars (ACI440.1R-15)*. Vol. 22.

ACI, 318-19. 2019 . *318M-19: Building Code Requirements for Concrete and Commentary*. 628.

Ahmed, Ghafur H., and Omar Q. Aziz. 2019. "Shear Strength of Joints in Precast Posttensioned Segmental Bridges during 1959–2019, Review and Analysis." *Structures* 20(April):527–42. https://doi: 10.1016/j.istruc.2019.06.007

Ahmed, Ghafur H., and Omar Q. Aziz. 2020. "Stresses, Deformations and Damages of Various Joints in Precast Concrete Segmental Box Girder Bridges Subjected to Direct Shear Loading." *Engineering Structures* 206(May 2019):110151. doi: 10.1016/j.engstruct.2019.110151 .

Al-Shaarbaf I.A., Aziz A.H., Askar O. F. 2012. "Experimental Study on the Shear Transfer in Joints of Precast Segmental Bridge." *Journal of Engineering and Development* 16(4):88–106.

Al-Tameemi, Haider Ali Abdulhussein. 2015. "Analysis For Behavior Of Spliced R . C. Girders Strengthened With (CFRP) Laminates." *Ph.D Thesis,University of Babylon*.

AL-Khafaji, Ali Ghanim Abbas, Ali Hameed Nasser Al-Mamoori, and Abathar Majid Abd Aoun. 2018. "Improvement of Flexural Strength of Precast Concrete Spliced Girder Using Reactive Powder Concrete in Splice Region." *Structures* 14(2017):197–208. doi: 10.1016/j.istruc.2018.03.012.

Al-Khazragy, Faten Fadhil Saleem. 2016. “Effect of Tensile Reinforcement Lap Splices on the Behavior of Reinforced Reactive Powder Concrete Beams Under Repeated Loading.” Ph.D. thesis , University of Technology.

Al-Mamuree, A. H. 2008. “Analysis of Prestressed Concrete Girders with Field Splices.” Ph.D. Thesis, University of Baghdad.

Al-Quraishy, Qassim Ali Husain. 2011. “Experimental And Theoretical Investigation For Behavior Of Precast Concrete Girders With Connections.” Ph.D thesis , University of Baghdad.

Al-Quraishy, Q. A. H. 2012 . *Experimental and Theoretical Investigations for Behavior of Precast Concrete Girders With*. *18*(5), 621–638.

Al-Rousan, Rajai, Ayman Ababneh, and Mohammad Alhassan. 2020. “Hybrid CFRP-Steel for Enhancing the Flexural Behavior of Reinforced Concrete Beams.” *Journal of King Saud University - Engineering Sciences* (xxxx). doi: 10.1016/j.jksues.2020.06.004.

Al-Shaarbaf I.A., Aziz A.H., Askar O. F. 2012. “Experimental Study on the Shear Transfer in Joints of Precast Segmental Bridge.” *Journal of Engineering and Development* 16(4):88–106.

Al-Tameemi, Haider Ali Abdulhussein. 2015. “Analysis For Behavior Of Spliced R . C. Girders Strengthened With (CFRP) Laminates.” *Ph.D Thesis,University of Babylon*.

Algorafi, M. A., A. A. A. Ali, I. Othman, M. S. Jaafar, and M. P. Anwar. 2010. “Experimental Study of Externally Prestressed Segmental Beam under Torsion.” *Engineering Structures* 32(11):3528–38. doi: 10.1016/j.engstruct.2010.07.021.

Aljanabi, A. Y., and A. H. Hassoon. 2020. "Experimental Behavior of Continuous Hybrid Reinforced Concrete Spliced Girders." *IOP Conference Series: Materials Science and Engineering* 871(1). doi: 10.1088/1757-899X/871/1/012004.

Aly, Ragi, Brahim Benmokrane, and Usama Ebead. 2006. "Tensile Lap Splicing of Fiber-Reinforced Polymer Reinforcing Bars in Concrete." *ACI Structural Journal* 103(6):857–64.

Aoun, Abathar Majid Abd. 2018. "Comparative Study for Different Types of Reinforced Concrete Spliced Girders." M.Sc. thesis , Kerbala University.

Arafa, Ahmed, Ahmed Sabry Farghaly, Ehab A. Ahmed, and Brahim Benmokrane. 2016. "Laboratory Testing of GFRP-RC Panels with UHPFRC Joints of the Nipigon River Cable-Stayed Bridge in Northwest Ontario, Canada." *Journal of Bridge Engineering* 21(11):05016006. doi: 10.1061/(asce)be.1943-5592.0000943 .

ASTM A820M-04. 2004 . *Standard Specification for Steel Fibers for Fiber-Reinforced Concrete* (Vol. 70).

ASTM D7205M-06. 2011 . *Standard Test Method for Tensile Properties of Fiber Reinforced Polymer Matrix Composite Bars*. https://doi.org/10.1520/D7205

ASTM A615M-15. 2015 . *Standard Specification for Deformed and Plain Carbon-Steel Bars for Concrete Reinforcement* (Issue April). https://doi.org/10.1520/A0615

ASTM C1240-15. 2015 . *ASTM C 1240, "Standard Specification for Use of Silica Fume as a Mineral Admixture in Hydraulic-Cement Concrete, Mortar, and Grout," American Society for testing and materials, Philadelphia, united states, 2015*. https://doi.org/10.1520/C1240-15.2

ASTM C494-15. 2015 . *Standard Specification for Chemical Admixtures for Concrete* (Vol. 311, Issue 7002). https://doi.org/10.1136/bmj.311.7002.404

ASTM C1856. 2017. "Standard Practice for Fabricating and Testing Specimens of Ultra-High Performance Concrete." *ASTM International* i:4. https://doi: 10.1520/C1856

ASTM C1856. 2017 . Standard Practice for Fabricating and Testing Specimens of Ultra-High Performance Concrete. *ASTM International*, *i*, 4. https://doi.org/10.1520/C1856

Azizinamini, A., Darwin, D., Eligehausen, R., Pavel, R., & Ghosh, S. K. 1999 . *Proposed Modifications to ACI 318-95 Tension Development and Lap Splice for High-Strength Concrete*. *June 2018*.

Basim, Shahnaz, Farzad Hejazi, and Raizal Saifulnaz Bin Muhammad Rashid. 2019. "Embedded Carbon Fiber-Reinforced Polymer Rod in Reinforced Concrete Frame and Ultra-High-Performance Concrete Frame Joints." *International Journal of Advanced Structural Engineering* 11(2016):35–51. doi: 10.1007/s40091-019-00253-7.

Brenkus, N. R., D. J. Wagner, and H. R. Hamilton. 2016a. "Experimental Evaluation of Flexural Static and Fatigue Strength of an Innovative Splice for Prestressed Precast Concrete Girders." *Journal of Bridge Engineering* 21(6):1–10. doi: 10.1061/(ASCE)BE.1943-5592.0000879.

Brenkus, N. R., D. J. Wagner, and H. R. Hamilton. 2016b. "Experimental Evaluation of Shear Strength of an Innovative Splice for Prestressed Precast Concrete Girders." *Journal of Bridge Engineering* 21(6):1–7. doi: 10.1061/(ASCE)BE.1943-5592.0000880.

BRENKUS, NATASSIA R. 2013. "Long Spans With Transportable Precast

Prestressed Girders."

BS EN 1992-1-1. 2004 . Eurocode 2: Design of concrete structures - Part 1-1 : General rules and rules for buildings. In *British Standards Institution* (Vol. 1, Issue 2004, p. 230).

Buyukozturk, Oral, Mourad M. Bakhoum, Student Member, and S. Michael Beattie. 1991. "Shear Behavior Of Joints In Precast Concrete Segmental Bridges." *Journal of Structural Engineering* 116(12):3380–3401.

Cao, Qi, Jianpu Zhou, Rongxiong Gao, and Zhongguo John Ma. 2017. "Flexural Behavior of Expansive Concrete Beams Reinforced with Hybrid CFRP Enclosure and Steel Rebars." *Construction and Building Materials* 150:501–10. doi: 10.1016/j.conbuildmat.2017.05.222.

Casanova, Maximilian, Christopher Clauson, Arya Ebrahimpour, and Mustafa Mashal. 2019. "High-Early Strength Concrete with Polypropylene Fibers as Cost-Effective Alternative for Field-Cast Connections of Precast Elements in Accelerated Bridge Construction." *Journal of Materials in Civil Engineering* 31(11):04019266. doi: 10.1061/(asce)mt.1943-5533.0002927.

Choi, Jinwoong, Sun Kyu Park, Hyeong Yeol Kim, and Sungnam Hong. 2015. "Behavior of High-Performance Mortar and Concrete Connections in Precast Concrete Elements: Experimental Investigation under Static and Cyclic Loadings." *Engineering Structures* 100:633–44. doi: 10.1016/j.engstruct.2015.06.009.

Clark, John H., John H. Allen, Gerald H. Anderson, Craig A. Ballinger, James M. Barker, Ostap Bender, T. Ivan Campbell, John L. Carrato, Gurdial Chadha, W. M. Davidge, William H. Epp, Noel J. Everard, Anthony L. Felder, Om P. Dixit, Ibrahim A. Ghais, Joseph D. Gliken, C. Stewart Gloyd, Nabil F. Grace, Hidayat N. Grouni, C. Donald Hamilton, Allan

C. Harwood, Thomas T. C. Hsu, Ray W. James, Richard G. Janecek, Richard A. Lawrie, James R. Libby, Clellon L. Loveall, John C. Payne, Paul N. Roschke, M. Saiid Saiidi, John J. Schemmel, A. C. Scordelis, Steven L. Stroh, James C. Tai, Marius B. Weschsler, and J. Jim Zhao. 1995. "Analysis and Design of Reinforced Concrete Bridge Structures Reported by ACI-ASCE Committee 343." *Design* 95(Reapproved):1–158.

Dagenais, Marc-André, and Bruno Massicotte. 2017. "Cyclic Behavior of Lap Splices Strengthened with Ultrahigh Performance Fiber-Reinforced Concrete." *Journal of Structural Engineering* 143(2):04016163. doi: 10.1061/(asce)st.1943-541x.0001652.

Dugat, J., N. Roux, and G. Bernier. 1996. "Mechanical Properties of Reactive Powder Concretes." *Materials and Structures/Materiaux et Constructions* 29(4):233–40. doi: 10.1007/bf02485945.

Eren, Ö., & Marar, K. 2010 . Effect of steel fibers on plastic shrinkage cracking of normal and high strength concretes. *Materials Research*, *13*(2), 135–141. https://doi.org/10.1590/S1516-14392010000200004

Fowler, John R., and Bob Stofko. 2007. "Precast Options for Bridge Superstructure Design." *TAC/ATC 2007 - 2007 Annual Conference and Exhibition of the Transportation Association of Canada: Transportation - An Economic Enabler* 1–18.

G. abtan, T. jaber. 2016. "Behavior of Hybrid Reinforced Concrete Beams Combining Reactive Powder Concrete and Varying Ytpes of Lightweight Concrete." *Journal of Engineering and Sustainable Development* 20(2):204–23.

Graybeal, B. A. 2007 . *Compressive Behavior of Ultra-High-Performance Fiber-Reinforced Concrete*. *146*(104).

Graybeal, B. A., & Russel, H. G. 2013 . *Ultra-High Performance Concrete: A State-of-the-Art Report for the Bridge Community. Publication N.º FHWA-HRT-13-060. June*, 176.

Graybeal. 2014. *Design and Construction of Field-Cast UHPC Connections, FHWA-HRT-14-084*.

Graybeal, Benjamin A. 2014. "Ultra-High-Performance Concrete Connections for Precast Concrete Bridge Decks." *PCI Journal* 59(4):48–62. doi: 10.15554/pcij.09012014.48.62.

Graybeal, Benjamin A., Igor De la Varga, and Zachary B. Haber. 2017. *Bond of Field-Cast Grouts to Precast Concrete Elements*.

Graybeal, Benjamin, and Zachary Haber. 2018a. "Ultra-High Performance Concrete for Bridge Deck Overlays (FHWA-HRT-17-097)." 16.

Graybeal, Benjamin, and Zachary Haber. 2018b. "Ultra-High Performance Concrete for Bridge Deck Overlays (FHWA-HRT-17-097)." (April):16.

Graybeal, Benjamin, Eugen Brühwiler, Byung-Suk Kim, François Toutlemonde, Yen Lei Voo, and Arash Zaghi. 2020. "International Perspective on UHPC in Bridge Engineering." *Journal of Bridge Engineering* 25(11):04020094. doi: 10.1061/(asce)be.1943-5592.0001630.

Haber, Zachary B., and Benjamin A. Graybeal. 2018. "Lap-Spliced Rebar Connections with UHPC Closures." *Journal of Bridge Engineering* 23(6):04018028. doi: 10.1061/(asce)be.1943-5592.0001239.

Hasgul, U., Turker, K., Birol, T., & Yavas, A. 2018 . Flexural behavior of ultra-high-performance fiber reinforced concrete beams with low and high reinforcement ratios. *Structural Concrete*, *19*(6), 1577–1590. https://doi.org/10.1002/suco.201700089

Hassoon, Alaa, and Ammar Aljanabi. 2020. "Improvement of Flexural Capacity of Hybrid, Reinforced Concrete Spliced Girders Using Steel

Fiber Concrete in Splice Region and near Surface Mounted Carbon Fiber-Reinforced Polymer Bars: Experimental Investigations." *Innovative Infrastructure Solutions* 5(3):1–11. doi: 10.1007/s41062-020-00315-w.

Hassoon, Alaa Hadi Hameed. 2021. "Experimental and Numerical Investigation for Structural Behavior of Hybrid Reinforced Concrete Spliced Beams." Ph.D. thesis , University of Babylon.

Helal, Yasser, Reyes Garcia, Kypros Pilakoutas, Maurizio Guadagnini, and Iman Hajirasouliha. 2016. "Strengthening of Short Splices in RC Beams Using Post-Tensioned Metal Straps." *Materials and Structures/Materiaux et Constructions* 49(1–2):133–47. doi: 10.1617/s11527-014-0481-6.

Huang, Z., and X. L. Liu. 2006. "Modified Skew Bending Model for Segmental Bridge with Unbonded Tendons." *Journal of Bridge Engineering* 11(1):59–63. doi: 10.1061/(ASCE)1084-0702(2006)11:1(59).

Hussein, Husam H., Kenneth K. Walsh, Shad M. Sargand, and Eric P. Steinberg. 2016. "Interfacial Properties of Ultrahigh-Performance Concrete and High-Strength Concrete Bridge Connections." *Journal of Materials in Civil Engineering* 28(5): 04015208.

Hung, Chung-Chan, Sherif El-Tawil, and Shih-Ho Chao. 2021. "A Review of Developments and Challenges for UHPC in Structural Engineering: Behavior, Analysis, and Design." *Journal of Structural Engineering* 147(9):03121001. doi: 10.1061/(asce)st.1943-541x.0003073.

Ismael, Murtada Ameer, Jasim Mahmood Al-Kafaji, and Hisham Mohammed Al-Hassani. 2015. "Flexural Behavior of Hybrid Tee Beams (Containing Reactive Powder Concrete and Normal Strength Concrete)." *Journal of Engineering and Development* 19(march):123–40.

Janssen, H. Hubert, and Leo Spaans. 1994. “Bulb-Tee Girders Used n Highland View Bridge.” *PCI JOURNAL* 34–49.

Jiang, Haibo, Rongbin Wei, Zhongguo John Ma, Yuhong Li, and Yuan Jing. 2016. “Shear Strength of Steel Fiber-Reinforced Concrete Dry Joints in Precast Segmental Bridges.” *Journal of Bridge Engineering* 21(11):1–13. doi: 10.1061/(ASCE)BE.1943-5592.0000968.

Jiang, Haibo, Yuhong Li, Airong Liu, Zhongguo John Ma, Li Chen, and Yuanhang Chen. 2018. “Shear Behavior of Precast Concrete Segmental Beams with External Tendons.” *Journal of Bridge Engineering* 23(8). doi: 10.1061/(ASCE)BE.1943-5592.0001249.

Jiqiu, Yuan, Benjamin A. Graybeal, and Kevin Zmetra. 2018. “Adjacent Box Beam Connections: Performance and Optimization.” (February).

Kadhim, M. M. A., Saleh, A. R., Cunningham, L. S., and Semendary, A. A. 2021 . Numerical investigation of non-shear-reinforced UHPC hybrid flat slabs subject to punching shear. *Engineering Structures*, *241*(May). https://doi.org/10.1016/j.engstruct.2021.112444

Kadhim, Majid M.A., Akram Jawdhari, and Abheetha Peiris. 2021. “Development of Hybrid UHPC-NC Beams: A Numerical Study.” *Engineering Structures* 233(November 2020): 111893. https://doi.org/10.1016/j.engstruct.2021.111893.

Kim, Jaeheung, Wonseok Chung, and Jang-ho Jay Kim. 2008. “Experimental Investigation on Behavior of a Spliced PSC Girder with Precast Box Segments.” 30(11):3295–3304. doi: 10.1016/j.engstruct.2008.04.029.

Le, Tan D., Thong M. Pham, Hong Hao, and Yifei Hao. 2018. “Flexural Behaviour of Precast Segmental Concrete Beams Internally Prestressed with Unbonded CFRP Tendons under Four-Point Loading.” *Engineering Structures* 168(April):371–83. doi: 10.1016/j.engstruct.2018.04.068.

Li, Guoping, Donghui Yang, and Yu Lei. 2013. “Combined Shear and Bending Behavior of Joints in Precast Concrete Segmental Beams with External Tendons.” *Journal of Bridge Engineering* 18(10):1042–52. doi: 10.1061/(ASCE)BE.1943-5592.0000453.

Liu, Tongxu, Zhen Wang, Jian Guo, and Jingquan Wang. 2019. “Shear Strength of Dry Joints in Precast UHPC Segmental Bridges: Experimental and Theoretical Research.” *Journal of Bridge Engineering* 24(1). doi: 10.1061/(ASCE)BE.1943-5592.0001323.

Marinela Bărbuţă, Constantin Gavriloaia and Ionuţ Ovidiu Toma. 2009. “Flexural Behavior of Short Reinforced Concrete Hybrid Beams – Experiment and Numerical Simulations.” *Journal of Intersection* 6(6):67–76.

Marzoq, Zahraa Hadi. 2020. “Combined Bending and Torsional Moments Effect on Hybrid Reactive Powder Concrete T-Beams.” M.Sc. thesis , University of Al- Qadisiyah.

Maya, L. F., & Graybeal, B. 2017 . Experimental study of strand splice connections in UHPC for continuous precast prestressed concrete bridges. *Engineering Structures*, *133*, 81–90. https://doi.org/10.1016/j.engstruct.2016.12.018

Michaud, Decebal, Amir Fam, and Marc André Dagenais. 2021. “Development Length of Sand-Coated GFRP Bars Embedded in Ultra-High Performance Concrete with Very Small Cover.” *Construction and Building Materials* 270(xxxx):121384. doi: 10.1016/j.conbuildmat.2020.121384.

Mohammed, Mohammed Hashim. 2013. “Flexural Behavior Of Hybrid Beams Containing Reactive Powder Concrete And Conventional Concrete.” Ph.D thesis , Al-Mustansiriya University.

Nicholls, jerome j., and Chuck Prussack. 1997. “Innovative Design and Erection Methods Solve Construction of Rock Cut Bridge.” *PCI JOURNAL* 42(4):42–55.

Park, Jongho, Jinwoong Choi, Yongjoon Jang, Sun Kyu Park, and Sungnam Hong. 2017. “An Experimental and Analytical Study on the Deflection Behavior of Precast Concrete Beams with Joints.” *Applied Sciences (Switzerland)* 7(11). doi: 10.3390/app7111198.

Peng, Keke, and Banfu Yan. 2021. “Experimental Study of the Flexural Behaviour of Ultra-High-Performance Concrete Beam with Wet Joint.” *Magazine of Concrete Research* 1–11. doi: 10.1680/jmacr.20.00078.

Qi, Jianan, Jingquan Wang, Zhongwen Zhang, Wenchao Li, and Yuqing Hu. 2020. “Flexural Behavior of an Innovative Dovetail Ultra-High Performance Concrete Joint Using Steel Wire Mesh Interface Treatment in Composite Bridges.” *Advances in Structural Engineering* 23(6):1142–53. doi: 10.1177/1369433219891531.

Qin, Renyuan, Ao Zhou, and Denvid Lau. 2017. “Effect of Reinforcement Ratio on the Flexural Performance of Hybrid FRP Reinforced Concrete Beams.” *Composites Part B: Engineering* 108:200–209. doi: 10.1016/j.compositesb.2016.09.054.

Qiu, M., Shao, X., Wille, K., Yan, B., & Wu, J. 2020 . Experimental Investigation on Flexural Behavior of Reinforced Ultra High Performance Concrete Low-Profile T-Beams. *International Journal of Concrete Structures and Materials*, *14*(1). https://doi.org/10.1186/s40069-019-0380-x

Qiu, M., Shao, X., Yan, B., Zhu, Y., & Chen, Y. 2022 . Flexural behavior of UHPC joints for precast UHPC deck slabs. *Engineering Structures*, *251*(PA), 113422. https://doi.org/10.1016/j.engstruct.2021.113422

Ramos, G., J. R. Casas, and A. Alarcón. 2004. “Repair and Strengthening of Segmental Bridges Using Carbon Fibers.” *Engineering Structures* 26(5):609–18. doi: 10.1016/j.engstruct.2003.12.008.

Russell, Henry G. 2011. “Adjacent Precast Concrete Box-Beam Bridges: State of the Practice.” *PCI Journal* 56(1):75–91. doi: 10.15554/pcij.01012011.75.91.

Saghafi, M. H., Shariatmadar, H., & Kheyroddin, A. 2019 . Seismic Behavior of High-Performance Fiber-Reinforced Cement Composites Beam-Column Connection with High Damage Tolerance. *International Journal of Concrete Structures and Materials*, *13*(1). https://doi.org/10.1186/s40069-019-0334-3

Saibabu, S., V. Srinivas, Saptarshi Sasmal, N. Lakshmanan, and Nagesh R. Iyer. 2013. “Performance Evaluation of Dry and Epoxy Jointed Segmental Prestressed Box Girders under Monotonic and Cyclic Loading.” *Construction and Building Materials* 38:931–40. doi: 10.1016/j.conbuildmat.2012.09.068.

Shafieifar, M., Farzad, M., & Azizinamini, A. 2017 . Experimental and numerical study on mechanical properties of Ultra High Performance Concrete (UHPC). *Construction and Building Materials*, *156*, 402–411. https://doi.org/10.1016/j.conbuildmat.2017.08.170

Shamass, Rabee, Xiangming Zhou, and Zongyi Wu. 2017. “Numerical Analysis of Shear-Off Failure of Keyed Epoxied Joints in Precast Concrete Segmental Bridges.” *Journal of Bridge Engineering* 22(1): 04016108.

SIMULIA. 2014. “Abaqus Theory Manual.” *Abaqus 6.13 documentation* (Dassault Systemes Simulia Corp., Providence, RI, USA.).

Siva Chidambaram, R., & Agarwal, P. 2015 . Seismic behavior of hybrid

fiber reinforced cementitious composite beam-column joints. *Materials and Design*, *86*, 771–781. https://doi.org/10.1016/j.matdes.2015.07.164

Song, X., Huang, Z., Shen, J., & Yao, Y. 2020 . Experimental study on cyclic behavior of hybrid CFRP grids-steel shear walls. *Structures*, *28*(August), 496–511. https://doi.org/10.1016/j.istruc.2020.08.063

Song, Shoutan, Guan Wang, Xinzhe Min, Ning Duan, and Yongming Tu. 2021. "Experimental Study on Cyclic Response of Concrete Frames Reinforced by Steel-CFRP Hybrid Reinforcement." *Journal of Building Engineering* 34:101937. doi: 10.1016/j.jobe.2020.101937.

Sun, Mingde, Ri Gao, Aili Li, and Yongjing Wang. 2016. "Bond of Reinforcement in Reactive Powder Concrete: Experimental Study." *ECCOMAS Congress 2016 - Proceedings of the 7th European Congress on Computational Methods in Applied Sciences and Engineering* 4(June):7771–78. doi: 10.7712/100016.2373.5785.

Tadros, Maher K., Amgad Girgis, and Robert Pearce. 2003. "SPLICED I-GIRDER CONCRETE BRIDGE SYSTEM." *Department of Civil Engineering University of Nebraska-Lincoln (UNL).Report No. SPR-PL-1 (038) P535* 7(2).

Takemura H, Kawashima K (1997) Effect of loading hysteresis on ductility capacity of reinforced concrete bridge piers. J Cent South Univ 43A:849

Tayeh, Bassam A., B. H. Abu Bakar, M. A. Megat Johari, and Yen Lei Voo. 2012. "Mechanical and Permeability Properties of the Interface between Normal Concrete Substrate and Ultra High Performance Fiber Concrete Overlay." *Construction and Building Materials* 36: 538–48. http://dx.doi.org/10.1016/j.conbuildmat.2012.06.013.

Tayeh, Bassam A., B. H. Abu Bakar, and M. A. Megat Johari. 2013. "Characterization of the Interfacial Bond between Old Concrete

Substrate and Ultra High Performance Fiber Concrete Repair Composite." *Materials and Structures/Materiaux et Constructions* 46(5):743–53. doi: 10.1617/s11527-012-9931-1.

Tekle, Biruk Hailu, Amar Khennane, and Obada Kayali. 2017. "Bond of Spliced GFRP Reinforcement Bars in Alkali Activated Cement Concrete." *Engineering Structures* 147:740–51. doi: 10.1016/j.engstruct.2017.06.040.

Tighiouart, Brahim, Brahim Benmokrane, and Phalguni Mukhopadhyaya. 1999. "Bond Strength of Glass FRP Rebar Splices in Beams under Static Loading." *Construction and Building Materials* 13(7):383–92. doi: 10.1016/S0950-0618(99)00037-9.

Verger-Leboeuf, Sébastien, Jean Philippe Charron, and Bruno Massicotte. 2017. "Design and Behavior of UHPFRC Field-Cast Transverse Connections between Precast Bridge Deck Elements." *Journal of Bridge Engineering* 22(7):1–11. doi: 10.1061/(ASCE)BE.1943-5592.0001064.

Villemure, & Ventura. 1995 . Damage Indices for Reinforced Concrete Frames: Evaluation And Correlation. *Department of Civil Engineering*, *Master of*(July), 196.

Wang, Huanzi. 2009. "An Analytical Study of Bond Strength Associated with Splitting of Concrete Cover." *Engineering Structures* 31(4):968–75. doi: 10.1016/j.engstruct.2008.12.008.

Wang, T., & Hsu, T. T. C. 2001 . Nonlinear finite element analysis of concrete structures using new constitutive models. In *Computers and Structures* (Vol. 79, Issue 32, pp. 2781–2791). https://doi.org/10.1016/S0045-7949(01)00157-2

Williams S.C. 2015. "Behavior of The Cast-In-Place Splice Region of Spliced I-Girder Bridges." Ph.D. Thesis, University of Texas, Austen, American

United States.

Xue, Junqing, Bruno Briseghella, Fuyun Huang, Camillo Nuti, Habib Tabatabai, and Baochun Chen. 2020. “Review of Ultra-High Performance Concrete and Its Application in Bridge Engineering.” *Construction and Building Materials* 260:119844. doi: 10.1016/j.conbuildmat.2020.119844.

Yang, I. H., Joh, C., & Kim, B. S. 2010 . Structural behavior of ultra high performance concrete beams subjected to bending. *Engineering Structures*, *32*(11), 3478–3487. https://doi.org/10.1016/j.engstruct.2010.07.017

Yoo, D. Y., & Yoon, Y. S. 2015 . Structural performance of ultra-high-performance concrete beams with different steel fibers. *Engineering Structures*, *102*, 409–423. https://doi.org/10.1016/j.engstruct.2015.08.029

Yuan, Jiqiu, and Benjamin A. Graybeal. 2011. “Bond Behavior of Reinforcing Steel in Ultra-High Performance Concrete.” *Engineering Structures* 1(6):228–35.

Yuan, Jiqiu, and Benjamin A. Graybeal. 2014. “Bond Behavior of Reinforcing Steel in Ultra-High Performance Concrete.” *Federal Highway Administration* 1(6):228–35.

Zhang, Qifeng, Yan Feng, Zhao Cheng, Yang Jiao, and Hang Cheng. 2022. “Large-Scale Testing and Numerical Study on an Innovative Dovetail UHPC Joint Subjected to Negative Moment Large - Scale Testing and Numerical Study on an Innovative Dovetail UHPC Joint Subjected to Negative Moment.” (September). doi: 10.12989/cac.2022.30.3.175.

Zheng, Wenzhong, Dehong Wang, and Yanzhong Ju. 2018. “Performance of Reinforced Reactive Powder Concrete Beam-Column Joints under Cyclic Loads.” *Advances in Civil Engineering* 2018. doi:

10.1155/2018/3914815.

Zhu, Zhenyu, Iftekhar Ahmad, and Amir Mirmiran. 2006. “Splicing of Precast Concrete-Filled FRP Tubes.” *Journal of Composites for Construction* 10(4):345–56. doi: 10.1061/(ASCE)1090-0268(2006)10:4(345).

Zuo, Jun, and David Darwin. 2000. “Erratum: Splice Strength of Conventional and High Relative Rib Area Bars in Normal and High-Strength Concrete (ACI Structural Journal (July-August 2000) 97:4).” *ACI Structural Journal* 97(5):796.

Supervisor's Certification

I certify that this thesis **"Structural Behavior of Spliced Hybrid Reinforced Concrete Deck Girders Under Effect of Monotonic and Cyclic Loads "** and submitted by the student **"Mustafa Kareem Moosa Abdulhassan"**, was prepared under my supervision at The Department of Civil Engineering/ College of Engineering/ University of Babylon, as a part of requirements for **the degree of Doctor of Philosophy in Civil Engineering (Structures).**

Signature:

Supervisor: ***Prof. Dr. Ammar Yaser Ali***

Date: / / 2023

I certify that this thesis mentioned above has been completed in Civil Engineering in the College of Engineering / University of Babylon.

Signature:

Head of Department: Prof.Dr. Thair J. Mizhir Alfatlawi

Date: / / 2023

Examining Committee Certificate

We certify that we have read this thesis entitled "**Structural Behavior of Spliced Hybrid Reinforced Concrete Deck Girders Under Effect of Monotonic and Cyclic Loads** ", and as an examining cee examined that student (**Mustafa Kareem Moosa Abdulhassan**), in its content and that in our opinion it meets a standard of the thesis for **the degree of Doctor of Philosophy in Engineering / Civil Engineering / Structures/.**

Signature: *Name : **Prof. Dr. Nameer A. Alwash*** *(Chairman)* *Date : / / 2023*	*Signature:* *Name : **Prof. Dr. Adel A. Al-Azzawi*** *(Member)* *Date : / / 2023*
Signature: *Name : **Asst.Prof. Dr. Najla'a H. AL-Shareef*** *(Member)* *Date : / / 2023*	*Signature:* *Name : **Asst.Prof. Dr. Nabeel Hassan Ali*** *(Member)* *Date : / / 2023*
Signature: *Name : **Asst. Prof. Dr. Majid M. Kadhim*** *(Member)* *Date : / / 2023*	*Signature:* *Name : **Prof. Dr. Ammar Yaser Ali*** *(Member and supervisor)* *Date : / / 2023*
Approval of Head of Civil Engineering Department *Signature:* *Name : **Prof. Dr. Thair J. Mizher*** *(Head of Civil Engineering Department)* *Date : / / 2023*	
Approve of the Dean of the College of Engineering *Signature:* *Name : **Prof. Dr. Laith Ali Abdul-Rahim*** *(Dean of the College of Engineering)* *Date : / / 2023*	